Group 10 dithiocarbamate complexes for biological applications and as single source precursors to metal sulphide nanoparticles

F.F. Bobinihi

orcid.org/ 0000-0002-0852-5704

Thesis submitted in fulfilment of the requirements for the degree *Doctor of Philosophy in Chemistry* at the North-West University

Promoter: Prof. DC Onwudiwe

Graduation: April 2019

Student number: 28169166

CERTIFICATION

This is to certify that the thesis titled Group 10 dithiocarmate complexes for biological applications and as single source precursors to metal sulphide nanoparticles is an authentic research work carried out by FELICIA FOLA BOBINIHI under the supervision of Prof. Damian Chinedu Onwudiwe at the Chemistry department of the North West University, Faculty of Natural and Agricultural Sciences, Mafikeng, South Africa.

---------- ----------

Date F.F Bobinihi

---------- ----------

Prof.D.C. Onwudiwe

Date Supervisor

DECLARATION

I, Felicia Fola Bobinihi declare that the thesis entitled **Group 10 dithiocarmate complexes for biological applications and as single source precursors to metal sulphide nanoparticles** which I submit to the North-West University, Mafikeng Campus, for the award of PhD Chemistry, is my own work, and has not been submitted to any other University. It has been indicated in the thesis wherever any information has been derived from other sources.

DEDICATION

This thesis is dedicated to my beloved brother, Rev. Fr. Martin Kehinde Alegbemi in appreciation of your unique love and support for me and my family.

Also to my little angel, St. Anne Boluwatife Bobinihi for the joy and blessings your presence has brought to the entire family.

ACKNOWLEDGEMENT

'My hope is in Christ who strengthens the weakest by His divine help; I can do all in Him who strengthens me. His power is infinite, and if I lean on Him, it will be mine. His wisdom is infinite, and if I look to Him for counsel, I shall not be deceived. His goodness is infinite, and if my trust is stayed in Him, I shall not be abandoned'.

Pope Saint Pius X

I am greatly indebted to my wonderful supervisor Prof.Damian.C.Onwudiwe, whose insight, knowledge, passion and creativity has given this work a huge success. He is not only an academic supervisor but also a God sent guardian, who takes delight to render help even on personal issues. Only God can reward you and your generation for the selfless sacrifices and generousity.

To the inorganic and materials research group, this is a repesentative of a small family unit whose team spirit and power of togetherness can inspire and motivate hardwork and success. I appreciate Dr. Jejenija Osuntokun's efforts on this project, he is the unofficial co-supervisor who can render assistance at any point in time he is called upon to do so. I also thank Dr. Elias Elemike for his unrelenting guidance and asistance at all times. A big thank you to Mr.Jerry Adeyemi, my PhD colleaque, he is tech savvy and ever ready to render help on any computer related issues to the group. To my other colleaques, Tshabo Papane my adopted daughter thanks for your special love and affection. Miss Mathatho Motaung, Mrs Tanzim Saiyed and Nkwe Violet, I am most grateful for your wonderful companionship throughout this study.

I thank the Chemistry department of the North West University for the oppourtunity given to me to make use of the departmental and University facilities for this research work. I thank the head of department Dr. Z.Mkhize and the school director Prof. S. Katata, for their assistance when and

where necesary. I appreciate the efforts of the technicians especillay Mr Kagiso Mokalane and Mr Sizwe for the prompt supply of chemicals and neccesary equipment whenever the need arose.

For my families in South Africa, I am mostly grateful to Prof. Raphael Funsho Kutu, who was instrumental in my coming to South Africa for this study, thank you for all your efforts and contributions to this success story. I am immensely grateful to his amiable wife, Mrs Mercy Kutu and the wonderful big boys in the house, may God bless your dreams greatly. For the family of Prof. Damian Onwudiwe and his wife Mrs Precious Onwudiwe a.k.a Lady Pee, and the adorable kids Chichi and Ngozi. I thank you for your hospitality, for giving me shelter and making me feel at home away from home. May God bless and reward you abundantly.

I recognize the contributions of my family members back home in Nigeria, I am very grateful to my parents, Mr Augustine and Mrs Florence Alegbemi. I am so happy that God still keeps you alive to share in the joy of this success story; the foundation of which was laid by your efforts. I pray that God will restore you back to sound health and keep you both for more years to still enjoy the fruits of your labour. To my amazing and wonderful husband, I thank God for your life and for making you who you are, so special, unique and selfless. I thank you for the trust and confidence you have in me to allow me travel this far and this long in pursuance of my dream. I pray the Lord will keep us both till old age to appreciate each other the more. To my wonderful children; Jude Adeniyi, thank you for your companionship, support and the special joy and priviledge of having you around me at this time. Joan Dammy, Maria Olufunke, Catherine Omoboni, Oluwashina, Blessing and my princess Anne Boluwatife, thank you all for your understanding and for bearing the pain of my absence for this period; and also for taking care of the house while I was away, may God bless your dreams and future richly. I am greatly indepted to my sisters who took charge of the home front in my absence; Mrs Felicia Adebola, Dr. Mrs Funmilayo Oniemayin, aunty Yetunde, Mrs Lydia Toluhi, Mrs Hellen Jide-Jimoh and Mrs Agnes Olonikadi, may God enrich you with heavenly bliss. I appreciate all members of St. Monica's society of sacred heart of Jesus parish, Kabba and Mrs Garuba Victoria, thank you all for your prayers and support. I thank my brothers; Mathias Alegbemi, Anthony and Sunday Bobinihi, Lekan Ibihunwa. I appreciate all who supported me financially in the course of this program; Mr Victor Adeniyi and Dr. James K. Samuel (USA), Mr. Steve Babaeko, Sir and Lady Johnson Jimoh, my wonderful brother Fr. Martin Alegbemi, I pray God reward your generousity towards me. For all the priests that surround me and my family; Rev. Frs: Loius Fowoyo, Mathew Bello, Gabriel Wada, Cyril Obanure, Donatus Ogunleye, Francis Ayeni, Nicolas Akindele, James Ḍukiya, Peter Dauda, Philip Otori, Sylvester Ajagbe (Canada),

Michael Eniolorunda and Christian Agbo. I appreciate your prayers on my behalf, I pray God bless your different ministries and grant you all faithful perseverance in His vineyard.

I cannot but remember the contribution of my School management back home, Federal college of Education, Okene, Nigeria. I am grateful for the priviledge and oppotunity of study leave given to me for this higher study. I promise with the grace of God for better efficiency and performance as soon as I resume back to work. I am highly indebted to Mr. Simeon Drisu, Mr. Nwona, A; my HOD, Mr.Avanza; the Dean School of Sciences, Pastor Audu and Mr. Lukan Aminu, Dr. J.K. Agunsoye, Hon Bamidele Owa and other colleaques. I thank you all for your support and for keeping in touch with me at all times.

For all the analyses carried out, I thank the efforts of Mr Romanus Uwaoma for the TGA analysis, Dr. Anthony Ekenia of University of Ibadan and Dr. Uche of UFH for the antimicrobial analysis of the synthesized complexes. I also appreciate the contributions of Drs: Jordan of NWU Potchefstroom and Munshi of UJ for the NMR analyses; Eric Hosten of NMU and Charmie Arderne of UJ for the X-ray single crystals diffraction.

Finally, to the omipotent and benevolence God, the giver of all that is good, in whom we live, we move and have our being; through whom nothing is impossible and whose timing is always perfect. I give unto Him the highest glory, honour and adoration both now and ever more, Amen. Alleluia!

RESEARCH OUTPUT

Felicia F. Bobinihi, Jejenija Osuntokun, Damian C. Onwudiwe (2018). "Synthesis and characterization of nickel(II)dithiocarbamate complexes containing NiS_4 and NiS_2PN moieties: Nickel sulphide nanoparticles from a single source precursor". *Journal of Saudi Chemical Society*, volume 22, pages 381-395

Felicia F. Bobinihi, Damian C. Onwudiwe, Eric C. Hosten (2018). "Synthesis and characterization of homoleptic group 10 dithiocarbamate complexes and heteroleptic Ni(II) complexes, and the use of the homoleptic Ni(II) for the preparation of nickel sulphide nanoparticles". *Journal of Molecular Structure*, volume 1164, pages 475-485.

Felicia Bobinihi, Damian C. Onwudiwe, Anthony Ekennia, Obinna Okpareke, Charmaine Arderne, Joseph Lane. "Group 10 metal complexes of dithiocarbamates derived from primary anilines: synthesis, characterization, computational and antimicrobial studies". *Polyhedron* volume158, pages 296-310.

ABSTRACT

The easy functionalization of dithiocarbamates has offered innovative possibilities to different structural moieties which are versatile in both materials and medicinal chemistry. They serve as precursors to metal sulphide nanoparticles, thin films and platforms for novel semiconductor nanomaterials. This is due to their ability to undergo clean thermal decomposition with little or no impurities, resulting into their respective metal sulphides in the nanometric dimension. In medicinal chemistry, the synergy exhibited by metals and the dithiocarbamate ligand provides new pathway for the discovery of useful therapeutic agents with enhanced activity. This thesis reports a series of dithiocarbamate ligands and complexes. Ten different dithiocarbamate ligands have been synthesized from primary and secondary amines, and also secondary amines prepared from the condensation reaction involving Schiff base compounds. The ligands were characterized using Fourier transform infrared (FTIR), ^{1}H, and ^{13}C nuclear magnetic resonance (NMR) spectroscopic techniques. The ligands were used to prepare thirty homoleptic complexes of group 10 metals [(Ni(II), Pd(II), Pt(II)]; six Ni(II) adducts of 2,2- bipyridine and 1,10-phenanthroline and six heteroleptic complexes containing triphenylphosphine (PPh_3) and thiocyanide (CN^-) or isothiocyanide (SCN^-) ions. All the compounds were characterized using elemental analysis, FTIR, UV-visible, ^{1}H and ^{13}C NMR and thermogravimetric analysis (TGA). Some of the Ni(II), Pd(II), Pt(II) homoleptic and heteroleptic complexes were further characterized by single crystal X-ray analysis. The X-ray crystal structure confirmed the adoption of non-centrosymmerical distorted square planar geometry by the Ni(II), Pd(II), Pt(II) complexes with two bidentate dithiocarbamate ligands. One of the complexes consists of the expected heteroleptic Ni(II) complex with a disordered triphenylphosphine molecule also forming part of the crystal structure.

The thermal decomposition profiles of the complexes followed a similar pattern, which ranges from one step to two step decompositions. The results showed that the introduction of Lewis bases and the formation of heteroleptic complexes increased the thermal stability of the parent complexes. All the complexes decomposed to their respective pure metal sulphides; hence, the complexes were utilized as single source precursors (SSP) for the synthesis of their respective metal sulphide nanoparticles. Three capping molecules: hexadecylamine (HDA), oleylamine (OLA), octadecylamine (ODA) were employed as stabilisers and the precursor compounds were thermolysed at varied temperatures and different growth times. The effects of the difference in capping molecules, growth temperature and time on the morphology of the different nanoparticles were discussed.

The structural properties of the nanoparticles were studied using TEM, SEM, EDX and XRD, while their optical properties were studied using UV-visible and photoluminescence (PL) spectroscopic techniques. Fourier transform infrared spectroscopy was used to explore the surface of the nanoparticles in order to establish the respective functional groups responsible for surface stabilization. From the UV-visible spectra, Tauc plots were used to estimate the band gap energies of the nanoparticles and the results confirmed the quantum confinement effects. An increase in band gap energy with growth time, which indicated decrease in size of nanoparticles with reaction time, was observed. The TEM/SEM results revealed the different morphologies which also occurred with slight widening of the particle size distribution as the thermolysis temperature increased. Different nanoparticle shapes such as dots, spheres, pseudo-spheres and triangular prism were observed with variation of the substituents on the dithiocarabamate group. The nanoparticles were monodispersed with narrow size distribution as confirmed by particles size distribution histogram and PL spectra. The XRD results revealed the formation of different phases of the nanoparticles: Ni_xS_y viz. α-NiS (hexagonal), α-NiS (vaestite), α-$NiS_{1.03}$, α-$NiS_{1.19}$ heazlewoodite-Ni_3S_2, Ni_9S_8 (godlevskite); Pd_xS_y phases: PdS (vysotskite), PdS_2, Pd_4S and Pd crystal; Pt_xS_y : PtS (cooprite), and Pt metal crystal. All the synthesized nanoparticles showed good crystallinity irrespective of the phases.

The antimicrobial potency of the complexes were screened against some gram positive bacteria such as *Bacillus cereus and Staphylococcus aureus,* gram negative bacteria such as *Escherichia coli, Klebsiella pneumonia* and *Pseudomonas aeruginosa*, and some fungi (*Candida albicans* and *Aspergillus flavus*). They exhibited good potential as antimicrobial agents, and in some cases were comparable with the standard drugs used as control. To evaluate their anticancer properties, the preliminary *in vitro* cytotoxic activity of the complexes was tested against tumor cell line of human cervix carcinoma (HeLa). The results of the IC_{50} value showed very good to moderate activity for all tested complexes. These indicate that the complexes could be useful as lead compounds in antimicrobial and anticancer studies.

\

TABLE OF CONTENTS

LIST OF FIGURES

LIST OF TABLES

LIST OF SCHEMES

LIST OF ABBREVIATION

DTC	Dithiocarbamate
FTIR	Fourier Transform Infrared
MS	Metal Sulphide
NPs	Nanoparticles
NMR	Nuclear Magnetic Resonance
PPh_3	Triphenylphosphine
THF	Tetrahydrofuran
SCN	Thiocyano
Ph	Ph
EtOH	Ethanol enyl
MeOH	Methanol
$NaBH_4$	Sodium borohydride
NH_4SCN	Ammonium thiocyanate
KCN	Potassium cyanide
XRD	X-ray Diffraction
TEM	Transmission Electron Microscopy
SEM	Scanning Electron Microscopy
DLS	Dynamic light scattering
UV	Ultra-violet
SSP	Single Source Precursor
HDA	Hexadecylamine

OLA	Oleylamine
ODA	OctadecylAmine
TOP	Trioctylphosphine
NaBH4	Sodiumborohydride
CHNS	Carbon, Hydrogen, Nitrogen, Sulphur
DTG	Derivative Thermogravimetric
Et_3N	Triethylamine
NH_4L^1	Ammonium *N*-phenyldithiocarbamate
NH_4L^2	Ammonium *N*-benzylphenyldithiocarbamate
NaL^3	Sodium *p*-methylphenyldithiocarbamate
NaL^4	Sodium *p*-ethylphenyldithiocarbamate
NaL^5	Sodium-1,6-hexamethelynediaminedithiocarbamate
$[Ni(L^1)_2]$	Ni(II) bis-(*N*-phenyldithiocarbamate)
$[Pd(L^1)_2]$	Pd(II) bis-(*N*-phenyldithiocarbamate)
$[Pt(L^2)_2]$	Pt(II) bis-(*N*-phenyldithiocarbamate)
$[Ni(L^2)_2]$	Ni(II) bis(*N*-benzyldithiocarbamate)
$[Pd(L^2)_2]$	Pd(II) bis(*N*-benzyldithiocarbamate)
$[Pt(L^2)_2]$	Pt(II) bis(*N*-benzyldithiocarbamate)
$[Ni(L^3)_2]$	Ni(II) bis (*p*-methylphenyldithiocarbamate)
$[Pd(L^3)_2]$	Pd(II) bis (*p*-methylphenyldithiocarbamate)
$[Pt(L^3)_2]$	Pt(II) bis (*p*-methylphenyldithiocarbamate)
$[Ni(L^4)_2]$	Ni(II) bis(*p*-ethylphenyldithiocarbamate)

$[Pd(L^4)_2]$	Pd(II) bis(*p*-ethylphenyldithiocarbamate)
$[Pt(L^4)_2]$	Pt(II) bis(*p*-ethylphenyldithiocarbamate)
$[Ni(L^5)_2]$	Ni(II) bis-(*N*-hexamethylenediaminedithiocarbamate
$[Pd(L^5)_2]$	Pd(II)bis-(*N*-hexamethylenediaminedithiocarbamate
$[Pt(L^5)_2]$	Pt(II) bis-(*N*-hexamethylenediaminedithiocarbamate
$[Ni(L^6)_2]$	Ni(II) bis-(*N*-methyl-*N*-ethanoldithiocarbamate
$[Pd(L^6)_2]$	Pd(II) bis-(*N*-methyl-*N*-ethanoldithiocarbamate)
$[Pt(L^6)_2]$	Pt(II) bis-(*N*-methyl-*N*-ethanoldithiocarbamate)
$[Ni(L^7)_2]$	Ni(II) bis-(*N*-ethyl-*N*-ethanoldithiocarbamate)
$[Pd(L^7)_2]$	Pd(lI) bis-(*N*-ethyl-*N*-ethanoldithiocarbamate)
$[Pt(L^7)_2]$	Pt(II) bis-(*N*-ethyl-*N*-ethanoldithiocarbamate)
$[Ni(L^8)_2]$	Ni(II) bis(*N*-naphtyl-1-carboxyl-*N*-phenyldithiocarbamate)
$[Pd(L^8)_2$	Pd(II) bis(*N*-naphtyl-1-carboxyl-*N*-phenyldithiocarbamate)
$[Pt(L^8)_2]$	Pt(II) bis(*N*-naphtyl-1-carboxyl-*N*-phenyldithiocarbamate)
$[Ni(L^9)_2]$	Ni(II) bis-(*N*-nitro-4-carboxyl-*N*-phenyldithiocarbamate)
$[Pd(L^9)_2]$	Pd(II) bis-(*N*-nitro-4-carboxyl-*N*-phenyldithiocarbamate)
$[Pt(L^9)_2]$	Pt(II) bis-(*N*-nitro-4-carboxyl-*N*-phenyldithiocarbamate)
$[Ni(L^{10})_2]$	Ni(II) bis-(*N*-3,4-dihydroxylbenzyl–*N*-hexamethylene-1,6-diamine DTC)
$[Pd(L^{10})_2]$	Pd(II) bis-(*N*-3,4-dihydroxylbenzyl–*N*-hexamethylene-1,6-diamine DTC)
$[Pt(L^{10})_2]$	Pt(II) bis-(*N*-3,4-dihydroxylbenzyl–*N*-hexamethylene-1,6-diamine DTC
$[Ni(L^1)_2bpy]$	Ni(II) (2,2′-bipyridyl(phenyldithiocarbamato)complex
$[Ni(L^1)_2ph]$	Ni(II) (1,10-phenantroline) (*N*-phenyldithiocarbamato) complex

$[Ni(L^3)_2bpy]$	Ni(II) (2,2′-bipyridyl) (*p*-methylphenyldithiocarbamato) complex
$[Ni(L^3)_2ph]$	Ni(II) (1, 10-phenantroline) (*p*-methylphenyldithiocarbamato) complex
$[Ni(L^4)_2bpy]$	Ni(II) (2,2′-bipyridyl) (*p*-ethylphenyldithiocarbamato) complex
$[Ni(L^4)_2ph]$	Ni(II) (1, 10-phenantroline) (*p*-ethylphenyldithiocarbamato) Complex
$[NiL^2(NCS)(PPh_3)]$	(*N*-benzyldithiocarbamato-S,S′)(isothiocyanato)(triphenylphosphine) nickel(II)
$[NiL^2(NC)(PPh_3)]$	(*N*-benzyldithiocarbamato-S,S′)(isocyano-*N*)(triphenylphoshine) nickel(II)
$[NiL^5(NCS)(PPh_3)]$	*N*-alkyl-*N*-methanoldithiocarbamato S,S′)(isothiocyanato) (triphenylphosphine) nickel(II)
$[NiL^5(NC)(PPh_3)]$	(*N*-alkyl-*N*-methanoldithiocarbamato S,S′)(isocyanato)(triphenylphosphine) nickel(II)
$[NiL^6(NCS)(PPh_3)]$	(*N*-alkyl-*N*-methanoldithiocarbamato S,S′)(isothiocyanato) (triphenylphosphine) nickel(II)
$[NiL^6(NC)(PPh_3)]$	(*N*-alkyl-*N*-ethanoldithiocarbamato S,S′)(isocyanato)(triphenylphosphine) nickel(II)

CHAPTER ONE

1.0 Introduction

1.1 Group 10 metals and their properties

Transition metals are one of the most resourceful elements in the Periodic Table with respect to human progress, conquest, war, and expensive works of art [1]. They have found a wide range of applications in all spheres of human endeavour, from electronics, industries to medicine [2]. The group 10 triad (Ni, Pd and Pt) offers much diverse chemistry with important therapeutic applications, especially in medicine. In the massive state, they are not reactive; thus, they are called "noble" metals. However, their ions are being studied as they play key roles in the treatment of various diseases [3]. The metals have variable oxidation states (Ni: 0,1,2,3, 4; Pd: 0, 2, 4; Pt: 0, 2, 4, 5, 6), and this imparts the differences in colours (white to light grey), reactivities, coordination complexes and magnetism of the metals. They are highly lustrous, ductile and resistant to tarnishing (oxidation) due to their strong intermetallic bonding, high ionization energies and are superconductors. The presence of the valence electrons in the d-orbitals significantly influences the metal ion coordination environment. Hence, the coordination numbers predict the structure of complexes and geometries. The different geometries that could be exhibited by the triads are: linear (from coordination number 2, not very common for first row transition metal ion complexes); tetrahedral or square planar (from coordination number 4); octahedral (from coordination number 6, most common geometry found for first row transition metal ions) [4]. The d^8 configuration in Pd(II) and Pt(II) particularly favours the square planar geometry where the ligand fields result in two paired electrons in both the e_g and t_{2g} energy levels (low spin/strong field). Ni(II), on the other hand, most times prefers the high spin/weak field configuration orbitals of a tetrahedral ligand field. This occurs when the metal is coordinated to very large ligands which might prefer the larger 109.5° of tetrahedral angles. However, real structures can be distorted most times due to steric effects (bulky ligands or stiff chelate rings) [5]. The group10 metal complexes are usually centro symmetric with the central metal in a distorted square planar structure, the distortion increases down the group in the order: Pt>Pd> Ni.

1.2. Group 10 triad in medicinal chemistry

The group 10 triad (Ni, Pd and Pt) offer much diverse chemistry with important therapeutic applications especially in medicine. They have more benefits compared to the more common organic-based drugs. Most of the unique properties are due to their wide range of coordination numbers and geometries, accessible redox states, 'tune-ability' of the thermodynamics and kinetics of ligand substitution, and wide structural diversity [6]. Medicinal inorganic chemistry is a thriving area of research. It was initially driven by the chance discovery of the metallo-pharmaceutical cisplatin. The cytotoxic activity of noble metal ions and their ability to revert tumour cells is higher than other metals. Thus, in the past 5000 years, noble metal ions have played significant roles in cancer treatment [7]. More than 30 years after its approval as a chemotherapeutic agent, cisplatin is still one of the world's best-selling anticancer drugs. It is mainly used in the treatment of ovarian, head and neck, bladder, cervical and lymphomas cancers. However, cisplatin has some undesirable side effects which include: limited application to short range of cancers, intrinsic resistance acquired by some cancer cells, and severe additional side-effects such as nausea, bone marrow suppression, and kidney toxicity. Hence, the development of inorganic anticancer agents with reduced toxicity is widening beyond cisplatin [8]. To find an alternative to cisplatin, different metal complexes are being developed with wide range of ligands or ligand combinations.

Palladium forms complexes similar to platinum, but with different kinetics and stability [9]. In addition, Pd compounds have low cost and higher solubility compared to Pt compounds. But, one of its demerits is the greater tendency to exchange the ligands, about 10^5 times higher than Pt(II), which results into rapid hydrolysis of the Pd-based drugs. Furthermore, the ligand dissociation generates very active sites that could easily interact with donor species. This could render palladium complexes inactive, but still toxic because of their higher reactivity. Besides, palladium compounds transform spontaneously into inactive trans derivatives compared to the cis configuration of Pt-drugs which exhibit higher anticancer activity [10]. However, these shortcomings of the Pd-based complexes could be overcome by incorporating into its backbone a bulky, chelating and a strongly coordinating ligand like dithiocarbamate coupled with non-labile leaving group(s) to achieve higher stabilization [11]. Since dithiocarbamates can coordinate strongly to transition metals, their Pt(II) and Pd(II) complexes can block metal interaction with sulphur-containing renal proteins, thus, preventing or at least reducing their renal-toxicity. These complexes may have antitumour activities similar to cisplatin, but without cross-resistance [12].

Nickel is also an essential element for biological systems and variation in its activities is widely reported [13]. Ni(II) complexes are very relevant in the search for novel compounds against drug resistance diseases and development of metal based pharmaceuticals. It is also very useful in the preparation of antibacterial and antifungal drugs. The kinetically labile, square-planar, divalent and low molecular weight complexes prove to be more beneficial against several diseases as they are part of the active centers of enzymes. When combined with monodentate phosphines of the type $[M(L)_2(PPh_3)]$, Ni(II) shows more effectiveness against the growth of fungi in various conditions [14]. The stability of +2 oxidation state in aqueous solution makes Ni(II) ions very important in biological system. This is a key factor that influences the production of secondary plant metabolites for plant resistance to diseases and in several animal enzyme systems. This is because it interacts with iron found in the haemoglobin and helps in oxygen and sugar transport to stimulate their metabolism [15].

The diverse characteristic properties and the pharmacological activities of the compounds of these metals depend also on the type of ligands to which they are bound. Dithiocarbamate ligands are, therefore, considered because they are good donors with excellent coordination ability.

1.3 Dithiocarbamates

Dithiocarbamates are highly versatile monoanionic chelating ligands which form stable complexes with all the transition elements and also the majority of main group, lanthanide and actinide elements. They are S and N containing ligands and display rich and varied coordination chemistry (Figure 1) [3].

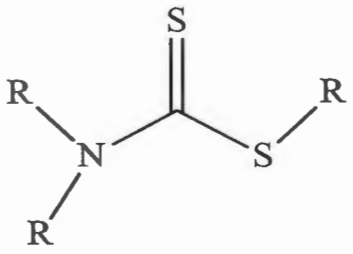

(R=Alkyl/phenyl)

Figure 1: Structure of dithiocarbamate derivative as an S and N containing compound

The presence of π-electron on the N makes dithiocarbamates more basic than other structurally related anions such as dithiocarboxylates ($R\text{-}CS_2^-$) and xanthates ($ROCS_2^-$) [16]. Dithiocarbamates tend to bind as monodentate, bidentate chelating or bidentate bridging ligands due to the diverse nature of their ligating character [17]. They are particularly useful for their ability to form complexes with all metals; stabilizing both high and low oxidation states. Related ligands such as xanthates cannot exhibit such property, because the electronegativity of the oxygen atom in the xanthates is too high to form the analogue of the 'thioureide' resonance form. So, it is less able to stabilise higher oxidation states [18]. The resonance forms of dithiocarbamate are shown in scheme 1.1. In the monoanionic form, there is a single bond between the N and S-bearing C atom and the delocalization of the negative charge between the C and S atoms. This gives rise to a soft ligand which is able to stabilize soft metals at lower oxidation states. In the thioureide form, the lone pair on the N atom is delocalised, resulting in double bond character between it and the CS_2 carbon, and both S atoms possess negative charges. The N here is sp^2 hybridized, and the result is a hard ligand able to stabilize hard metal centres at higher oxidation states. Dithiocarbamate ligands are, therefore, considered as good donors with excellent coordination ability which forms metal complexes resulting in different forms as shown in scheme 1.2 [3].

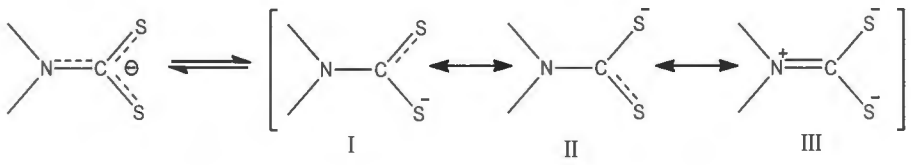

Scheme 1.1: Main resonance structure of a dithiocarbamate anion [18].

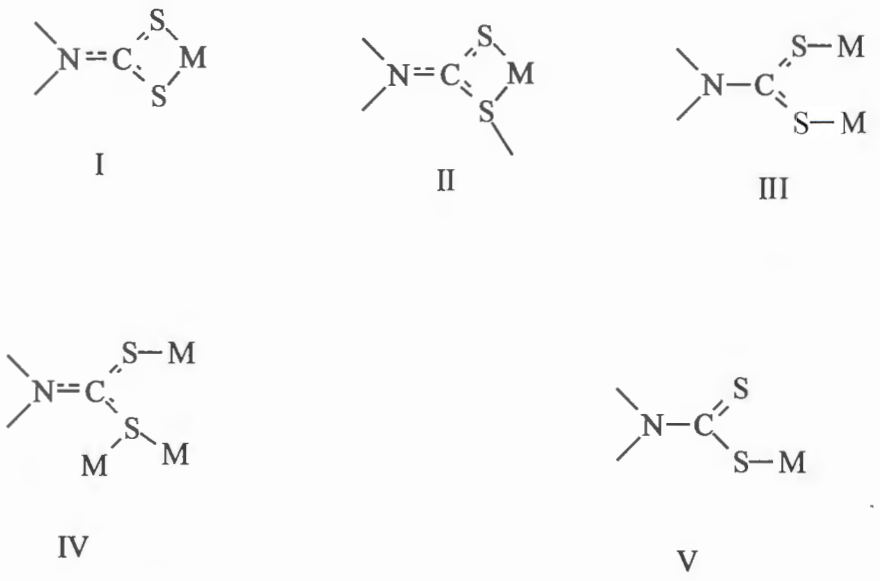

Scheme 1.2: Binding forms of dithiocarbamate metal complexes [3]

The extent to which the resonance (thioureide) forms contributes to the structure and their effects on the physical and chemical properties of dithio compounds have been the subject of considerable study. This contribution to the structure of the dithiocarbamate ligands and complexes has been offered as a possible explanation for the varying antifungal activities of these compounds.

Dithiocarbamates have small bite angle, (~2.8–2.9 ◦) whose major advantage on the dithiocarbamato moiety is its unique ability to remain intact under a variety of reaction conditions [19]. Complexation reaction by dithiocarbamate, thus, occurs either at refluxing (heat), at room temperature, or at extremely low temperature (in ice) condition.

They also have ability to stabilize novel stereochemical configurations, unusual mixed oxidation states (e.g., Cu), intermediate spin states (e.g., Fe(III), S = 3/2), and to form a variety of tris chelated complexes of Fe(II) [20].

Due to their versatile metal chelating properties, they are used extensively in analytical and medicinal chemistry.

When primary dithiocarbamates are used, the presence of the labile hydrogen atom; -NH a hydrophilic group, can easily be deprotonated to increase the rate of DNA interaction and thereby assist in promoting the lipophilicity of the compound [21]. In the presence of secondary dithiocarbamates carrying hydroxyl groups, the solubility of the compounds could be enhanced leading to increased hydrophilicity of these compounds with significant biological implications [22]. Furthermore, incorporation of these metal complexes to Schiff base backbone shows some degree of antibacterial, antifungal, antitumor and anti -inflammatory activities. Adduct and mixed

ligand formations allow the increase in coordination number of metal ions in a complex giving rise to different physical and chemical properties from the parent complexes, and so can enhance their biological activities [23].

Dithiocarbamates have also been used extensively in agriculture, polymer and environmental chemistry. A derivative of the compound has been used to increase the soil fertility, and is used for the prevention of wireworm damage to potatoes. It can be used as a control element in organic reactions like epoxidation and epoxide opening as well as in the removal of heavy metal ions from aqueous solution. In addition, they serve as modifiers in latex coagulation, rubber-reinforcing agent, an accelerator of vulcanization [19]. Other derivatives are applicable of forming highly concentrated, stable and porous emulsion materials. Dithiocarbamates are lipophilic and their characteristic complexing properties, combined with the poor solubility of the metal complexes in aqueous media are responsible for the extensive use of these compounds in various areas of environmental importance [15].

1.4 Synthesis of dithiocarbamate

Dithiocarbamates could easily be prepared, from the reaction of carbon disulphide with a primary or secondary amine in the presence of a base [24]. At the early stage, the synthesis of dithiocarbamates suffered from many drawbacks such as long reaction time, harsh reaction conditions, and the use of expensive and toxic reagents [25]. However, due to the wide applications of dithiocarbamates, several new, fast, convenient and safe methods with different substituent groups for the synthesis of these compounds have been developed. Dithiocarbamates have been prepared from primary and secondary amines, and also from the one-pot reduction of amines, and electrophiles such as alkyl halides, epoxides, carbonyl compounds and Schiff bases [26]. The presence of multisites on the dithiocarbamate moiety gives room for multiple interactions and this enhances their biological activities on different proteins and enzymes in medicinal applications.

The simplest member of the series H_2NCSSH was obtained as an unstable crystalline solid by the acidification of a concentrated solution of the ammonium salt. Studies involving dithiocarbamate ligands obtained from primary amines are rare due to their low stability and difficult synthetic procedure. The low stability is ascribed to the presence of acidic hydrogen on the nitrogen atom of the dithiocarbamate which facilitates the loss of H_2S, and also the formation of isothiocyanate as an intermediate during the thermal decomposition [15, 16] according to reaction (1).

$RNHCS_2M^+ \longrightarrow RNCS + H_2S$ ..... (1)

Although disubstituted dithiocarbamates are more stable, their stability is pH dependent as they could also decompose under acidic conditions to give the free amine and carbon disulphide as presented in reaction (2)

$R_2NCS_2^- + H^+ \longrightarrow R_2NH + CS_2$ ..... (2)

1.5 Dithiocarbamate complexes of group 10 metals

The chemistry of group 10 metal dithiocarbamate complexes has been studied in considerable detail [27]. Most of the complexes display distorted square planar and/or tetrahedral arrangement and the extent of distortion increases when one of the two dithiocarbamate groups is substituted by other bidentate ligands. The effect of the type of substituents on the dithiocarbamate ligand can manifest in many ways on the properties of the d^{10} complexes produced. These include: the thermal stability, optical properties, magnetic susceptibility and electronic properties. The stability of the complexes increases with increase in the size of the R-group due to the electronic shifts in the dithiocarbamate ligand [28]. The inductive effect (positive or negative) of the substituent on the nitrogen atom, also dictates the flow of electrons towards the ligating CS_2 group [29].

Dithiocarbamate complexes have proven to be efficient single source precursor for the synthesis of metal sulphide (MS) nanoparticles. The efficiency of the dithiocarbamate complex in materials chemistry depends on the nature of the substituents which could be varied to suit a particular purpose [30].

1.6 Nanoparticles (Overview)

Nanoparticles (NPs) are materials with at least one dimension in the nanometer ($1x10^{-9}m$) range, and this dimension matters for nearly all material properties [34]. They behave as a whole unit with respect to their transport and properties. Thus, they allow materials to be used in areas that are too small for the bulk to reach and bring with it new capabilities. It is the intermediate size range between bulk materials and molecules, and possesses properties distinct from these two species.

Particles can be classified by size as coarse (10000 - 2500 nm), fine (2500 -100 nm) and ultrafine (1-100 nm). They exist in the natural world and are also created as a result of human activities. Due to their sub microscopic size, they have unique material characteristics when compared to their larger (bulk) or smaller (single-atom) counterparts [35]. These unique properties are highly required for commercialization, with considerable efforts by current researchers on the large scale production of smarter and cost effective materials.

Nanoparticles could be amorphous or crystalline, and in the latter case are sometimes referred to as nanocrystals [36]. Dispersions of nanoparticles in liquid media are referred to as colloids and themselves possess distinct properties. As a result of their submicroscopic size, nanoparticles offer more unique characteristics over their bulk counterparts (minute particles, infinite possibilities). For example, they can be used to (a) improve drug solubility and bioactivity and allow multiple drugs to be incorporated into the same delivery system, (b) reduce toxicity and can easily be taken up by phagocytic cells, and (c) target to particular cell or tissue [37]. They can also contribute to stronger, lighter, smarter and cleaner surfaces. Physical and chemical properties that change at the nanoscale due to surface area and quantum effects are: colour, melting temperature, crystal structure, chemical reactivity, electrical conductivity, magnetism and mechanical strength. Different diversities are also exhibited at the nanoscale like chemical composition, form or shape and surface treatments [38].

Nanoscience has advanced at an alarming rate and this is mostly driven by consumer demand for smaller, speedy and more powerful electronic devices. And so, currently, nanoscience and nanotechnology have come to surround particulate science, nanostructured devices and atomic scale manipulation of matter [39].

The unique properties offered by nanoparticles remain highly desirable for commercialization and a great deal of efforts is now focused on the large scale generation of high performance, cost-effective materials. Nanoparticles are of great importance in the areas of medicine, computing, energy materials, sensing and detection, water treatment and catalysis [40]. It is swiftly gaining renovation in a large number of fields such as health care, cosmetics, biomedical, food and feed, drug-gene delivery, environment, health, mechanics, optics, chemical industries, electronics, space industries, energy science, light emitters, single electron transistors, nonlinear optical devices and photo-electrochemical applications.

Since nanoparticles have more surface area to volume ratio, using the nanoparticle drug delivery system can improve their biological applications [41]. This is because the compounds in the nanometre range will have faster dissolution, greater bioavailability and specific target delivery [42]. All these can combine to help curb drug resistance and toxicity.

1.7 Historical perspective of nanometer length scale

The nanometer length scale was been ignored for a certain period of time called the world of neglected dimension, when there was no colloid science but replaced with 0.1-1 μm, the scale of visible light [43]. Not until in the speech of Dr. Richard Feynman, at the American Chemical Society annual meeting in December 1959, 'There is plenty of room at the Bottom', where he visualized the technical potential of the very small materials. He predicted a version of the Encyclopedia Britannica that could fit on the head of a pin [44]. About 20 years later, there was a technological breakthrough when Eric Drexler pioneered molecular manufacturing. He introduced the term 'nanotechnology' where he described the act of engineering materials on a very small scale [45]. Since then, the production of nanomaterial and nanoparticles has progressed greatly. Developments in the field of nanoscience have necessarily accompanied developments in analytical techniques and equipment, exemplified in the 1925 Nobel Prize in Chemistry, awarded to Richard Zsigmondy for his work on metal colloids and the ultramicroscopic [46].

Though the human manipulation of nanoparticles is considered a relatively new technology, nanoparticles or ultra-fine particles have existed in our atmosphere in numerous ways such as fires, mineral composites, volcanoes, viruses and sea spray [47]. There are also many activities engaged by humans that produce nanoscale particles as an unintentional waste product of the process such as cooking smoke, sand blasting, diesel exhaust and welding fumes. Nanoparticles were used by artisans as far back as 9th century to generate a glittering effect on the surfaces of pots by dispersing gold and silver nanoparticles on the transparent surface of the ceramic glaze. Size effects on gold nanoparticles were famously investigated by Michael Faraday in 1857 [48]. He, thus, provided the first description in scientific terms of the optical properties of nanometre scale metals.
Nanotechnology has since then found growth in several fields of research such as (i) nanomedicine, (ii) solar derived power, (iii) bio-sensors and Nano-electronics, (v) production, processing and food packaging [49].

1.8. Nanoparticle synthesis

The end use of the nanoparticle dictates the materials and methods of their synthesis, since nanoparticle syntheses are engineered towards maximizing the performance of the products.
There are two general approaches to the synthesis of nanoparticles: the top-down (physical destruction of larger materials) and bottom-up (build up from molecular precursors, often colloidal)

approaches. The bottom-up approach is often used because it allows a stepwise build-up of nanoparticles into desired sizes and shapes, while the top-down approach introduces surface imperfection on the product [50]. The bottom-up approach includes photochemical, electrochemical, chemical reduction and solvothermal (which could either be hot injection or heat-up) methods [51, 52]. One of the mostly used bottom-up approach is the solvothermal method. This is a solution based thermal synthesis route, which typically involves the dissolution of the molecular precursor in a high boiling solvent with subsequent decomposition at high temperature. A capping agent is used to protect the prepared nanoparticles from agglomeration. The solvothermal synthesis has several advantages over the other methods. It is simpler, and occurs at lower temperature and pressure. The variables involved include, solvent, precursors, decomposition temperature and duration of reaction. The solvent should be a high boiling point compound which is able to coordinate to the resulting nanoparticles in order to prevent agglomeration e.g., ethylene glycol, hexadecylamine, oleylamine, octadecylamine, dodecylamine, dodecanethiol, oleic acid. [53]. There are two main types of solvothermal decomposition which differ by the temperature at which the precursors are introduced into the solvent, namely the 'hot injection' and 'heat up' methods.

In the 'heat up' method, all the reagents are put together at the start of the reaction which proceeds through monomer accumulation, nucleation and then to particle growth in order to form nanoparticles. The precursors are dissolved in a high boiling point solvent at room temperature, often in an oxygen free atmosphere, and heated to the desired temperature. The reactions are typically held at this temperature for a specified time, to allow for complete decomposition of the precursors [54].

The 'hot injection' method could involve the use of binary precursors or single source precursor. In the former, one of the precursors is heated in a high boiling solvent to a temperature which on injection of the other precursor will be high enough to overcome the nucleation barrier and cause instantaneous burst nucleation. In the later, a single precursor is used and upon addition of room temperature (RT) precursor solution, decomposition and surpersaturation of precursor monomer occurred rapidly, producing burst nucleation. External heating is removed prior to injection and the addition accompanied by a net temperature drop. This is to prevent multiple nucleations by providing a distinct energy barrier between the nucleation and crystal growth phases. Heating is then reapplied to the system to allow for particle growth (but not high enough for nucleation), all of which will lead to well defined, 'temporally discrete', nucleation and growth phases, and nanoparticles with a low polydispersity (< 5 %) [55]. The 'hot injection' method has advantages

over the 'heat up' method, particularly the temporal separation of the nucleation and growth phases of particle formation, leading to small particles of low polydispersity. Polydispersity is defined as the degree at which particle sizes differ with respect to each other; this is often detrimental to nanoparticle properties. Monodispersity is desired as the entire sample will behave in the same way to enhance the effectiveness of the nanoparticle [56].

Another method of synthesis, termed Biosynthesis/Green synthesis, involves the use of plant extracts from the root, shoot, leaves or fruits and microorganisms for the synthesis of nanoparticles. Since plant extracts contain various secondary metabolites, they could act as both reducing and stabilizing agents for the synthesized nanoparticles. Metals such as cobalt, copper, silver, gold, palladium, platinum, and some metal oxides have been reported using this technique. One of the benefits of biosynthesis of nanoparticles using plants extracts is that some plants with therapeutic benefits are able to transfer those properties to the nanoparticles, hence enhances the potentials of the nanoparticles for medicinal applications [57].

1.9 Conclusion

The discovery of the metallopharmaceutical cisplatin has aided the relevance of medicinal inorganic chemistry and transition metals in particular have been considered to offer more opportunities for therapeutic applications. The role of the central metal is important because of the advantage of metals to easily lose the electrons from the metallic state to form positively charged ions which is soluble in biological fluids and so have specific DNA interaction and cleavage properties under physiological conditions [58]. The group 10 triad (Ni, Pd, Pt) with a high affinity for sulphur containing ligands can thus be combined with dithiocarbamates which can efficiently coordinate to transition metals to promote ligand exchange reactions.

In materials chemistry, there are changes in materials' properties when sizes are reduced. The nanoparticles have increased surface to volume ratio as compared to the bulk, and this imparts new and unusual properties on the material. As the particle diameter decreases, the surface area per unit mass increases extremely, such that their activity towards any processes that occur at their surface like catalysis and sensing is greatly increased [59]. Quantum size and quantum confinement effects are also important outcome of the nanometre scale. These changes in properties as materials move from macro to nano size are very unique and can be used for a variety of applications.

With the growing interest in biologically relevant molecules, there is the need for efficient synthetic methods to prepare compounds with interesting physiological activities. It is hoped that this work

could add up to the current drive in the design and development of novel and active metal complexes with greater potential for biological activities and production of metal chalcogenides for a variety of applications in many fields.

1.10 Research aim and objectives

Aim: To synthesize a new class of dithiocarbamate complexes with improved biological properties that could also serve as precursor to group 10 chalcogenide nanoparticles.

To achieve the research aim, the following objectives have been set:

- synthesis and characterization of different dithiocarbamate ligands from different primary and secondary amines,
- synthesis and characterization of some homoleptic and heteroleptic complexes of Ni(II), Pd(II), and Pt(II) dithiocarbamates,
- synthesis and characterization of nickel sulphide, palladium sulphide and platinum sulphide nanoparticles using solvothermal approach,
- Evaluation of the antibacterial, antifungal and anticancer properties of the complexes.

REFERENCES

[1] S. Medici, M. Peana, V.M. Nurchi, J.I. Lachowicz, G. Crisponi, M.A. Zoroddu, Coord. Chem. Rev. 284 (2015) 329.

[2] G. Hogarth, Mini Rev. Med. Chem. 12 (2012) 1202.

[3] G. Hogarth, Prog. Inorg. Chem. 53 (2005) 71.

[4] H. Khan, A. Badshah, M. Said, G.Murtaza, M S Jamil, S.Butler, Inorg. Chim.Acta, 447 (2016) 176.

[5] D C. Onwudiwe, A. C. Ekennia, E. Hosten J. Coord. Chem., 69 (2016) 2454.

[6] A.C. Ekennia, D.C. Onwudiwe, C. Ume, E .E, Ebenso, Bioinorg. Chem. Appl. 2015 (2015) 1.

[7] B.A Prakasam, M Lahtinen, A. Peuronen, M. Muruganandham, E. Kolehmainen, E Haapaniemi, M. Sulanpaa, J. Mol. Struc. 1108 (2015) 195.

[8] N. Singh, S. B. Charya, J. Organomet. Chem. 700 (2012) 69.

[9] D .C. Onwudiwe, P. A. Ajibade, Polyhedron 29 (2010) 1431.

[10] B. Escobar, S.A. Gamboa, U. Pal, R. Guardian, Int. J. Hydr. Energy. 35 (2010) 4215.

[11] D. C. Onwudiwe, T. Arfin, C. A. Strydom, R. J. Kriek, Electrochim. Acta. 104 (2013) 19.

[12] D. Buac, S. Schmitt, G. Ventro, F.R. Kona, Q.P. Dou, Mini Rev. Med. Chem. 12 (2012) 1193.

[13] I. Ali, W. A. Wani, K. Saleem, M. Hseih, Polyhedron 56 (2013) 134.

[14] P. Mittal, V. Uma, Der Chemica Sinica, 1 (2010) 124.

[15] E. Yousif, J. Saudi Chem. Soc. 18 (2014) 269.

[16] R. Y. Pelgrift, A. J. Friedman, Adv. Drug Delivery Rev. 65 (2013) 1803.

[17] A. Roffey, N. Hollingsworth, H.UbaydaIslam, M. M. G.Sankar, C. Richard A. Catlow, G. Hogarth, N. H. deLeeuwa, Nanoscale, 8(2016) 11067.

[18] K.S. Saddiqi, S.A.NamiLutfulla, Y.Chebude, J.Braz. Chem.Soc.17 (2006)107.

[19] D. C. Onwudiwe, J. N.Mugo, H. Madalina, H. Eric, J. Sulfur Chem. 36 (2015) 36.

[20] D. Coucouvanis, J. P. Fackler Jr., Inorg.Chem.6 (1967) 2047,

[21] H. Kubinyi, J. Braz. Chem. Soc.13 (2002) 717.

[22] G. M. de Lima, D. C. Menezes, C. A. Cavalcanti, J. A.F. dos Santos, I. P. Ferreira, E. B Paniago, J. L. Wardell, S. M.S.V. Wardell, K. Krambrock, I. C. Mendes, H. Beraldo, J. Mol. Struct. 988 (2011) 1.

[23] R. Johari, G. Kumar, S. Singh, J. Indian Chem. Council., 26 (2009) 23.

[24] A. N. Vasiliev, A. D. Polackov, Molecules 5 (2000) 1014.

[25] A. W. M Lee, W. H Chan, H. C Wong, M. S. Wong, Synth.commn.19 (1989) 547.

[26] A.Z. Halimehjani, S. Torabi, V. Amani, B. Notash, M.R. Saidi, Polyhedron. 102 (2015) 201.

[27] E. Sathiyaraj, G. Gurumoorthy, S. Thirumaran, New J. Chem.39 (2015) 5336.

[28] F.Trudu, F. Amato, P. Vanhama, T. Pivetta, E. M. Pena-Mendez, J. Have. J. Appl. Biomed. 132 (2015) 79.

[29] S. A. Bhat, J. T. Mague, M. S. Balakrishna J. Organ. Chem. 809 (2016) 21.

[30] R. R. Martinez, R. M. Huicochea, J.A G. Alvarez, H. Hopfl, H. Tlahuext, Ark. V (2008) 19.

[31] A. Goicu, Springer Sci. Bus Media 31 (2006) 405.

[32] S. C. Bajia, A. Mishra, J. Coord. Chem. 64 (2011) 2727.

[33] M.J. Hajipour, K. M. Fromm, A. A. Ashkarran, D. Jimenez de Aberasturi, Trends Biotech. 30 (2012) 499.

[34] T.S. Sreeprasad, T. Pradeep, Noble Metal Nanoparticles.Springer Handbook of Nanomaterials.Springer, Berlin, Heidelberg. (2013).

[35] P. Christopher, H. Xin, A. Marimuthu, S. Linic, Nat. Mater. 11 (2012) 1044.

[36] R. Anthony, K. Uwe, Phys. Rev. B. 80 (2009) 115407.

[37] G.A.Ozin, A.C.Arsenault, L. Cademartiri, Nanochemistry: A Chemical Approach to Nanomaterials, RSC Publishing, 2nd edn., (2009).

[38] S. Raoux, C.T. Rettner, J .Appl.Phys. 102 (2007).

[39] W. Ostwald, Z. Phys. Chem. 37 (1901) 385.

[40] M. Donbrow, Microcapsules and Nanoparticles in Medicine and Pharmacy, CRC press, Amazon.com (1991).

[41] M. Caldorera-Moore, N. Guimard, L. Shi, K. Roy.Drug. Deliv. 7 (2010) 479.

[42] K. Xiao, Y. Li, J. Luo, Biomaterials 32 (2012) 3435.

[43] H. Weller, Angew. Chem. 105 (1993) 43.

[44] R.P.Feynman, J.Microelectromechanical Syst. 1(1992) 49.

[45] K. Eric Drexler Proc. Natl. Acad. Sci. USA 78 (1981) 5275.

[46] R. Zsigmondy, Coloids and the Ultramicroscope: a Manual of Coilloid Chemistry and Ultramicroscopy, J. Wiley, 1st edn. (1914).

[47] B. Le Ouay, F. Stellacci, NanoToday 10 (2015) 339.

[48] M.Faraday, Philos.Trans.R.Soc.London, 147 (1857) 145.

[49] K. Miyazaki, N. Islam, Technovation 27 (2007) 661.

[50] A. N. Gupta, V. Kumar, V. Singh, K. K. Manar, M. G. B. Drew, N. Singh, Crys. Engr. Comm.39 (2014) 1.

[51] D. C. Onwudiwe, P. A. Ajibade, Int. J. Mol. Sci. 12 (2011) 5538.

[52] J. Silva, A. S. Rodrigues, P. A.Videria, J. L Adilia, Inorg. Chim. Acta. 423 (2014) 156.

[53] A. M. Prodan, S. L. Iconaru, C. M. Chifinuc, C. Bleotu, J. Nanomat. 2013 (2013) 1.

[54] S. Gu Kwon, T. Hyeon, Acc. Chem. Res. 41 (2008) 1696.

[55] C. de Mello Doneg, P. Liljeroth, D. Vanmaekelbergh, Small 1 (2005) 1152.

[56] M. Dunne, O .Corrigan, Z .Ramtoola, Biomaterials 21 (2000) 1659.

[57] P. Mohanpuria, N.K.Rana, S.K.Yadav. J. Nanopart. Res.10 (2008) 507.

[58] S.P. Fricker, Dalton Transc. 43 (2007) 4903.

[59] J. WYoo, N. Doshi, S.Mitragotri, Adv. Drug Deliv. Rev. 63 (2011) 1247.

[60] I.P.Ferreira, G.M. de Lima, E.B. Paniago, J.A. Takahashi, Inorg. Chim. Acta 423 (2014) 44.

CHAPTER TWO

2.0 Literature Review

2.1. The chemistry of dithiocarbamates (DTCS).

Dithiocarbamate is a sulphur containing compound whose property owns to a certain degree the chemistry of the sulphur elements in its structural constituents. Among the most common sulphur containing ligands in literature in the past few years are xanthates, dithiocarbamates and other similar ligands which form four-membered chelate rings with sulphur as the sole donor atom such as dithiocarboxylates, dithiophosphates, and dithiophosphinates.

Sulphur is one of the most versatile elements in the main group chemistry. It exhibits a remarkable property in its capacity to bond to other elements especially those in the d-group. It has a peculiar donor property because of its low electronegativity. This decreases its ionic character and helps to reduce the strength of hydrogen bonding in its compounds, thereby making it stable with various types of bonds. [1].

Dithiocarbamates belong to the 1,1-dithiolate family, but occupy a special place with quite different properties from the other members of the same family with interesting organosulphur chemistry. Due to their water insoluble nature, they have become relevant to many applications; in inorganic analysis separation of different metal ions by high-performance liquid chromatography (HPLC) and capillary gas chromatography (GC) [2], and are useful as rubber vulcanization accelerators [3], fungicides and pesticides [4].

Many properties of this class of ligand have brought them to limelight in metal complex formation. For example, they are strong electron donors, as an extra π - electron flow from the N to S through a planer delocalised π - orbital system. The S atom can, thus, form multiple bonds due to the vacant $d\pi$ orbitals. They have a small bite angle (ligand–metal–ligand angle) which makes them flexible, pulling the ligands together to reduce activation energy and, thus, withstand various reaction conditions [5]. They can stabilize both high and low oxidation states in transition metals and delocalize positive charge from the metal towards the surface of the complex. They have, therefore, become a very important class of organometallic compounds, which also possess rich electrochemistry.

Dithiocabarmates are usually prepared when a primary or secondary amine reacts with carbon disulphide (CS_2) in the presence of a strong base such as sodium/potassium/ammonium hydroxide and at very low temperature [6] as represented in Scheme 2.1.

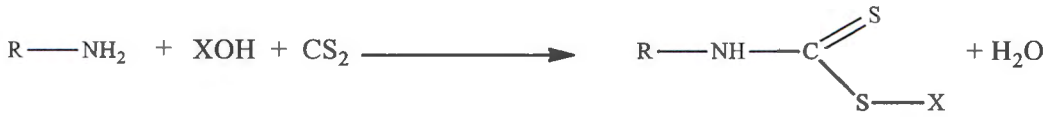

(a)

(b)

Scheme 2.1: Synthetic route for the formation of dithiocarbamate ligands from (a) primary amine and (b) secondary amine. X =Na/K/NH_4.

The process could also take place in the absence of a strong base, but with very low yield since in this case; the yield of dithiocarbamate corresponds to about half the amount of the consumed amine. Indeed, the base catalysed reaction makes an essential contribution to the dithiocarbamate formation rate [7].

To allow molecular interactions, the solvents involved have important roles to play during synthesis. Solvents such as methanol, ethanol, or tetrahydrofuran are mostly used and sodium, potassium or ammonium hydroxides typically serve as the base. Some reactions are carried out at very low temperature in ice, or at room temperature (under nitrogen atmosphere). Reaction rates are fast and in high yield. The sodium and potassium salts can be isolated as white solids, often with good solubility in water but rarely soluble in common organic solvents and are stable at room temperature. However, the ammonium salts may appear white or faint yellowish (creamy off-white), display much better solubility in organic solvents, and are unstable at ambient temperature. This might be due to the lability of the ammonium ion, thereby resulting into an S-S linked thiuram molecule.

The chemistry of transition metal-sulphur compounds has attracted much interest due to their importance in the field of metalloenzymes, material precursors, and catalysis [1]. Special interest in the study of metal dithiocarbamates was aroused because of the striking structural features presented by this class of compounds and also because of its diversified applications. Metal dithiocarbamate complexes can generally be prepared through simple ligand displacement reactions of the solution of the respective metal salt to an aqueous/ alcoholic solution of the dithiocarbamate salt. The oxidation state of the metal remains unchanged all through the reaction process [8].

Various bis(dithiocarbamate) complexes derived from primary amines, have been prepared and their chemistry investigated. Thus, different complexes including those derived from simple amines [9], amines with hydroxyl groups [10], benzyl [11], and from Schiff bases [12] exist in literature. In the context of this research objective, only the metal dithiocarbamates obtained from the nickel triad will be highlighted.

[a]

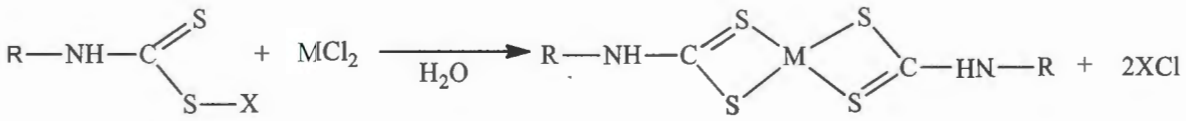

[b]

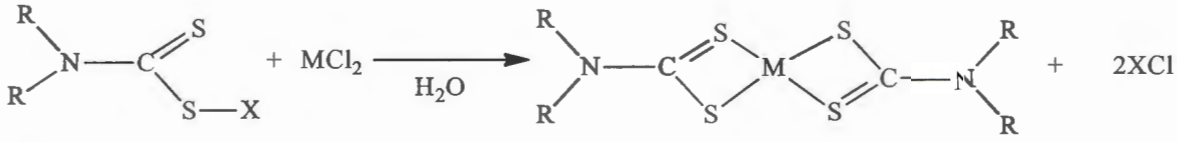

Scheme 2.2: Synthetic route of the metal complexes from dithiocarbamate obtained from (a) primary and (b) secondary amines (X = Na, K or NH_4).

2.2. Classification of dithiocarbamate based on the amine sources

Dithiocarbamates could be classified on the basis of the different types of amines used in the preparation. The type of amine used in the synthesis plays an important role in influencing the properties of the compound. At the early stage, the synthesis of dithiocarbamates suffered from many drawbacks such as long reaction time, harsh reaction conditions, the use of expensive and toxic reagents [13]. The disulphides were first prepared in 1850 when Debus reported the synthesis of dithiocarbamic acids [14]. Although incorrectly prepared at the initial stage, in 1907 Dele´pine reported the synthesis of a range of aliphatic dithiocarbamates and also the salts of di-iso-butyldithiocarbamate with different transition metals [15]. In recent years, significant progress has been made leading to several new, fast, convenient and safe methods with different substituent groups for the synthesis of these compounds.

The structure of dithiocarbamate presents an electronegative nitrogen atom directly bonded to the carbon disulphide, with a special ability to conform to variations of the substituents on the N atom. Hence, they could be grouped into various categories.

2.2.1 Dithiocarbamate complexes from primary amines

Dithiocarbamates prepared from primary amines are not as stable as those from the secondary amines; they can decompose to give the corresponding isothiocyanate. The poor stability of the former has been ascribed to the presence of the acidic proton on the nitrogen atom of the thioureide group [16]. The NH site stimulates the transfer of proton between ligands through the N-H···S hydrogen bonds. This instability can be improved upon by storing the ligands below room temperature, in a refrigerator and also by complexation with metal ions.

The presence of the acidic proton (NH) could be utilized for many beneficial purposes. For instance, the NH site promotes the lipophilicity of the compounds. This allows easy inhibition of bacteria cells, making them more active as anti - microbial agents than their N, N counterperts [17]. They are also capable of providing hydrogen bonding for basic anion N-H deprotonation, which can serve as the signal-output of certain anion-receptor interaction [17].

Kaul and Pandeya [18] reported several substituted aniline derived dithiocarbamate salts, by the addition of the aniline to an ice-cold mixture of carbon disulphide and aqueous ammonia. The ligand was obtained as white solids, which tend to decolourise and decompose within few days. Hence, they are best used as prepared.

Different group 10 dithiocarbamate complexes derived from primary amines have been reported. The synthesis of cyclohexylamine-*N*-dithiocarbamate, and some mixed-ligand complexes containing triphenylphosphine adducts of nickel(II), reported by Mamba *et al.,* [19], confirmed that both dithiocarbamate ligands and the metal complexes exhibit antibacterial activity against different bacterial species.

Yan *et al.,* [20] reported nickel(II) complexes of dithiocarbamate ligands derived from the ortho and para isomers of sulforhodamine B fluorophores, and compared their selectivity with nitrogen dioxide. Platinum complexes in different oxidation states, obtained using dithiocarbamate from different aniline derivatives, have been reported [21]. The cytotoxicity studies showed that the complexes bind and denature DNA at extremely low concentration. The synthesis and antitumour activity of palladium(II) complexes bearing bulky amine dithiocarbamate ligand from primary amine have been studies [22]. The complexes showed similar antitumor activity against HeLa cells when compared with the activity of the standard references, cisplatin, carboplatin and oxaliplatin.

2.2.2. Dithiocarbamate complexes from primary diammines

Dithiocarbamates from diammines can afford the formation of dinuclear metal complexes, M_2L_2. They have many benefits over mononuclear complexes such as coordinated reactiveness of substrates with the adjoining metal centres, improved catalysis via multi-electron processes, reduced oxidation or reduction potentials needed for multiple redox equivalents on the complex and the interactions between the metal centres are potentially beneficial to catalysis [23]. These ligands may be able to dictate a given metal-metal bond length with controlled electronic interactions between the metal centres. In addition, the number and positions of donor atoms can be controlled to achieve particular coordination geometry [24]. Spacer units such as benzene and methylene groups are necessary between coordinating diammine units in order to provide the required metal-metal bond length. The length and tunability of the spacer unit determines the intermetallic bond length and hence the level of interaction between the two metal centres.

The ligands can be prepared by the reaction of two equivalents of carbon disulphide and the diamine at a very low temperature. The dithiocarbamate compound involving 1, 2-diaminoethane was reported as early as 1872 [25], and was followed later by longer spacer unit of 1,6-diaminohexane in an exothermic reaction [26].

In the complexation, the metals could be the same to produce homodinuclear complexes or different to yield heterodinuclear complexes [27]. Davenport and Tilley utilized 1,8-naphthpyridine dithiocarbamate with late first-row transition metals in which the two metal centres are held apart in the range 2.7826(5)–3.2410(11) Å. Pseudo-octahedral metal centres with one-atom bridging ligands which gave "diamond-shaped" dinuclear complexes were obtained [23]. The *in situ* preparation of homodinuclear dithiocarbamates from 2-aminobenzoylhydrazide bis(dithiocarbamate) and first row transition metals have been reported by Nami *et al.,* [28]. The Ni(II) was octahedrally bonded to dithiocarbamate resulting in a complex that structurally resembles macromolecules and is also a non-electrolytes.

2.2.3. Dithiocarbamate complexes from secondary amines

Dithiocarbamate ligands derived from secondary amines are more stable than the compounds from primary amines. Consequently, more reports on metal complexes of dithiocarbamate derived from secondary amines abound in literature. The instability of dithiocarbamate from primary amines is mainly due to the absence of the acidic proton which, thus, hinders the easy elimination of sulphide (H_2S or CS_2) via heterolytic desulphurization at slightly elevated temperature [29]. Different

approaches have been reported for the synthesis of this class of dithiocarbamate. Due to the stability of the ligand, some reports involved the isolation of the ligand prior to complexation while others involved direct *in situ* complexation. For example, a one-pot three-component method of synthesis of *S*-trifluoromethyldithiocarbamates have been described, and a higher rotational barrier in the fluorinated dithiocarbamates than in the nonfluorinated analogue was reported [30]. *N*-butyl-*N*-phenyldithiocarbamate complexes of platinum and palladium were studied by Onwudiwe *et al.,*[31]. The ligands were first isolated as ammonium salts before complexation and the structure showed that the two complexes are centrosymmetrical with distorted square planar geometry.

N-(R) ethanolamine dithiocarbamate ligands and their Ni(II) and Pt(II) complexes were prepared by Ramos-Espinosa *et al.,* . The dithiocarbamate ligands were isolated and characterized; the complexation with the metal ions was confirmed to be bidentate and distorted square planar geometry around the matal atoms. Evaluation of the in vitro anticancer activity of the derivatives showed the Pt(II) complex had a better activity against the studied cell lines [32].

2.2. 4. Dithiocarbamate complexes from Schiff base compounds

Schiff base compounds are formed by the condensation of primary amine with an active carbonyl compound [33]. The presence of an azomethine group –RC=NR' is responsible for the lone pair of electron in their sp^2 hybridised orbital. They play a central role in coordination chemistry, and are capable of forming stable complexes with metal ions. They behave as a flexidentate ligand, coordinating through the O and N atoms. The chemistry of imino-phosphine compounds originated from the discovery of the ligand 2-(diphenylphosphino)benzaldehyde by Rauchfuss *et al.,* [34]. Since then, several works on Schiff base metal dithiocarbamates have been recorded [12].

The dithiocarbamate from Schiff base can be prepared by refluxing the primary amine with an aldehyde/ketone to afford the imine linkage (C=N) formation through condensation reaction. This is then followed by reaction with sodium borohydride ($NaBH_4$) at a very low temperature (in ice) to facilitate the imine linkage consumption by reduction process, triethylamine (Et_3N) is then added to pick up the proton so formed and to create the space for the carbon disulphide (CS_2) attachment on the N atom. The complexes are prepared by the *in-situ* addition of the aqueous solution of the metal salt to the prepared dithiocarbamate at room temperature [35].

The condensation reaction of benzaldehyde with 1, 6-hexamethylenediamine in ethanol, then the reduction of the Schiff base with $NaBH_4$ in methanol and subsequent formation of dinuclear diorganotin(IV) dithiocarbamate macrocycles was carried out by Reyes-Martínez *et al.,*[35].

Spectroscopic characterization showed that the ligands are coordinated to the metal atoms in the anisobidentate manner, both in solution and the solid state.

Transition metal complexes of symmetrical and asymmetrical Schiff bases have so far been shown to be important class of compounds, such that variation in the substituents can play further significant roles in the field of coordination, inorganic and bioinorganic chemistry as models for biological, analytical and industrial applications.

2.2.5 Mixed ligand dithiocarbamate complexes bearing compounds with P and N donor atoms

Compounds which contain P donor atom (e.g triphenylphosphine) and N donor atom (e.g bipyridine and phenanthroline) are able to form complexes with transition metals. They are π- deficient, thus are good π-acceptors, with their complexes stabilized by back bonding into the π* orbitals of the P or N ring. They are often incorporated into many bridging ligands as classical bidentate chelating heterocyclic ligands to impart significant effects on the properties of their metal complexes [36]. They can expand the coordination numbers of metal dithiocarbamate complexes in cases where the central metal atom is coordinatively unsaturated. On coordination with transition metals, they create dissymmetry in the metal orbitals, which then regulates the reactivity of complexes bearing these ligands [37]. They impart better physical properties on parent metal complexes and enhanced biological activities because of their resemblance with biomolecules such as amino acids, proteins, enzymes, and vitamins. Dithiocarbamates influence adducts formation through the mesomeric effect of their $-NR_2$ group [38].

Several dithiocarbamate adducts have been reported in literature. Gerald *et al.,* [39] studied the effect of changing the R groups on the sulphur-metal bonding in dithiocarbamate complexes and the subsequent effects on pyridine adduct formation with Ni(II) dithiocarbamate. The results showed that complex stability (base donor ability) increased with increase in the size of the R (CH_3- < C_2H5~- <n-C_3HT. Ni(II) dithiocarbamate complexes involving triphenylphosphine and isothiocynate have been reported.

The electronic spectral suggest square planar geometry. The presence of triphenylphosphine in the nickel complexes increased the C=N double bond character, while the additional coordination of the nitrogen donors decreases it.

Ekennia *et al.,*[40] described a series of pyridine adducts of *N*-methyl-*N*- phenyl dithiocarbamate which showed enhanced biological activities. Different Pd and Pt complexes containing both dithiocarbamate and α-diimine moieties have been reported [41]. Subsequently, their mixed ligand

complexes containing bipyridine and phenanthroline were synthesized which showed interesting biological properties. Ni(II) complexes of two unsymmetrical dithiocarbamate ligands, containing furfuryl and 2-thiophenylethyl substituents, and the reactivity of these complexes toward PPh_3 have been reported by Rani *et al.,* The nickel was shown to be in a distorted square planar arrangement with the NiS_2PN chromophore [42].

Keter *et al.,* [43] reported *N*-heterocyclic dithiocarbamate complexes of platinum(II) prepared from diazoles, which form stable platinum complexes. However, in the presence of a phosphine ancillary ligand, the obtained diphosphinoplatinum *N*-heterocycle-dithiocarbamate complexes transformed in solution into oxodithiocarbonate.

Some Ni(II) dithiocarbamate complexes with NiS_4, NiS_2PN and NiS_2PCl coordination spheres have been reported by Prakasam *et al.,* [44]. A distorted square planar geometry around the Ni(II) metal center was confirmed for all the complexes. Two heteroleptic palladium(II) dithiocarbamates complexes were studied by Khan *et al.,* [45]. The Pd exhibited pseudo square planner geometry mediated by SS chelate, P and Cl. Some heteroleptic-bis(diphenylphosphino)ferrocene-dithiocarbamate complexes of Ni, Pd and Pt have been described. The studies showed that the metal lies at the center of a distorted square planar environment and the distortion varies in the order Pd~Pt>Ni [46].

Different metal dithiocarbamates can, thus, be easily prepared from readily available starting materials. They are thermally stable with good decomposition patterns. The side-products are volatile and stable which is an added advantage as this makes their removal easy from the desired sulphide products [47]. They have continued to be widely explored as single source precursor (SSP) for the synthesis of metal sulphide nanoparticles.

2.3 Dithiocarbamate in Materials chemistry

Different substituents on the nitrogen atom of dithiocarbamates influence the properties of nanoparticles obtained from them as precursor compounds. Therefore, a useful tuning of the molecular precursors could be devised to synthesize nanoparticles with different morphologies and optical properties. The C−S bonds in dithiocarbamate complexes are relatively easy to break, which is important in the decomposition pathway for nanoparticles synthesis since volatility of the by-product is ensured [47]. The formation of undesired impurities (metal oxides) could be avoided (by carrying out the reaction under inert atmosphere) because the dithiocarbamate precursors yield chemically metal sulphide as residue [48]. Besides, ligands with high steric bulk can prevent nanoparticle agglomeration by providing physical barrier between nanoparticles, preventing inter-

particle interaction and this makes dithiocarbamate an effective precursor for metal sulphide nanoparticles. This is particularly useful because nanoscopic properties of nanoparticles are maximized when they are monodispersed [49].

Nanotechnology allows matter to be manoeuvred on an atomic, molecular, and supramolecular scale. It involves the design, preparation, characterization and application of different nanoscale materials in various areas to provide novel technological advances in many fields of study [50]. Nanomaterials find practical applications in a variety of areas such as, engineering, catalysis, environmental remediation, optical and electronic fields [51]. They also have great potentials in medicine, being able to convert poorly soluble, poorly absorbed and labile biologically active substance into promising deliverable substances [52]. Various characteristics and brief applications of nanostructured materials are presented in Table 2.1.

2.4 Classification of nanomaterials

Nanomaterials are broadly classified into four, based on the number of dimensions which do not confine to the nanoscale range (<100 nm). We have several categories.

(a) Zero-dimensional (0-D) nanomaterials: These are materials in which all the dimensions are measured within the nanoscale. That is, no dimension is larger than 100 nm. Examples are nanoparticles and quantum dots. A quantum dot is a semiconductor nanostructure which can restrict the motion of conduction band electrons, valence band holes, or excitons in all three spatial directions [53]. Each quantum dot acts as a quantum well, where electron-hole activity occurs, and all of the dots in the grid are close enough to each other to ensure interactions. Spacing and size of the dots can be varied in order to vary the band gap, which determines the wavelength of light it emits, with the size, energy and wavelength (colour) inter-dependent, the optical properties of the particles can be tuned depending on its size to match the application .

(b) One dimensional (1-D) nanomaterials: These are materials in which only one of the dimensions is outside the nanoscale. They are restricted in only one dimension, resulting in a quantum well or plane where the magnitudes of length and width are much greater than the thickness that is only a few nanometers in size. This confers needle like-shape on the materials. It utilizes the large surface area from the nanoparticles together with the tunability of their optical properties for the various successful applications examples are nanotubes, nanorods, and nanowires [54].

(c) Two-dimensional (2-D) nanomaterials: In this type of materials, two of the dimensions do not confine to the nanoscale and they exhibit plate-like shapes as metallic or as semiconductors. Examples include nanofilms, nanolayers, and nanocoatings [55].

(d) Three-dimensional (3-D) nanomaterials. They are bulk materials in which none of the dimension is confined to the nanoscale. Thus, the three dimensions are arbitrarily above 100 nm. They possess a nanocrystalline structure where they can be composed of a multiple arrangement of nanosize crystals in different orientations. They can also contain dispersions of nanoparticles, bundles of nanowires, and nanotubes as well as multinanolayers. Their properties are intermediate between bulk semiconductors and discrete molecules as they behave as single objects with bound, discrete electronic states.

Table 2.1 Various characteristics and brief applications of nanostructured [56].

Types of Nanosystems	Size (nm)	Characteristics	Applications
Micelles	10–100	Block amphiphilic copolymer micelles, high drug entrapment, payload, biostability	Long circulatory, target specific active and passive drug delivery, diagnostic value
Dendrimer	<10	Highly branched, nearly monodisperse polymer system produced by controlled polymerization; three main parts core, branch and surface	Long circulatory, controlleddelivery of bioactives, targeted delivery of bioactives to macrophages, liver targeting
Liposome	50–100	they are completely biodegradable, compatible, non-toxic and non immunogenic, versatile, good entrapment efficiency, offer easy.	Long circulatory, offer passive and active delivery of gene, protein, peptide.
Compact polymeric (nanospheres, nanocapsules	10–1000	Biodegradable, biocompatible, offer complete drug protection. Stealth and surface modified nanoparticles	Excellent carrier for controlled and sustained delivery of drugs used for active and passive delivery of bioactives.
Fullerenes (Carbon nanotubes)	0.5–3, 20–1000	A rigid icosahedron with 60 carbon atoms. In its structure, single bounds form pentagons and double bounds form Hexagons, unique optic, electric and magnetic properties (such as superconductivity	medical diagnosis and imaging, Functionalization enhanced solubility, penetration to cell cytoplasm and to nucleus, as carrier for gene delivery, peptide delivery
Nanocrystals Quantum dots	2–9.5	Semi conducting material synthesized with II-VI and III-V column element; Size between 10 and 100 Å; Bright fluorescence, narrow emission, Broad UV excitation and high photo stability	imaging, detection and targeting, are luminescent semiconductor crystal
Metallic nanoparticles	<100	Gold and silver colloids, verysmall size resulting in highsurface area available for functionalization and stable.	Drug and gene delivery, highly sensitive diagnostic assays, thermal ablation and radiotherapy enhancement.

2.5 Synthesis of nanomaterials

The synthesis of nanomaterials may either be from the break-down of larger molecules 'top-down' (physical destruction of larger material), or step-wise build up from atoms 'bottom-up' (to nucleate and grow particles from fine molecular distributions in liquid or vapour phase). The 'top-down' approach is based mainly on the milling of larger materials including film deposition and growth, lithographic, laser beam processing and mechanical (grinding and polishing) techniques. It is vastly used in semiconductor technology, as there are very few applications of nanomaterials prepared by these methods because size and morphology cannot be easily controlled and results are usually non-reproducible [57].

The 'bottom-up' method includes: electrochemical, sonolysis, thermal decomposition, colloidal aggregation, co-precipitation and laser ablation. It involves the use of chemical, electrical or physical forces to build the nanomaterial atom by atom, molecule by molecule, from their constituent materials [58]. Processing steps can be scaled up to synthesize reproducible monodispersed nanomaterials.

In all the methods, monodispersity is preferred to polydispersity where majority of particles are within 5% of the mean particles size [59]. Within this size distribution, they can behave in uniform way to amplify the effectiveness of the nanomaterials properties. This can be achieved if the van der Waals interactions between particles are overcome either electrostatically (charge the surface leading to Columbic repulsion between particles) or sterically (attach sterically bulky ligands to the surface, typically macromolecules). Nucleation and growth govern nanoparticle morphology and size, a brief single nucleation period is necessary as different size nuclei growing at the same rate will lead to polydispersed products just as same size nuclei growing at different rate lead to broadening of the particle size distribution [60].

Nucleation involves several processes; the precursor monomer can either move to the interfacial layer about the particles or add to the surface. The monomer in the particle could also redissolve back into the solution. The process that is favourable depends on the radius (r) of the particle as presented in the Gibbs free energy (ΔG). The energy difference, ΔG, must be negative for the growth of the particle, and a supersaturated concentration of the precursor in solution must be reached. For ΔG to be negative, $r >> r^*$ (r= radius of particle and r^* = critical radius). However, if it is less, the gamma term of equation (1) prevails, the ΔG becomes positive and particle formation will not be favoured.

$\Delta G = -4/3\pi r^3 \Delta G_v + 4\pi r^2 \gamma$..... (1)

This equation assumes a spherical nanoparticle, where r is the particle radius, ΔGv is the change in energy per unit volume (of solvent molecules) and γ is the surface energy per unit area [60].

Nucleation can only occur when monomer units are able to assemble into a lattice (a favourable process), after all interactions with surrounding solvent molecules have been broken. If formation of the lattice is able to overcome the removal of coordinated solvent molecules and the formation of dangling bonds on the surface of the new particle, then it is a favourable process and there will be nucleation. Otherwise, the monomer units will redissolve back into the solution (an unfavourable process).

LaMer proposed a model for the formation of nanoparticles when he described the nucleation and growth of sulphur colloids [61]. The model has three main phases:

Phase 1- monomer generation as the precursor monomer increases until critical supersaturation is reached.

Phase 2 - rapid nucleation of the particles occur. Nucleation has to be a single event so as to prevent nanoparticle growth at different rates. As nanoparticles grow, monomer concentration decreases since it is consumed by nucleation and falls below the critical nucleation level. The remaining monomers enter into the next phase.

Phase 3- the particles continue to grow by diffusion onto the surface of others. The criteria for monodispersity is instantaneous particle growth called 'burst nucleation', this is the general principle of the LaMer model [62].

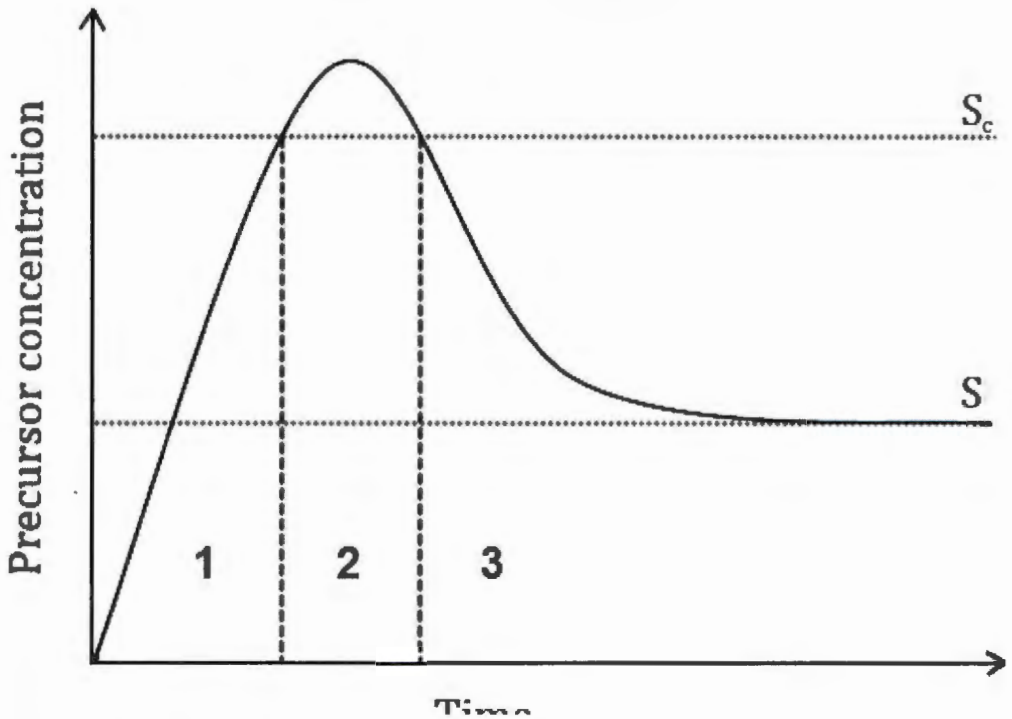

Figure 2.2: The LaMer plot showing the three stages of particle formation [60]

As particles grow, at equillibrium concentration, Ostwald ripening takes place. This is when larger particles grow faster than smaller ones which dissolve into the system. The process reduces the number of particles in the system and can also decrease polydispersity of a sample. It is a thermodynamically more feasible process for small particles to lose monomer and for large particles to gain, driven by the favourable reduction of the percentage of surface particles with dangling bonds. Therefore, this increases the monomer coordination and reduces particle surface energy [63].

2.5.1. Methods of nanomaterials synthesis

There are diverse methods for the synthesis of nanoparticles. Generally, the process could either proceed by the precipitation of the nanoparticles from solution (e.g reduction of a metal salt) or the decomposition of precursors using heat or other process.

2.5.1.1. Precipitation methods

This involves controlled formation of precipitates, where nucleation and growth determine the size of the particle produced. The reaction is carried out in the presence of stabilizers to prevent agglomeration and growth [64]. Other factors that control the particle size are precursor type, concentration, reaction temperature, pH of the solution and diffusion and sorption properties of the precursors. The right choice of solvent (effective for low solubility of nanoparticles) and passivating

agent makes the method an effective one. This method was employed by Faraday in his early experiments on gold colloids where he used aqueous solutions of auric chloride reduced with phosphorus to yield gold nanoparticles [65]. In that reaction, the formation of a solid interface drives the reaction towards the production of the nanocrystals [66].

2.5.1.2. Thermal Decomposition Methods

This method could be carried out in the solid, liquid and gas phases. The solid state synthesis is a solventless route which involves the use of a Teflon lined autoclave where the precursor solid is heated up in a vessel [67]. No solvent is involved here, so size control is difficult. This problem could be solved by the incorporation of capping/ stabilizing agent into the precursor complex [68]. Chemical vapour deposition (CVD) represents the gas or vapour phase synthesis especially for thin films. It involves the vaporization of the precursor at reduced pressure and when brought in contact with a heated substrate, it decomposes to form thin film or ultra-fine particles of the precursor. This method gives rise to large particle size distributions due to the absence of capping/stabilizing agent. It was first utilized in the decomposition of $Ni(CO)_4$ for the formation of pure nickel metal [69].

2.5.1.3. Solvothermal Synthesis

It is the liquid phase thermal decomposition method. A solution based thermal synthesis that involves the decomposition of the molecular precursor in a high boiling solvent at high temperature. The solvent serves a dual function, as a capping agent in order to control particle size and as a heat sink to protect the produced nanoparticles from oxidation. It could follow the 'heat up' or the 'hot injection' route [70].

2.5.1.4. Single source precursor method (SSP)

The single source precursor (SSP) approach implies that all the constituent elements required in the nanomaterial have been incorporated into one compound. The compound is then utilized as a precursor for the desired product. It is mostly subjected to thermal decomposition in the presence of a coordinating solvent which are usually long chain, high boiling point amine such as hexadecylamine (HDA), octadecylamine (ODA) and oleylamine (OLA). This route is one of the most commonly used methods as it affords stable monodispersed colloidal quantum dots whose size distribution could be approximately ~5%. Compared to other routes which require exact control over stoichiometry, the SSP routes offers mildness, safety and the fabrication procedure is very simplified [72]. Typical of solvothermal approach, formation of nanoparticle is consistent with the

LaMer model for colloid formation and Ostwald ripening for growth of the nuclei [73]. This method has been used for the synthesis of many transition metal sulphide nanocrystals.

In order to obtain a metal sulphide, the single-source precursors must be metal complexes made up of sulphur-containing organic ligands such as alkyldithiocarbamates or mercaptobenzothiazol. Different metal sulphides and various phases have been prepared using the single source precursors (SSPs) synthesis route. Among the group 10 metal complexes, nickel sulphide has been the most widely explored. It is more economical and easy to synthesize. Ludolph *et al.,* prepared good quality, highly mono-dispersedtrioctylphosphineoxide (TOPO) capped NiS quantum dots from stable, non-air sensitive single molecule precursors of Ni(II) complex [74].

Nickel(II) complexes of piperidine and tetrahydroquinoline have been utilized as single source precursors which gave nickel sulphide nanoparticles of different phases via solvothermal decomposition in oleylamine (OLA), dodecylamine (DDA) and hexadecylamine (HDA) at different temperatures. The results showed that Ni_3S_4 nanoparticles prepared at 230 °C using DDA were ferromagnetic, while the rhombohedral Ni_3S_2 obtained at 230 °C using HDA displayed paramagnetic property [75].

Spherically shaped nickel sulphide nanoparticles have been synthesized using bis(*N*-(pyrrol-2-ylmethyl)-*N*-furfuryldithiocarbamato-S,S')nickel(II) as single source precursor in ethylenediamine [76]. X-ray diffraction analysis confirmed the formation of cubic-NiS_2, cubic-Ni_3S_4 and Rhombohedral-Ni_3S_2) phases.

Abdelhady utilized nickel(II) complexes of 1,1,5,5-tetra-iso-propyl-2-thiobiuret as single-source precursor for the synthesis of nickel sulphide nanoparticles by thermolysis in hot solution of different solvents used as capping agents including oleylamine, octadecene, and dodecanethiol. The precursor compound gave mostly Ni_3S_4 in different morphologies (wires, rods, spheres, and triangles). However, injection of the oleylamine solution of the precursor compound into hot octadecene afforded only nanowires of NiS [77]. Beal *et al.,* reported that metal polysulphide complexes are viable single-source precursors for a range of transition metal sulphide nanocrystals. Different metal polysulphide complexes were utilized as single-source precursors for the synthesis of metal sulphide nanocrystals, and all samples demonstrated high degree of crystallinity and excellent phase-purity [78]. The solvothermal conversion of some Ni(II) complexes as precursors in oleylamine at 200°C was studied by Christine Buchmaier *et al.,* X-ray diffraction measurements confirmed that hexagonal NiS and cubic Ni_3S_4 as secondary phase were produced [79].

Platinum and palladium dithiocarbamate and diselenoimidodiphosphinato complexes have been synthesized and used as single source precursors for the deposition of platinum and palladium

chalcogenide thin film. The corresponding dithiocarbamate complexes gave PdS, while only Pt films were obtained from the platinum analogue [80]. Bis(n-hexyl(methyl)dithiocarbamato)platinum(II) and bis(n-hexyl(methyl)dithiocarbamato) palladium(II) have been utilized to grow nanocrystals of PtS or PdS by thermolysis in trioctylphosphine oxide (TOPO) [80]. The tetragonal phases of both PtS and PdS were obtained and the TEM image showed well defined, close to monodispersed particles.

The synthesis of bimetallic Pt-Pd nanoparticles by reduction through a solvothermal method was reported by Yunqi Li *et al.,* [81]. Their results showed the formation of homogeneous Pt-Pd nanoparticles which exhibited an enhanced electrocatalytic activity and stability compared with commercial Pt black.

Regardless of the achievements of metal dithiocarbamates in materials chemistry and particularly in metal sulphides nanoparticles synthesis; and knowing the high level of ligands control on the reactivity and properties of transition metal ions, the exploration of other relevant nitrogenous molecules as efficient synthetic methods cannot be over emphasized. The ligands provide a platform for functional group transformation to give interesting physiological, catalysis, biological and other important activities, and also to provide a lot of improvements needed for routine use in all these relevant applications.

2.6. Characterization of Nanoparticles

To fully understand the potential of the synthesized nanoparticles, a broad and clear insight of their properties is required for the correct application, hence their characterization using a variety of different techniques. The following characterization techniques are employed for synthesized nanoparticles.

2.6.1. UV-visible spectroscopy

This is a technique used to quantify the extinction, which is the sum of absorbed and scattered light by a sample. The sample is placed between a light source and a photodetector, and the intensity of a beam of UV/visible light is measured before and after passing through the sample. Since nanoparticles have optical properties that are sensitive to size, shape, concentration, agglomeration state, and refractive index near the nanoparticle surface, the UV/vis spectroscopy is a valuable tool for characterizing nanomaterials [82].

2.6.2. Transmission electron microscopy (TEM)

This is a method that directly measures the particle size, grain size, size distribution, and morphology of nanoparticles by imaging the transmission of a beam of electrons through a sample. Nanoparticles are dried on a copper grid that is coated with a thin layer of carbon and it uses electrons to illuminate the sample for imaging. Variations in the transmitted beam provide imaging contrast depending on the thickness and material of the sample [83].

2.6.3. Scanning electron microscopy (SEM)

The interactions between the beam electrons and sample atoms are similar to those described for a transmission electron microscope, but the column is shorter and specimen chamber is larger. Specimen preparation is simplified as it may not need to be thin since it is not necessary to penetrate the specimen. The signal varies with the topography of the sample surface [84].

2.6.4. Fourier transform infrared (FTIR) spectroscopy

FTIR helps to determine the conformational and structural changes of the coordinating self-assembled functional groups on the nanoparticles surface and the surrounding environment [85]. It is a powerful tool used to determine the nature of the chemical surface species as well as the reactive sites and also to determine the purity of the prepared nanoparticles. Since the surface charge of the nanoparticle can change due to the adsorption of ligands and functional groups, FTIR spectroscopy is an analytical tool that can be used effectively for the probing of a functionalized nanoparticle surface, and its interface with the surrounding medium [85].

2.6.5. Dynamic light scattering (DLS)

DLS measures light scattered from a laser that passes through a colloidal solution, the scattered light intensity is measured as a function of time and provides information on the size of the particle in solution. Its analysis is based on Brownian motion where larger particles move more slowly and scatter more light than smaller particles. It gives a complementary measurement to TEM as it provides information on the aggregation state of nanoparticle solutions [86].

2.6.6. Powder X-ray diffraction (XRD)

XRD is an analytical technique used for phase identification of a crystalline material and gives information on unit cell dimensions. The X-ray source provides energy with the correct frequency for inter-atomic-scale diffraction. By satisfying Bragg's Law ($n\lambda=2d \sin\theta$), which is used to explain

the interference pattern of X-rays scattered by crystals, the incident rays interact with the sample to produce the diffracted ray. This law relates the wavelength of electromagnetic radiation to the diffraction angle and the lattice spacing in a crystalline sample. Random orientation of the powdered material is attained as the sample is scanned through a range of 2θ angles in all possible diffraction directions of the lattice. The diffraction peaks are converted to d-spacings which are then compared to that of standard reference patterns for the identification of the unknown compound, because each mineral has a unique set of d-spacings [87].

REFERENCES

[1] S.C. Bajia, A. Mishra, J. Coord. Chem. 64 (2011) 2727.

[2] G. Schwedt, Chromatographica, 11 (1978) 145

[3] D. Ondrušová, E. Jóna, P. Šimon, J. Therm. Anal. Calorim. 67 (2002) 147.

[4] G.W.Ware, D. M. Whitcare, The Pesticide Book. 6th Edition. Meister P Information Resources, Willoughby, OH (2004).

[5] W.J. Van Zeist, R. Visser, F. Matthias Bickelhaupt, Chem. - A Eur. J. 15 (2009) 6112.

[6] R.T. Li, P.Y. Ding, M. Han, M.S. Cai, Synth. Commun. 28 (1998) 295.

[7] C.A. Tsipis, I.J. Meleziadis, G.A. Katsoulos, D.P. Kessissoglou, Preparation of the Complexes, 90 (1984) 1984.

[8] G. Hogarth, 1978-2003, Prog. Inorg. Chem. 53 (2005) 1978.

[9] C.S. Chamberlain, R.S. Drago, Inorg. Chim. Acta 32(1979) 75.

[10] I.P. Ferreira, G.M.D. Lima, E.B. Paniago, J.A. Takahashi, K. Krambrock, C.B. Pinheiro, J.L. Wardell, L.C. Visentin, J. Mol. Struct. 1048 (2013) 357.

[11] P.C. Christidis, Acta Crystallogr., Sect. C, 42 (1986) 781.

[12] G.E. Manoussakis, C.A. Bolos, Inorg. Chim. Acta, 108 (1985) 215.

[13] R. Ghorbani-Vaghei, M. Amiri, H. Veisi, Bull. Korean Chem. Soc. (2012) 4047

[14] H. Debus, Ann. Chem. (Liebigs), 73 (1850) 26.

[15] M. Dele´pine, Compt. Rend. Chim, 144 (1907) 1125.

[16] D.C. Onwudiwe, J.N.Mugo, H. Madalina, H. Eric, J. Sulfur Chem. 36 (2015) 36.

[17] K.C. Chang, S.S. Sun, M.O. Odago, A.J. Lees, Coord. Chem. Rev. 284 (2015) 111.

[18] B.B. Kaul, K.B. Pandeya, J. Inorg. Nucl. Chem., 40 (1978) 229.

[19] S.M. Mamba, A.K. Mishra, B.B. Mamba, P.B. Njobeh, M.F. Dutton, E. Fosso-Kankeu, Spectrochim. Acta - Part A Mol. Biomol. Spectrosc. 77 (2010) 579.

[20] Y.Yan, S. Krishnakumar, H.Yu, S. Ramishetti, L.Wen Deng, S. Wang, L. Huang, D. Huang. J. Am. Chem. Soc. 135(2013) 5312.

[21] A.S. Abu-Surrah, K.A. Abu Safieh, I.M. Ahmad, M.Y. Abdalla, M.T. Ayoub, A.K. Qaroush, A.M. Abu-Mahtheieh, Eur. J. Med. Chem. 45 (2010) 471.

[22] A.M. Alafeefy, A. A. Kadi, O. A. Al-Deeb, K.E.H. El-Tahir, N. A. Al-jaber, Eur. J. Med. Chem. 45 (2010) 4947.

[23] T.C. Davenport, T.D. Tilley, Dalt. Trans. 44 (2015) 12244.

[24] D.G. McCollum, B. Bosnich, Inorg. Chim. Acta. 270 (1998) 13.

[25] D.M. Hoffman, D. Lappas, Polyhedron 15 (2000) 1539.

[26] J.W. Beattie, Synthesis Of Dinucleating Ligands And Their Dinuclear Metal Complxes : applications In Sensing And Small Molecule Activation, (2016).

[27] A.Z. Halimehjani, S. Torabi, V. Amani, B. Notash, M.R. Saidi, Polyhedron. 102 (2015) 643

[28] S.A.A. Nami, A. Husain, I. Ullah, Spectrochim. Acta - Part A Mol. Biomol. Spectrosc. 118 (2014) 380.

[29] K. Ghosh, V. Mohan, P. Kumar, S.W. Ng, E.R.T. Tiekink, Inorganica Chim. Acta. 416 (2014) 76.

[30] N. Manav, A.K. Mishra, N.K. Kaushik, Spectrochim. Acta - Part A Mol. Biomol. Spectrosc. 60 (2004) 3087.

[31] D.C. Onwudiwe, A.C. Ekennia, B.M.S. Mogwase, O.O. Olubiyi, E. Hosten, Inorg. Chim. Acta. 450 (2016) 69.

[32] Á. Ramos-Espinosa, H. Valdés, M. Teresa Ramírez-Apan, S. Hernández-Ortega, B. Adriana Aguilar-Castillo, R. Reyes-Martínez, J.M. Germán-Acacio, D. Morales-Morales, Inorg. Chim. Acta. 466 (2017) 584.

[33] W.M. Motswainyana, M.O. Onani, A.M. Madiehe, M. Saibu, N. Thovhogi, R.A. Lalancette, Phosphorus, Sulfur Silicon Relat. Elem. 188 (2013) 778.

[33] H. Mansouri-Torshizi, M. Saeidifar, F. Khosravi, A. Divsalar, A.A. Saboury, F. Hassani, Bioinorg. Chem. Appl. 2011 (2011).

[34] J.E. Hoots, T. Rauchfuss, D.A. Wrobleski, Inorg. Synth. 21 (1982) 175.

[35] R. Reyes-Martínez, R. Mejia-Huicochea, J. A. Guerrero-Alvarez, H. Höpfl, H. Tlahuext ARKIVOC 2008 (v) 19.

[36] W.M.Motswainyanaa,M.O.Onania, M.Madieheb, M. Saibub, N. Thovhogib, R. A.Lalancettec, J. Inorg. Biochem.129 (2013) 112.

[37] S. Kanchi, P. Singh, K. Bisetty, Arab. J. Chem. 7 (2014) 11.

[38] A.C. Ekennia, D.C. Onwudiwe, C. Ume, E.E. Ebenso, Bioinorg. Chem. Appl. 2015 (2015) 1.

[39] G. S.Vigees, L.W.J. Charles, Inorg, nucL Chem. 34 (1972) 3936.

[40] A.C. Ekennia, D.C. Onwudiwe, C. Ume, E.E. Ebenso, Bioinorg. Chem. Appl. 2015 (2015) 1.

[41] N. Aryanpour, H. Mansouri-Torshizi, M. Nakhjavan, F. H. Shirazic. Iran J Pharm Res. 11 (2012) 689.

[42] P. J. Rani, S. Thirumaran, S. Ciattini, J. Phosphorus, Sulfur, Silicon and the Related Elements, 188 (2013) 778.

[43] F.K. Keter, I.A. Guzei, J. Darkwa, Inorg. Chem. Commun. 27 (2013) 60.

[44] A.P. Balasubramaniam, A. Peuronen, M. Lahtinen, M. Manickavachagam, E. Kolehmainen, E. Haapaniemi, M. Sillanp Polyhedron. 123 (2017) 453.

[45] S.Z. Khan, Zia-ur-Rehman, M.K. Amir, I. Ullah, M.S. Akhter, F. Bélanger-Gariepy, Heteroleptic J. Mol. Struct. 1156 (2018) 564.

[46] S.K. Singh, R. Chauhan, K. Diwan, M.G.B. Drew, L. Bahadur, N. Singh, J. Organomet. Chem. 745–746 (2013) 190.

[47] D.C. Onwudiwe, E.C. Hosten, J. Mol. Struct. 1152 (2018) 409.

[48] M.S.G. Desechos, L. Counts, L. Msg, M.S.G. Ii, L. Cps, M.S.G. Cobaltos, M.-C.N. De, M.S.G. Nickel, M.S.G.D. De Extralum, C. Msg, M.S.G. B-, D. De, M.-C. Diat, M.S.G. Coo, C. Diatomita, N. Diatomita, 2-Theta - Scale, 1467 (2000) 95520.

[49] L. Counts, 2-Theta - Scale, 0566 (2000) 2000.

[50] A.R. Roffey, Dithiocarbamate Complexes as Single Source Precursors to Metal Sulfide Nanoparticles for Applications in Catalysis, PhD Thesis, University College London (2012) 178.

[51] K. Miyazaki, N. Islam, Technovation. 27 (2007) 661–675.

[52] H. Hazards, C. Compounds, W.A. Report, Nanomaterials Commission for the Investigation of Health Hazards of Chemical Compounds in the Work Area Report, (2012).

[53] J.N. Tiwari, R.N. Tiwari, K.S. Kim, Prog. Mater. Sci. 57 (2012) 724.

[54] J. Lu, X. Zeng, H. Liu, W. Zhang, Y. Zhang, Appl. Surf. Sci. 258 (2012) 8538.

[55] R. Zsigmondy, Z. Physic. Chem. 56 (1906) 65.

[56] A. Hett, Nanotechnology: small matters, many unknown. (2004).

[57] S. Hasan, S. Hasan, Res. J. Recent Sci. Res. J. Recent. Sci. Uttar Pradesh (Lucknow Campus). 4 (2016) 3.

[58] D. V. Talapin, E. V. Shevchenko, Chem. Rev. 116 (2016) 10343.

[59] A. Luísa, P. Cartaxo, Nanoparticles types and properties – understanding these promising devices in the biomedical area, (2016) 1.

[60] V.K.LaMer, M.D. Barnes, J. Colloid Sci. 1 (1946) 71.

[61] E. E.Finneyan R.G.Finke, J.Colloid Interface Sci., 317 (2008) 351.

[62] E.C. Vreeland, J. Watt, G.B. Schober, B.G. Hance, M.J. Austin, A.D. Price, B.D. Fellows, T.C. Monson, N.S. Hudak, L. Maldonado-Camargo, A.C. Bohorquez, C. Rinaldi, D.L. Huber, Chem. Mater. 27 (2015) 6059.

[63] S. G.Kwon ,T. Hyeon, Small, 7 (2011) 2685.

[64] H. Method, Chapter 2 Hydrothermal Method, (1893) 18.

[65] Y. Chen, X. Gu, C.-G. Nie, Z.-Y. Jiang, Z.-X. Xie, C.-J. Lin, Chem. Commun. 1 (2005).

[66] A. Islam, M. Anwarul Kabir Bhuiya, M. Saidul Islam, J. Energy Environ. 1 (2014) 107.

[67] J. J.Cryst.Growth Des. 9 (2009) 353.

[68] B. Yuan, W. Luan, Functional Materials Letters 7 (2014) 6.

[69] H. Wang, J.-R. Zhang, X.-N. Zhao, S. Xu, and J.-J. Zhu. , Materials Letters. 55(2002) 253.

[70] C.B.Murra, C.R.Kagan M.G.Bawendi Annu Rev Mater Sci. 30 (2000) 545.

[71] G. Nichols, S. Byard, M.J. Bloxham, J. Botterill, N.J. Dawson, A. Dennis, V. Diart, N.CNorth, J.D. Sherwood, J. Pharm. Sci. 91 (2002) 2103.

[72] M. Azad Malik, N. Revaprasadu, P. O'Brien, Chem. Mater., 2001, 13 (3) 913.

[73] Y.C Zhang, G.Y Wang, X.Y Hu, J Alloys Compds 437 (2007) 47.

[74] B. Ludolph, M.A. Malik, P. O'Brien, N. Revaprasadu, Chem. Commun. 3 (1998)1849.

[75] C. Gervas, S. Mlowe, M.P. Akerman, I. Ezekiel, T. Moyo, N. Revaprasadu, Polyhedron. 122 (2017)16.

[76] E. Sathiyaraj, G. Gurumoorthy, S. Thirumaran, New J. Chem. 39 (2015) 5336.

[77] A.L. Abdelhady, M.A. Malik, P. O'Brien, F. Tuna, J. Phys. Chem. C. 116 (2012) 2253.

[78] J.H.L. Beal, P.G. Etchegoin, R.D. Tilley, J. Phys. Chem. C. 114 (2010) 3817.

[79] C. Buchmaier, M. Glänzer, A. Torvisco, P. Poelt, K. Wewerka, B. Kunert, K. Gatterer, G. Trimmel, T. Rath, J. Mater. Sci. 52 (2017) 10898.

[80] P.L. Musetha, N. Revaprasadu, G.A. Kolawole, R.V.S.R. Pullabhotla, K. Ramasamy, P. O'Brien, 519 (2010) 197.

[81] Y. Li, S. Ishihara,B.PrasadBastakoti,C. Li, V. Malgras,Y.Yamauchi, Electrochim Acta. 183 (2015) 119.

[82] B. Faust, Mod. Chem. Tech. 3 (1997) 92.

[83] N. Sonker, J. Bajpai, A.K. Bajpai, A. Mishra, 14 (2018) 1.

[84] P.B. Taunk, R. Das, D.P. Bisen, R. kumar Tamrakar, J. Radiat. Res. Appl. Sci. 8 (2015) 433.

[85] M. Jackson, H.H. Mantsch, Crit. Rev. Biochem. Mol. Biol. 30 (1995) 95.

[86] D.L. Scattering, E. Equation, P. Size, P. Motion, Dynamic Light Scattering, (2018) 1.

[87] P.S. Nayak, B.K. Singh, Bull. Mater. Sci. 30 (2007) 235.

[88] Z.J. Wang, Y. Xie, C.J. Liu, J. Phys. Chem. C. 112 (2008) 19818.

[89] C. Wei, Q. Ru, X. Kang, H. Hou, C. Cheng, D. Zhang, Appl. Surf. Sci. 435 (2018) 993.

[90] Z. Haghighi Pak, H. Abbaspour, N. Karimi, A. Fattahi, Appl. Sci. 6 (2016) 69.

[91] F. Fievet, J.P. Lagier and M. Figlarz, 14 (1989) 29.

CHAPTER THREE

3.0 Synthesis and characterization of Ni(II), Pd(II) and Pt(II) dithiocarbamate complexes

Chapter Summary

This chapter presents the synthesis of dithiocarbamate ligands and their Ni(II), Pd(II) and Pt(II) complexes; and it has been divided into four sections:

(i) The synthesis of dithiocarbamate ligands from primary amines and their Ni(II), Pt(II) and Pd(II) complexes,

(ii) The synthesis of dithiocarbamate ligands from secondary amines.and their Ni(II), Pt(II) and Pd(II) complexes,

(iii) The synthesis of dithiocarbamate ligands from secondary amines derived from Schiff base condensation reactions, their Ni(II), Pt(II) and Pd(II) complexes, and

(iv) The synthesis of adducts/mixed ligand complexes from dithiocarbamate prepared from both primary and secondary amines.

3.1. Materials and instrumentation

All chemicals were used as obtained without further purification. The following reagents were obtained from Sigma Aldrich Co: aniline, *p*-methylaniline, *p*-ethylaniline, benzylaniline, hexamethelenediamine, 2-(methylamino)ethanol, 2-(ethylamino)ethanol, and benzaldehyde. The solvents were procured from Merck and they include: methanol, ethanol, tetrahydrofuran, chloroform, dichloromethane, acetonitrile, toluene, and diethyl ether. Sodium hydroxide and ammonia solution were purchased from BDH. The metal salts, nickel chloride hexahydrate, nickel acetate, sodium tetrachloropalladate(II), and potassium tetrachloroplatinate(II) were purchased from Sigma Aldrich chemicals.

3.1.1 Physical Measurements

Elemental analyses were carried out by Elementar, Vario EL Cube, set up for CHNS analysis. FTIR analyses were obtained using Bruker alpha-P FTIR spectrophotometer between 4000–400 cm^{-1}. NMR spectra analysis was conducted using 600 MHz Bruker Avance III NMR spectrophotometer. Thermogravimetric analysis (TGA) was carried out using SDTQ 600 Thermal analyser. UV/visible

spectra were measured using a Perkin-Elmer λ20 UV-vis spectrophotometer. Melting point was recorded using the Stuart melting point SMP10.

3.1.2. X-ray crystallography

The single crystal suitable for X-ray diffraction was obtained for some of the compounds using the slow evaporation method in different solvent systems. The X-ray diffraction was performed at 200 K using a Bruker Kappa Apex II diffractometer with graphite monochromated Mo Ka radiation (λ = 0.71073 Å). APEXII was used for data collection and SAINT for cell refinement and data reduction [1]. The structures were solved with SHELXT-2014 [2] and refined by least-squares procedures using SHELXL- 2017 [3] with SHELXLE [4] as a graphical interface. All non hydrogen atoms were refined anisotropically. Carbon and oxygen bound H atoms were placed in calculated positions and were included in the refinement in the riding model approximation, with Uiso(H) set to 1.2 Ueq(C) and 1.5 Ueq(O). The H atoms of the alkyl group were allowed to rotate with a fixed angle around the C=C bond to best fit the experimental electron density (HFIX 137 in the SHELX program suite [3], with Uiso(H) set to 1.5 Ueq(C). Data were corrected for absorption effects by the numerical methods using SADABS [1].

3.2. Preparation of dithiocarbamate ligands from primary amines

The ligands were prepared by the reaction of either sodium or ammonium hydroxide with the primary or secondary amines and carbon disulphide under a very cold temperature (in ice) following reported literature procedure [5]. The dithiocarbamate precipitated out of the solution as white solids for the sodium salts and pale yellow solids for the ammonium salts.

The preparative details for the different dithiocarbamates are presented as follows:

3.2.1. Ammonium *N*-phenyldithiocarbamate [NH_4L^1]

To an equimolar mixture of ammonium hydroxide (15 mL, 0.05 mol) and *N*-phenyl aniline (4.6 mL, 0.05 mol) in an ice bath at 0 °C, carbon disulphide (3.0 mL, 0.05 mol) was added in small portions. After stirring for 3 h, the solidified mass was filtered under suction, rinsed with very cold ethanol, followed by diethyl ether to give a white precipitate and stored in the refrigerator.

[NH_4L^1]: Yield: 6.9 g (75%); Selected IR, ν(cm^{-1}): 1452 (C=N), 1226 (C_2—N), 911 (C=S), 3035 (=CH—H), 2818 (C—H), 3283 (NH); ^{1}H NMR ($CDCl_3$) δ ppm = 6.89 - 7.88 (m, 10H, $C_6\underline{H}_5$), 10.12 (s, 2H, N$\underline{H}$); ^{13}C NMR ($CDCl_3$) δ= 121.96 - 128.23 ($\underline{C}_6H_5$), 196.1 (–$\underline{C}S_2$).

3.2.2. Ammonium *N*-benzyldithiocarbamate [NH_4L^2]

Benzylaniline (5.50 mL, 0.05 mol) was stirred with ammonium hydroxide (15 mL, 0.05 mol) for 30 min in ice bath. To this solution, cold carbon disulphide (3 mL, 0.05 mol) was added in drop wise and the mixture was agitated for 3 h while maintaining a temperature of 4 °C. A crude yellowish-white solid substance precipitated out, separated using suction pump and rinsed with very cold ethanol, followed by several rinsing with ether. The white solid product was stored under reduced temperature.

[NH_4L^2]: Yield: 0.62 g (62%); Selected IR, (cm^{-1}): 1372 (C=N), 1312 (C_2-N), 927 (C=S), 3393 (N–H), 3171 (=C-H) and 2962 (–C–H); ^{1}H NMR ($CDCl_3$) δ (ppm) = 6.89- 7.88 (m, 10H, $C_6\underline{H}_5$–CH_2–NH), 10.45 (s, 4H, C_6H_5–CH_2–N$\underline{H}$), 4.59 (s, 4H, C_6H_5–$C\underline{H}_2$–NH); ^{13}CNMR ($CDCl_3$) δ (ppm) = 121.96- 128.23 ($\underline{C}_6H_5$), 52.3($\underline{C}H_2$), 196.1 (–$\underline{C}S_2$).

3.2.3. Sodium *p*-methylphenyldithiocarbamate [NaL^3]

p-methylaniline (2.70 g, 0.025 mol) was dissolved in 20 mL THF and added to a 20 mL THF solution of sodium hydroxide (1.00 g, 0.025 mol). Then, carbon disulphide (1.5 mL, 0.025 mol) was added and the solution was stirred for 6 h under N_2 atmosphere. The yellowish-white precipitate obtained was filtered, washed with diethyl ether and reprecipitated in acetone to give white solids which were dried in vacuum.

[NaL^3]: Yield: 4.0 g (74%); Selected IR, ν(cm^{-1}): 1502 (C=N), 1215 (C_2–N), 988 (C=S), 3031 (=CH–H), 2920 (H_2C–H), 3326 (N-H); ^{1}H NMR ($CDCl_3$) δ (ppm) = 6.96- 7.81 (m, 10H, $C_6\underline{H}_5$), 10.10 (s, 2H, N$\underline{H}$), 2.34 (s, 6H, $C\underline{H}_3$); ^{13}C NMR ($CDCl_3$) δ= 123.5 – 128.9 ($\underline{C}_6H_5$), 21.3 ($\underline{C}H_3$), 196.5 (–$\underline{C}S_2$).

3.2.4. Sodium *p*-ethylphenyldithiocarbamate [NaL^4]

Sodium hydroxide (2.0 g, 0.05 mol) was dissolved in 5 mL of water, and carbon disulphide (3.0 mL, 0.05 mol) was added in small portions and stirred in ice bath at 0 °C for 30 min. 4-ethylphenyl aniline (6.2 mL, 0.05 mol) was then added and further stirred for 3 h. The solidified mass was filtered, reprecipitated in acetone and rinsed with diethyl ether to give a white precipitate which was dried in vacuum.

[NaL^4]: Yield: 7.10 g (65%); Selected IR, ν(cm^{-1}): 1507 (C=N), 1225 (C_2–N), 1014 (C=S), 3019 (=CH–H), 2921 (H_2C–H), 3201 (N-H); ^{1}H NMR ($CDCl_3$) δ (ppm) = 7.09 - 7.46 (m, 10H, $C_6\underline{H}_5$),

10.10 (s, 2H, N<u>H</u>), 1.19 (t, 6H, C<u>H</u>$_3$), 2.58 (q, 4H, C<u>H</u>$_2$); ^{13}C NMR ($CDCl_3$) δ (ppm) = 120.50 – 144.0 (<u>C</u>$_6$H$_5$), 15.73 (<u>C</u>H$_3$), 27.72 (<u>C</u>H$_2$), 179.30 (–<u>C</u>S$_2$).

3.2.5. Sodium-1,6-hexamethelynediaminedithiocarbamate [NaL^5]

Hexamethylene-1, 6-diamine, (5.41 g, 0.05 mol) was dissolved in 20 mL THF and added to 8 mL aqueous solution of sodium hydroxide (4.0 g, 0.1 mol). Carbon disulphide (6.0 mL, 0.1 mol) was added to the solution and stirred for 3 h in ice bath. The yellowish-white precipitate obtained was filtered under suction, washed with cold ethanol and diethylether to give a white precipitate which was dried under vacuum.

[NaL^5]: Yield: 9.86 g (82%); Selected IR, ν(cm^{-1}): 1508 (C=N), 1305 (C$_2$–N), 941 (C=S), 2920 *ass*(CH$_2$), 2815 *sy* (CH$_2$), 3316 (N-H); ^{1}H NMR ($CDCl_3$) δ (ppm) 8.80 (s, 2H, NH), 4.70 (t, 4H, C<u>H</u>$_2$CH$_2$CH$_2$), 3.50 (m, 4H, CH$_2$C<u>H</u>$_2$CH$_2$), 1.56 (t, 4H, CH$_2$CH$_2$C<u>H</u>$_2$); ^{13}C NMR ($CDCl_3$) δ = 46.0, C<u>H</u>$_2$CH$_2$CH$_2$; 29.1, CH$_2$C<u>H</u>$_2$CH$_2$, 26.4, CH$_2$CH$_2$C<u>H</u>$_2$; 200.4, CS$_2$.

3.3. Metal complexation of dithiocarbamate ligands from primary amines

The dithiocarbamate complexes were prepared through simple ligand displacement reactions, by the addition of aqueous solution of the metal salts to an aqueous solution of the corresponding dithiocarbamate salts at room temperature [6].

3.3.1. Preparation of M(II) bis-(*N*-phenyldithiocarbamate) complexes (M = Ni, Pd, Pt)

About 10 mL aqueous solution of the respective 0.625 mmol of metal salts ($NiCl_2.6H_2O$: 0.149 g; $Na_2(PdCl_4)$: 0.184 g; $K_2(PtCl_4)$: 0.259 g), was added with stirring to 20 mL aqueous solution of 1.25 mmol **[NH$_4$L^1]** (0.233 g). The reaction mixture was stirred for 1 h, and the different coloured precipitated complexes were filtered off, washed thoroughly with water and dried under vacuum.

(1) [Ni(L^1)$_2$]; Yield: 1.10 g (81%); M.pt: 205 – 207 °C; Selected IR, ν(cm^{-1}): 1468 (C=N), 1292 (C$_2$–N), 994 (C=S), 3166 (=CH–H), 2953 (–CH$_2$–H), 3166 (NH), 411 (Ni-S); ^{1}H NMR ($CDCl_3$) δ (ppm) = 7.2 - 7.4 (m, 10H, C$_6$<u>H</u>$_5$), 8.56 (s, 2H, N<u>H</u>); ^{13}CNMR ($CDCl_3$) δ (ppm)= 129 – 137 (<u>C</u>$_6$H$_5$), 196.7 (–<u>C</u>S$_2$); $C_{14}H_{12}N_2S_4Ni$ (395.21): Calculated: C, 42.55; H, 3.06 N, 7.08; S, 32.22. Found: C, 42.05; H, 3.46 N, 7.50; S, 32.62%.

(2) [Pd(L^1)$_2$]; Yield 0.75g (55%); M.pt: 210 – 215 °C; Selected IR, 1475 (C=N), 1298 (C_2–N), 965 (C=S), 3226 (=CH–H), 2999 (–CH_2–H), 3155 (NH), 408 (Pd–S). ^{1}H NMR ($CDCl_3$) δ (ppm) = 7.3-7.6 (m, 10H, $C_6\underline{H}_5$), 9.79 (s, 2H, N$\underline{H}$); ^{13}CNMR ($CDCl_3$) δ (ppm) = 134 - 145 ($\underline{C}_6H_5$), 196.7 (–$\underline{C}S_2$); $C_{14}H_{12}N_2S_4Pd$ (442.94): Calculated: C, 37.96; H, 2.73, N, 6.33; S, 28.95. Found: C, 37.45; H, 2.34, N, 6.86; S, 28.40%.

(3) [Pt(L^1)$_2$]; Yield: 0.65 g (70%); M.pt: 240 – 243 °C; Selected IR, ν(cm^{-1}): 1494 (C=N), 1312 (C_2–N), 977 (C=S), 3154 (=CH–H), 3001, 3155 (NH), 424 (Pt–S); ^{1}H NMR ($CDCl_3$) δ (ppm) = 7.3- 7.9 (m, 10H, $C_6\underline{H}_5$), 9.25 (s, 2H, N$\underline{H}$).^{13}CNMR ($CDCl_3$) δ (ppm) = 135 - 145 (C_6H_5), 196.9 (–CS). $C_{14}H_{12}N_2S_4Pt$ (531.60): Calculated: C, 31.63; H, 2.28; N, 5.27; S, 24.13. Found: C, 32.22; H, 2.52; N, 5.20; S, 24.67%.

3.3.2. Preparation of M(II) bis(*N*-benzyldithiocarbamate) complexes (M = Ni, Pd, Pt)

About 10 mL aqueous solution of the respective 0.625 mmol of metal salts [($NiCl_2.6H_2O$: 0.149 g; $Na_2(PdCl_4)$: 0.184 g; $K_2(PtCl_4)$: 0.259 g], was added, with stirring, to 10 mL aqueous solution of 1.25 mmol ammonium *N*-benzyldithiocarbamate **[NH_4L^2]**. The reaction mixture was stirred for 1 h, and the different coloured precipitated complexes were filtered off, washed thoroughly with water and dried under vacuum.

(4) [Ni(L^2)$_2$]: Yield, 0.22 g (84%), M.pt. 200-202°C; Selected IR, ν (cm^{-1}): 1446 (C=N), 1326 (C_2-N), 923 (C=S), 3056 (=CH-H), 2932 (–CH_2-H), 3232 (-NH), 1542 s(-NH), 427 (Ni-S); ^{1}H NMR (DMSO) δ (ppm) = 7.38–7.26 (m, 10H, $C_6\underline{H}_5$–CH_2–NH), 4.59 (s, 4H, C_6H_5–C$\underline{H}_2$–NH), 9.60 (s, 2H, C_6H_5–CH_2–N$\underline{H}$); ^{13}CNMR (DMSO) δ (ppm) = 134.68, 129.11, 128.45, 127.56 ($\underline{C}_6H_5$–CH_2–NH), 47.46 (C_6H_5–$\underline{C}H_2$–NH), 211.05 (–$\underline{C}S_2$). $C_{16}H_{16}N_2S_4Ni$ (423.26): Calculated: C, 45.40; H, 3.81; N, 6.61; S, 30.30; Found: C, 45.10; H, 3.41; N, 6.55; S, 30.18%.

(5) [Pd(L^2)$_2$]: Yield, 0.25 g, (86 %); M.Pt. 230 – 232 °C; Selected IR, ν(cm^{-1}): 1534 (C=N), 1401 (C_2–N), 964 (C=S) 3239 (=CH–H), (–CH_2–H) 2924, 3229 (-NH), 452 (Pd-S); ^{1}H NMR (DMSO) δ (ppm) = 7.38–7.26 (m, 10H, $C_6\underline{H}_5$–CH_2–NH), 4.15 (s, 4H, C_6H_5–C$\underline{H}_2$–NH), 8.32 (s, 2H, C_6H_5–CH_2–N$\underline{H}$); ^{13}CNMR (DMSO) δ (ppm) = 128.5, 126.5, 137.9 (C_6H_5–CH_2–NH), 52.3 (C_6H_5–$\underline{C}H_2$–NH), 209.00 (–CS_2). $C_{16}H_{16}N_2S_4Pd$ (470.99), Calculated: C, 40.80; H, 3.42; N, 5.95; S, 27.23. Found: C, 40.40; H, 3.12; N, 6.15; S, 27.50%.

(6) [Pt(L^2)$_2$]: Yield, 0.28 g (80%); M.pt: 234 – 236 °C; Selected IR, ν(cm^{-1}): 1539 (C=N), 1404 (C_2–N), 922 (C=S) 3244 (=CH–H), 2926 (H_2C–H), 3244 (-NH), 403 (Pt-S); ^{1}HNMR (DMSO) δ (ppm) = 7.38–7.26 (m, 10H, $C_6\underline{H}_5$–CH_2–NH), 4.15 (s, 4H, C_6H_5–$C\underline{H}_2$–NH), 2.50 (t, 2H, C_6H_5–CH_2–N$\underline{H}$). ^{13}CNMR (DMSO) δ (ppm)= 128.5, 126.5, 136.9 ($\underline{C}_6H_5$–CH_2–NH), 52.3 (C_6H_5–$\underline{C}H_2$–NH), 210 (–CS_2).

$C_{16}H_{16}N_2S_4Pt$ (559.66), Calculated: C, 39.34; H, 2.88; N, 5.01; S, 22.92. Found: C, 39.96; H, 2.58; N, 5.63; S, 23.35%.

3.3.3. Preparation of M(II) bis (*p*-methylphenyldithiocarbamate) complexes (M = Ni, Pd, Pt)

About 10 mL aqueous solution of the respective 0.625 mmol of metal salts [($NiCl_2.6H_2O$: 0.149 g; $Na_2(PdCl_4)$: 0.184 g; $K_2(PtCl_4)$: 0.259 g], was added, with stirring, to 10 mL aqueous solution of 1.25 mmol sodium bis(*p*-methylphenyldithiocarbamate) **[NaL^3]**. The reaction mixture was stirred for 1 h, and the different coloured precipitated complexes were filtered off, washed thoroughly with water and dried under vacuum.

(7) [Ni(L^3)$_2$]: Yield, 0.60g, (44%); M.Pt-215-217 °C; Selected IR, ν(cm^{-1}): 1508 (C=N), 1208 (C_2–N), 996 (C=S), 3001 (=CH–H), 2917 (H_2C–H), 3185 (N-H), 411 (Ni–S); ^{1}H NMR ($CDCl_3$) δ (ppm) = 7.0 - 7.4 (m, 10H, $C_6\underline{H}_5$), 7.25 (s, 2H, N$\underline{H}$), 2.34 (s, 6H, $C\underline{H}_3$).^{13}CNMR ($CDCl_3$) δ (ppm) = 123.5 – 128.9 ($\underline{C}_6H_5$), 21.3 ($\underline{C}H_3$), 196.5 (–$\underline{C}S_2$); $C_{16}H_{16}N_2S_4Ni$ (423.26): Calculated: C, 45.18; H, 4.26; N, 6.59; S, 30.16. Found: C, 45.10; H, 4, 23; N, 6.60; S, 30.20%.

(8) [Pd(L^3)$_2$]: Yield, 0.71g (51%); M.pt: 230 – 233 °C; Selected IR, ν(cm^{-1}): 1511 (C=N), 1209 (C_2–N), 979 (C=S), 3032 (=CH–H), 2920 (H_2C–H), 3183 (N-H), 405 (Pd–S); ^{1}H NMR ($CDCl_3$) δ = 7.0- 7.5 (m, 10H, $C_6\underline{H}_5$), 9.68 (s, 2H, N$\underline{H}$), 2.34 (s, 6H, $C\underline{H}_3$); ^{13}CNMR ($CDCl_3$) δ = 123 – 137 ($\underline{C}_6H_5$), 21.2 ($\underline{C}H_3$), 207.2 (–$\underline{C}S_2$). $C_{16}H_{16}N_2S_4Pd$ (470.99): Calculated: C, 40.63; H, 3.84; N, 5.92; S, 27.11. Found: C, 40.54; H, 3.57; N, 5.90; S, 26.93%.

(9) [Pt(L^3)$_2$]: Yield, 0.64g (55%); M.pt: 248 – 250 °C; Selected IR, ν(cm^{-1}): 1512 (C=N), 1210(C_2–N), 974 (C=S), 3025 (=CH–H), 2980 (H_2C–H), 3180 (N-H), 420 (Pt–S); ^{1}H NMR ($CDCl_3$) δ (ppm) = 7.09 - 7.50 (m, 10H, $C_6\underline{H}_5$), 9.64 (s, 2H, N$\underline{H}$), 2.30 (s, 6H, $C\underline{H}_3$).^{13}CNMR

($CDCl_3$) δ (ppm) = 123 – 137 ($\underline{C}_6H_5$), 21.04 ($\underline{C}H_3$), 210.0 (–$\underline{C}S_2$). Anal cal. $C_{16}H_{16}N_2S_4Pt$ (559.66): , 3, 03; N, 4.99; S, 22.52%. C, 34.21; H, 3.23; N, 4.99; S, 2.83. Found: C, 34.03; H, 3.43; N, 5.03; S, 2.75%

3.3.4. Preparation of M(II) bis(*p*-ethylphenyldithiocarbamate) complexes (M= Ni, Pd, Pt)

About 10 mL aqueous solution of the respective 0.625 mmol of metal salts [($NiCl_2.6H_2O$: 0.149 g; $Na_2(PdCl_4)$: 0.184 g; $K_2(PtCl_4)$: 0.259 g], was added, with stirring, to 10 mL aqueous solution of 1.25 mmol sodium bis(*p*-ethylphenyldithiocarbamate) **[NaL^4]**. The reaction mixture was stirred for 1 h, and the different coloured precipitated complexes were filtered off, washed thoroughly with water and dried under vacuum.

(10) [$Ni(L^4)_2$]: Yield, 0.50 g (83%); M.pt: 209 – 212 °C; Selected IR, ν(cm^{-1}): 1533 (C=N), 1298 (C_2–N), 995(C=S), 3205 (=CH–H), 2961 (H_2C–H), 3205 (N-H), 442 (Ni–S); ^{1}HNMR ($CDCl_3$) δ (ppm) = 6.50 - 7.18 (m, 10H, $C_6\underline{H}_5$), 8.31 (s, 2H, N$\underline{H}$), 1.25 (t, 6H, $C\underline{H}_3$), 2.6 (q, 4H, $C\underline{H}_2$); ^{13}CNMR ($CDCl_3$) δ (ppm) = 115.0 – 129.0 ($\underline{C}_6H_5$), 14.5 ($\underline{C}H_3$), 28.2 ($\underline{C}H_2$), 220.0 (–$\underline{C}S_2$). $C_{18}H_{22}N_2S_4Ni$ (453.33): Calculated: C, 47.70; H, 4 .89; N, 6.19; S, 28.29. Found: C, 47.20; H, 4. 45; N, 6.60; S, 28.65

(11) [$Pd(L^4)_2$]: Yield, 0.56 g (84%); M.pt: 240 – 243 °C; Selected IR, ν(cm^{-1}): 1535 (C=N), 1298 (C_2–N), 965 (C=S), 3206 (=CH–H), 2961 (H_2C–H), 3208 (N-H), 419 (Pd–S); ^{1}H NMR δ = 6.80 - 7.30 (m, 10H, $C_6\underline{H}_5$), 8.44 (s, 2H, N$\underline{H}$), 1.20 (t, 6H, $C\underline{H}_3$), 2.58(q, 4H, $C\underline{H}_2$); ^{13}CNMR ($CDCl_3$) δ (ppm) = 120.0 – 145.0 ($\underline{C}_6H_5$), 20.8 ($\underline{C}H_3$), 45.2 ($\underline{C}H_2$), 185.0 (–$\underline{C}S_2$); $C_{18}H_{22}N_2S_4Pd$ (501.06): Calculated: C, 43.15; H, 4.43; N, 5.59; S, 25.59. Found: C, 41.25; H, 4.80; N, 5.30; S, 25 %;

(12) [$Pt(L^4)_2$]: Yield, 0.45 g, (61%); M.Pt. 248 – 250 °C; Selected IR, ν(cm^{-1}): 1534 (C=N), 1298 (C_2–N), 964 (C=S), 3205 (=CH–H), 2961 (H_2C–H) 2961, 3205 (N-H), 419 (Pt-S); ^{1}HNMR (CDCl3) δ (ppm) = 6.96 - 7.78 (m, 10H, $C_6\underline{H}_5$), 9.80 (s, 2H, N$\underline{H}$), 1.25 (t, 6H, $C\underline{H}_3$), 2.65(q, CH_2); ^{13}CNMR ($CDCl_3$) δ (ppm) = 120.50 – 144.07 ($\underline{C}_6H_5$), 15.73 ($\underline{C}H_3$), 27.74 ($\underline{C}H_2$), 179.30 (–$\underline{C}S_2$); $C_{18}H_{22}N_2S_4Pt$ (589.72): Calculated: C, 36.66; H, 3.16; N, 4.75; S, 21.74; Found: C, 36.20; H,3.35; N, 4.20; S, 21.20%

3.3.5. Preparation of M(II) bis-(*N*-hexamethylenediaminedithiocarbamate) complexes (M = Ni, Pd, Pt)

About 10 mL aqueous solution of the respective 2.5 mmol of metal salts [($NiCl_2.6H_2O$: 0.149 g; $Na_2(PdCl_4)$: 0.184 g; $K_2(PtCl_4)$: 0.259 g], was added, with stirring, to 10 mL aqueous solution of 2.5 mmol sodium bis-(*N*-hexamethylenediaminedithiocarbamate) **[NaL^5]**. The reaction mixture was stirred for 1 h, and the different coloured precipitated complexes were filtered off, washed thoroughly with water and dried under vacuum.

(13) [$Ni(L^5)_2$]: Yield, 1.15 g (93%); M.pt: 216 – 218 °C; Selected IR, $\nu(cm^{-1})$: 1508 (C=N), 1213 (C_2—N), 943 (C=S), 2924 *as*(CH_2), 2851 *sy*(CH_2), 3263 (N-H), 432 (Ni–S); ^{1}HNMR ($CDCl_3$) δ (ppm) = 7.29 (s, 2H, N<u>H</u>), 2.65 (t, 4H, C<u>H</u>$_2$$CH_2CH_2$), 1.29 (m, 4H, CH_2C<u>H</u>$_2$$CH_2$), 1.55 (t, 4H, CH_2CH_2C<u>H</u>$_2$); ^{13}C NMR ($CDCl_3$) δ = 45.0, C<u>H</u>$_2$$CH_2CH_2$; 28.1, CH_2C<u>H</u>$_2$$CH_2$), 26.0, CH_2CH_2C<u>H</u>$_2$; 200.10 (–CS_2); $C_{16}H_{28}N_4S_8Ni_2$ (650.33): Calculated: C, 29.55; H, 4.34; N, 8.62; S, 39.44; Found: C, 29.15; H, 4.14; N, 8.02; S, 39.70%.

(14) [$Pd(L^5)_2$]: Yield, 0.77g (81%); M.pt: 235 – 238 °C; Selected IR, $\nu(cm^{-1})$: 1540 (C=N), 1212 (C_2—N), 945 (C=S), 2924 *as*(CH_2), 2855 *sy*(CH_2), 3264 (N-H), 455 (Pd–S); ^{1}HNMR ($CDCl_3$) δ (ppm) = 8.09 (s, 2H, NH), 3.38 (t, 4H, C<u>H</u>$_2$$CH_2CH_2$), 2.09 (m, 4H, CH_2C<u>H</u>$_2$$CH_2$), 2.50 (t, 4H, CH_2CH_2C<u>H</u>$_2$). ^{13}CNMR ($CDCl_3$) δ (ppm) = 40.0, C<u>H</u>$_2$$CH_2CH_2$, 30.70, CH_2C<u>H</u>$_2$$CH_2$, 28.0, CH_2CH_2C<u>H</u>$_2$ 206.90 (–CS_2). $C_{16}H_{28}N_4S_8Pd_2$ (745.78): Calculated: C, 25.77; H, 3.78; N, 7.51; S, 34.40. Found: C 25.28; H, 3.38; N, 6.90; S, 34.10%.

(15) [$Pt(L^5)_2$]: Yield: 0.71g, (70%); M.Pt. 258-260 °C; Selected IR, $\nu(cm^{-1})$: 1545 (C=N), 1214 (C_2—N), 949 (C=S), 2979 *as*(CH_2), 2930 *sy*(CH_2), 3266 (N-H), 466 (Pt–S); ^{1}HNMR ($CDCl_3$) δ (ppm) = 8.15 (s, 2H, N<u>H</u>), 3.40 (t, 4H, C<u>H</u>$_2$$CH_2CH_2$), 2.20 (m, 4H, CH_2C<u>H</u>$_2$$CH_2$), 2.50 (t, 4H, CH_2CH_2C<u>H</u>$_2$); ^{13}C NMR ($CDCl_3$) δ (ppm) = 40.0, C<u>H</u>$_2$$CH_2CH_2$, 30.01, CH_2C<u>H</u>$_2$$CH_2$ 28.4, CH_2CH_2C<u>H</u>$_2$, 207.20 (–CS_2); $C_{16}H_{28}N_4S_8Pt_2$ (923.10): Calculated: C, 20.82; H, 3.06; N, 6.07; S, 27.79; Found: C, 20.44; H, 3.36; N, 5.75; S, 26.70%.

3.4. Discussions on the metal(II) dithiocarbamate complexes from ligands obtained from primary amines

3.4.1. General synthesis of the dithiocarbamate ligands obtained from primary amines and their respective metal complexes

The ligand formation from the primary amines involved the nucleophilic attack of the amine on the carbon disulphide, in an alkaline medium, to generate the dithiocarbamate salt as shown in schemes 3.1 and 3.2.

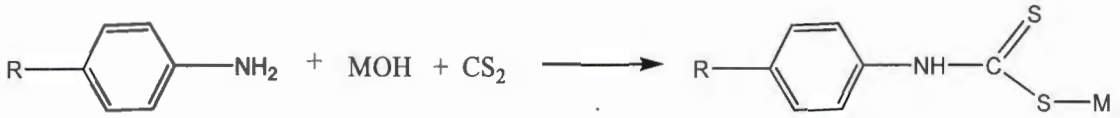

Scheme 3.1: General synthetic route for the preparation of dithiocarbamate ligands from primary amines (R = H, CH_3, CH_2CH_3; M = NH_4/Na).

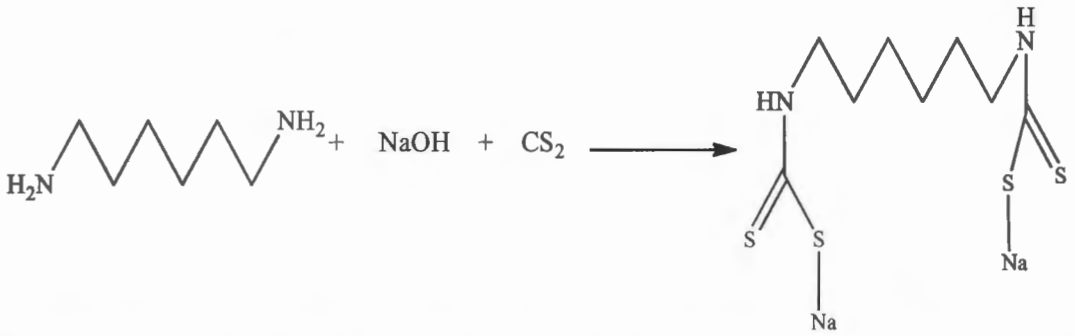

Scheme 3.2: The synthetic route for the preparation of dithiocarbamate ligand from primary diamine.

The ammonium salts precipitated out as faint yellow solids, very unstable (decompose) at room temperature but more stable in a cold environment; while the sodium salts precipitated out as pure white solids and are stable at room temperature. The yield for both the ammonium and sodium salts was high, and they are all soluble in water at room temperature. All the complexes were prepared by the direct reaction of aqueous solutions of metal salts and ligand (1:2 molar ratio) as presented in Schemes 3.3 and 3.4. These reactions were carried out at room temperature because of the high aqueous solubility of the dithiocarbamate ligands, and the nature of the reactions (simple displacement reaction). All complexes formed were intensely coloured conforming to one of the properties of d^8 metals (formation of coloured ions), with different shades of green for the nickel, orange for palladium and yellow for platinum complexes. They are all insoluble in water but soluble in different solvents such as chloroform, dichloromethane, methanol, ethanol, acetonitrile with the

exception of the hexamethylenediamine DTC complexes which are only soluble in the more coordinating solvents THF (with heat), DMF and DMSO.

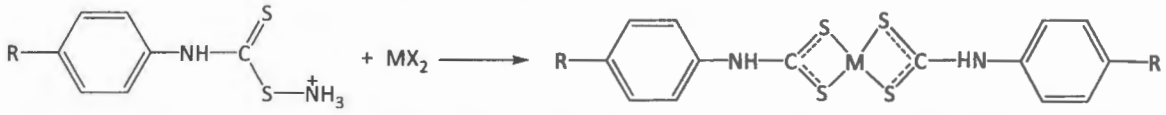

Scheme 3.3: General synthetic route for the formation of complexes from dithiocarbamate ligands obtained from primary amines (R = H, CH_3, CH_2CH_3; M= Ni, Pd, Pt).

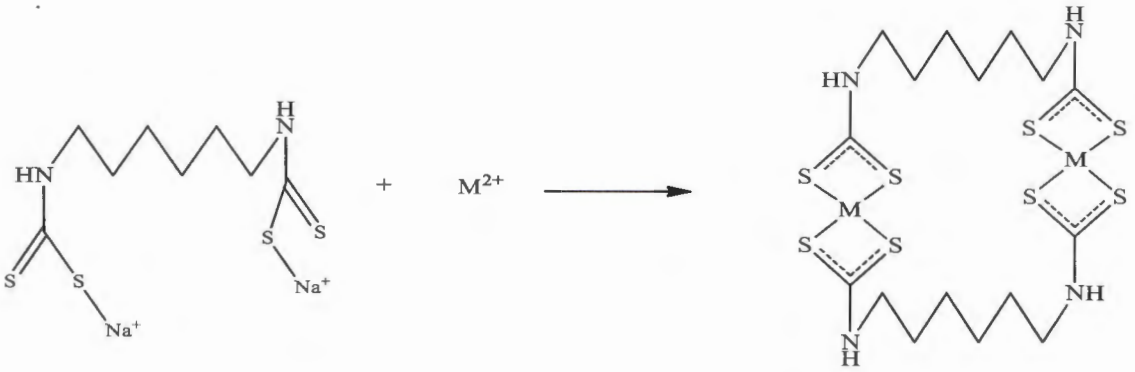

Scheme 3.4: Synthetic route for the formation of complexes from dithiocarbamate ligand obtained from primary diamine (M= Ni, Pd, Pt).

3.4.2. Infrared spectral studies of the metal(II) complexes of dithiocarbamate obtained from primary amines

In dithiocarbamate compounds, the major regions of particular interest are: the 1450-1580 cm^{-1}, which is the stretching vibration of the thiouriede band (C=N), the 950-1050 cm^{-1} region associated with ν(C-S) vibration, and the band between 450 and 550 cm^{-1} associated with the metal-sulphur vibration [7]. In these studies, a single sharp band of high intensity occurred around 1452, 1453, 1502, 1507 and 1508 cm^{-1} for the **$[NH_4L^1]$, $[NH_4L^2]$, $[NaL^3]$, $[NaL^4]$, $[NaL^5]$** ligands respectively, which are ascribed to the thioureide bond. These bands were observed around 1491 – 1545 cm^{-1} in the Ni(II), Pd(II), Pt(II) complexes on all the ligands respectively. These characteristic dithiocarbamate bands generally found around 1500 cm^{-1} indicate a C-N bond order between a (C-N) single bond around 1250 – 1350 cm^{-1} and a (C=N) double bond around 1640 – 1690 cm^{-1} [8]. A comparison of the absorption bands of the complexes and the uncoordinated free ligand revealed higher modes observed in the complexes as a result of an increase in the carbon–nitrogen double

bond character due to the mesomeric movements of the electrons from the dithiocarbamate moiety towards the central metal; thus confirmed the coordination of the metal ions to the ligands [9]. The *v*(C=N) increases down the triad due to increase in electron accepting abilities from Ni to Pt which also implies an increase in Lewis acid properties. The π donor property also gets weaker down the group, thus increasing the C=N vibrations [10]. The effect of the strength of electron donating substituents (H, CH_3 and CH_2CH_3) on the para position of the phenyl ring was observed as the value of the thiouriede bands were observed in the order $L^1<L^2<L^3$.

The *v*(C–S) band appeared around 1018 – 1040 cm^{-1} for the ligands, and in the range 983 –1018 cm^{-1} in all the metal complexes without any splitting, thus indicated a symmetrically bidentate coordination of the $–CS_2$ group to the metal centre. According to the Bonati and Ugo reports, the number of bands detected around 1000±70 cm^{-1} determines the mode of bonding of the dithiocarbamate ligands [11]. The *v*(C-S) frequencies for the uncoordinated dithiocarbamate ligands shift to lower frequencies for the metal complexes which could be ascribed to an increase in the double bond character of *v*(C=S) in the formation of the complexes [12]. The trend is an increase in the C=S vibrations as the chain length of the substituents on the phenyl group increases. The magnitude of the C-S bands were also in the order $L^1<L^2<L^3$.

In the far IR region, the appearances of new bands around 408– 466 cm^{-1} (which was absent in all the ligands) was due to M-S bond vibrations [13]. In both the ligands and the complexes, the (N—H) stretching vibrations occurred around 3283 – 3316 cm^{-1} and 3166 – 3266 cm^{-1} respectively, a decrease in N-H vibration as a result of complexations.

The vibrations which occurred around 2920 – 2979, 2875 – 2930 cm^{-1} in both ligands and complexes represent *as*(C–H) and *sym*(C–H) respectively for the $\mathbf{L^5}$ compounds.

3.4.3. Electronic spectral studies of the metal(II) complexes of dithiocarbamate obtained from primary amines

The electronic spectra gives possible information about electronic transitions of the group 10 complexes in the d^8 configuration and square planar geometry. This d^8 configuration imposes a ^3F ground term on the spectral which splits into three energy levels and can be treated as an inverted $A_2g \rightarrow T_2g \rightarrow T_1g$ in the ^3F and ^3P orbitals. They can have structural adjustments from 4-coordinate square planar to tetrahedral or to 6-coordinate octahedral geometry [14]. For the complexes $\mathbf{[Ni(L^1)_2]}$ to $\mathbf{[Ni(L^5)_2]}$, the electronic spectra of the complexes gave absorption bands due to electronic transitions within the ligands at 300- 390 nm which is assigned to $n \rightarrow p^*$, $p \rightarrow p^*$ (metal to ligand and ligand to metal charge transfer transitions) [15]. The two bands in the range 400-567

nm in all the complexes are typical of square planar group10 dithiocarbamate complexes, and are assigned to metal d-d transitions [16].

3.4.4 NMR spectral studies of the metal(II) dithiocarbamate complexes obtained from primary amines

The phenyl protons of the ligands appeared as multiplets in the range 6.96 – 7.88 , 7.24 – 7.47, 6.96 – 7.81, 7.09 – 7.46 ppm for the ligands $\mathbf{L^1}$, $\mathbf{L^2}$, $\mathbf{L^3}$ and $\mathbf{L^4}$ while that of the complexes appeared around 6.50 - 7.18 (Ni(II)), 6.80 - 7.30 (Pd(II)) and 6.96 - 7.78 ppm (Pt(II)). The position of these peaks indicated a slight deshielding, and could be attributed to the shift of electron density towards the nitrogen of the NRR′ thereby enhancing the electron density on the sulphur via the thioureide π-system [17]. The different magnetic environments reflect the different chemical shifts of the metal complexes. In the spectrum of $\mathbf{L^5}$, α methylene proton appeared at 4.70 ppm, the β and γ protons appeared at 1.56 and 3.50 ppm respectively. In the complexes, α methylene protons appeared as triplets around 2.65 - 3.40 ppm and highly deshielded due to the release of electrons of the nitrogen atom which forces a high electron density towards the sulphur via the thioureide π-system. The β protons appeared around 1.29 - 2.20 ppm as multiplets and the γ protons at 2.09 - 2.10 ppm as triplets.

Many signals in the spectra of the complexes were observed to be shifted compared to those in the uncoordinated ligands. The coordination shifts ($\Delta\delta$), which gives the differences between the corresponding chemical shifts in the signals of the complexes and the uncoordinated organic compounds could be calculated using the relationship: ($\Delta\delta = \delta_{complex} - \delta_{ligand}$) [18]. In these studies, $\Delta\delta$ for the phenyl protons were obtained as 0.24 - 0.48, 0.34 - 0.48, 0.02 - 0.34 ppm for the Ni(II), Pd(II), Pt(II) respectively, and for the methylene protons as 1.30-2.05, 0.27-0.64 and 1.40-1.41 ppm for all the complexes.

The signals due to the NH protons in the compounds containing the phenyl ring appeared in the range 10.10 -10.12 ppm for the uncoordinated ligands, and between 7.25 – 9.60, 8.32 -9.68, 8.31-9.80 ppm in the spectra of the Ni(II), Pd(II), Pt(II) complexes, with $\Delta\delta$ of 2,85 – 0.32 ppm. The signals which appeared at 8.80 ppm have been assigned to the N-H protons of the $\mathbf{L^5}$ ligand while these peaks occurred in the range 7.29 - 8.15 ppm in the spectra of the corresponding complexes. These differences may be attributed the different distribution of electron densities within the aromatic rings as a result of the coordination to the metal ions. The singlet signal at 3.36 ppm in the $\mathbf{L^2}$ complexes corresponded to the $-CH_2$ protons on a highly deshielding nitrogen atom.

The ^{13}C NMR show the characteristic quaternary carbon peak, but in different environments, in the spectra of the uncoordinated ligands at 196.1, 196.5, 179.3 ppm. These peaks resonated around 196.7-220.0, 196.7-206.9, 196.9-210 ppm in the spectra of the Ni(II), Pd(II) and Pt(II) complexes, with $\Delta\delta$ in the range 0.60 - 23.90, 0.50 - 10.40, 17.60 - 30.70 respectively. In the $\mathbf{L^5}$ complexes, the carbon atoms shift displacements were observed with $\Delta\delta$ in the range 0.2 – 2.0 ppm and the NCS_2 carbon atoms gave signals at δ =200.10– 207.20 ppm. An increase in -NCS_2 signals is observed down the group of each series confirming that heavier atom complexes have higher δ values than the lighter atoms in the same group [18].

3.5. Single crystal X-ray diffraction for paladium(II) bis-(*N*-phenyldithiocarbamate) $[Pd(L^1)_2]$ and platinum(II) bis-(*N*-phenyldithiocarbamate) $[Pt(L^1)_2]$ complexes

3.5.1. Data collection for $[Pd(L^1)_2]$ and $[Pt(L^1)_2]$

A clear, pale yellow crystal of $\mathbf{[Pd(L^1)_2]}$ with approximate dimensions of 0.069 x 0.231 x 0.287 mm, and $\mathbf{[Pt(L^1)_2]}$ with dimensions of 0.086 x 0.134 x 0.282 mm was selected under oil at ambient conditions and attached to the tip of a MiTeGenMicroMount©. Each of the crystal was mounted in a stream of cold nitrogen at 100(2) K and centered in the X-ray beam using a video camera. The crystal evaluation and data collection were performed on a Bruker APEXII CCD DUO diffractometer with Mo K (λ = 0.71073 Å) radiation and the diffractometer to crystal distance of 6.00 cm [1]. The initial cell constants were obtained from three series of scans at different starting angles. Each series consisted of 12 frames collected at intervals of 0.5° in a 6° range about with the exposure time of 10 seconds per frame. The reflections were successfully indexed by an automated indexing routine built in the APEX2 program suite. The final cell constants were calculated from a set of 6500 strong reflections from the actual data collection. These highly redundant datasets were corrected for Lorentz and polarization effects. The absorption correction was based on fitting a function to the empirical transmission surface as sampled by multiple equivalent measurements [2].

3.5.1.1 X-ray crystal structures of paladium(II) bis-(*N*-phenyldithiocarbamate) ($[Pd(L^1)_2]$ and platinum(II) bis-(*N*-phenyldithiocarbamate) $[Pt(L^1)_2]$)

The crystallographic parameters and the interatomic bond angles and distances for both Pd and Pt complexes of $\mathbf{L^1}$ have been summarized in Table 3.1 and 3.2 respectively. In each of the complexes, the dithiocarbamate ligands are bonded at opposite ends in a bidentate fashion to the central metal as shown in Figures 3.1(a) and 3.2(a). The crystallographic packing shows that the crystal exists as 4 monomers per unit cell for each of the complexes as presented in Figures 3.1(b) and 3.2(b). There is one symmetry-independent molecule in the asymmetric unit, consisting of one half of the

Pd(II)/Pt(II) complex. The N–H···S interactions are also shown as red dashed lines and symmetry positions for the two structures are identical at: (i) 3/2–*x*, ½+*y*, *z*, (ii) 1–*x*, –*y*, 1–*z*, (iii) –½+*x*, –½–*y*, 1–*z* as shown in Figures 3.1(c) and 3.2(c). The metal is in the 2+ oxidation state and charge balance comes from the bound dithiocarbamate molecule connected by only two S atoms (S1 and S2) where the negative charge is localized on S1 and S2 respectively. The other half of the molecule is generated by symmetry with the Pd/Pt atom residing on a special position (0.5, 0, 0.5).The final least-squares refinement of 101 parameters against 1899 reflections resulted in residuals *R* (based on *F* for all data) of 0.0233 and 0.0587 respectively. The coordination environment of the Pd(II) and Pt(II) complexes shows symmetric bond lengths for Pd-S as observed from Table 3.2, [Pd(1)-S(1) = 2.3232(5) and Pd(1)- S(2) = 2.3399 (5) Å]; Pt-S bond lengths Pt1-S1=2.3201(7) and Pt1-S2=2.3313(7). Both complexes have distorted square planar geometry due to the small S-Pd-S bite angle S1-Pd1-S2i =75.134 (17)° and S1-Pt-S2 = 74.75 (3)°. The C-S and C-N bond lengths of the corresponding dithiocarbamate ligands are: S1-C1=1.724(2), S2-C1=1.707(2); N1-C1=1.324(20, N1-C2=1.390(2) for the Pd, and S1-C1=1.731(3); S2-C1=1.704(3); N1-C1=1.327(3), N1-C2=1.426(4) for the Pt complex. The phenyl groups make angles of 86.17(7) and 86.03(7)°; 87.20(10) and 86.95(10) with their respective dithiocarbamate planes. The bond length for both Pd-S and Pt-S are relatively close, 2.32-2.34; 2.32-2.33, with similar intermolecular hydrogen bonding interactions which supports their similar coordination modes and chemical properties. This also justifies why they are usually studied as a pair [17].

Table 3.1: Summary of crystal data and structure refinement for **[Pd(L^1)$_2$]** and **[Pt(L^1)$_2$]**

Complex	[Pd(L^1)$_2$]	[Pt(L^1)$_2$]
Empirical formula	$C_{14}H_{12}N_2PdS_4$	$C_{14}H_{12}N_2PtS_4$
Formula weight	442.90	531.59
Crystal size (mm)	0.29 × 0.23 × 0.07	0.28 × 0.13 × 0.09
Crystal system	orthorhombic	orthorhombic
Crystal habit	Plate, yellow	Plate, yellow
Space group	*Pbca* (no. 61)	*Pbca* (no. 61)
a (Å)	9.5470(8)	9.6947(9)
b (Å)	6.5224(6)	6.4818(6)
c (Å)	24.393(2)	24.299(2)
Space group	*Pbca* (no. 61)	*Pbca* (no. 61)
α (°)	90	90
β (°)	95.021(2)	96.111(2)

γ (°)	90	90
V [Å**3]	1518.9(2)	1527.0(2)
Z	4	4
Dcalc (g cm-3)	1.937	2.312
F(000)	880	1008
Dataset	-12:12, -8:8, -32:32	12:12, -8:8, -32:32
μ(MoKa) (/mm)	1.763	9.728
Tot.,Uniq.Data, R(int)	30730,4612, 0.0645	21080, 2295, 0.024
Observed reflections $I > 2\sigma(I)$	1630	1476
Nref, Npar	4612, 209	2295, 110
Final R, wR2, S	0.0233, 0.0587, 1.09	0.0198, 0.0384, 1.03
Max.residual density [e/Å3]	0.00, 0.00	0.00, 0.00
Min. residual density [e/Å3]	-0.35, 0.49	-0.64, 0.49
θrange(°)	2.7–28.3	2.7-28.3

Table 3.2: Selected bond lengths and angles for for **[Pd(L^1)$_2$]** and **[Pt(L^1)$_2$]**

[Pd(L^1)$_2$]		[Pt(L^1)$_2$]	
Bond	Distances (Å)	Bond	Distances (Å)
Pd1—S1	2.3232 (5)	Pt1—S1	2.3201 (7)
Pd1—S1i	2.3232 (5)	Pt1—S1 i	2.3202 (7)
Pd1—S2i	2.3399 (5)	Pt1—S2	2.3313 (7)
Pd1—S2	2.3399 (5)	Pt1—S2 i	2.3314 (7)
S1-C1	1.724 (2)	S1—C1	1.731 (3)
S2-C1	1.707 (2)	S2—C1	1.704 (3)
N1—H1	0.80 (2)	N1—H1	0.80 (4))
N1—C1	1.324 (2)	N1—C1	1.327 (4)
N1—C2	1.420 (2)	N1—C2	1.426 (4)
C2—C3	1.390 (3)	C2—C3	1.389 (4)
Bond	Angle (°)	Bond	Angle (°)
S1—Pd1—S1i	180.0	S1—Pt1—S1i	180.0
S1—Pd1—S2i	75.134 (17)	S1—Pt1—S2	74.75 (3)
S1—Pd1—S2	104.866 (17)	S1—Pt1—S2	105.24 (3)
S1—Pd1—S2i	104.864 (17)	S1—Pt1—S2i	105.25 (3)
S1—Pd1—S2	75.136 (17)	S1—Pt1—S2i	74.76 (3)
S2—Pd1—S2	180.00 (2)	S2—Pt1—S2	180.000 (19)
C1—S1—Pd1	86.17 (7)	C1—S1—Pt1	86.95 (10)
C1—S2—Pd1	86.03 (7)	C1—S2—Pt1	87.20 (10)
C1—N1—H1	112.5 (17)	C1—N1—H1	117 (2)

C1—N1—C2	129.33 (18)	C1—N1—C2	129.1 (3)
C2—N1—H1	117.9 (17)	C2—N1—H1	113 (2)
S2—C1—S1	111.92 (11)	S2—C1—S1	110.61 (16)
N1—C1—S1	120.46 (16)	N1—C1—S1	120.5 (2)
N1—C1—S2	27.58 (16)	N1—C1—S2	128.9 (2)
C3—C2—N1	117.43 (19)	C3—C2—N1	117.5 (3)

(a)

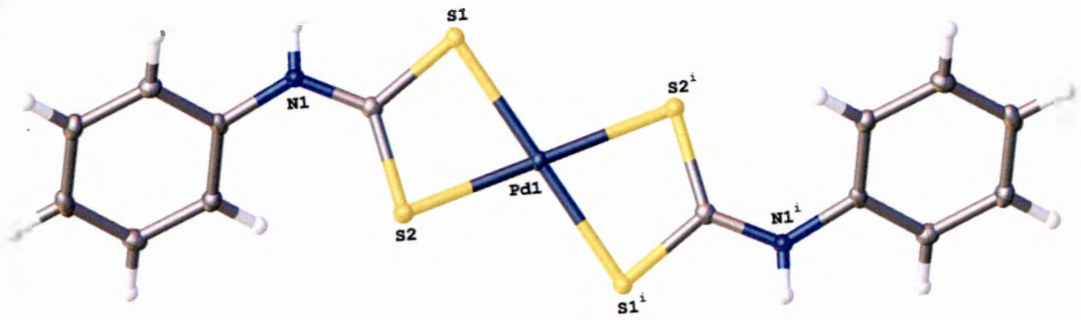

(b)

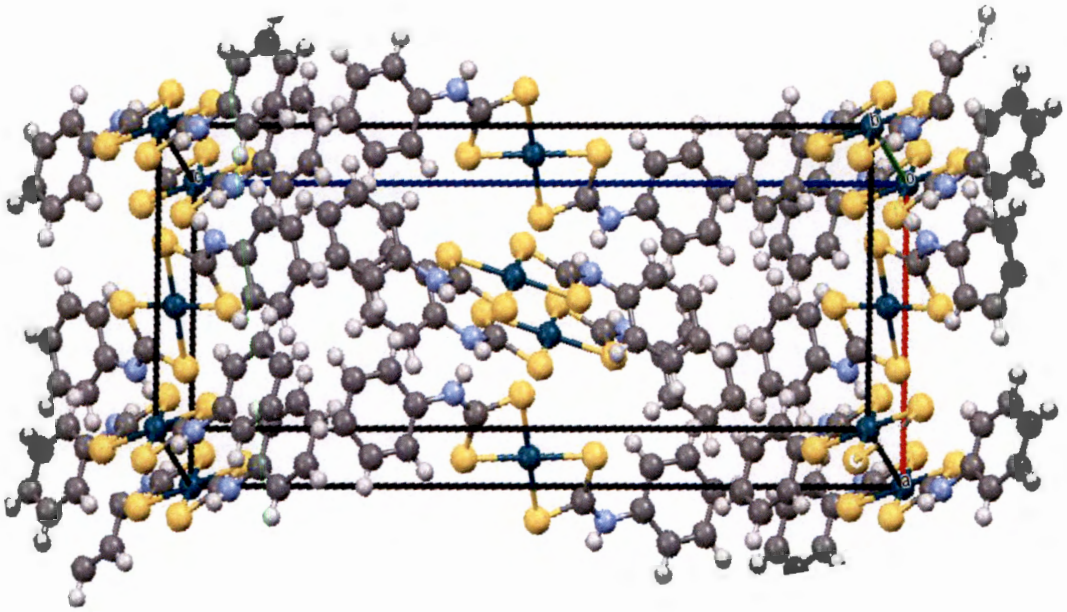

(c)

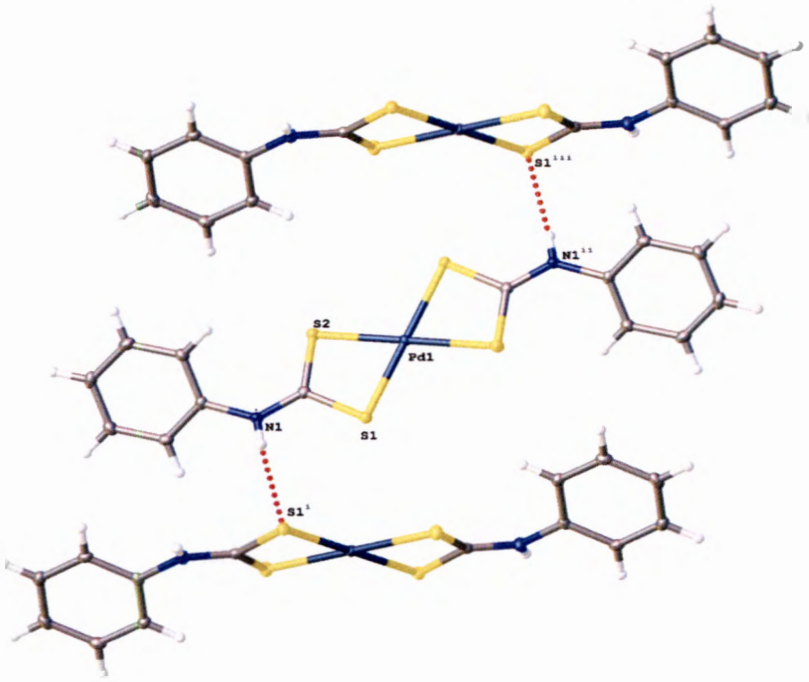

Figure 3.: (**a**) A molecular drawing of **[Pd(L^1)$_2$]** shown with 50% probability ellipsoids, showing the full molecule in the unit cell, **(b)** molecular structure diagram showing the packing of **[Pd(L^1)$_2$]**, **(c)** intermolecular hydrogen bonding contacts.

(a)

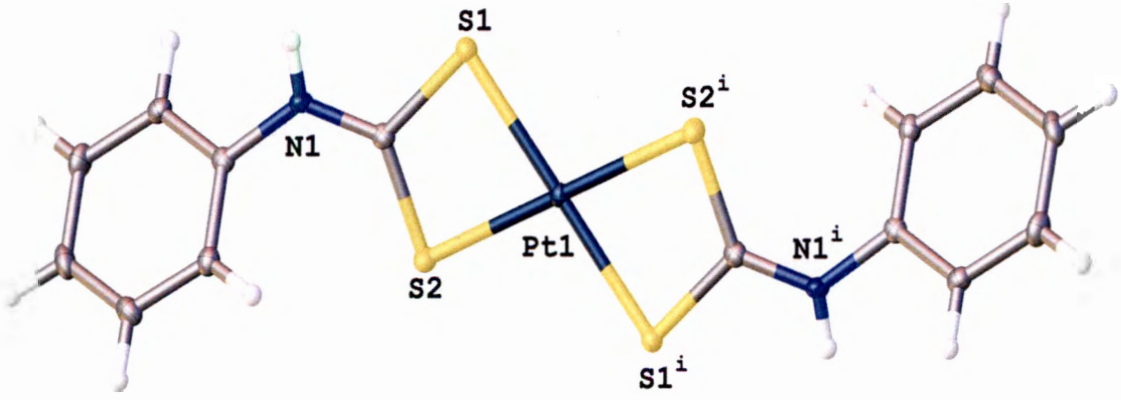

(b)

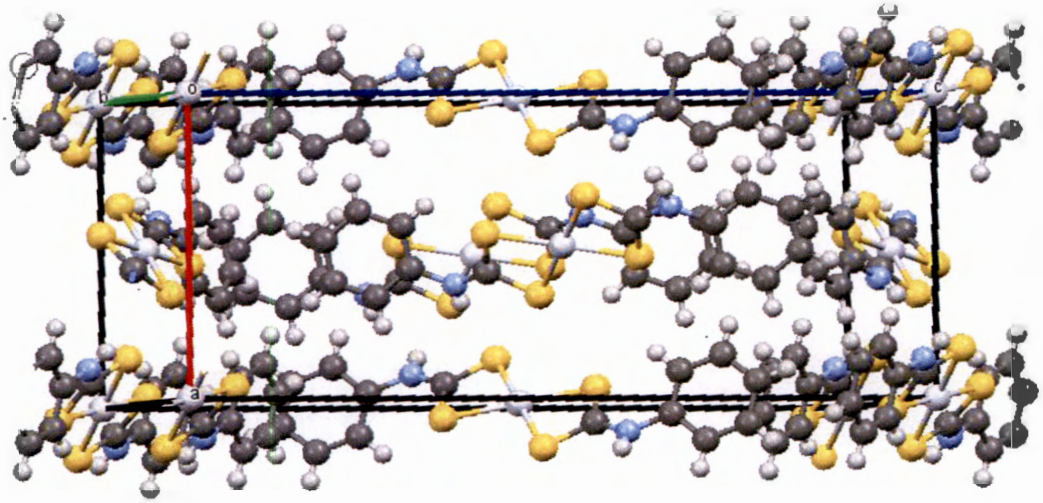

(c)

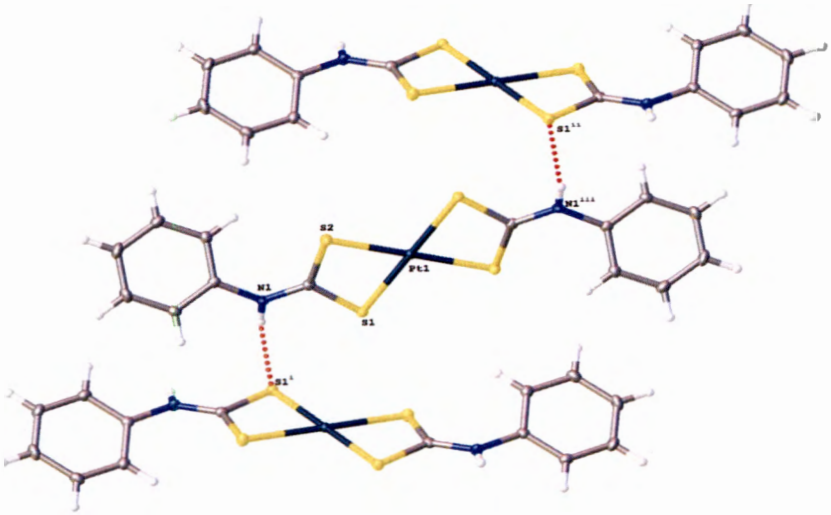

Figure 3.2: (a) A molecular drawing of **[Pt(L^1)$_2$]** shown with 50% probability ellipsoids, showing the full molecule in the unit cell, **(b)** molecular structure diagram showing the packing of **[Pt(L^1)$_2$]**, **(c)** intermolecular hydrogen bonding contacts.

3.5.1.2. X-ray crystal structures of nickel(II) bis-(*N*-benzyldithiocarbamate) $[Ni(L^2)_2]$ and platinum(II) bis-(*N*-benzyldithiocarbamate) $[Pt(L^2)_2]$

A green crystalline block with approximate dimensions of 0.17 x 0.23 x 0.47 mm for **$[Ni(L^2)_2]$**, and a light orange block of **$[Pt(L^2)_2]$** with dimension of 0.03 x 0.16 x 0.20 mm was selected under oil at ambient conditions and attached to the tip of a MiTeGenMicroMount©.

The systematic absences reported in the diffraction data were found to be consistent for the *P*1 space group which yielded stable results of refinement that are chemically and computationally reasonable [1-4].

The crystallographic parameters and the interatomic bond angles and distances for both Ni(II) and Pt(II) complexes of L^2 have been summarized in Table 3.3 and 3.4 respectively. In each of the complexes, the dithiocarbamate ligand moiety bonded at opposite end in a bidentate fashion to the central metal as shown in Figures 3.3(a) and 3.4(a). The crystallographic packing shows that the crystals exist in two monomers per unit cells for each of the complexes as presented in Figures 3.1(b) and 3.2(b). The structures of both complexes are square planar geometry with two dithiocarbamate ligands in each molecule. The complexes both appeared centro symmetrical, with $P2_1/n$ space group and an inversion point at the metal centre. The resulting structure has a high wR2 of 0.289. In the non-centrosymmetrical space group $P2_1$, the wR2 is more acceptable at 0.076. The least square planes formed by the two dithiocarbamate ligands make a dihedral angle of 2.0(8) with each other. The minimum and maximum Pt—S bond lengths are 2.276(4) and 2.385(4) Å to S22 and S12; while for Ni-S, the bond lengths are 2.1817(10) and 2.2173(10) respectively. This implies that the bond lengths increase down the group. The phenyl groups make angles of 89.6(6) and 86.8(5)°; 85.72(12) and 84.73(12) with their respective dithiocarbamate planes.

Each dithiocarbamate ligand in **$[Pt(L^2)_2]$** has one intramolecular C---H...S hydrogen interaction with lengths 2.73 and 2.75 to S12 and S22 respectively as seen in Figure 3.5. On either side of the complex there are two N—H…S interactions of length 2.73 and 2.75 to S12 and S22.In the structure of **$[Ni(L^2)_2]$,** there is a C---H...S hydrogen interaction with distances of 2.74 and 3.198 Å to S12 and S22. Another hydrogen bonding interaction occurred with N—H…S with distances of 2.57 and 3.366 Å to S12 and S22 respectively, forming infinite chain with base vector [1-4]. The Ni-S bond length is shorter at 2.18-2.22 than the Pt-S bond length at 2.28-2.39, this implies a higher bond strength in Ni-S than in Pt-S, so more intramolecular interactions are recorded for the **$[Ni(L^2)_2]$** complex than the **$[Pt(L^2)_2]$.**

Table 3.3: Summary of crystal data and structure refinement for **$[Ni(L^2)_2]$** and **$[Pt(L^2)_2]$**

Complex	**$[Ni(L^2)_2]$**	**$[Pt(L^2)_2]$**
Empirical formula	C_{16} H_{16} N_2 Ni S_4	C16 H16 N2 Pt S4
Formula weight	423.24	559.63
Crystal size (mm)	0.19 x 0.27 x 0.35	0.03 x 0.16 x 0.20
Crystal system	Monoclinic	monoclinic
Space group	P21/c (No.14)	P21(No.4)
a (Å)	6.3418(3)	5.3914(2)
b (Å)	5.5322(3	26.2291(11)
c (Å)	26.4224(13)	6.5787(3)
α (°)	90	90
β (°)	96.055(2)	94.472(2)
γ (°)	90	90
V [Å**3]	921.84(8)	927.47(7)
Z	2	2
Dcalc (g cm-3)	1.5248(1)	*2.004*
F(000)	436.0 [437.74]	*536*
Dataset	-8: 8; -7:7 -34:35	-6:7; -34:35; -8:8
μ(MoKa) (/mm)	1.504	*8.013*
Tot.,Uniq.Data, R(int)	16894,2304,0.023	30730,4612,0.033
Observed reflections *I*> 2σ(*I*)	2083	4248
Nref, Npar	2304, 110	4612, 209
Final R, wR2, S	0.0350, 0.0724, 1.27	0.0408, 0.0761, 1.21
Max.residual density [e/Å3]	-0.51	-2.18
Min. residual density [e/Å3]	0.42	4.50
θrange(°)	1.5, 28.3	3.1, 28.3
Temperature (K)	200	200

Table 3.4: Selected bond distances and angles for **$[Ni(L^2)_2]$** and **$[Pt(L^2)_2]$**

$[Ni(L^2)_2]$		**$[Pt(L^2)_2]$**	
Bond	**distances (Å)**	**Bond**	**distances (Å)**
Ni1-S1	2.1817(10)	Pt1-S11	2.312(3)
Ni1-S2	2.2173(10)	Pt-S12	2.385(4)
Ni1-S1a	2.1817(10)	Pt1-S21	2.316(3)
Ni11-S2a	2.2173(10)	Pt1-S22	2.276(4)
S1-C1	1.711(3)	S11-C11	1.684(16)
S2-C1	1.706(3)	S12-C11	1.725(16)
N1-C1	1.335(19)	S21-C21	1.729(14)
N1-C2	1.301(5)	S22-C21	1.714(12)
		N1-C11	1.335(19)
		N1-C12	1.43(2)
		N2-C21	1.289(17)
		N2-C22	1.50(2)
Bond	**angles (°)**	**Bond**	**angles (°)**
S1-Ni1-S2	79.20(4)	S11-Pt1-S12	73.60(18)
S1-Ni1-S1a	100.80(4)	S11-Pt1-S21	175.7(3)
S1-Ni1-S2a	100.80(4)	S11-Pt1-S22	107.22(19)
S1a-Ni1-S2	100.80(4)	S12-Pt1-S21	103.06(15)
S2-Ni1-S2a	180.00	S12-Pt1-S22	177.43(16)
S1a-Ni1-S2a	79.20(4)	S21-Pt1-S22	76.00(15)
Ni1-S1-C1	85.72(12)	Pt1-S11-C11	89.2(5)
Ni1-S2-C1	84.73(12)	Pt1-S12-C11	85.9(5)
C1-N1-C2	126.7(3)	Pt1-S21-C21	86.0(4)
S1-C1-S2	110.28(18)	Pt1-S22-C21	87.6(5)
S1-C1-N1	123.2(3)	C11-N1-C12	128.2(13)
S2-C1-N1	126.6(3)	C21-N2-C22	125.7(11)

N1 -- H....S1	0.83(4)	2.57(4)	3.366(3)	3.666
C2 --H2A...S2	0.9900	2.7400	3.198(4)	109.00.

(a)

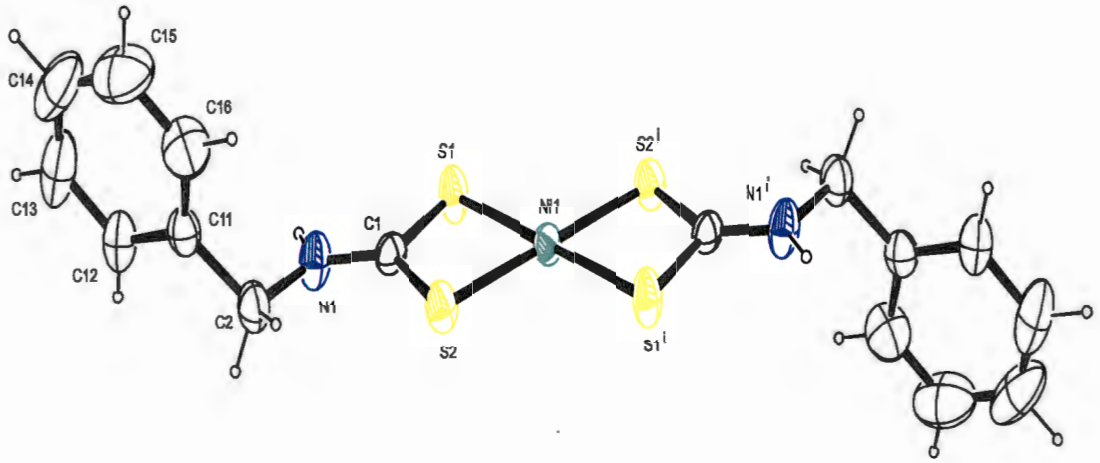

(b)

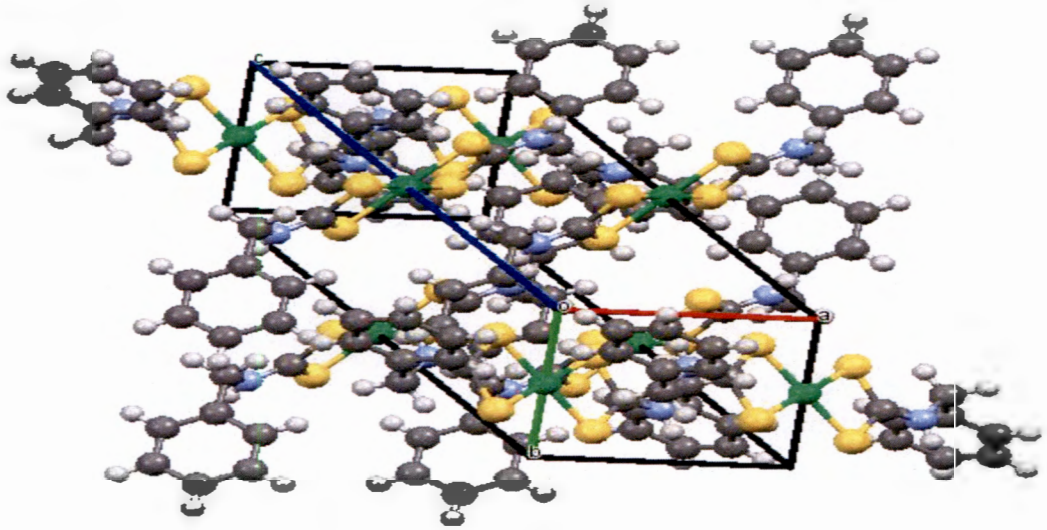

Fig.3.3: **(a)** A molecular drawing of **[Ni(L^2)$_2$]**, and **(b)** molecular structure diagram showing the packing of **[Ni(L^2)$_2$]**

(a)

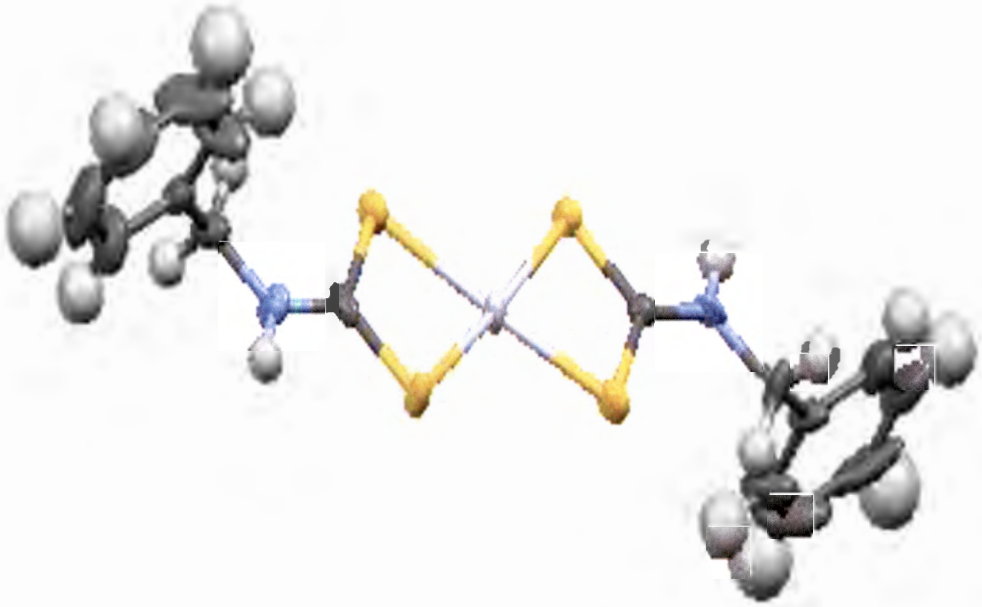

(b)

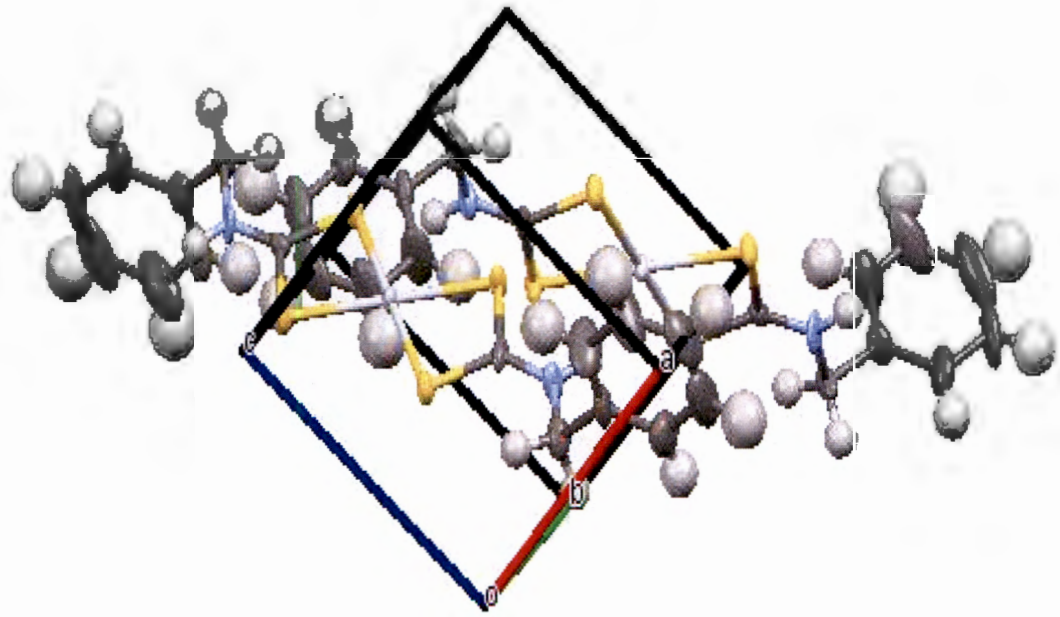

Figure 3.4. **(a)** A molecular drawing of **[Pt(L^2)$_2$]**, and **(b)**Molecular structure diagram showing the packing of **[Pt(L^2)$_2$].**

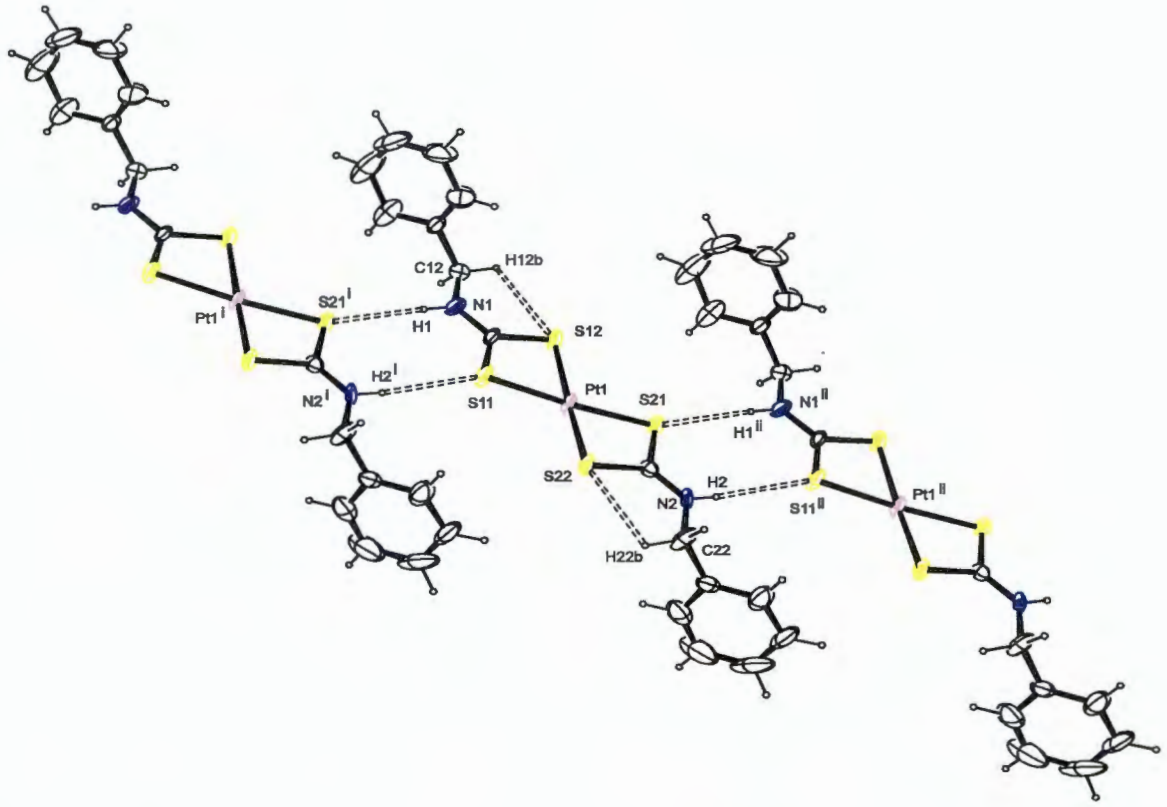

Figure 3.5: Ortep diagram for **[Pt(L^2)$_2$]** showing the hydrogen interactions ellipsoids drawn at 50 % probability. Symmetry element: (i) 1+x,y,-1+z; (ii) -1+x,y,1+z.

3.5.3. X-ray crystal structures of platinum(II) bis-(*N*-ethylphenyldithiocarbamate) [Pt(L^4)$_2$]

A yellow crystalline block with approximate dimensions of 0.47 × 0.37 × 0.26 mm of **[Pt(L^4)$_2$]** was selected under oil at ambient conditions and attached to the tip of a MiTeGenMicroMount©. The systematic absences reported in the diffraction data were found to be consistent for the *P*21/*n* space group which yielded stable results of refinement that are chemically and computationally reasonable.

The crystallographic parameters and the interatomic bond angles and distances for Pt complex of L^4 are summarized in Tables 3.5 and 3.6 respectively. Figure 3.6(a) show the bonded dithiocarbamate ligands at opposite end in a bidentate fashion to the central metal. The crystallographic packing shows that the crystal exists as 2 monomers per unit cell of the complex as presented in Figure 3.6(b). The coordination environment of the Pt(II) complex show symmetric bond lengths for Pt-S as observed from Table 3.6, [Pt(1)- S(1) = 2.3163 (6) and Pt(1)- S(2) = 2.3216 (6) Å. The complex

has distorted square planar geometry due to the small S-Pt-S bite angle S1-Pt-S2 = 74.93 (2)°. The C-S and C-N bond lengths of the corresponding dithiocarbamate ligands are: S1-C1=1.726 (3), S2-C1=1.716 (2); N1-C1=1.327 (3), N1-C2=1.423 (3) for the Pt complex and the N–H···S interactions are also shown as red dashed lines as presented in Figure 3.6(c) with symmetry positions at: (i) 3/2–*x*, ½+*y*, *z*, (ii) 1–*x*, –*y*, 1–*z*, (iii) –½+*x*, –½–*y*, 1–*z*.

The phenyl groups make angles of 87.40 (8) and 87.47 (9)° with the dithiocarbamate planes. The bond length for Pt-S in the unsubstituted phenyl complex of **L**[1] is 2.3201-2.3202 while Pt-S of the ethyl substituted in **L**[4] is 2.3163-2.3216. This revealed that the bond length is slightly reduced by the presence of the ethyl group which increases the intramolecular interactions between the atoms. This justifies the improved activities over the unsubstituted phenyl complex in most of their applications.

Table 3.5: Summary of crystal data and structure refinement of **[Pt(L[4])$_2$]**

Complex	**[Pt(L[4])$_2$]**
Empirical formula	C18H20N2PtS4
Formula weight	587.6
Crystal size (mm)	0.47 × 0.37 × 0.26
Crystal system	Monoclinic
Temperature (K)	100
Crystal habit	Block, yellow
Space group	*P*21/*n* (no. 14)
a (Å)	10.9519 (8)
b (Å)	8.2161 (6)
c (Å)	11.7276 (9)
α (°)	90
β (°)	114.009(2)
γ (°)	90
V [Å**^{3}]	963.97 (12)
Z	2
*D*calc (g cm^{-3})	2.025
F(000)	568
Dataset	-1414; -10□8;- -15□15

μ(MoKa) (/mm)	0.71073
Index range	16217, 2952
Tot.,Uniq.Data, R(int)	72891, 2086, 0.027
Observed reflections $I > 2\sigma(I)$	2157
Nref, Npar	2427, 119
Final *R*, w*R2, S*	0.018, 0.043, 1.09
Max.residual density [e/Å^3]	28.4
Min. residual density [e/Å^3]	2.2
θ range (°)	3.1–28.4

Table 3.6: Selected bond distances and angles of complex **[Pt(L^4)$_2$]**

Bonds	Distances(Å)
Pt1-S1	2.3163 (6)
Pt1—S1i	2.3163 (6)
Pt1– S2	2.3216 (6
Pt1—S2i	2.3216 (6)
S1– C1	1.726 (3)
S2– C1	1.716 (2)
N1-C1	1.327 (3)
N1-C2	1.423 (3)
N1—H1	0.80 (3)
Bond	Angle (°)
S1 – Pt1 – S11	180
S1– pt1 – S21	105.07 (2)
S1—Pt1—S2	74.93 (2)
S1—Pt1—S2i	74.93 (2)
S1—Pt1—S2i	105.07 (2)
S2—Pt1—S2	180.0

Pt1–S1 –C1	87.40 (8)
Pt1–S2– C1	87.47 (9)
C1—N1—H1	117 (2)
C1—N1—C2	130.4 (2)
C2—N1—H1	113 (2)
S2—C1—S1	110.08 (14)
N1—C1—S1	127.61 (19)
N1—C1—S2	122.30 (19)
C3—C2—N1	123.6 (2)

(a)

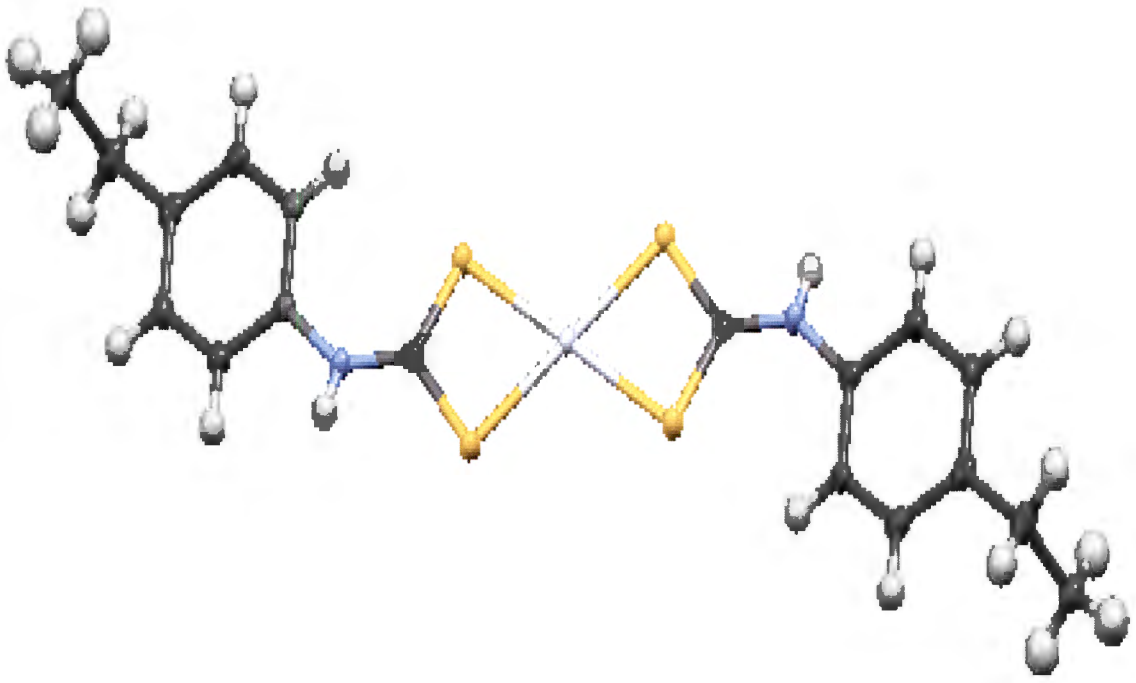

(b)

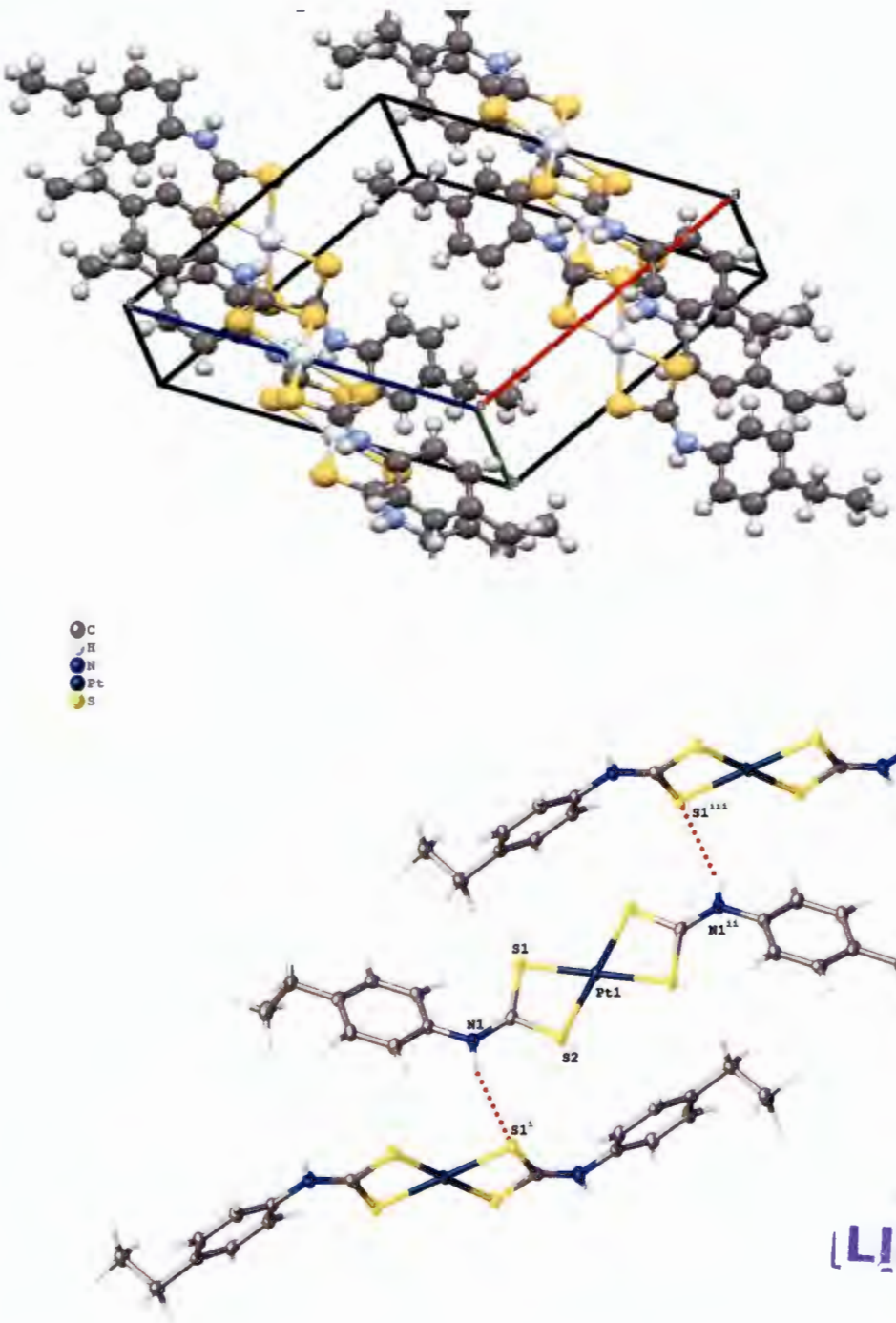

Figure 3.6. **(a)** A molecular drawing of **[Pt(L^4)$_2$]**, **(b)**Molecular structure diagram showing the packing of **[Pt(L^4)$_2$],** and **(c)** intermolecular hydrogen bonding contacts.

3.6. Thermal studies of the Ni(II), Pd(II) and Pt(II) dithiocarbamate complexes derived from primary amines

Dithiocarbamate metal complexes exhibit good thermal stability. The complexes could be classified as volatile or non-volatile. It is volatile when the solid compounds sublime at elevated temperature or the molten chelates evaporates. This generally depends on the temperature and also the nature of the ligands attached to the central metal ion. Delepine reported the thermal analysis of metal DTC. In the studies, the reported Ni(II) and Cu(II) DTCs sublime in vacuum without decomposition [19]. Benard and Borel [20] studied the thermal behaviour of some metal dithiocarbamates obtained from primary amines, and reported that the compounds decomposed with the evolution of H_2S or CS_2. The decomposition process was described to either proceed via a two-step pattern through the formation of thiocyanate as an intermediate, which then proceed to the formation of the metal sulphide or the complex could decompose directly through one-step decomposition pattern to form the metal sulphide.

Figures 3.7-3.11 present the overlapped TGA/DTG graphs of the complexes, while the relevant data from the decomposition process are presented in Table 3.7. The **[ML^1]** complexes show single step decomposition pattern from 163 to 294 °C. The Ni(II) and Pd(II) complexes yielded residues with mass 2.78/2.60 and 3.84/4.10 mg (calculated/found), which corresponded to a metal to sulphur molar ratio of 1:1 (NiS, PdS). The Pt(II) decomposed to give a residue with mass of 5.66 mg, which agreed with the calculated value of 5.57 mg and corresponded to a molar ratio 1:2 of the metal : sulphur (PtS_2)

The decomposition of **[ML^3]** and **[ML^4]** complexes followed similar single-step pattern, with the onset temperatures around 114 and 174 °C which continued to 295 and 423 °C, respectively. All conform to ratio 1:1 of metal: sulphur product to give NiS, PdS, PtS with 78, 81%, 67, 75 % and 60, 66 % weight loss for the Ni(II), Pd(II) and Pt(II) complexes respectively. The presence of the methyl and ethyl substituents on the phenyl ring decreased the volatility and increased the thermal stability of the complexes.

The **[ML^2]** complexes showed well-defined two step decomposition (Figure 3.8). The first step occurred between 169 and 194 °C, with a 35% mass loss which corresponded to the loss of the benzyl group, and the formation of thiocyanate intermediate. The second step started instantaneously after the first with a 73% loss in the range 194 – 255 °C to yield NiS_2 (46%) as residue [21], [22] (mass: found 3.03; calculated, 3.22).

In the thermal graph of **[ML^5]** complexes, two distinct decomposition patterns were also observed for the Ni(II), the first step started around 176 °C and continued to 226 °C with 23% decomposition

of the organic portion of the ligand to give the metal thiocyanate. The second step decomposition occurred in the range 261 - 535 °C, with about 66% mass loss which corresponded to the formation of Ni_2S_3. However, the graphs of Pd(II) and Pt(II) complexes of $\mathbf{L^5}$ showed a single-step decomposition which occurred between 181 and 254 °C, resulting into the formation of the metal sulphides Pd_4S and Pt_2S_4 respectively.

To show the variation in the temperature of maximum rate of decomposition within the complexes of similar ligand moiety, their respective DTG graphs were overlapped. Figures 3.6b - 3.10b present the overlapped DTG graphs which conspicuously show the changes in their decomposition peaks as a function of both the types of central metal ions and also the ligand type.

All of the complexes studied showed good thermal stability, and gave the respective metal sulphides. Hence, could be used as single source precursors (SSP) for the preparation of their respective metal sulphide nanoparticles [23]

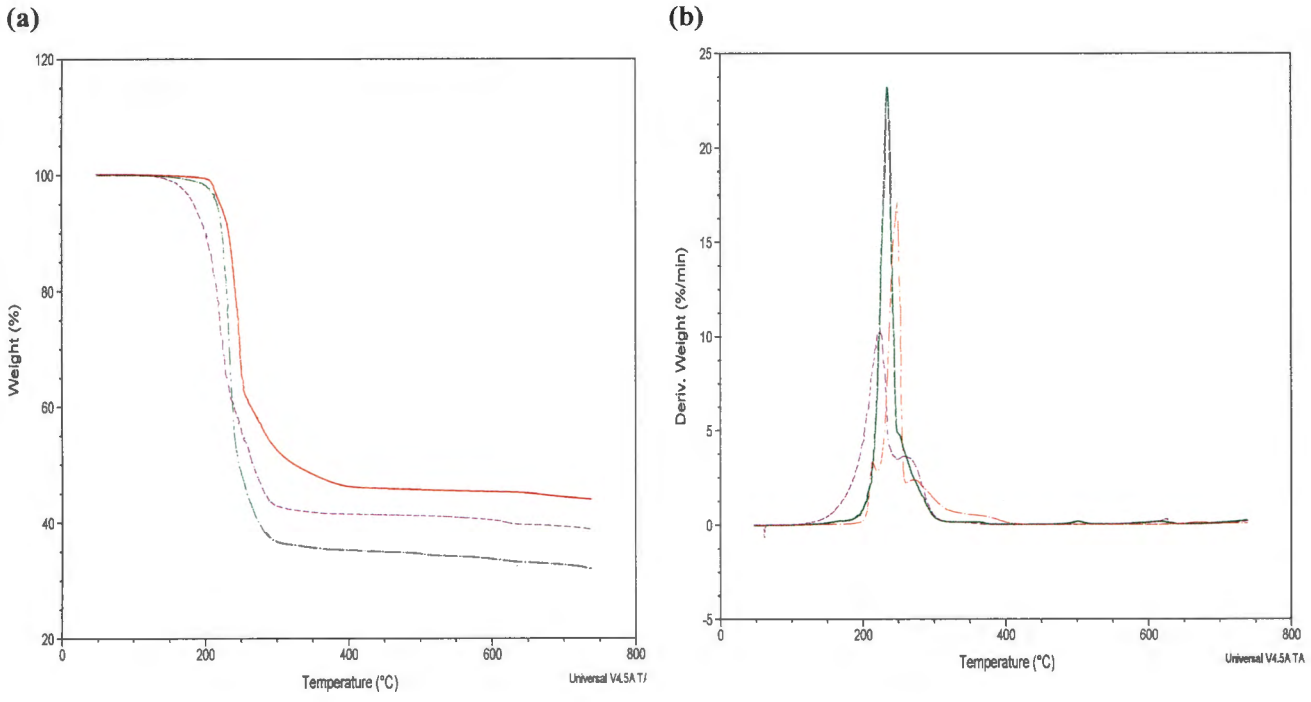

Figure 3.7: (a) TG and (b) DTG of Ni (green), Pd (purple), and Pt (red) complexes of $\mathbf{L^1}$

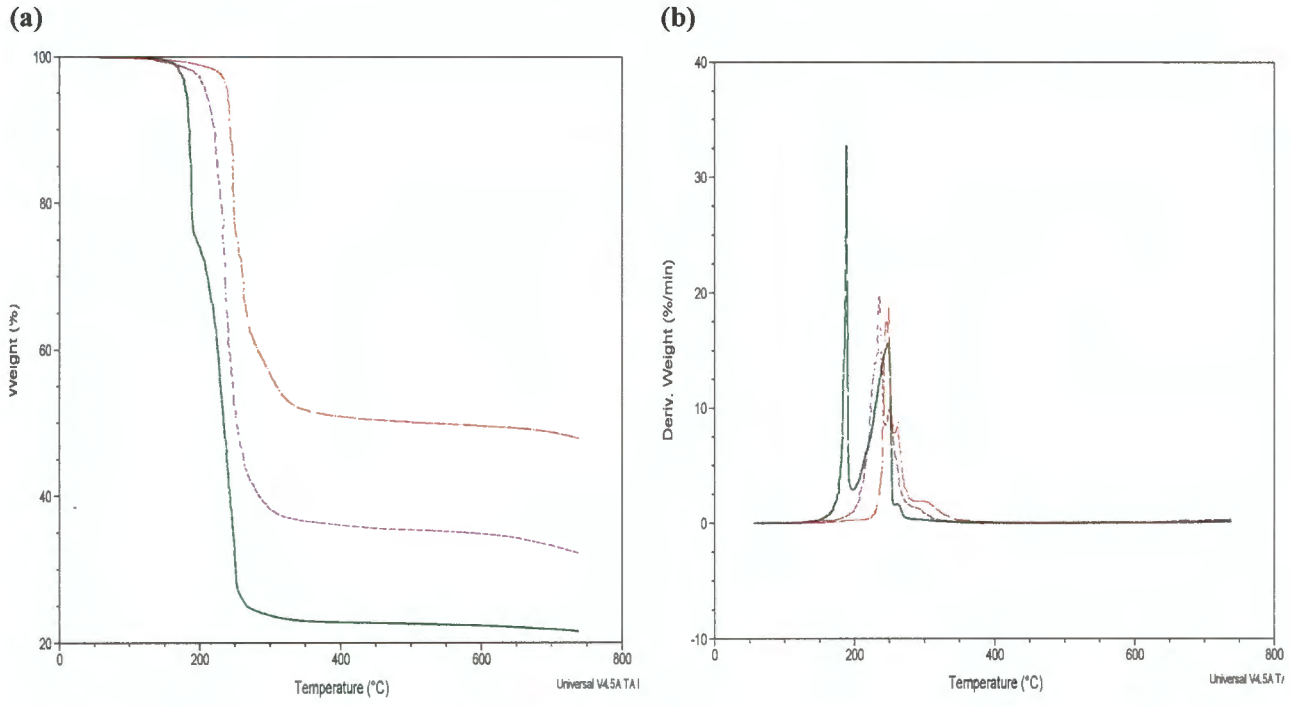

Figure 3.8: (a) TG and (b) DTG of Ni (green), Pd (purple), and Pt (red) complexes of

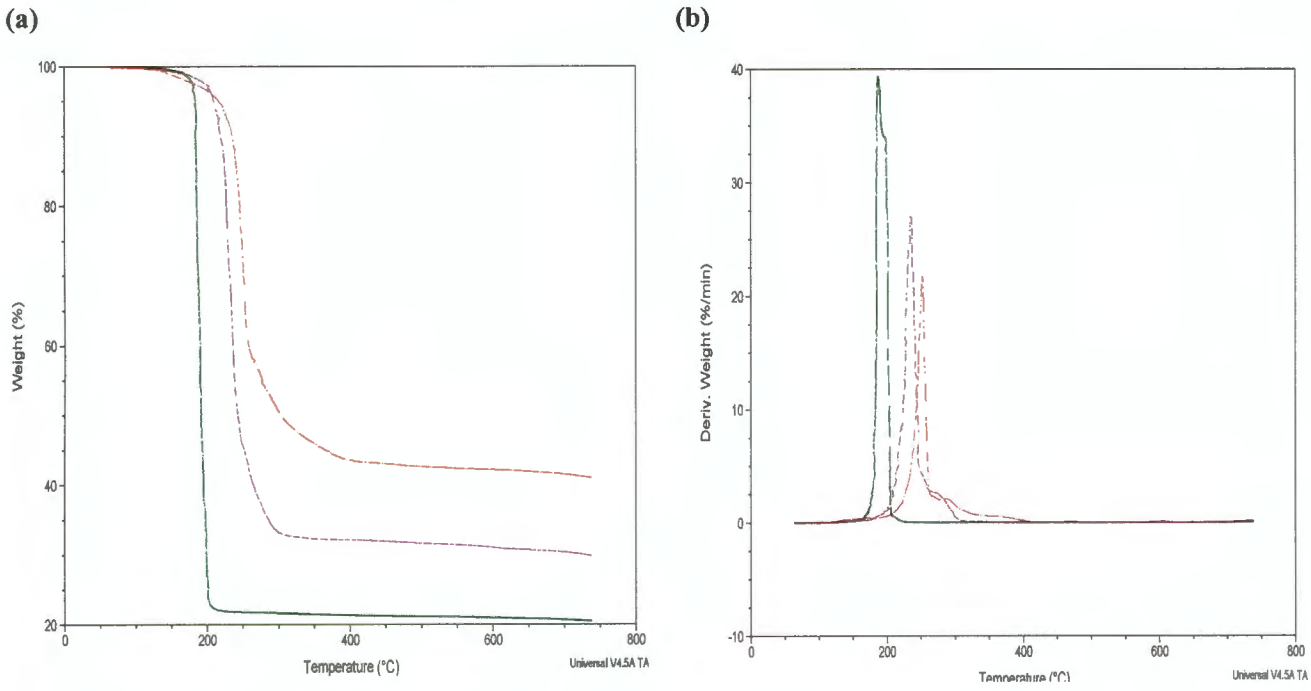

Figure 3.9: (a) TG and (b) DTG of Ni (green),Pd (purple), and/Pt (red) complexes of $\mathbf{L^3}$

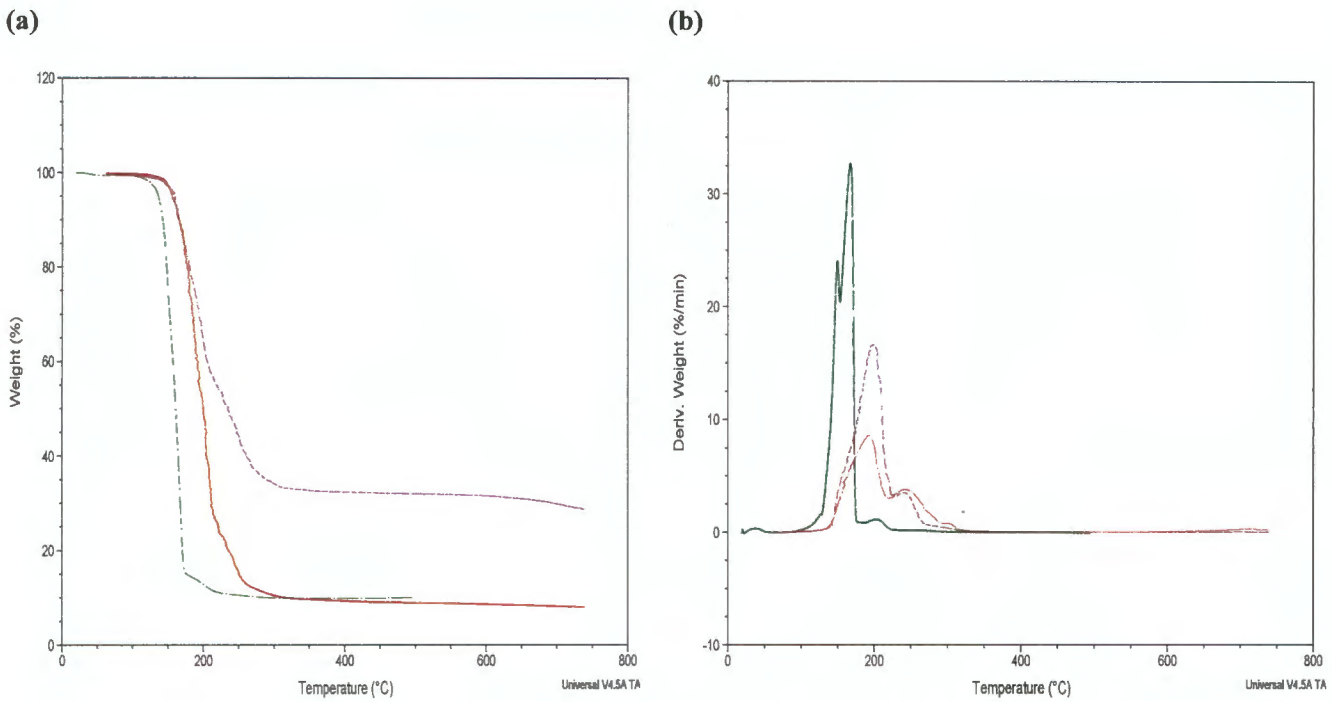

Figure 3.10: (a) TG and (b) DTG of Ni (green), Pd (purple), and/Pt (red) complexes of $\mathbf{L^4}$

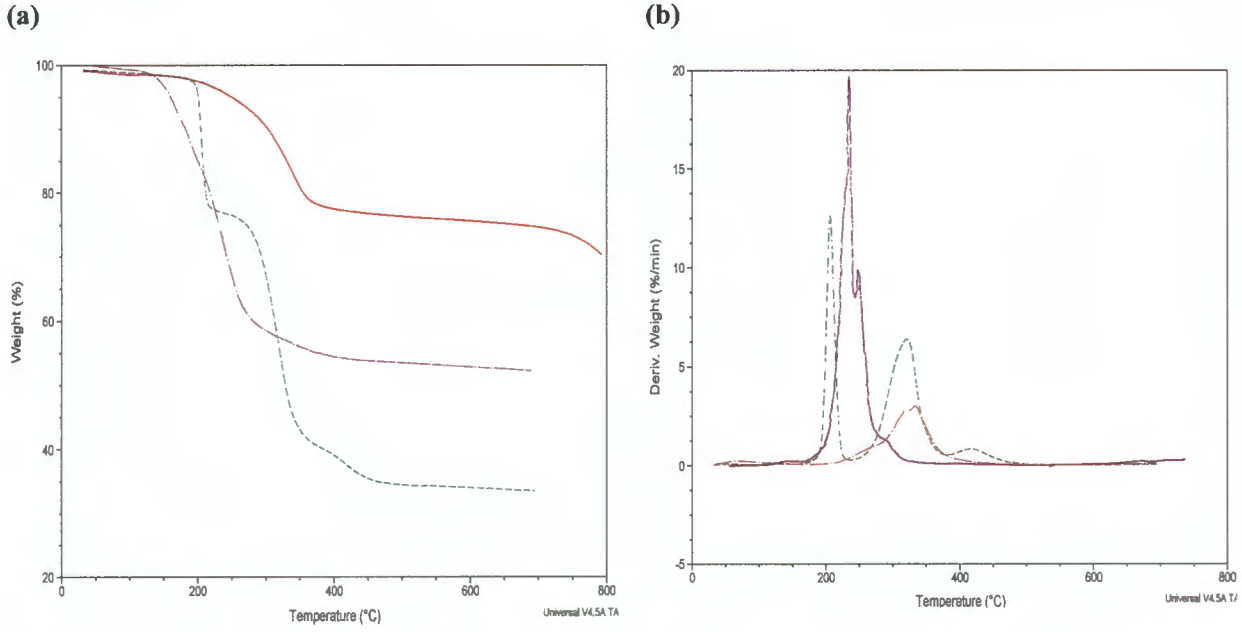

Figure 3.11: (a) TG and (b) DTG of Ni (green), Pd (purple), and/Pt (red) complexes of $\mathbf{L^5}$

Table 3.7: Thermal stability data for the prepared complexes

Compound	Decomposition range (◦C)	Peak Temp (◦C)	Weight Loss (%)	Product obtained	Mass change (mg) (calc/Found)
$[Ni(L^1)_2]$	163 - 215	192	75	NiS	2.78/2.60
$[Pd(L^1)_2]$	269 - 290	232	68	PdS	3.84/4.10
$[Pt(L^1)_2]$	199 - 300	250	54	PtS_2	5.65/5.57
$[Ni(L^2)_2]$	174 - 209	187	78	NiS	2.39/2.23
$[Pd(L^2)_2]$	171 - 305	234	67	PdS	3.40/3.24
$[Pt(L^2)_2]$	213 - 380	252	60	PtS	4.95/4.59
$[Ni(L^3)_2]$	127-170	165	81	NiS	0.64/0.67
$[Pd(L^3)_2]$	144 - 274	200	75	PdS	3.30/3.60
$[Pt(L^3)_2]$	138 - 450	191	66	PtS	4.40/4.70
$[Ni(L^4)_2]$	169 -194	187	25	$HNCS_2Ni$	3.03/2.50
	194-255		74	NiS_2	
$[Pd(L^4)_2]$	168 - 306	234	62	PdS_2	4.48/4.23
$[Pt(L^4)_2]$	228 - 309	248	50	PtS_2	5.81/5.34
$[Ni(L^5)_2]$	176 – 226	207	23	$2NCS_2Ni$	15.89/14.90
	261 - 535	321	66	Ni_2S_3	7.07/6.83
$[Pd(L^5)_2]$	181 -248	333	50	Pd_4S	7.27/6.46
$[Pt(L^5)_2]$	191 -254	335	30	Pt_2S_4	1.97/1.56

3.7. Preparation of dithiocarbamate ligands from secondary amines

A one-pot, three-component synthetic route to dithiocarbamates [24]was employed for the synthesis of the ligands from two secondary amines.

3.7.1. Synthesis of ammonium *N*-methyl-*N*-ethanoldithiocarbamate (L^6)

N-methyl–*N*-ethanolamine (0.8 mL, 0.01 mol) was added to CS_2 (0.6 mL, 0.01 mol) and the solution was stirred in ice. After 30 min, NH_4OH (3.0 mL, 0.01mol) was added and stirred for 3 h resulting into faint yellowish solution of ammonium *N*-methyl-*N*-ethanoldithiocarbamate.

3.7.2 Synthesis of M(II) bis-(*N*-methyl-*N*-ethanoldithiocarbamate) complex (M = Ni, Pd, and Pt)

To the aqueous solution of ammonium *N*-methyl-*N*-ethanoldithiocarbamate (L^7), 15 mL aqueous solution of 0.005 mol of the respective metal salts ($NiCl_2{\cdot}6H_2O$, 1.19 g; Na_2PdCl_4, 1.48 g; K_2PtCl_4, 2.08g), was added and the solution was stirred for 40 min to give different coloured precipitates. The product was filtered, rinsed thoroughly with water and dried under vacuum.

(16) $[Ni(L^6)_2]$: Yield, 1.66 g (92%); M.pt: 215 – 217 °C; Selected IR, $\upsilon(cm^{-1})$: 1470 (C=N), 1237 (C_2–N), 980 (C=S), 2996 (H_2C–H), 412 (Ni-S), 3132 (O-H); ^{1}HNMR ($CDCl_3$) δ (ppm)= 3.1 (s, 6H, CH_3), 2.5 (t, 4H, $C\underline{H_2}CH_2OH$), 3.5 (t, 4H, $CH_2C\underline{H_2}OH$), 5.0 (s, 2H, $O\underline{H}$).^{13}C NMR ($CDCl_3$) δ (ppm)= 57.7 ($CH_2\underline{C}H_2OH$), 54.4 ($\underline{C}H_2CH_2OH$), 40.0 ($\underline{C}H_3$), 205.2 (–$\underline{C}S_2$); $C_8H_{16}N_2O_2S_4Ni$ (359.18): Calculated: C, 26.75; H,4.49, N, 7.80; S, 35.75. Found: C, 26.50; H, 4.20, N, 7.43; S, 35.55%.

(17) $[Pd(L^6)_2]$: Yield, 1.93 g (95%); M.pt: 220 – 223 °C; Selected IR, $\upsilon(cm^{-1})$: 1461(C=N), 1253 (C_2–N), 974 (C=S), 2867 (H_2C–H), 413 (Pd-S), 3206 (O-H); ^{1}H NMR (DMSO) δ = 3.5 (s, 6H, CH_3), 2.0 (t, 4H, $C\underline{H_2}CH_2OH$), 2.6 (t, 4H, $CH_2C\underline{H_2}OH$), 5.0 (s, 2H, OH). ^{13}C NMR (DMSO) δ (ppm)=57.1 ($CH_2\underline{C}H_2OH$), 54.1 ($\underline{C}H_2CH_2OH$), 30.8 (NCH_3), 206.9 (–CS_2); $C_8H_{16}N_2O_2S_4Pd$ (406.90): Calculated: C, 23.61; H,3.96, N, 6.88; S, 31.52. Found: C, 23.67; H, 3.40, N, 6.44; S, 31.80%.

(18) $[Pt(L^6)_2]$: Yield, 2.11 g (85.1%); M.pt: 240 – 242 °C; Selected IR, $\upsilon(cm^{-1})$: 1473 (C=N), 1254 (C_2–N), 974 (C=S), 2867 (H_2C–H), 417 (Pt-S), 3239 (O-H); ^{1}H NMR (DMSO) δ (ppm) = 3.7 (t, 6H, $C\underline{H_3}$), 2.5 (t, 4H, $C\underline{H_2}CH_2OH$), 2.7 (t, 4H, $CH_2C\underline{H_2}OH$), 5.0 (t, 2H, $O\underline{H}$); ^{13}C NMR(DMSO) δ (ppm)= 31.2 (CH_3), 58.4 ($CH_2\underline{C}H_2OH$), 53.9 ($\underline{C}H_2CH_2OH$), 207.3 (–$\underline{C}S_2$); Calculated:– $C_8H_{16}N_2O_2S_4Pt$ (495.57): C, 19.39; H,3.25; N, 5.65; S, 25.88. Found: C, 19.80; H, 3.45; N, 5.20; S, 25.40%.

3.7.3. Synthesis of ammonium *N*-ethyl-*N*-ethanoldithiocarbamate ($\bar{L}^7$)

N-ethyl-*N*-ethanolamine, (0.98 mL, 0.01 mol) was reacted with CS_2 (0.6 mL, 0.01 mol) in ice for 30 min. To this mixture, NH_4OH (3.0 mL, 0.01 mol) was added and the solution was stirred for 3 h to afford a yellowish white solution.

3.7.4 Preparation of M(II) bis-(*N*-ethyl-*N*-ethanoldithiocarbamate) complexes (M = Ni, Pd, Pt)

A water-ethanol (1:1) solution of 0.005 mol of the respective metal salts ($NiCl_2.6H_2O$, 1.19 g; Na_2PdCl_4, 1.48 g; K_2PtCl_4, 2.08 g) was added to the aqueous solution of ammonium-*N*-ethyl-*N*-ethanoldithiocarbamate ($\mathbf{L^7}$) in separate reaction systems and stirred for 1 h. The respective complex was filtered, rinsed with ethanol: water solution and dried in vacuum.

(19) [Ni($\mathbf{L^7}$)$_2$]: Yield, 1.83 g (94%); M.pt: 220 – 222 °C; Selected IR, υ(cm^{-1}): 1461 (C=N), 1256 (C_2-N), 989 (C=S), 2871 (H_2C=H), 413 (Ni-S), 3318 (O-H); ^{1}HNMR (DMSO) δ (ppm)= 1.15 (t, 6H, $CH_2C\underline{H_3}$), 3.36 (q, 4H, $C\underline{H_2}CH_3$), 2.50 (t, 4H, $C\underline{H_2}CH_2OH$), 3.60 (t, 4H, $CH_2C\underline{H_2}OH$), 5.0 (s, 2H, CH_2CH_2OH); ^{13}C NMR (DMSO) δ (ppm) = 12.3 ($CH_2\underline{C}H_3$), 45.5 ($\underline{C}H_2CH_3$), 51.0 ($\underline{C}H_2CH_2OH$), 58.1 ($CH_2\underline{C}H_2OH$), 204.7 (-$\underline{C}S_2$); Calculated: ($C_{10}H_{20}N_2O_2S_4Ni$ (387.32): C, 31.02; H, 5.10; N, 7.23; S, 33.12; Found: C, 31.63; H, 5.40; N, 7.12; S, 32.72%. Single crystals suitable for X-ray analysis was obtained for the Pd(II) by the slow evaporation of two solvent systems, methanol: acetonitrile (4:1).

(20) [Pd($\mathbf{L^7}$)$_2$]: Yield: 1.84 g (84.7%); M.pt: 230 – 233 °C; Selected IR, υ(cm^{-1}): 1490 (C=N), 1267 (C_2-N), 984 (C=S), 2869 (H_2C=H), 442 (Pd-S), 3326 (O-H) ; ^{1}HNMR (DMSO) δ (ppm) = 1.18 (t, 6H, $CH_2C\underline{H_3}$), 3.36 (q, 4H, $C\underline{H_2}CH_3$), 2.50 (t, 4H, $C\underline{H_2}CH_2OH$), 3.74 (t, 4H, $CH_2C\underline{H_2}OH$), 5.0 (s, 2H, $CH_2CH_2\underline{OH}$); ^{13}C NMR (DMSO) δ (ppm)=12.3 ($CH_2\underline{C}H_3$), 46.1 ($\underline{C}H_2CH_3$), 51.0 ($\underline{C}H_2CH_2OH$), 60.0 ($CH_2\underline{C}H_2OH$), 208.4 (-CS_2). Calculated: $C_{10}H_{20}N_2O_2S_4Pd$ (434.96): C, 27.60; H, 4.63; N, 6.44; S, 29.49. Found: C, 27.20; H, 4.20; N, 6.65; S, 29.80%.

(21) [Pt($\mathbf{L^7}$)$_2$]: Yield: 1.55 g (59.2%); M.pt: 245 – 247 °C; Selected IR, υ(cm^{-1}): 1506 (C=N), 1290 (C_2-N), 983 (C-S), 2869 (H_2C=H), 443 (Pt-S), 3327 (O-H); ^{1}HNMR (DMSO) δ (ppm) = 1.2 (t, 6H, $CH_2C\underline{H_3}$), 3.3 (q, 4H, $C\underline{H_2}CH_3$), 2.5 (t, 4H, $C\underline{H_2}CH_2OH$), 3.6 (t, 4H, $CH_2C\underline{H_2}OH$), 5.0 (s, 2H, CH_2CH_2OH).^{13}CNMR (DMSO) δ (ppm) = 11.7 ($CH_2\underline{C}H_3$), 45.5 ($\underline{C}H_2CH_3$), 51.2 ($N\underline{C}H_2CH_2OH$), 57.8 ($NCH_2\underline{C}H_2OH$), 208.9 (-$\underline{C}S_2$). Calculated: $C_{10}H_{20}N_2O_2S_4Pt$ (523.62): C, 22.94; H, 3.85; N, 4.70; S, 24.50. Found: C, 22.56; H, 3.50; N, 5.35; S, 24.75%.

3.8. Results and discussion of Ni(II), Pd(II) and Pt(II) complexes of dithiocarbamate prepared from secondary amines

3.8.1. General synthesis of dithiocarbamate complexes from ligands obtained from secondary amines

The ligands were produced by one-pot, three-component route as presented in Scheme 3.5 a by stirring the amine, CS_2 and the base in ice for 3 h. After the formation of the ligands, aqueous solutions of the respective metal salts were added in-situ to afford the different coloured precipitates. The complexes were prepared with differing ligand chain length (R = CH_3, CH_2CH_3) (Scheme 3.5 b) and different shades of green colour for the nickel, orange for the palladium and yellow for the platinum complexes were generated immediately the solution of the metal salts were added to the dithiocarbamate solutions. Good yields ranging from 60 to 95% were obtained compared to the yields when primary amines were used. They were soluble in different organic solvents such as chloroform, dichloromethane, methanol, ethanol, acetonitrile.

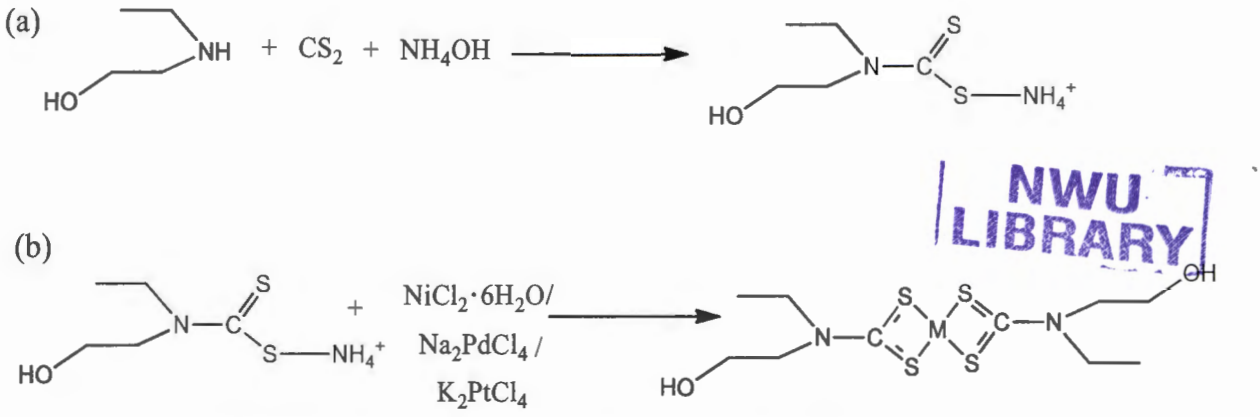

Scheme 3.5: General synthetic route for the preparation of (a) dithiocarbamate ligands (L^6 and L^7) and (b) complexes from secondary amines (R= CH_3, CH_2CH_3; M= Ni, Pd, Pt).

3.8.2. Infrared spectral studies of Ni(II), Pd(II) and Pt(II) complexes of dithiocarbamate btained from secondary amines sources

The thioureide bands were observed in the range 1433 – 1473 and 1470 – 1518 cm^{-1} in the spectra of the complexes of L^9 and L^{10} respectively. These bands define the carbon-nitrogen bond order between a single bond in the range 1250 – 1350 cm^{-1} and a double bond in the range 1640 – 1690 cm^{-1} [25]. The peak due to the (C-S) stretching vibration occurred in the range 974 – 980 cm^{-1} and 983 – 996 cm^{-1} for the **L^6** and **L^7** complexes, indicating a bidentate chelating form of the ligand towards the metal ion through the two sulphur atoms [26]. The O-H stretching vibration, which

occurred as a broad band around 3300 cm^{-1}, increased down the group from the nickel to the platinum of the L^6 and L^7 complexes. The bands which appeared at the far IR region around 412-443 cm^{-1} represent the metal-sulphur bands. The results observed revealed increase in the vibrations for all the peaks as a result of increase in chain length of the substituent on the nitrogen atom.

3.8.3. Electronic spectral studies of the metal(II) complexes of dithiocarbamate obtained from primary ammine

For the complexes **$[Ni(L^6)_2]$** to **$[Ni(L^{10})_2]$**, the electronic spectra of the complexes gave absorption bands due to electronic transitions within the ligands at 320- 390 nm which are assigned to $n \rightarrow p^*$, $p \rightarrow p^*$ (metal to ligands and ligand to metal charge transfer transitions) [27]. The two bands in the range 400-540 nm in all the complexes are typical of square planar group10 dithiocarbamate complexes, and are assigned to metal d-d transition.

3.8.4. NMR Spectral studies of Ni(II), Pd(II) and Pt(II) complexes of dithiocarbamate prepared from secondary amines

In the H NMR spectra of the complexes, the signals of the methyl protons ($-CH_3$) appeared in the range 2.5 - 3.7 ppm for the L^6 and at 1.15-1.20 ppm for the L^7 complexes. The signals around 2.50 - 3.36 ppm, which appeared as a quartet in L^7 complexes, correspond to the protons of the $-CH_2$ attached to the nitrogen atom. The triplet signals around 2.5 - 3.5 ppm and at 3.60 - 3.74 ppm correspond to the proton of the CH_2 bearing the hydroxyl group in the complexes. The proton of the hydroxyl group appeared around 5.0 ppm as a singlet in all the complexes. The presence of the highly electronegative oxygen confers a higher resonant value due to deshielding effect.

The ^{13}C NMR spectra of the complexes showed three signals ascribed to the aliphatic carbons in the range 27.7- 58.4 for the L^6 complexes, while four signals were observed for the L^7 complexes in the range 12.0 - 58.1 ppm. The most important signal is the low field $-CS_2$ resonance, which in all the complexes, was observed in the range 205 -207 ppm and 204 - 208.9 for the complexes of L^6 and L^7 respectively. A gradual increase down the triad was observed. This shows that apart from complexation, ionic radii have some effect on the chemical shifts of the complexes as heavier atom complexes have higher resonant values than their lighter atom complexes.

3.8.5. Description of crystal structure of Pd(II) bis-(*N*-ethyl-*N*-ethanoldithiocarbamate) $[Pd(L^7)_2]$ complex

Crystallographic data for **$[Pd(L^7)_2]$** are given in Table 3.9, and selected bond lengths and angles are presented in Table 3.10. Figure 3.14a presents the molecular drawing of **$[Pd(L^7)_2]$** with 50% probability ellipsoids, while Figure 3.14b presents the packing diagram. The structure is a square

planar centrosymmetrical complex of Pd with two bidentate dithiocarbamate ligands. The Pd-S bond lengths are 2.3156(5) and 2.3208(6) Å, and the C1-N1 and C4-N1 bond lengths are 1.319(3) and 1.48(2) Å respectively. The distances are comparable to the normal bond distances for C=N and C-N (1.28 and 1.47 Å). The ethanol group of the ligand has positional disorder in a 0.68:0.32 ratio. There are intermolecular hydrogen bonds between adjacent ethanol groups of distance 1.64 Å between major disordered components and 2.10 Å between the major and minor disordered components. These O-H...O interactions form two infinite chains in the structure. There are two intramolecular C-H....S interactions of length 2.57 and 2.65 Å (C4-H4....S2 and C2-H2...S1 respectively), and three longer intermolecular interactions of 2.94, 3.00 and 2.99 Å (C3-H3B...S1, C2-H2A … S2 and C5-H5A … S2 respectively).

Each complex has two C-H …π ring interactions with the rings formed by Pd1, S1, C1 and S2. The hydrogen to centroid distance is 2.81 and 2.74 Å with the major C5-H5A component and minor C7-H7B component respectively.

Table 3.8: Summary of crystal data and structure refinement of **[Pd(L^7)$_2$]**

Complex	**[Pd(L^7)$_2$]**
Empirical formula	$C_{10}H_{20}N_2O_2PdS_4$
Formula weight	434.92
Crystal size (mm)	0.13 x 0.13 x 0.44
Crystal system	Tetragonal
Temperature (K)	200
Crystal habit	green blocks
Space group	P42/n(No. 86)
a (Å)	16.465(5)
b (Å)	16.465(5)
c (Å)	6.177(3)
α (°)	90
β (°)	95.021(2)
γ (°)	90
V [Å**3]	2843.9(3)
Z	4
*D*calc (g cm^{-3})	1.725
F(000)	880

Dataset	-21:21;-21:21;-8:8
μ(MoKa) (/mm)	1.605
Index range	16217, 2952
Tot.,Uniq.Data, R(int)	72891, 2086,0.023
Observed reflections $I > 2\sigma(I)$	1901
Nref, Npar	2086, 100
Final *R*, w*R2*, *S*	0.0242,0.0676,1.07
Max.residual density [e/Å^3]	1.00
Min. residual density [e/Å^3]	-0.45
θ range (°)	1.2- 28.3

Table 3.9: Selected bond distances and angles of complex **[Pd(L^7)$_2$]**

[Pd(L^7)$_2$]	
Bonds	Distances (Å)
Pd1-S1	2.3156(5)
Pd1– S2	2.3208(6)
S1– C1	1.724(2)
S2– C1	1.720(2)
N1-C1	1.319(3)
N1-C4	1.48(2)
Bond	Angle (°)
S1 – Pd1 – S1^1	180
S1– pd1 – S2^1	104.32(2)
Pd1–S1 –C1	86.48(8)
Pd1–S2– C1	86.42(8)
C1–N1 –C4	121.3(19)

(a)

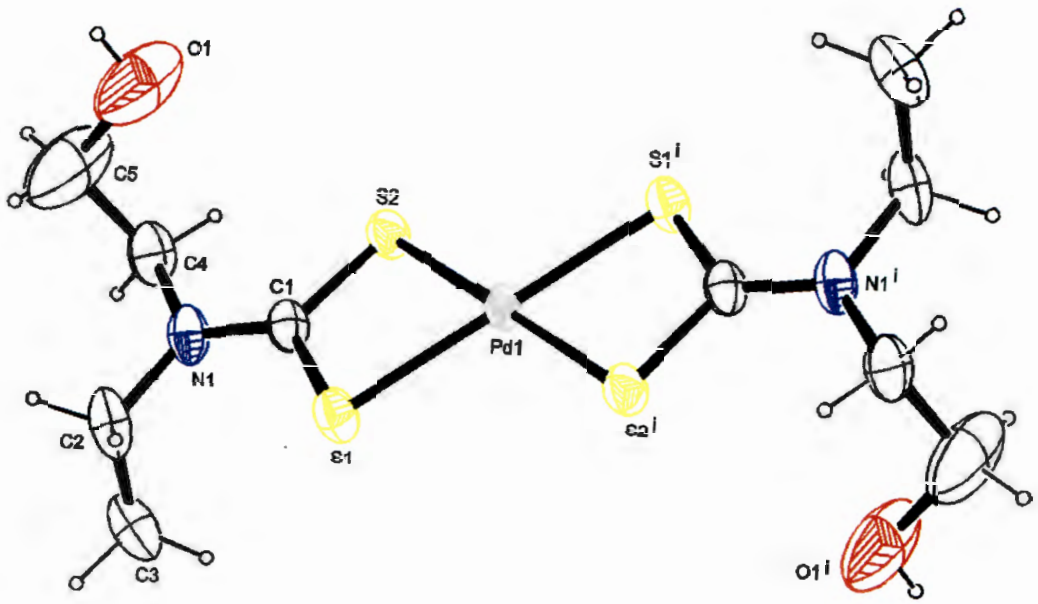

(b)

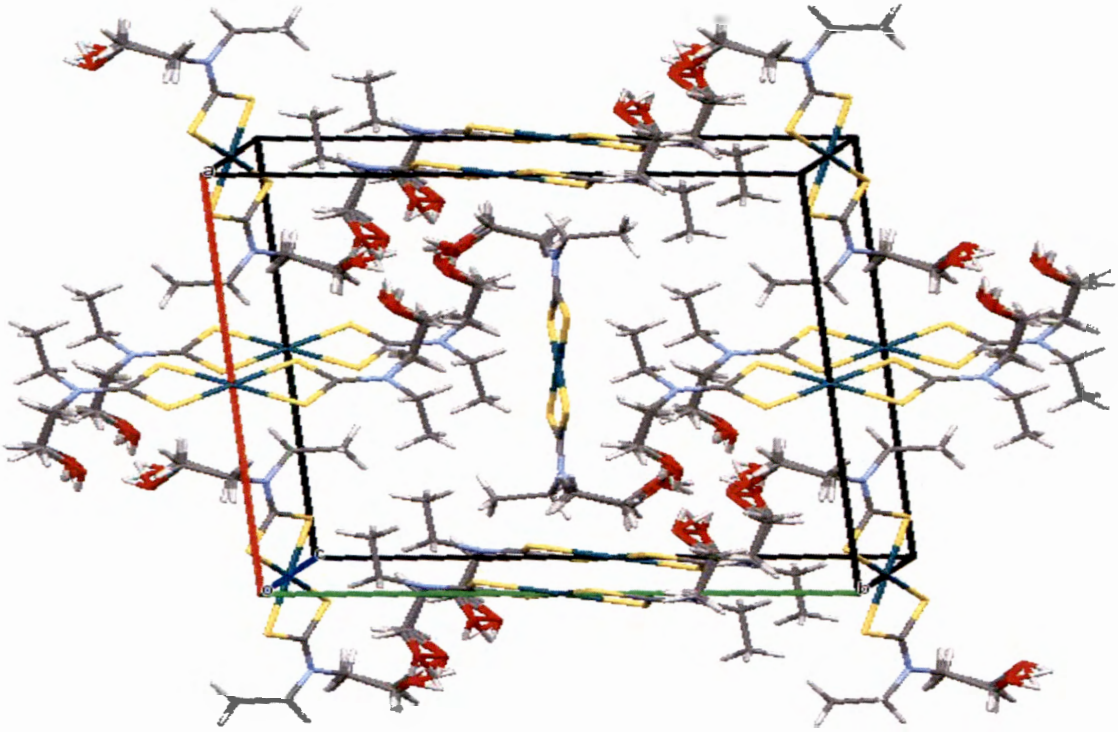

Fig.3.14: **(a)** A molecular drawing of **[Pd(L^7)$_2$]** shown with 50% probability ellipsoids, showing the major disorder component of the molecule of the asymmetric unit, and **(b)** The packing diagram with hydrogen bonding interactions. Only major disorder components are shown.

3.8.6. Thermal studies of of Ni(II), Pd(II) and Pt(II) complexes of dithiocarbamate prepared from secondary amines

The relevant data from the thermal decomposition process are presented in Table 3.11. The thermal graphs of the Ni(II), Pd(II) and Pt(II) complexes of $\mathbf{L^6}$ and $\mathbf{L^7}$ are presented in Figures 3.15-3.16, and they showed decomposition occurred in the range (195-275, 224 – 256 and 217 – 285), (212-258, 225-302 and 203-690) °C, with 75, 59 and 48; 76, 61 and 50.0% loss respectively. In all the complexes, the onset of decomposition temperature was about 200 °C, and this indicated there was no loss of solvent molecules. The ligand components have close temperatures of desorption; so, they underwent a simultaneous decomposition, yielding the metal sulphides directly in a single step. The calculated mass of nickel, palladium and platinum sulphides left as residue from the complexes after decomposition were 25% (2.77 mg), 31% (5.27 mg), 42% (5.97 mg) for the $\mathbf{L^6}$ complexes; 24% (3.10 mg), 41% (4.60 mg), and 50% (5.61 mg) for the $\mathbf{L^7}$ complexes. These values were in good agreement with the weight of NiS, PdS_2, PtS_2 for all the complexes.

The thermogravimetric data revealed that the complexes from secondary amine dithiocarbamates are thermally more stable than those from the primary amines, with decomposition occurring in the range 195-690 °C and 138-450 °C respectively. All the complexes have good thermal stability and decomposed to their respective metal sulphides on heating. They can therefore serve as single source precursors (SSP) for metal sulphide nanoparticle synthesis.

Table 3.10: Thermal data for the complexes prepared from secondary amines

Compounds	Decomposition Range (°c)	Peak temp (°c)	Weight loss (%)	Product obtained	Residual mass Found/cald (mg)
$[Ni(L^6)_2]$	195 -275	221	75	NiS	2.77/2.79
$[Pd(L^6)_2]$	224 - 256	232	59	PdS_2	5.27/5.28
$[Pt(L^6)_2]$	217 - 285	254	48	PtS_2	5.97/5.91
$[Ni(L^7)_2]$	212 – 258	222	76	NiS	3.10/2.97
$[Pd(L^7)_2]$	225 - 325	240	61	PdS_2	4.60/4.59
$[Pt(L^7)_2]$	203 - 690	234	50	PtS_2	5.61/5.59

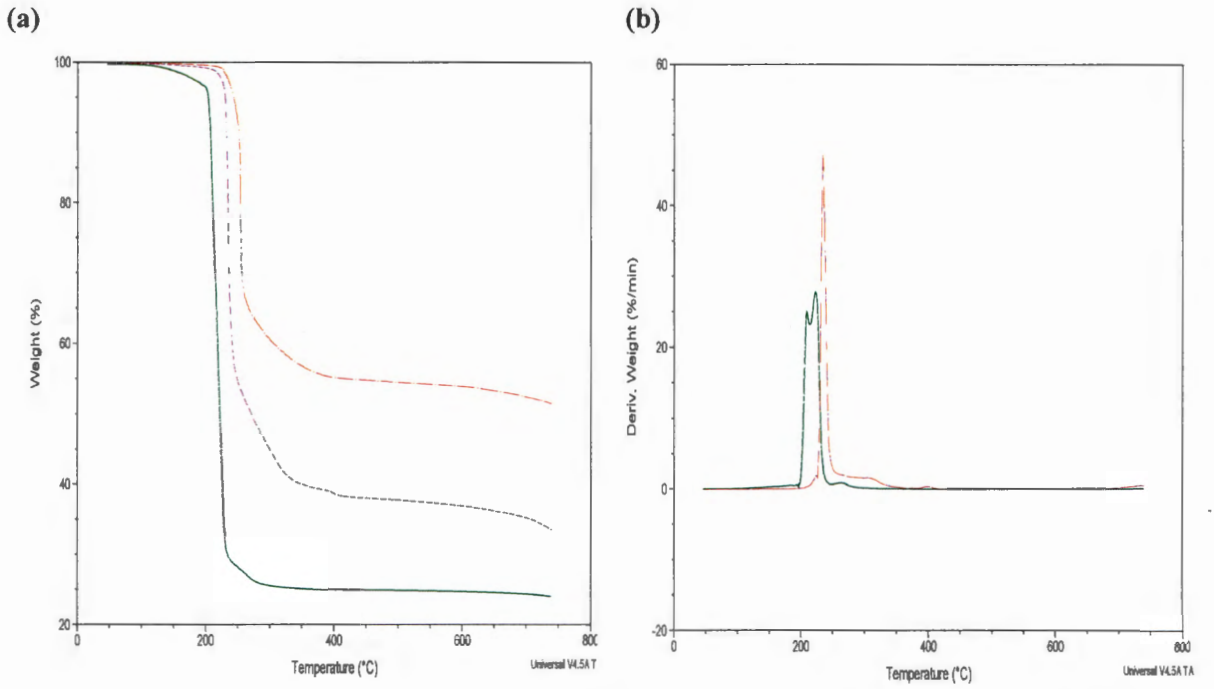

Figure 3.15: **(a)** TG and **(b)** DTG graphs of **[Ni(L^6)$_2$]** (green), **[Pd(L^6)$_2$]** purple), and **[Pt(L^6)$_2$]** (red) complexes.

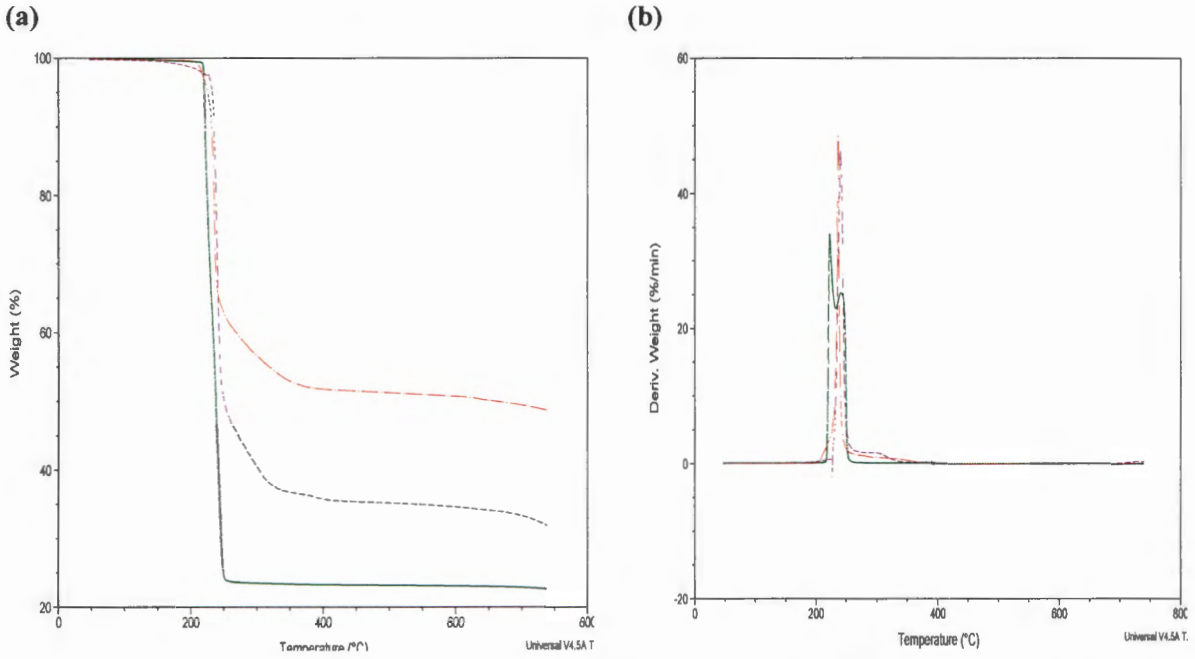

Figure 3.16: **(a)** TG and **(b)** DTG graphs of **[Ni(L^7)$_2$]** (green), **[Pd(L^7)$_2$]** purple), and **[Pt(L^7)$_2$]** (red) complexes.

3.9. Preparation of dithiocarbamate ligands from secondary amines derived from Schiff base via condensation reactions.

The dithiocarbamate ligands from Schiff bases were synthesized in three stages:

(i) Conversion of the primary amine via Schiff base condensation reaction with an aldehyde (reflux) to form an imine. A few drops of acetic acid were added as acid buffer to activate the C=O and also facilitate the dehydration process, but without inhibiting the nucleophile.

(ii) Reduction of the imine by the addition of $NaBH_4$ [(1: 3) (in ice)] to give the secondary amine.

(iii) Dithiocarbamate formation through the reaction of the secondary amine with CS_2 (1:1) and Et_3N (1:3), to trap H_2 and other impurities.

3.9.1. Preparation of carboxyl-4- naphty-1-amine

About 20 mL ethanol solution of naphtyl-1-aniline (1.43 g, 0.01 mol) was refluxed with 20 mL ethanol solution of carboxyl-4- formaldehyde (1.5 g, 0.01 mol) for 2 h, with the addition of few drops of acetic acid as shown in Scheme 3.5. A yellow precipitate of carboxyl-4- naphty-1-imine was formed which was filtered, rinsed and dried. Selected IR- $\nu(cm^{-1})$: 3045 (-C=H), 3323 (OH), 1606 (C=N), 760 (naphthalene ring), 1674 (C=O)

^1H NMR ($CDCl_3$) δ = 7.02 - 7.30 (m, 10H, C_6H_5), 7.50-8.62 (m, naphthalene ring), 3.75 (s, 1H, CH), 10.15 (COOH); $^{13}CNMR$ ($CDCl_3$) δ= 129.80 – 131.09 ($\underline{C}_6H_5$), 120.00-126.05 (naphthalene ring), 46.50 ($\underline{C}H$), 162.40 ($\underline{C}OOH$),

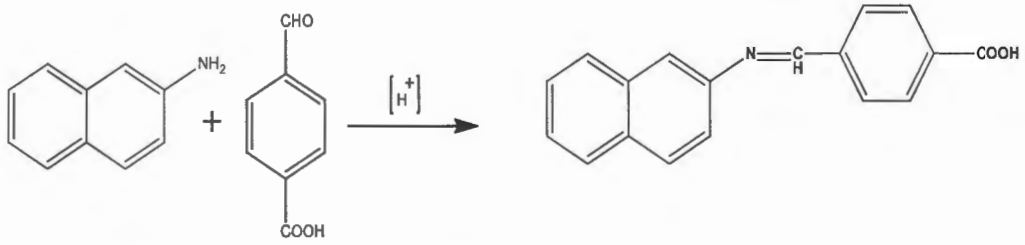

Scheme 3.6: General synthetic route for the preparation of carboxyl-4- naphty-1-imine).

The reduction process was carried out by reacting 20 mL methanol solution of carboxyl-4-naphtyl-1- imine (1.619 g; 0.006 mol) with 5 mL methanol solution of $NaBH_4$ (0.68 g, 0.018 mol) which was added in small portions as shown in Scheme 3.7. After the reaction, the solution was cooled to 0°C, and the stirring was continued overnight. A yellow solution was produced and the solvent was

removed under vacuum, the resulting viscous liquid was washed with water and dichloromethane was added in order to extract the product. The organic layer was removed and the solvent was evaporated in air.

Selected IR- ν(cm^{-1}): 3340 (N-H), 3047 (-C=H), 3323 (OH), 760(naphthalene ring), 1685(C=O)

^{1}H NMR ($CDCl_3$) δ = 6.11 - 7.07 (m, 10H, C_6H_5), 7.25-7.86 (m, naphthalene ring), 4.10 (s, 2H, CH_2), 9.50 (COOH), 8.60(NH); ^{13}CNMR ($CDCl_3$) δ= 129.50 – 130.00 ($\underline{C}_6H_5$), 120.05-126.05 (naphthalene ring), 49.50 ($\underline{C}H_2$), 160.40 ($\underline{C}$OOH).

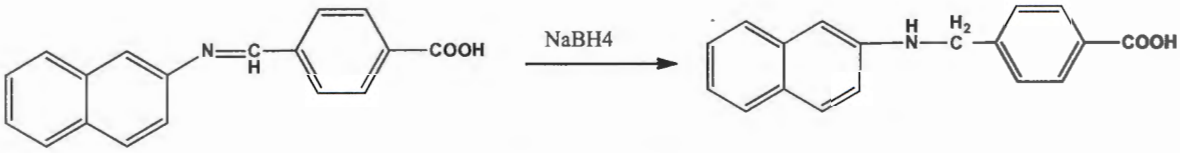

Scheme 3.7: General synthetic route for the preparation of carboxyl-4- naphty-1-amine.

3.9.2. Preparation of M(II) bis(*N*-naphtyl-1-carboxyl-*N*-phenyldithiocarbamate) complexes (M = Ni, Pd, Pt)

The synthesis of the dithiocarbamate complexes was carried out as follows: About 5 mL methanol solution of carboxyl-4-naphtyl-1-amine (1.385 g, 0.005 mol) was added to CS_2 (0.3 mL, 0.005 mol). To the stirred solution, Et_3N (1.01 mL, 0.01 mol) was added and the solution was stirred in ice as shown in Scheme 3.8. After 2 h, about 10 mL aqueous solution of 0.0025 mol of the respective metal salts ($NiCl_2$.$6H_2O$, 0.519 g; Na_2PdCl_4, 0.74 g; K_2PtCl_4, 1.04 g) was added. The solution yielded some precipitates which was stirred for 1 h, filtered and rinsed thoroughly with water.

(22) [Ni(L^8)$_2$]: Yield- 1.27 g (35%); M.pt: > 300∘C; Selected FTIR- ν(cm^{-1}): 3601 (OH), 3047 (H-C=H), 1541 (C=N), 760 (naphthalene ring), 1215 (C_2-N), 976 (CS_2), 1675(C=O), 414 (Ni-S); ^{1}HNMR ($CDCl_3$) δ = 5.8- 7.2 (m, 10H, $C_6\underline{H}_5$), 7.25-8.82 (m, naphthalene ring), 2.65 (s, 4H, $C\underline{H}_2$), 9.11(s, 2H, COOH).^{13}CNMR ($CDCl_3$) δ= 128.50 – 130.09 ($\underline{C}_6H_5$), 118-126.05 (naphthalene ring), 48.50 ($\underline{C}H_2$), 159.40 ($\underline{C}$OOH), 204.50 (–$\underline{C}S_2$); Anal calc. $C_{38}H_{28}N_2O_4S_4Ni$ (763.59): C, 59.77; H, 3.70; N, 3.67; S, 16.81; Found: C, 59.27; H, 3.40; N, 3.25; S, 16.35%.

(23) [Pd(L^8)$_2$]: Yield- 0.43 g (43%); M.pt:> 300∘**C;** Selected FTIR- ν(cm^{-1}): 3602 (OH), 3047 (H-C=H), 1545 (C=N), 760 (naphthalene ring), 1218 (C_2-N), 1000 (CS_2), 1678(C=O) 466 (Pd-S); ^{1}H NMR ($CDCl_3$) δ = 6.98 - 7.07 (m, 10H, C_6H_5), 7.25-8.07 (m, naphthalene ring), 4.0 (s, 4H, CH_2), 9.10 (COOH). ^{13}CNMR ($CDCl_3$) δ = 108.50 – 130.09 (C_6H_5), 118.04 -126.05 (naphthalene ring), 46.40 (CH_2), 160.05 (COOH), 205.90 (–CS_2); Anal calc. $C_{38}H_{28}N_2O_4S_4Pd$ (811.32): C, 56,25; H, 3.48; N,3.45; S, 15.81. Found: C, 56.77; H, 3.75; N, 4.05; S, 16.20

(24) [Pt(L^8)$_2$]: Yield- 0.49 g (44%); M. pt: > 300∘**C.** Selected IR- ν(cm^{-1}): 3601 (OH), 3047 (H-C=H), 1548 (C=N), 760 (naphthalene ring), 1210 (C_2-N), 1003 (CS_2), 1678 (C=O), 466 (Pt-S); ^{1}HNMR ($CDCl_3$) δ = 6.30 - 7.24 (m, 10H, C_6H_5), 7.40 - 8.12 (m, naphthalene ring), 2.90 (s, 4H, CH_2), 9.80 (s, 2H, COOH).^{13}CNMR ($CDCl_3$) δ= 129.30 – 131.50 (C_6H_5), 113.70-126.60 (naphthalene ring), 48.50 (CH_2), 161.40 (COOH), 207.50 (–CS_2). Anal calc. $C_{38}H_{28}N_2O_4S_4Pt$ (899.98): C, 50.71; H, 3.14 N, 3.11; S, 14.25. Found: C, 50.25; H, 3.50 N, 3.65; S, 14.60%.

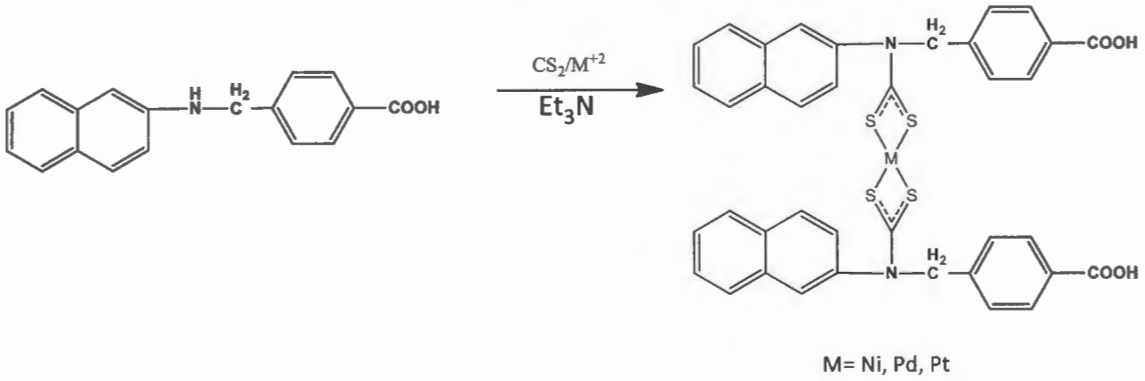

Scheme 3.8: General synthetic route for the preparation of M(II) bis-(*N*-naphtyl-1-carboxyl-*N*-phenyldithiocarbamate) (M =Ni, Pd, Pt).

3.9.3. Preparation of carboxyl-4- nitro-4-amine

About 20 mL ethanol solution of nitro-4- amine (1.38 g, 0.01 mol) was refluxed for 2 h with 20 mL ethanol solution of carboxyl-4- formaldehyde (1.5 g, 0.01 mol) with 3 drops of acetic acid as shown in Scheme 3.9. A brownish- yellow precipitate was formed which was filtered, and the filtrate was reprecipitated to give a yellow product. This was filtered, rinsed with cold ethanol and dried.

Selected IR- ν(cm^{-1}): 3044 (-C=H), 1682 (C=N), 1573, 1505 (-C=C-), 1328 (NO_2), 1684 (C=O)

^{1}H NMR ($CDCl_3$) δ = 6.76 - 7.40 (m, 10H, C_6H_5), 3.70 (s, 1H, CH), 10.07 (COOH); ^{13}CNMR ($CDCl_3$) δ= 99.70 – 120.50 ($\underline{C}_6H_5$), 60.20 ($\underline{C}H$),160 .90 ($\underline{C}OOH$),

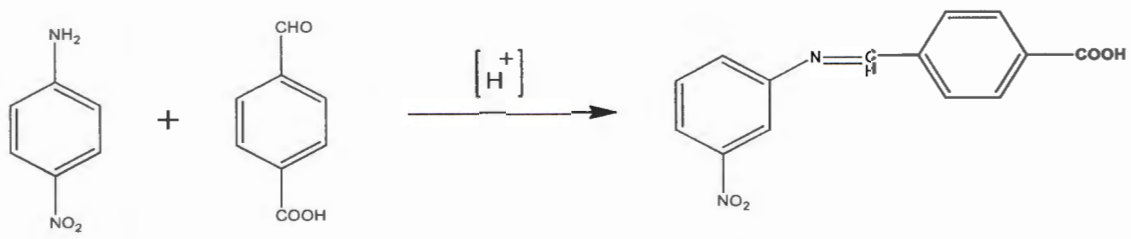

Scheme 3.9: General synthetic route for the preparation of carboxyl-4- nitro-4-imine.

The reduction process: The precipitate, carboxyl-4- nitro-4-imine (0.673 g, 0.605 mmol) was dissolved in 5 mL methanol and cooled to 0 °C in ice. A solution of $NaBH_4$ (0.069 g, 1.815 mmol) was added in small portions and stirred overnight (Scheme 3.10). A yellow solution was produced and the solvent removed under vacuum. The resulting viscous liquid was washed with water, and dichloromethane was added in order to extract the product. The organic layer was removed and dried in air. Selected IR- $\nu(cm^{-1})$: 3357 (OH), 3247 (N-H), 3046 (-C=H-), 1588, 1542 (-C=C-), 1328 (NO_2), 760 (naphthalene ring). 1691(C=O). ^1H NMR ($CDCl_3$) δ = 6.24 - 7.60 (m, 10H, C_6H_5), 3.50 (s, 2H, CH_2), 9.40 (COOH), 8.72 (NH); $^{13}CNMR$ ($CDCl_3$) δ= 98.90 – 120.20 ($\underline{C}_6H_5$), 60.04 ($\underline{C}H_2$), 160 .40 ($\underline{C}OOH$),

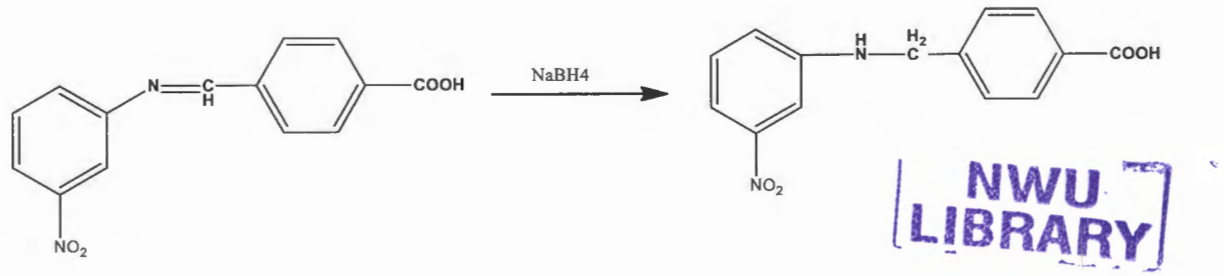

Scheme 3.10: General synthetic route for the formation of **of carboxyl-4- nitro-4-amine**

3.9.4. Preparation of M(II) bis-(*N*-nitro-4-carboxyl-*N*-phenyldithiocarbamate) complexes (M = Ni, Pd, Pt)

The secondary amine (0.34 g, 1.25 mmol) was added to a solution of CS_2 (0.1 mL, 1.25 mmol) and Et_3N (0.5 mL, 2.50 mmol) and stirred in ice. After 2 h, about 0.625 mol water: ethanol solution of the respective metal salts: ($NiCl_2$, 0.149 g; Na_2PdCl_4, 0.184 g; K_2PtCl_4, 0.259 g) was added to the solution to afford precipitates with different colours which were stirred for 1 h, filtered, rinsed with water: ethanol solution and dried in vacuum (Scheme 3.11).

(25) [Ni(L^9)$_2$]: Yield: 0.56 g (30%); M.pt: > 300 ∘**C**; Selected IR- ν(cm^{-1}): 3371 (OH), 1502 (C=N), 1637 (C=O), 1304 (C_2-N), 1057 (CS_2), 1588, 1542 (-C=C-), 1349 (NO_2), 470 (Ni-S); ^{1}H NMR ($CDCl_3$) δ = 6.19 - 7.24 (m, 10H, $C_6\underline{H}_5$), 3.64 (s, 4H, $C\underline{H}_2$), 2.20 (s, 2H, COO$\underline{H}$). ^{13}CNMR ($CDCl_3$) δ= 98.70 – 119.50 ($\underline{C}_6H_5$), 59.00 ($\underline{C}H_2$), 158.90 ($\underline{C}$OOH), 205.90 (–$\underline{C}S_2$). Anal calc. $C_{30}H_{22}N_4O_4S_4Ni$ (753.14): C, 47.82; H, 2.94; N, 7.44; S, 17.02. Found: C, 47.42; H, 2.50; N, 7.82; S, 17.60%.

(26) [Pd(L^9)$_2$]: Yield: 0.71 g (35%); M.pt> 300∘**C.** Selected IR- ν(cm^{-1}): 3327 (OH), 1503 (C=N), 1637(C=O), 1243 (C_2-N), 1057 (CS_2), 1588, 1542 (-C=C-), 1349 (NO_2), 760 ν(COOH), 473 (Pd-S); ^{1}H NMR (CDCl3) δ = 6.19 - 7.24 (m, 10H, C_6H_5), 3.64 (s, 4H, CH_2), 2.20 (s, 2H, COOH). ^{13}CNMR ($CDCl_3$) δ = 98.70 – 119.50 (C_6H_5), 59.00 (CH_2), 158.90 (COOH), 205.90 (–CS_2). Anal calc. $C_{30}H_{22}N_4O_4S_4Pd$ (801.20): C, 44.97; H, 2.77; N, 6.99; S, 16.01. Found: C, 44.30; H, 2.45; N, 6.51; S, 15.30%.

(27) [Pt(L^9)$_2$]: Yield: 0.83 g (37%); M.pt: > 300∘**C** Selected FTIR ν(cm^{-1}): 3326 (OH), 1503 (C=N), 1638(C=O), 1245(C_2-N), 1057 (CS_2), 1588, 1542 (-C=C-), 1349 (NO_2), 760 ν(COOH), 475 (Pt-S); ^{1}H NMR (CDCl3) δ = 6.80 - 7.38 (m, 10H, C_6H_5), 7.50 - 8.90 (m, C_6H_5,ring), 3.80 (s, 4H, CH_2), 6.60 (s, 2H, COOH). ^{13}CNMR ($CDCl_3$) δ = 83.70 – 119.50 (C_6H_5), 59.00 (CH_2), 168.00 (COOH), 200.40 (–CS_2). Anal calc. $C_{30}H_{22}N_4O_4S_4Pt$ (889.86): C, 40.49; H, 2.49; N, 6.30; S, 14.41. Found: C, 40.80; H, 2.70; N, 5.80; S, 14.88%.

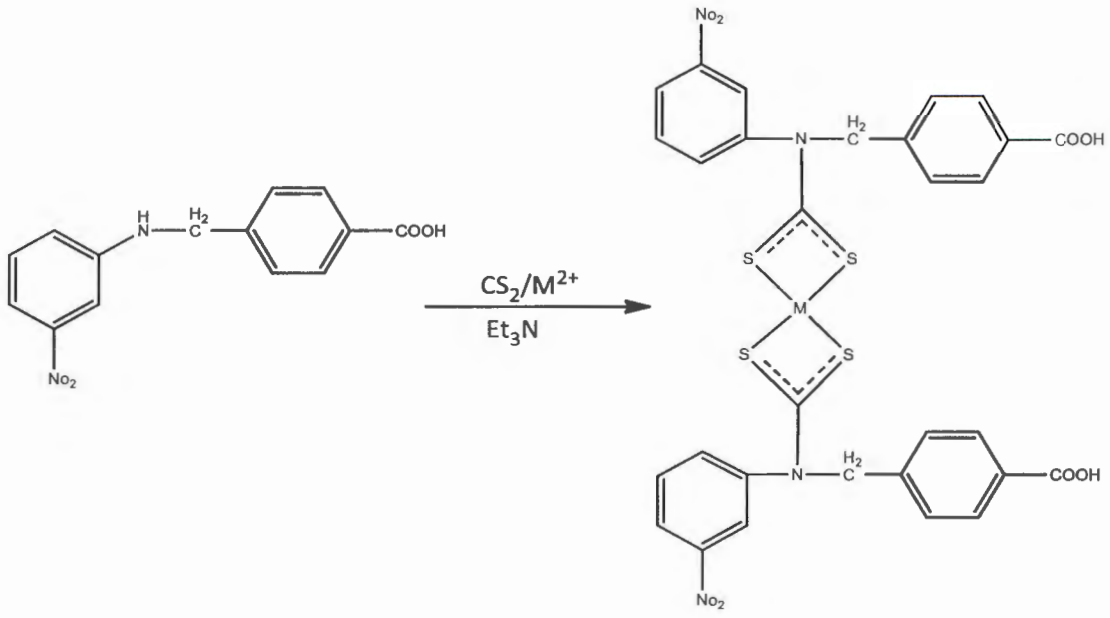

Scheme 3.11: General synthetic route for the preparation of M(II) bis(*N*-nitro-4-carboxyl-*N*-phenyldithiocarbamate) (M = Ni, Pd, Pt)

3.9.5. Preparation of *N*-3, 4-dihydroxylbenzyl–*N*- hexamethylene-1, 6-diamine.

Dihydroxyl-3,4-benzaldehyde (6.90 g, 0.05 mol) was dissolved in 25 mL ethanol and added to a 40 mL ethanol solution of hexamethylene-1,6-diamine (2.70 g, 0.025 mol) and stirred. To this solution, 3 drops of acetic acid was added and refluxed for 2 h (Scheme 3.11). A yellow solution was produced and the solvent was removed under vacuum. The resulting viscous liquid was washed with water, and dichloromethane was added in order to extract the product. The organic layer was removed and dried in air.

Selected IR- ν(cm^{-1}): 33376 (OH), 3047 (-C=H), 2924 *ass*(-CH_2), 2640 *sy*(CH_2), 1689 (C=N), 1589, 1542 (C=C)^{1}HNMR ($CDCl_3$) δ (ppm) = 1.15 (t, 4H, $C\underline{H}_2CH_2CH_2$), 1.75 (m, 4H, $CH_2C\underline{H}_2CH_2$), 3.45 (t, 4H, $CH_2CH_2C\underline{H}_2$); 7.32 - 7.63 (m, C_6H_5,ring), ^{13}C NMR ($CDCl_3$) δ = 47.80, $C\underline{H}_2CH_2CH_2$; 29.2, $CH_2C\underline{H}_2CH_2$), 32.20, $CH_2CH_2C\underline{H}_2$; 135.80, 126.30(C_6H_5).

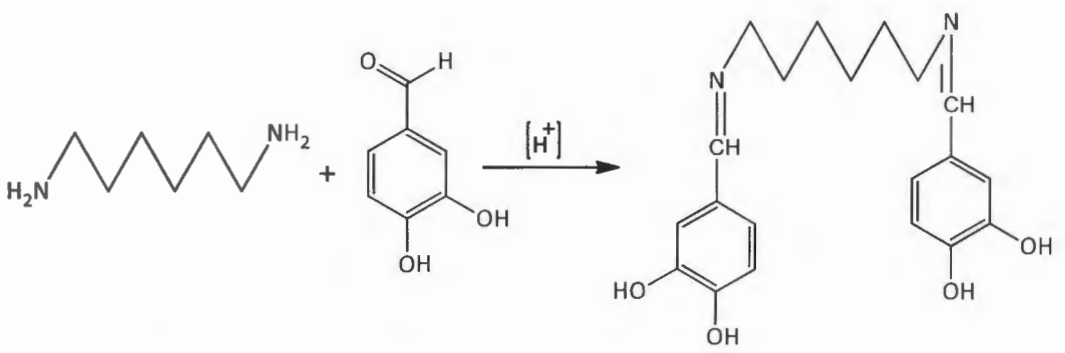

Scheme 3.12: General synthetic route for the preparation of *N*-3,4-dihydroxylbenzyl–*N*-hexamethylene-1,6-diimine.

The reddish- yellow solid of *N*-3, 4- dihydroxylbenzyl–*N*- hexamethylene-1, 6-diimine (6.36 g, 0.027 mol) was dissolved in 40 mL methanol and a solution of $NaBH_4$ (3.02 g, 0.08 mol) was added. The solution was first stirred in ice for 2 h and then at room temperature overnight (Scheme 3.13). A reddish-yellow solution was obtained, and the solvent was removed under vacuum. The resulting viscous liquid was washed with water, and dichloromethane was added in order to extract the product. The organic layer was removed which was kept for the solvent to evaporate given a red

yellowish oil.Selected IR- $\nu(cm^{-1})$: 3383 (OH), 3159 (N-H), 3047 (-C=H), 2924 *ass*($-CH_2$), 2640 *sy*(CH_2), 1638(C=N), 1589,1542 ν(C=C), ^{1}HNMR ($CDCl_3$) δ (ppm) = 1.13 (t, 4H, $C\underline{H}_2CH_2CH_2$), 1.45 (m, 4H, $CH_2C\underline{H}_2CH_2$), 2.70 (t, 4H, $CH_2CH_2C\underline{H}_2$); 7.22 - 7.55 (m, C_6H_5,ring), ^{13}C NMR ($CDCl_3$) δ = 46.40, $C\underline{H}_2CH_2CH_2$; 28.60, $CH_2C\underline{H}_2CH_2$), 30.20, $CH_2CH_2C\underline{H}_2$; 132.80, 124.30(C_6H_5)

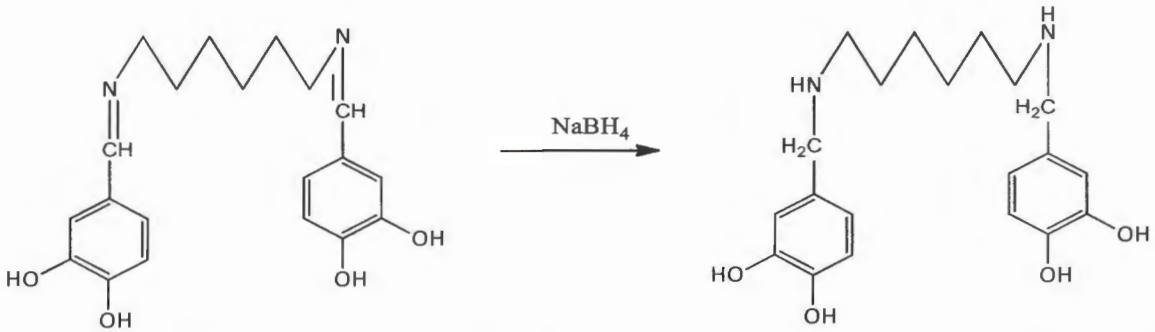

Scheme 3.13: General synthetic route for the preparation of *N*-3, 4- dihydroxylbenzyl–*N*-hexamethylene-1- 6-diamine.

3.9.6. Preparation of M(II) bis-(*N*-3,4-dihydroxylbenzyl–*N*-hexamethylene-1,6-diamine dithiocarbamate) complexes (M = Ni, Pd, Pt)

Carbon disulphide (1.52 mL, 0.04 mol) and Et_3N (5.0 mL, 0.12 mol) were added to 20 mL methanol solution of *N, N´*- dihydroxylbenzylhexamethylene-1, 6 – diamine (9.56 g, 0.04 mol) in a round bottom flask placed in ice. After stirring the solution for 2 h, about 20 mL aqueous solution of 0.0025 mol of the respective metal salts ($NiCl_2.6H_2O$, 0.59 g; Na_2PdCl_4, 0.74 g; K_2PtCl_4, 1.04 g) was added to the solution and stirred for another 1 h (Scheme 3.14). The different coloured precipitates produced was filtered, washed with water and dried under vacuum.

(28) [Ni(L^{10})$_2$]: Yield: 1.30 g (45%); M.pt: > 300 ∘**C**; Selected FTIR ν(cm^{-1}): 3644 (OH), 3066 (-C=H), 2938 *ass*(-CH_2), 2358 *sy*(CH_2), 1500 (C=N), 1214 (C_2N), 965 (CS_2), 1456, 1020 (C=C), 471 (Ni-S); ^{1}HNMR ($CDCl_3$) δ (ppm) = 1.10 (t, 4H, C$\underline{H_2}CH_2CH_2$), 1.35 (m, 4H, $CH_2C\underline{H_2}CH_2$), 2.05 (t, 4H, $CH_2CH_2C\underline{H_2}$); 7.02 - 7.63 (m, C_6H_5,ring), ^{13}C NMR ($CDCl_3$) δ = 45.80, C$\underline{H_2}CH_2CH_2$; 28.2, $CH_2C\underline{H_2}CH_2$), 30.20, $CH_2CH_2C\underline{H_2}$; 131.80, 124.30 (C_6H_5), 202.10 (–CS_2). $C_{44}H_{56}N_4S_8O_8Na_2$ (1071.43): Calculated: C, 49.32; H, 5.27; N, 5.23; S, 23.97. Found: C, 49.63; H, 5.52; N, 5.10; S, 23.60%.

(29) [Pd(L^{10})$_2$]: Yield: 1.28 g (41%); MPt. > 300 ∘**C;** Selected FTIR ν(cm^{-1}): 3642 (OH), 3067 (-C=H), 2938 *ass*(-CH_2), 2357 *sy*(CH_2), 1500 (C=N), 1203 (C_2N), 965 (CS_2), 1456, 1019 (C=C), 473 (Pd-S); ^{1}HNMR ($CDCl_3$) δ (ppm) = 1.10 (t, 4H, C$\underline{H_2}CH_2CH_2$), 1.35 (m, 4H, $CH_2C\underline{H_2}CH_2$), 2.09 (t, 4H, $CH_2CH_2C\underline{H_2}$); 7.26 - 7.65 (m, C_6H_5, ring),^{13}C NMR ($CDCl_3$) δ = 46.00 (C$\underline{H_2}CH_2CH_2$); 28.2 $CH_2C\underline{H_2}CH_2$), 30.20 ($CH_2CH_2C\underline{H_2}$); 131.80,124.30(C_6H_5), 202.50 (–CS_2). $C_{44}H_{56}N_4S_8O_8Pd_2$ (1238.02): Calculated: C, 42.68; H, 4.56; N, 4.52; S, 20.72. Found: C, 43.20; H, 4.15; N, 4.90; S, 21.20%

(30) [Pt(L^{10})$_2$]: Yield, 1.40 g (40%); M.pt. > 300 ∘**C;** Selected FTIR- ν(cm^{-1}): 3642 (OH), 3075 (-C=H), 2937 *ass*(-CH_2), 2853 *sy*(CH_2), 1502 (C=N), 1200 (C_2N), 962 (CS_2), 1456, 1043 (C=C), 473 (Ni-S) ; ^{1}HNMR ($CDCl_3$) δ (ppm) = 1.10 (t, 4H, C$\underline{H_2}CH_2CH_2$), 1.35 (m, 4H, $CH_2C\underline{H_2}CH_2$), 2.05 (t, 4H, $CH_2CH_2C\underline{H_2}$); 7.02 - 7.63 (m, C_6H_5,ring), ^{13}C NMR ($CDCl_3$) δ = 45.80 (C$\underline{H_2}CH_2CH_2$); 28.2 ($CH_2C\underline{H_2}CH_2$), 30.20 ($CH_2CH_2C\underline{H_2}$); 131.80,124.30(C_6H_5), 202.10(–CS_2). $C_{44}H_{56}N_4S_8O_8Pt_2$(1415.61). Calculated: C, 37.33; H, 3.99; N, 3.96; S, 18.12. Found: C, 37.20; H, 3.60; N, 3.70; S, 18.42%

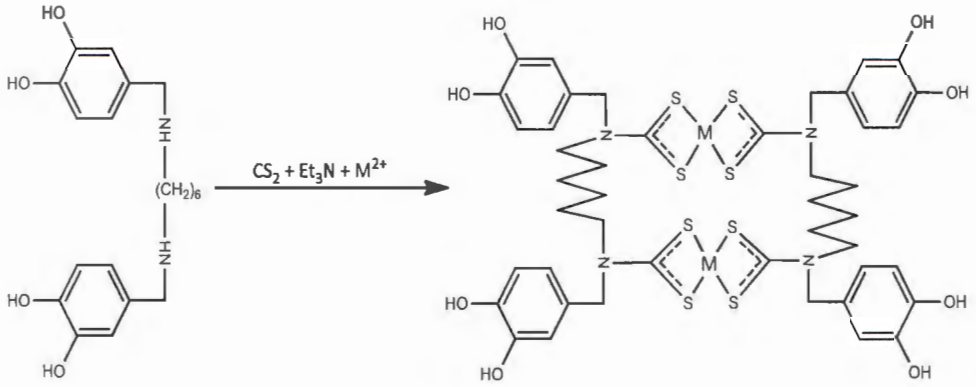

Scheme 3.14: General synthetic route for the preparation of of M(II) bis-(*N*-3, 4-dihydroxylbenzyl–*N*-hexamethylene-1, 6-diamine dithiocarbamate) (M = Ni, Pd, Pt) complexes.

3.10. Results and discussion of Ni(II), Pd(II) and Pt(II) complexes of dithiocarbamates derived from Schiff bases

3.10.1 General synthesis of M(II) dithiocarbamate complexes prepared from amines derived from Schiff bases

The ligands were obtained as yellow solids and upon complexation with the metal ions, they yielded precipitates of different shades of colour: green, orange and yellow for the Ni(II), Pd(II) and Pt(II) complexes respectively. The yields were low compared to the complexes obtained from other dithiocarbamates. The low yield might be due to the absence of a strong base which could catalyse the reaction and increase the rate of DTC formation [28]. The complexes were insoluble in water and were only soluble in coordinating high boiling point organic solvents, DMF and DMSO. The insolubility of the complexes in low boiling solvents also made the crystal growth of the complexes very difficult, and all efforts to grow the crystals were futile.

3.10.2. Infrared spectral studies of Ni(II), Pd(II) and Pt(II) complexes of dithiocarbamates derived from Schiff bases

In the infrared spectra of the immine compounds, the band due to the characteristic azomethine appeared as a sharp peak around 1682 cm^{-1}. The absence of a band due to the carbonyl group (around 1700 cm^{-1}) indicated the formation of the Schiff base. The imine linkage was consumed during condensation reaction, and so disappeared upon the formation of the amino group through

the reduction reaction. This subsequently resulted into the formation of the N-H bond. The C=N bond reappeared as thiouriede bond but now shifted to lower vibrations after complexation reaction. The band appeared around 1541-1548, 1637-1641, 1500-1502 cm–^{1} with decreased intensity to indicate the coordination of N to the metal ions. This suggested partial double bond character and delocalization of pi-electron density within the dithiocarbamate functions. This confirmed the formation of the dithiocarbamates and the coordination to the metal ions.

The aromatic C-H vibrations around 3045 cm^{-1} and the strong deformation bands of COOH around 1674- 1691 cm^{-1} were common to the imino, amino and the complexes of **L^{8}** and **L^{9}**. The aromatic NO_2 asymmetric vibrations appear at 1328 and 1329 cm^{-1} in ligand **L^{9}** and the complexes. The N-H stretching vibrations which appeared around 3200 cm^{-1} were observed for the amino compounds. This functional group was used up upon dithiocarbamate formation and the protons released were removed upon the addition of triethylamine (Et_3N). The vibrations in the range 1200-1300 cm^{-1} were ascribed to C_2-N, while the single band within 962 – 1003 cm^{-1} was due to the CS_2 vibration. The band found in the far IR region in the range 414-475 cm^{-1} were M-S vibrations, and appeared only in the spectra of the complexes. The single peak of the $\nu(CS_2)$ confirmed bidentate mode of coordination of the central metal to the two sulphur atoms.

3.10.3. NMR spectral studies of Ni(II), Pd(II) and Pt(II) complexes of dithiocarbamates derived from Schiff bases

The proton ^{1}H NMR spectrum of the carboxyl-4- naphty-1-amine ligand showed multiplets in the range 6.11-7.07 and 7.50-8.62 for the aromatic carboxyl and naphthalene ring system respectively; they are shifted to higher delta values in the range 6.30-8.07 and 7.25-8.82 in the complexes. The –CS_2 values show an upward shifts from 204-207 ppm from the Ni(II) – Pt(II) complexes.

In the ^{1}H NMR spectrum of carboxyl-4- nitro-4-amine, the resonantfrequency values appeared around 6.24 - 7.60 and 7.65-8.60 ppm; while the values for the complexes appeared in the downfield shift at 6.19 - 7.24 and 7.10 - 8.20 ppm. This could be ascribed to the presence of the electron withdrawing and deshielding nature of NO_2 in the compounds. The –CS_2 values were observed around 200.40-205.90 ppm for all the complexes, showing an increasing delta value down the group.

For the *N*-3,4-dihydroxylbenzyl–*N*-hexamethylene-1,6-diamine, there is a significant shift displacement to lower fields from the amine to the complexes produced as observed in the ^{1}H NMR spectrum, from 1.13- 2.70 ppm of the methylene hydrogen atoms in the diamine to 1.10-2.09 ppm of the methylene hydrogen atoms in the complexes. The same direction of shifts displacement was also observed for the carbon atoms. This confirmed the formation of dithiocarbamate complexes.

3.10.4. Thermal decomposition studies of Ni(II), Pd(II) and Pt(II) complexes of dithiocarbamates derived from Schiff bases

From the observed thermal decomposition graphs presented in Figure 3.11 -3.13, all the compounds displayed different decomposition patterns. The **[Ni(L^8)$_2$]** complex decomposed with 68% weight loss and residue of about 2.67 mg. The direct one-step decomposition indicated nickel sulphide of 3:4 molar ratios. The **[Pd(L^8)$_2$]** complex went through a three step decomposition pattern with the first step between 80 – 180 °C, and involved about 19% weight loss to give 5.58 mg of residue corresponding to the loss of the carboxylic component. The second decomposition occurred in the range 193 – 244 °C, with the loss of the naphthalene component and the formation of thiocyanate intermediate giving 5.07 mg residual mass. The last stage occurred in the range 259 – 650 °C, with 51% decomposition and 3.40 mg residual mass. This corresponded to the formation of Pd_4S. The **[Pt(L^8)$_2$]** complex decomposed in two stages with the formation of the thiocyanate intermediate. The first step was about 15% weight loss, which further broke down to a residue of 8.82 mg equivalent to the mass of Pt_2S_4.

In the carboxylnitro compounds, both the **[Ni(L^9)$_2$] and [Pd(L^9)$_2$** complexes went through two stage decomposition patterns via the formation of thiocyanate intermediate. The final decomposition resulted into the respective sulphides with 50 and 58% weight loss, and residue of 6.60 and 10.10 mg in the Ni and Pd complexes respectively. The **[Pt(L^9)$_2$** complex decomposed in just one-step with 64% loss and 4.40 mg residual mass to form PtS_2.

The **[Ni(L^{10})$_2$]** complex decomposed via the formation of the thiocyanate intermediate with 21% weight loss which further broke down to nickel sulphide of composition Ni_3S_4. The **[Pd(L^{10})$_2$** complex decomposed with 44% loss to form palladium sulphide Pd_4S, while the **[Pt(L^{10})$_2$** complex exhibited three steps pattern with initial 15% loss which corresponded to the loss of the dihydroxyl group. The first step decomposition was followed by a 28% weight loss of the hexamethylene segment and the formation of the thiocyanate intermediate. Final decomposition occurred with 57% weight loss, leaving residue of 6.08 mg and subsequent formation of Pt_2S_4. The entire decomposition temperatures ranged between 176 and 434 °C.

All the complexes were thermally stable, with the final decomposition temperatures above 500 °C, and all gave their respective metal sulphides. Table 3.8 presents the TGA data.

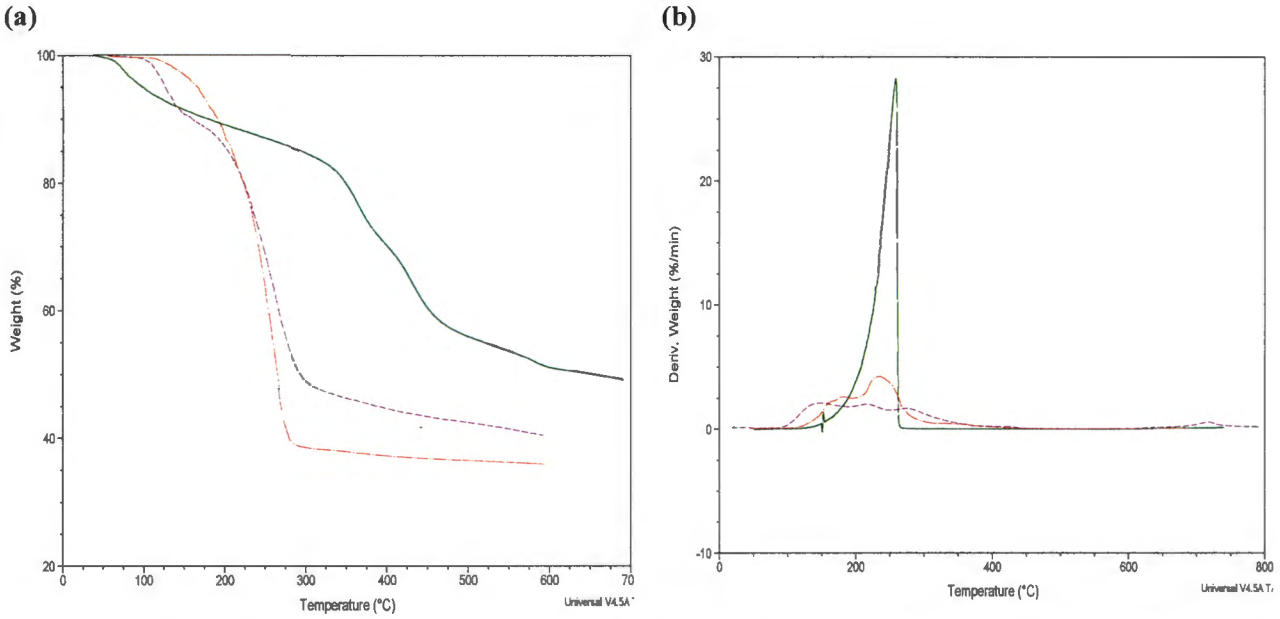

Figure.3.11: **(a)** TG, and **(b)** DTG graph of **[Ni(L^8)$_2$]** (green), **[Pd(L^8)$_2$]** purple), **[Pt(L^8)$_2$]** (red) complexes

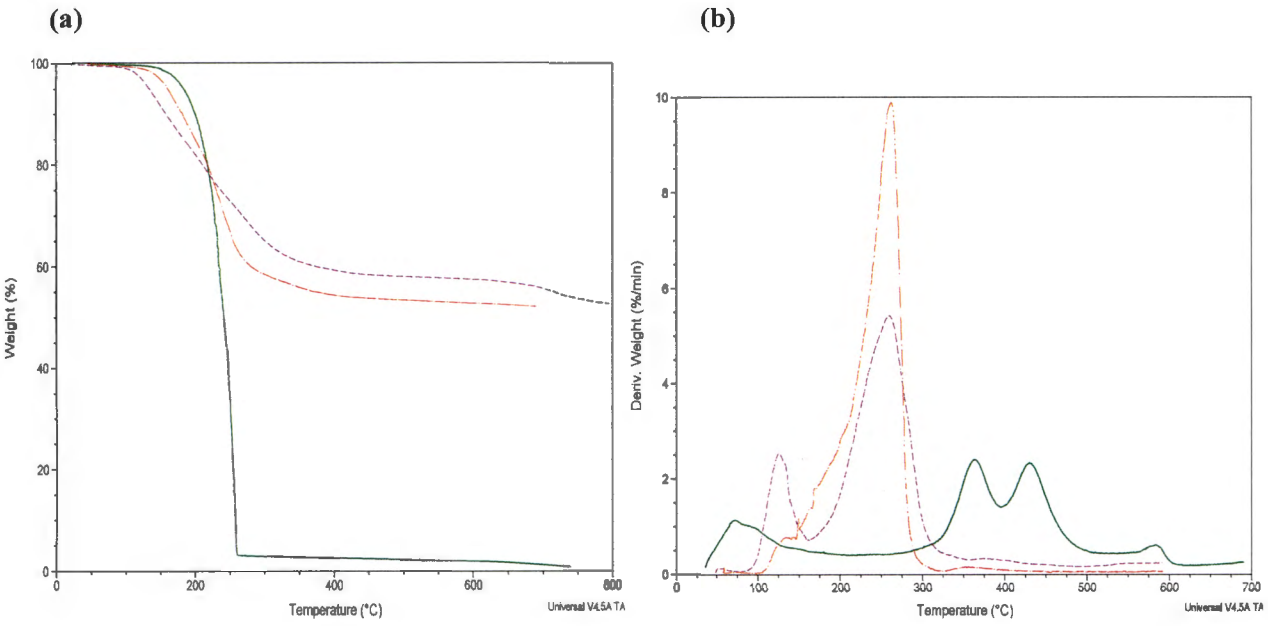

Figure.3.12: **(a)** TG and **(b)** DTG graphs of **[Ni(L^9)$_2$]** (green), **[Pd(L^9)$_2$]** purple), and **[Pt(L^9)$_2$]** (red) complexes.

(a) (b)

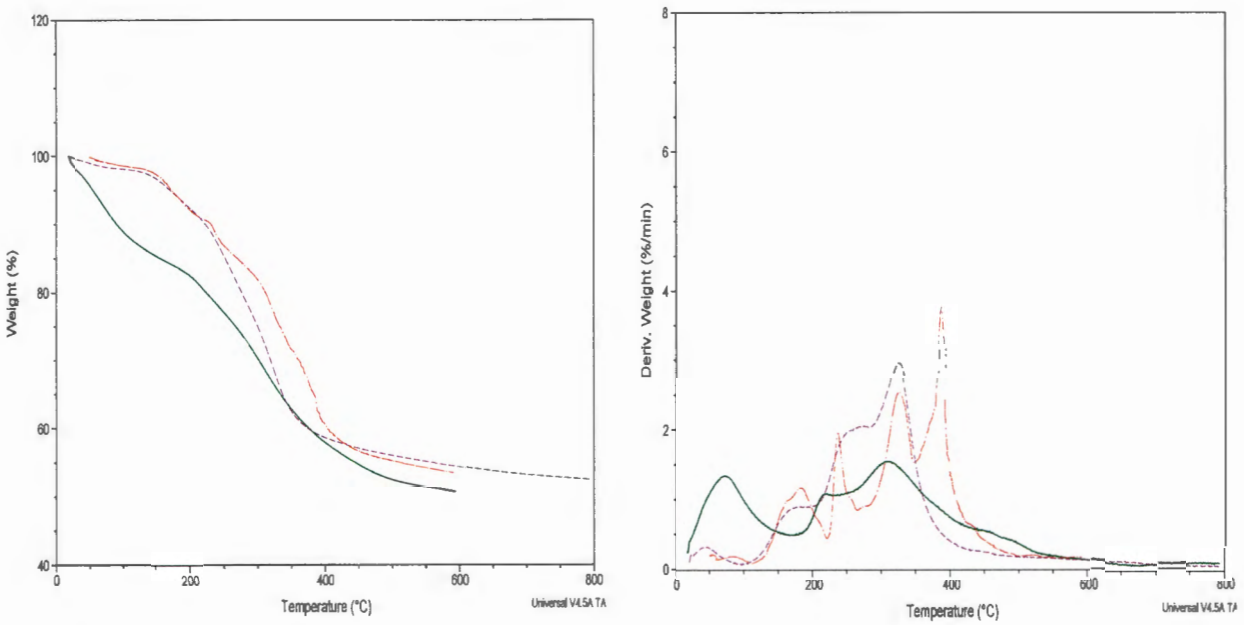

Figure 3.13: (a) TG and **(b)** DTG graphs of **[Ni(L^{10})$_2$]** (green), **[Pd(L^{10})$_2$]** purple), and **[Pt(L^{10})$_2$]** (red) complexes

Table 3.11: Showing Thermal stability data for the complexes prepared from Schiff base secondary amines.

Compounds	**Decomposition Range (°C)**	**Peak Temp (°C)**	**Weight Loss (%)**	**Product Obtained**	**Residual Mass (mg) Found/Calc**
[Ni(L^8)$_2$]	320 -652	391	68	Ni_3S_4	2.60/2.70
	80 – 180	147	19	$RNCS_2Pd$	5.58/5.87
[Pd(L^8)$_2$]	193 – 244	217	26	NCS_2Pd	5.07/4.96
	259 – 650	274	51	Pd_4S	3.40/3.88
	120 – 200	183	15	$RNCS_2Pt$	14.30/14.80
[Pt(L^8)$_2$]	209 – 670	235	53	Pt_2S_4	8.82/9.40
	240 – 397	364	29	$RNCS_2Ni$	9.34/8.74
[Ni(L^9)$_2$]	400 – 676	428	50	Ni_3S_4	6.60/6.20
	52 – 160	125	10	$RNCS_2Pd$	21.70/
[Pd(L^9)$_2$]	187 – 520	262	58	Pd_4S	10.10/10.20
[Pt(L^9)$_2$]	170 – 520	262	64	PtS_2	4.40/3.60
	176 – 240	218	21	$RNCS_2Ni$	23.23/22.36
[Ni(L^{10})$_2$]	271 – 437	314	43	Ni_3S_4	16.50/15.81

$[Pd(L^{10})_2]$	281 – 502	325	44	Pd_4S	8.70/8.84
	228 – 266	234	15	$RNH(CH_2)_6CS_2Pt$	11.99/11.33
$[Pt(L^{10})_2]$	300 – 351	323	28	$RNCS_2Pt$	10.05/10.85
	358 - 434	390	57	Pt_2S_4	6.08/5.18

3.11. Adducts and mixed ligands complexes of Ni(II) dithiocarbamate complexes

3.11.1. Syntheses of adducts and mixed ligands complexes

The ability of metal complexes to form adducts differs and is closely related to the geometry of the compounds. It is also dependent on the ability of the Lewis base to accept π-electrons and also the ionic size of the central metal ion [29]. In order to incease the number of functional groups around the nickel and also to study the effect of coordinating flexibility and easy kinetic tuning on the properties of metal complexes, *N* donor molecules (2, 2-bypiridine and 1, 10-phenanthroline) were incorporated into the complexes. The preparative details are presented below:

3.11.1.1. Synthesis of Ni(II) (2,2′-bipyridyl) (*N*-phenyldithiocarbamate) complex $[Ni(L^1)_2bpy]$

About 15 mL hot chloroform solution of the complex **$[Ni(L^1)_2]$**, (0.187 g, 0.5 mmol) and a 15 mL hot chloroform solution of 2, 2-bypyridine (0.156 g, 0.1 mmol) were added together and the solution was refluxed for 2 h. The dark purple solution produced was cooled, filtered and the filtrate was left to form precipitate.

(31) $[Ni(L^1)_2bpy]$: Yield: 0.13 g (48%); M.pt: 118 – 120 °C; Selected FTIR, (cm^{-1}): 1472 (C=N), 1267 (C_2–N), 986 (C=S), 3112 (=CH–H), 2953 (H_2C–H), 3130 (NH), 453 (Ni-S); Anal calc-$C_{24}H_{30}N_4S_4Ni$ (561.40): C, 51.34; H, 5.39; N, 9.98; S, 22.84. Found: C, 51.20; H, 5.20; N, 10.10; S, 22.50%.

3.11.1.2. Synthesis of Ni(II) (1, 10-phenantroline) (*N*-phenyldithiocarbamate) complex $[Ni(L^1)_2ph]$

About 15 mL hot chloroform solution of the complex **$[Ni(L^1)_2]$**, (0.187 g, 0.5 mmol) and a 15 mL hot chloroform solution of 1, 10 phenanthroline (0.180 g, 0.1 mmol) were added together and the solution was refluxed for 2 h. The dark purple solution produced was cooled, filtered and the filterate was left to form precipitate.

(32) [Ni(L^1)$_2$ph]: Yield, 0.13 g (46%); M.pt: 115 – 118 °C; Selected FTIR, (cm^{-1}): 1519 (C=N), 1277 (C_2—N), 988 (C=S), 3133 (=CH–H), 2953 (H_2C–H), 3133 (NH), 442 (Ni-S); Anal calc-$C_{26}H_{20}N_4S_4Ni$ (575.42): C, 56.58; H, 3.50; N, 7.44; S, 17.02. Found: C, 56.20; H, 3.10; N, 7.04; S, 16.95%.

3.11.1.3. Synthesis of Ni(II) (2,2′-bipyridyl) (*p*-methylphenyldithiocarbamate) complex [Ni(L^3)$_2$bpy]

About 15 mL hot chloroform solution of the complex **[Ni(L^3)$_2$]**, (0.22 g, 0.5 mmol) and a 15 mL hot chloroform solution of 2, 2 bipyridine (0.156 g, 0.1 mmol) were added together and the solution was refluxed for 2 h. The dark purple solution produced was cooled, filtered and the filterate was left to form precipitate.

(33) [Ni(L^3)$_2$bpy]: Yield, 0.15 g (52%); M.pt: 114 – 116 °C;
Selected FTIR, (cm^{-1}): 1513 (C=N), 1209 (C_2—N), 987 (C=S), 3001 (=CH–H), 2917 (H_2C–H), 3165 (NH), 451 (Ni-S); $C_{25}H_{33}N_4S_4Ni$ (576.51): Calculated: C, 52.68; H, 5.77; N, 9.72; S, 22.25. Found: C, 53.39; H, 5.45; N, 8.77; S, 22.10%.

3.11.1.4. Synthesis of Ni(II) (1, 10-phenantroline) (*p*-methylphenyldithiocarbamate) complex [Ni(L^3)$_2$ph]

About 15 mL hot chloroform solution of the complex **[Ni(L^3)$_2$]**, (0.22 g, 0.5 mmol) and a 15 mL hot chloroform solution of 1, 10 phenanthroline (0.180 g, 0.1 mmol) were added together, and the solution was refluxed for 2 h. The dark purple solution produced was cooled, filtered and the filterate was left to form precipitate.

(34) [Ni(L^3)$_2$ph]: Yield, 0.17 g (57%); M.pt. 100 – 103 °C; Selected FTIR, (cm^{-1}): 1543 (C=N), 1238 (C_2—N), 988 (C=S), 3024 (=CH–H), 2920 (H_2C–H), 3155 (NH), 425 (Ni-S). $C_{27}H_{23}N_4S_4Ni$ (590.45): Calculated: C, 54.92; H, 3.93; N, 9.49; S, 21.72. Found: C, 54.20; H, 3.65; N, 9. 04; S, 21.95%.

3.11.1.5. Synthesis of Ni(II) (1, 10-phenantroline) (*p*-ethylphenyldithiocarbamate) complex [Ni(L^4)$_2$bpy]

About 15 mL hot chloroform solution of the complex **[Ni(L^4)$_2$]**, (0.57 g, 1.25 mmol) and a 15 mL hot chloroform solution of 2,2 bipyridine (0.39 g, 2.5 mmol) were added together and the solution

was refluxed for 2 h. The dark purple solution produced was cooled, filtered and the filterate was left to form precipitate.

(35) [Ni(L^4)$_2$bpy]: Yield, 0.35 g (52%), M.pt: 97 - 100 °C Selected FTIR, (cm^{-1}): 1510 (C=N), 1226 (C_2—N), 977 *asy*(C=S), 730 *sy*(C=S), 3100 (=CH−H), 2960 (H_2C−H), 3204 (NH), 437 (Ni-S); $C_{25}H_{33}N_4S_4Ni$ (576.51): Calculated: C, 52.08; H, 5.77; N, 9.72; S, 22.25. Found: C, 52.00; H, 5.45; N, 10.40; S, 22.10%.

3.11.1.6. Synthesis of Ni(II) (1, 10-phenantroline) (*p*-ethylphenyldithiocarbamato) complex [Ni(L^4)$_2$ph]

About 15 mL hot chloroform solution of the complex **[Ni(L^4)$_2$]**, (0.57 g, 1.25 mmol) and a 15 mL hot chloroform solution of 1, 10 phenanthroline (0.45 g, 2.50 mmol) were added together and the solution was refluxed for 2 h. The dark purple solution produced was cooled, filtered and the filterate was left to form precipitate.

(36)[Ni(L^4)$_2$ph]: Yield, 0.43 g (54%); M.pt: 95 - 98 °C; Selected FTIR, (cm^{-1}): 1508 (C=N), 1225 (C_2—N), 984 (C=S), 3011 (=CH−H), 2924 (H_2C−H), 3193 (NH), 420 (M-S); $C_{30}H_{28}N_4S_4Ni$ (631.52): Calculated: C, 57.06; H, 4.47; N, 8.87; S, 20.31; Found: C, 56.20; H, 4.20; N, 8.04; S, 20.95%.

3.12. Results and discussion of the adducts and mixed ligands complexes of the Ni(II) dithiocarbamate complexes

3.12.1. General synthesis of the adducts and mixed ligands complexes of the Ni(II) dithiocarbamate complexes

The observed properties of the resulting adducts, represented in Scheme 3.15, are quite different from their parent complexes. The adduct formation influenced the properties of the metal complexes. In addition to the M-S bond, two additional M-N bonds have been created by the Lewis base from its two coordinate bonds. Thus, charge compensation comes from the two DTC atoms through the S atoms but the N donor atoms direct the framework pattern [30]. These adducts were brownish- purple in colour and were soluble in solvents such as chloroform and dichloromethane. The geometry and coordination properties of the central metal ions also changed from four-coordinate to six coordinate octahedral. Since Ni(II) in an octahedral geometry is paramagnetic, the NMR measurements were not done.

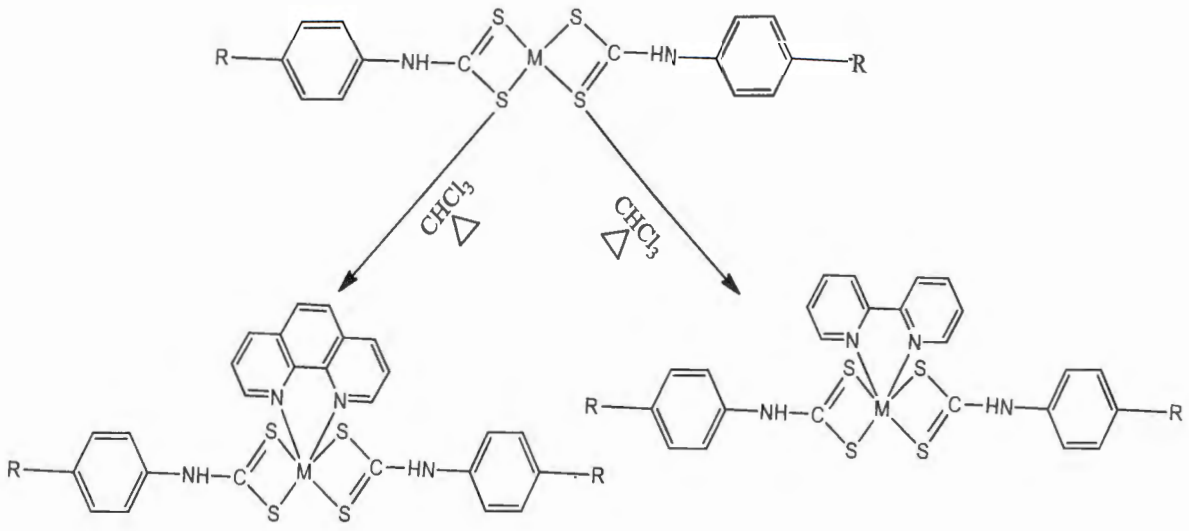

(R= H, CH_3, CH_2CH_3; M= Ni)

Scheme 3.15: Synthetic route for the preparation of 2,2-bpy and 1,10 phen adducts of the Ni(II) dithiocarbamate complexes.

3.12.2. Infrared spectral studies of the adduct and mixed ligand complexes of the synthesized Ni(II) dithiocarbamate complexes

In the FTIR spectra of the adducts, the ν(C=N) which was observed around 1468, 1508 and 1511 cm^{-1} in the parent complexes of **L^1**, **L^3** and **L^4** respectively, shifted to higher frequencies above 1510 cm^{-1} for the bypiridine and phenanthroline adducts. These revealed the effect of the additional bypiridine and phenantroline rings due to the shift of electrons density to the carbon-nitrogen bond in the N–CSS group towards the nickel centre. The ν(C=N) vibrations increased with increase in chain length of the substituents. The ν(C-S) vibrations also shifted to lower values for the adducts compared to the parent complexes, which is due to the effect of increase in coordination number of the central metal ion from four to six and change in geometry from four to six coordinate. Consequently, this led to an increase in the double bond character of ν(C=S) in the complexes. The presence of a single bond without splitting in each compound indicated bidentate mode of bonding. The N-H vibrations were observed in the range 3130 - 3204 cm^{-1} in all the adducts. The new band not observed in the spectra of the ligands but in the far IR region around 420 - 453 cm^{-1} in all the complexes represented the Ni-S vibrations. These vibrations shifted to higher frequencies compared

to those of the parent complexes at 411-442 cm^{-1} and increased as the chain length of the substituents increased.

3.12.3 Thermal decomposition studies of the adducts and mixed ligand complexes of the synthesized Ni(II) dithiocarbamate complexes

Single step decomposition patterns were observed in all the bpy adducts of Ni dithiocarbamate complexes. The temperature ranges of the decomposition were 138-610, 131-350 and 170-475 °C for the **$[Ni(L^1)_2bpy]$**, **$[Ni(L^3)_2bpy]$**, **$[Ni(L^4)_2bpy]$** complexes respectively, as presented in Table 3.11 and Figures 3.17 – 3.19 . The residual masses obtained after the decomposition of each compound were 2.80, 2.0 and 2.52 mg respectively, and these corresponded to about 80, 83 and 84% mass loss. The calculation based on stoichiometry was NiS in all the complexes. This suggested that the bipyridine and the dithiocarbamate molecules decomposed collectively in a single step.

The phenanthroline complexes have onset of decomposition around 240 °C, which continued up till 502 °C; the decomposition peak was at 298 up to 475 °C with two step decomposition patterns for the L^1 and L^4 complexes. The removal of the Lewis base (phenanthroline) occurred with about 64 and 67% loss which preceded the decomposition of the DTC The masses of the residues left after this step were 3.21/2.70 mg and 4.55/4.32 mg (calculated/found), resulting into the formation of isothiocyanate intermediate. The second step occurred in the range 385-502 °C with about 84 and 86% decomposition, resulting in residual masses of 1.39/1.35 and 1.96/1.95 mg (calculated/found). Only the L^3 exhibited single step decomposition in the range 223-335 °C with 83% weight loss leaving residual masses of 2.14/1.89 mg, which corresponded to the mass of NiS.

All the complexes indicated the formation of NiS as final product. Introduction of the adducts into the parent complexes led to increase in decomposition temperatures compared to the parent complexes, which implies that introduction of the adducts increases the thermal stability of the parent compounds.

Table 3.12: Thermal stability data for the bpy and phen adducts of **[Ni(L^1)$_2$]**, **[Ni(L^3)$_2$]** and **[Ni(L^4)$_2$]**

Compound	Decomposition Range (°c)	Peak temp (°c)	Weight loss (%)	Product obtained	Residual mass Found/cald
[Ni(L^1)$_2$bpy]	138-610	223	80	NiS	2.80/2.70
[Ni(L^1)$_2$ph]	240-317	298	64	$RNCS_2Ni$	3.21/2.70
	385-492	594	84	NiS	1.39/1.35
[Ni(L^3)$_2$bpy]	131-350	191	83	NiS	2.0/1.8
[Ni(L^3)$_2$ph]	223-335	298	83	NiS	2.14/1.89
[Ni(L^4)$_2$bpy]	170-475	230	84	NiS	2.52/2.59
[Ni(L^4)$_2$ph]	267-341	296	67	$RNCS_2Ni$	4.55/4.32
	440-502	471	86	NiS	1.96/1.95

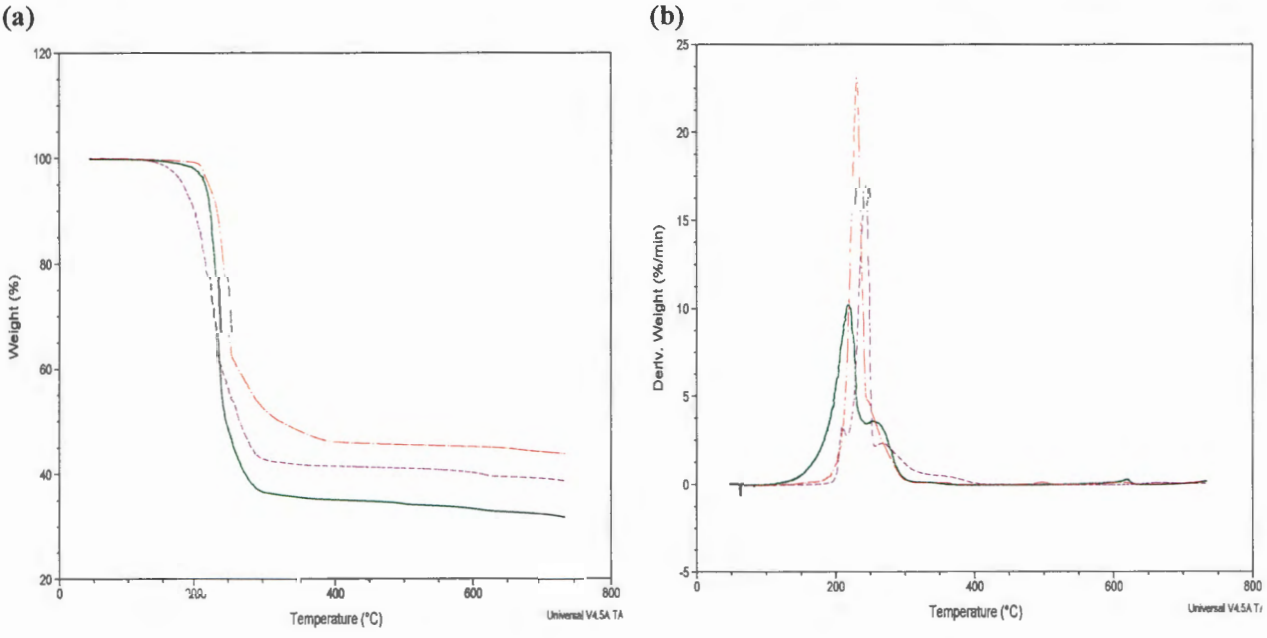

Figures 3.17: Overlapped (a) TG and (b) DTG curves of: **[Ni(L^1)$_2$]** (green), **[Ni(L^1)$_2$bpy]** (Purple) and **[Ni(L^1)$_2$ph]** (red).

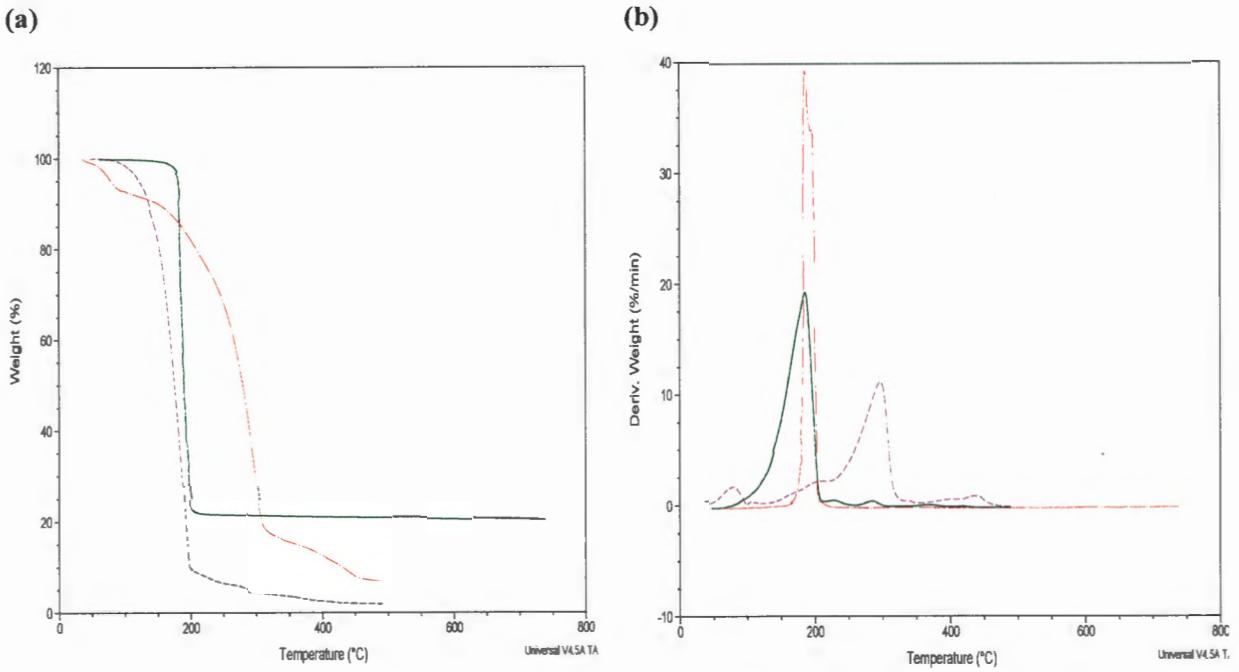

Figures 3.18: Overlapped (a) TG and (b) DTG curves of: **[Ni(L^3)$_2$]** (green), **[Ni(L^3)$_2$bpy]** (Purple) and **[Ni(L^3)$_2$ph]** (red).

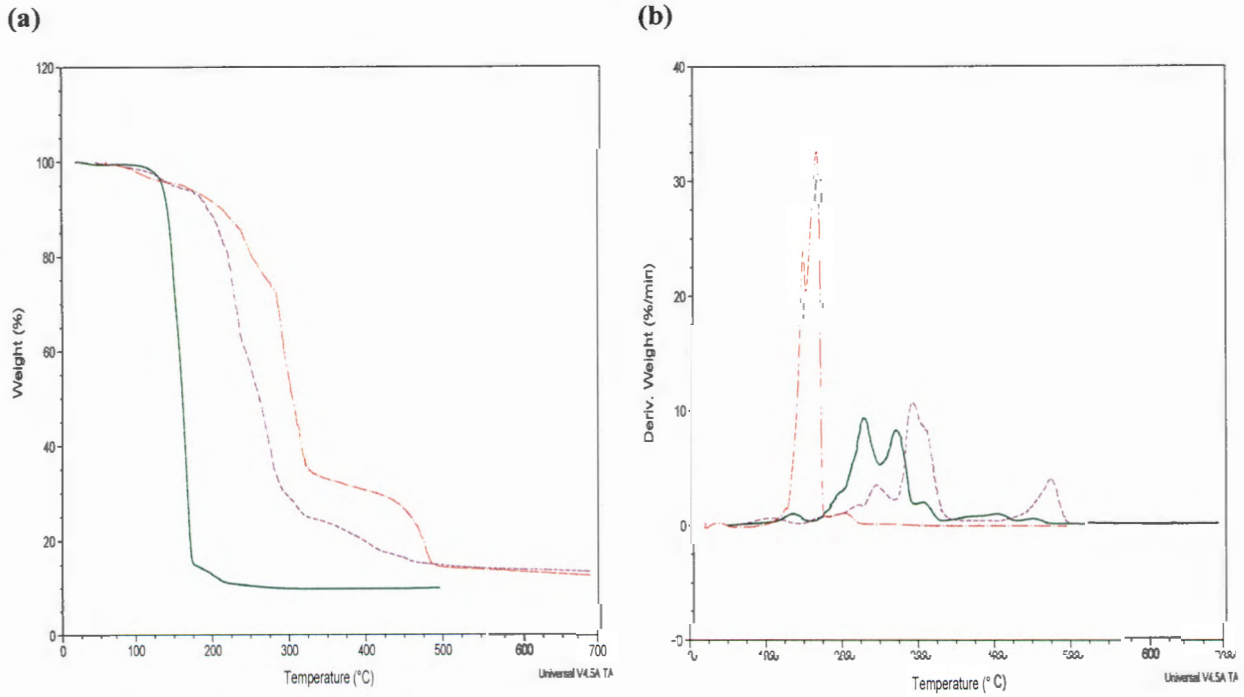

Figures 3.19: Overlapped (a) TG (b) DTG curves of: **[Ni(L^4)$_2$]** (green), **[Ni(L^4)$_2$bpy]** (purple) and **[Ni(L^4)$_2$ph]** (red).

3.13. Mixed ligand complexes of the synthesized Ni(II) dithiocarbamate complexes

Nickel(II) dithiocarbamate complexes in four coordinate geometry have mononuclear structure, and their reactions with Lewis bases having P and N donor atoms show interesting variation [31]. The reaction of dithiocarbamate with the nitrogenous and phosphines ligand is significantly influenced by the steric and electronic nature of the dithiocarbamato ligands [32]. To obtain new functionalized complexes with the aim of improving the biological profile of the parent compounds, P and N donor atoms: triphenylphosphine (PPh_3), isothiocyanate (SCN) and isocyanate (CN) were incorporated into the backbone of the parent complexes. The preparative methods are as detailed below:

3.13.1. Synthesis of (*N*-benzyldithiocarbamato-S,S′)(isothiocyanato)(triphenylphosphine) nickel(II) [$NiL^2(NCS)PPh_3$] .

A mixture of bis(*N*-benzyldithiocarbamato-S,S')nickel(II) (**NiL^2**) (0.06 g, 0.13 mmol), triphenylphosphine (0.065 g, 0.25 mmol), nickel(II) chloride hexahydrate (0.03 g, 0.13 mmol), ammonium thiocyanate (0.02 g, 0.25 mmol) was refluxed for 3 h in acetonitrile –methanol mixture (2:1, 35 mL). A dark purple-red mixture was obtained which was filtered after cooling to room temp. Single crystals appropriate for X-ray structural analysis were obtained by slow evaporation of the solvent.

(37) [$NiL^2(NCS)PPh_3$]: Yield, 0.12 g (85 %); M.pt: 203 – 205 °C: Selected FTIR ν (cm^{-1}): 1486 (C=N), 1386 (C_2-N), 971 (C=S), 3102 (=CH-H), 2981 (H_2C-H), 3378 (-NH), 1521 (-NH), 468 (Ni-S), 2139 (CN), 862 (CS) of –NCS; ^{1}HNMR (DMSO) δ (ppm)= 7.43–7.24 (m, 10H, $C_6\underline{H_5}$–CH_2–NH), 4.50 (s, 4H, C_6H_5–$C\underline{H_2}$–NH), 8.40 (s, 2H, C_6H_5–CH_2–$N\underline{H}$); ^{13}CNMR (DMSO) δ (ppm)= 136.91, 136.15, 133.59, 129.49 ($\underline{C}_6H_5$–CH_2–NH), 129.31, 129.04, 128.40, 128.13 ($\underline{C}_6H_5$-P), 46.76 (C_6H_5–$\underline{C}H_2$–NH), 144.30 (S$\underline{C}$N), 206.67 (–$\underline{C}S_2$). $C_{27}H_{23}N_2S_3NiP$ (561.33): Calculated: C, 57.77; H, 4.13; N, 4.99; S, 17.14; Found: C, 57.27; H, 4.40; N, 4.60; S, 17.75%

3.13.2. Synthesis of (*N*-benzyldithiocarbamato-S,S′)(isocyano-*N*)(triphenylphosphine) nickel(II) [$NiL^2(NC)(PPh_3)$].

A mixture of bis(*N*-benzyldithiocarbamato-S,S')nickel(II) (**NiL^2**) (0.21 g, 0.5 mmol), triphenylphosphine (0.26 g, 1 mmol), nickel(II) chloride hexahydrate (0.03 g, 0.13 mmol), potassium cyanide (0.07 g, 1 mmol) was refluxed for 3 h in dichloromethane – methanol mixture (1:1, 50 mL). The dark purple-red solution obtained was filtered after cooling down, and the filtrate was left to evaporate. After a few days, the product separated as a precipitate which was filtered off, rinsed with ethanol and dried in desiccator.

(38) [NiL^2(NC)(PPh$_3$)]: Yield, 0.20 g (74 %); M.pt 123 – 125 °C; Selected FTIR, *v* (cm-1): 1457 (C=N), 1351 (C2-N), 966 (C=S), 3060; (=CH-H), 2983(H2C-H), 3380 (-NH), 1557 s(-NH), 477 (Ni-S), 2188 (CN); ^{1}HNMR (DMSO) δ (ppm)= 7.47–7.24 (m, 10H, $C_6\underline{H}_5$–CH_2–NH), 4.52 (s, 4H, C_6H_5–$C\underline{H}_2$–NH), 8.55 (t, 2H, C_6H_5–CH_2–$N\underline{H}$).^{13}CNMR (DMSO) δ (ppm)= 136.14, 133.86, 133.64, 130.44 ($\underline{C}_6H_5$–CH_2–NH), 129.36, 129.07, 128.36, 128.10 ($\underline{C}_6H_5$-P), 46.79 (C_6H_5–$\underline{C}H_2$–NH), 133.20 ($\underline{C}$N) 206.84 (–$\underline{C}S_2$); $C_{27}H_{23}N_2S_2NiP$ (529.20): Calculated: C, 61.27; H, 4.38; N, 4.99; S, 12.12. Found: C, 61.73; H, 4.50; N, 4.78; S, 11.75%.

3.13.3. Synthesis of (*N*-alkyl-*N*-ethanoldithiocarbamato S,S′)(isothiocyanato) (triphenylphosphine) nickel(II), [NiL(NCS)(PPh$_3$)] (L= L^6, L^7 and alkyl = CH_3, CH_2CH_3).

A mixture of bis(*N*-alkyl-*N*-ethanoldithiocarbamate) Ni(II), (0.09 g, CH_3; 0.097 g, CH_2CH_3, 0.25 mmol); triphenylphosphine (0.13 g, 0.5 mmol), nickel(II) chloride hexahydrate (0.06 g, 0.25 mmol), ammonium thiocyanate (0.04 g, 0.5 mmol) was refluxed in acetonitrile-methanol mixture (2:1, 30 mL) for 4 h. The solution obtained was dark purple-red which was allowed to cool down, filtered, and left for slow evaporation of the solvent.

(41) [NiL^6(NCS)(PPh$_3$)]: Yield, 0.12 g (85 %); M.pt: 193 – 195 °C; Selected IR, v(cm^{-1}): 1431 (C=N), 1200 (C_2–N), 1067 (C=S), 3366 (OH), 2894 (-H_2C-H), 2920(CN) and 741(CS) of –NCS, 432 (Ni-S); ^{1}H NMR ($CDCl_3$) δ 3.1 (s, 3H, CH_3), 3.5(t, 2H, $\underline{C}H_2CH_2OH$), 5.0(t, 2H, $CH_2\underline{C}H_2$ OH), 2.90 (s, 1H, OH) δ 7.41- 7.5 (m, 10H, C_6H_5), 7.40–7.60 (m, 6H, C_6H_5), 2.50 (s, 1H, OH).^{13}CNMR ($CDCl_3$) δ (ppm) = 132,127.0 (C_6H_5), 40.5 (-CH_3), 77.0(CH_2CH_2OH), 134.8(SCN),198.6 (–CS_2). $C_{23}H_{23}N_2S_3ONiP$ (529.30): Calculated: C, 52.19; H, 4.38; N, 5.29; S, 18.17. Found: C, 52.27; H, 4.52; N, 5.60; S, 17.75%

(42) [NiL^7(NCS)(PPh$_3$)]: Yield, 1.05 g (69.5%); M.pt: 207 – 210 °C; Selected IR, v(cm^{-1}): 1518 (C=N), 1278 (C_2-N), 987 (C=S), 2920 (H_2C-H), 424 (Ni-S), 3321 (O-H); ^{1}HNMR (DMSO) δ (ppm) = 2.2 (t, 3H, CH_2CH_3), 3.4 (q, 2H, CH_2CH_3), 3.6(t, 2H, CH_2CH_2OH), 5.0 (t, 4H, CH_2CH_2OH), 2.9 (s, 1H, CH_2CH_2OH), 7.0-7.6 (m, PPh_3).^{13}CNMR (DMSO) d (ppm) =77.1 (CH_2OH), 11.3 (CH_2CH_3),59.4 (CH_2OH), 50.8 (NCH_2), 134.2 (NCS), 204.6 (-CS_2); $C_{24}H_{25}N_2OS_3NiP$ (543.33): Calculated: C, 53.05; H, 4.64; N, 5.16; S, 17.70% Found: C, 53.45; H, 4.30; N, 5.50; S, 17.25%.

3.13.4. Synthesis of (*N*-alkyl-*N*-ethanoldithiocarbamatoS,S)(isocyano) (triphenylphosphine) nickel(II), [NiL(NC)(PPh_3)] (L= L^6, L^7 and alkyl = CH_3, CH_2CH_3).

Bis(*N*-alkyl-*N*-ethanoldithiocarbamate)Ni(II), (0.18 g, CH_3; 0.194 g, CH_2CH_3; 0.5 mmol) was mixed with triphenylphosphine (0.26 g, 1.0 mmol), nickel(II) chloride hexahydrate (0.12 g, 0.5 mmol), and potassium cyanide (0.065 g, 1.0 mmol), and refluxed in methanol-dichloromethane mixture (1:1, 40 mL) for 4 h. The solution obtained which was dark purple-red in colour was cooled, filtered, and left to slowly evaporate the solvent at room temperature to afford single crystals suitable for X-ray analysis.

(43) [NiL^6(NC)(PPh_3)]: Yield, 0.20 g (74%); M.pt: 137-139 °C; Selected IR, ν(cm^{-1}): 1432 (C=N), 1282 (C_2—N), 1094 (C=S), 3285 (OH), 2932 (-H_2C-H), 2867(CN) and 743(CN) of –N≡C, 420 (Ni-S); ^{1}HNMR (DMSO) δ (ppm)= 3.0 (s, 3H, CH_3), 3.5(t, 2H, $\underline{C}H_2CH_2OH$), 4.1(t, 2H, $CH_2\underline{C}H_2$ OH), 2.90 (s, 1H, OH), 7.42 (m, 10H, C_6H_5), 7.38–7.26 (t, 6H, C_6H_5), ^{13}CNMR (DMSO) δ (ppm)= 129.1, 129.5, 133.8 (C_6H_5), 39.4(CH_3), 49.4 (-NCH_2), 54.4 (-CH_2OH), 207.8 (–CS_2), 134.8 (CN); $C_{23}H_{23}N_2S_2ONiP$ (497.24): Calculated: C, 55.56; H, 4.66; N, 5.63; S, 12.90. Found: C, 55.12; H, 4.26; N, 5.78; S, 11.75%.

(44) [NiL^7(NC)(PPh_3)]: Yield, 1.02 g (53.2%); M.pt. 128 – 130 ◦C; Selected IR, ν(cm^{-1}): 1515 (C=N), 1280 (C_2—N), 996 (C=S), 3318 (O-H), 2850 (H_2C–H), 422 (Ni-S). ^{1}HNMR (DMSO) δ =1.1 (t, 3H, $CH_2\underline{CH_3}$), 3.4 (q, 2H, $\underline{CH_2}CH_3$), 3.6 (t, $CH_2\underline{CH_2}OH$), 2.9 (s, 1H, $\underline{CH_2}CH_2OH$), 7.2-7.4 and 7.5-7.7 (m, PPh_3).^{13}CNMR (DMSO) 77.0 (NCH_2OH), 12.2 (NCH_3), 61.0 (CH_2OH), 51.3 (NCH_2), 128-134 (PPh_3), 135 (CN), 205 (-CS_2). $C_{23}H_{25}N_2OS_3NiP$ (531.32): Calculated: C, 51.99; H, 4.74; N, 5.27; S, 18.10%; Found: C, 51.45; H, 4.35; N, 5.50; S, 18.25%.

3.14. Results and discussion of the mixed ligand complexes of the synthesized Ni(II) dithiocarbamate complexes

3.14.1. General synthesis of the mixed ligand complexes of the synthesized Ni(II) dithiocarbamate complexes

The presence of the P and N donor atoms (to afford NiS_2PN and NiS_2PC) on the parent complexes, created an imbalance in the metal orbitals due to the additional donor atoms provided [33]. The new complexes responded by regulating their reactivities by a change in geometry and coordination properties. Schemes 3.16 and 3.17 present the synthetic routes to the preparation of the different adducts of the nickel(II) complexes of benzyldithiocarbamate and *N*-alkyl-*N*-ethanol dithiocarbamate respectively.

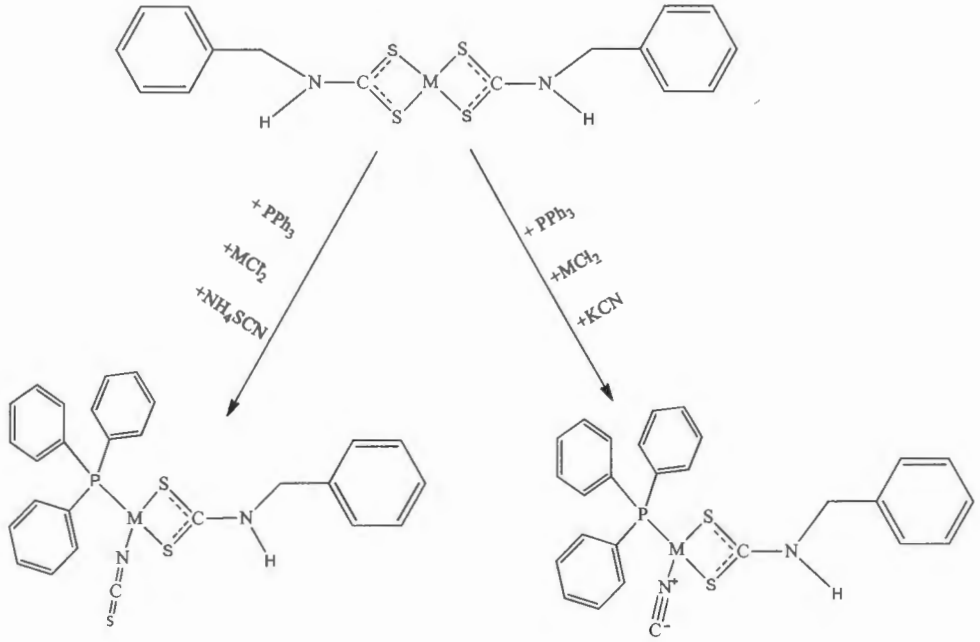

Scheme 3.16: Synthetic route for the heteroleptic complexes **[NiL²(NCS)(PPh₃)]** and **[NiL²(NC)(PPh₃)]**

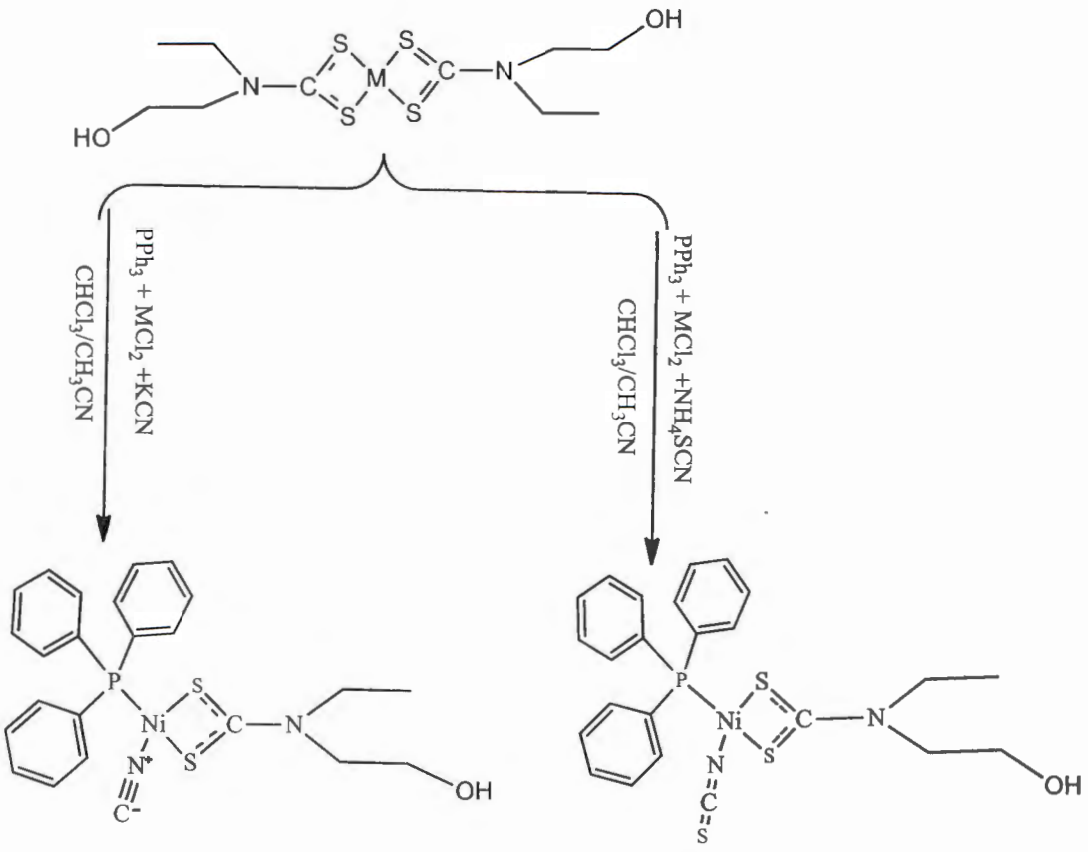

Scheme 3.17: Synthetic route for the heteroleptic **[NiL(NC)(PPh3)]** and **[NiL(NCS)(PPh3)]** complexes [R = CH_3 , CH_2CH_3].

3.14.2 Infrared studies of the mixed ligand Ni(II) dithiocarbamate complexes

The IR bands due to ν(CN) in complexes **[NiL^2(NCS)(PPh3)]** and **[NiL^2(NC)(PPh3)]** appeared around 1486 and 1457 cm^{-1} respectively, and are higher than that of the parent dithiocarbamate (1446 cm^{-1}). This is indicative of an increase in the strength of the thioureide bond as a result of the presence of the pi-accepting phosphine, and also the redistribution of electron density from the P toward the Ni due to the bonding of the triphenylphosphine to the nickel [5]. The ν(C–S) band which appeared around 966 and 971 cm^{-1} without any splitting in all the complexes, indicated a symmetrically bidentate coordination of the $-CS_2$ group to the metal centre. It also shows higher values than that of the parent at 923 cm^{-1}. The number of bands detected around 1000±70 cm^{-1} is indicative of the mode of bonding of the metal to the dithiocarbamate ligands [34]. In the far IR region, the appearances of new bands around 468 and 477 cm^{-1} due to the Ni-S vibration has higher values in the mixed ligands than the parent complex which may be as a result of higher coordination

number around the central metal ion [35]. The (N—H) stretching vibration occurred around 3232 cm^{-1} for the parent complex but at higher values around 3378 and 3380 cm^{-1} in the mixed ligands.

In the spectra of **[NiL^5(NCS)(PPh$_3$)]** and **[NiL^5(NC)(PPh$_3$)]** complexes, the ν(CN) peaks were observed around 1621 and 1543 cm^{-1}. These were higher than the parent which appeared around 1508 cm^{-1}. The ν(C–S) peaks around 995 and 996 cm^{-1} are slightly higher than the parent (923 cm^{-1}). The ν(Ni-S) found around 413 and 420 cm^{-1} are comparable to 528 cm^{-1} in the parent, the (N—H) stretching vibrations around 3392 and 3378 cm^{-1} were slightly below the value for the parent at 3439 cm^{-1}. The difference has been ascribed to the increase in the strength of the thioureide bond due to the presence of the pi-accepting phosphine, and the effect of the triphenylphosphine on the complex.

The presence of bands in the range 980 – 990 cm^{-1}, without any splitting, in the spectra of **[NiL(SNC)(PPh$_3$)]** and **[NiL(NC)(PPh$_3$)]** complexes, correspond to ν(C-S) vibrations. This was indicative of bidentate coordination mode of the dithiocarbamate moiety through the two sulphur donor atoms. The thioureide bands in these complexes were observed in the range 1433 to 1432 cm^{-1} for the CH_3; and 1518 to 1515 cm^{-1} for CH_2CH_3 containing compounds respectively. These were larger than that of the parent dithiocarbamate (1431 and 1470 cm^{-1}) and indicated the partial double bond character due to the electron releasing ability of the nitrogen atom toward the sulphur atoms via the thioureide π-system [5]. The higher vibrational frequency observed for the heteroleptic complexes compared to the parent complex indicate a mesomeric drift of electron density from the dithiocarbamate moiety towards the nickel(II) centre [33]. In addition, the broad bands around 3132-3366 cm^{-1} in all the complexes are assigned to O-H of the ethanol group. The bands at the far IR region of 424-432 cm^{-1} are due to the Ni-S bond. Finally, the bands which appeared around 2900 cm^{-1} and 742 cm^{-1} for the heteroleptic complexes are attributed to the N-coordinated isocyanate and isothiocyanate anions respectively.

3.14.3 Electronic studies of the mixed ligand Ni(II) dithiocarbamate complexes

The electronic spectra of the **[Ni(L)$_2$bpy]**, and **[Ni(L)$_2$ph]** complexes were the octahedral nickel(II) complexes with three low intensity bands. The bands at 220-233 nm, 307-313 nm which represent the $^3A_{2g} \rightarrow {}^3T_{1g}(F)$, $^3A_{2g} \rightarrow {}^3T_{1g}(P)$ transitions, and 340-350 nm could be assigned to π–π^* transition of the C═N in the bipyridine and phenanthroline ligands [36].

In the [NiL(PPh_3)(NCS)] and [NiL(PPh_3)(NC)](PPh_3) complexes, electronic transitions with incomplete electrons in the d-orbitals were observed. This gave absorption bands due to metal d-d transition and charge transfer transitions ($n\rightarrow\pi*$, $\pi\rightarrow\pi*$). As expected for square planar complexes, the diamagnetic nickel(ll) complex displayed a weak d-d transition. In this study, the bands at 320-390 nm is ascribed to the ligand to metal charge transfer transitions which supports the bonding of the ligand to the metal ion through sulphur atoms, while the bands at 420- 480 nm arise due to the transfer of electrons from the incompletely filled d-orbital of the metal ions to the ligand ($d\pi\rightarrow p\pi$). Other absorption bands at 460-540 nm are due to the nickel d-d transitions which could be assigned to d_{yz}-d_{xy}, d_{xz} -d_{xy} and d_{x2-y2}-d_{xy} transitions [37].

3.14.4 NMR spectra studies of the mixed ligand Ni(II) dithiocarbamate complexes

The ^{1}H NMR of complexes **[NiL^2(NCS)(PPh_3)]** and **[NiL^2(CN)(PPh_3)]** showed a set of similar signals between 7.40 and 7.43 ppm due to asymmetric NiS_2PN and NiS_2PC moieties. The protons due to the methylene (-CH_2) and amine (-NH) groups appeared as singlets at 4.50 and 4.52 ppm; 8.40 and 8.55 ppm respectively. The fast isothiocyanate and isocyanide ligand exchange is responsible for the broadening of the aliphatic protons. The signals observed in the downfield region, 7.25–7.41 ppm, are due to aromatic protons in the dithiocarbamate and triphenylphosphine [38].

In ^{13}C NMR spectra, the chemical shifts of the characteristic thioureide carbon (N–$^{13}CS_2$) of dithiocarbamate were observed at 206.6 and 206.8 ppm respectively. There is a significant up-field shift of 3.2 ppm in the thioureide carbon peak, relative to the parent **[Ni(L^2)$_2$]**, 210 ppm. This was supported by the higher vibrational frequency of C–N observed in the FTIR **[NiL^2(NCS)(PPh_3)]** and **[NiL^2(NC)(PPh_3)]**, and confirmed the presence of a π-accepting group [39]. The N–^{13}CS and N—^{13}C carbon signals were at 136.4 and 130.5 ppm respectively. The observed signal (at 130.5 cm^{-1}) in the CN complex indicated coordination of the cyanide via the electronegative nitrogen. The position of the peak corroborates the observed IR vibrational frequency for ν(NC) and indicated the presence of a N-coordinated cyanide.

In the spectra of the heteroleptic complexes **[NiL(NCS)(PPh_3)]** and **[NiL(NC)(PPh_3)],** the methylene proton (-CH_2) of the ethyl group resonated around 1.1 - 2.2 ppm, an up-field shift of 1.0 ppm compared to the parent complex. For the methyl proton of the- *N*-methyl-*N*-ethanoldithiocarbamato group appeared as broad singlets around 3.0 and 3.1 ppm. They appeared as quartet at 3.40 ppm in the **L^{10}** complexes. A slight up field shift was observed from the positions of their appearance in the parent complex at 3.36 ppm. The fast ligand exchange process in the heteroleptic complexes resulted in more broadening of the proton signals. Similarly, the signal due

to the proton of the –OH group appeared around 2.9 ppm, which was an up-field shift of 0.4 ppm from their positions in the parent complexes. The set of multiplets in the range 7.0 - 7.7 ppm are due to the phenyl protons of the triphenyl phosphine in the asymmetric NiS_2PN and NiS_2PC. The $-CS_2$ peaks appeared in the range 207.2 - 207.8 ppm for all the complexes, with an up-field shift of 2.6 ppm compared to the parent. The shift is a consequence of the attachment of π-accepting triphenylphosphine group [40]. The peaks due to the carbon of the NCS and NC appeared around 134.0 - 135.0 ppm for the **[NiL(NCS)(PPh_3)]** and **[NiL(CN)(PPh_3)]** respectively. Thus, these established the attachment of the isocyanide and cyanide groups to the parent complex via the electronegative nitrogen atom. Besides these signals, the heteroleptic complexes displayed additional four peaks between 128.00 – 134.00 ppm, due to the carbons of the triphenylphosphine molecule.

3.14.5. X-ray crystallography of the [NiL^2(NCS)(PPh_3)] and [NiL^7(NC)(PPh_3)]

3.14.5.1. Description of crystal structures of [NiL^2(NCS)(PPh_3)]

The systematic absences reported in the diffraction data for **[NiL^2(NCS)(PPh_3)]** were found to be consistent for the *P*1 space group which yielded stable results of refinement that are chemically and computationally reasonable [1-4]. The crystal and structure refinement data for complex **[NiL^2(NSC)(PPh_3)]** are presented in Table 3.13. The ORTEP diagram is shown in Figure 3.20, while the selected bond length and angles are summarised in Table 3.14 There is one symmetry-independent molecule in the asymmetric unit, consisting of the entire Ni(II) complex. The nickel is in the +2 oxidation state and charge balance comes from the one bound isothiocyanate and one dithiocarbamate molecule where the negative charge is spread over both S atoms in the dithiocarbamate. Around the nickel atom, the *cis* angles: N1—Ni1—P1 = 97.62(4)°, S1—Ni1—P1 = 93.482 (17)°, N1—Ni1—S2 = 91.26(4)° and S1—Ni1—S2 = 78.68(2)° and *trans* angles N1—Ni1—S1 = 167.85(5) and P1—Ni1—S2 = 166.80(2)° make the molecule to adopt a non-centrosymmetrical distorted square planar. Due to the bidentate chelation of the nickel atom by two sulphur atoms from the dithiocarbamate, one of the *cis* angles S1—Ni1—S2 = 78.68(2)° is significantly small compared to the 90° expected for a square planar geometry [41]. A portion of the molecule in the asymmetric unit exhibits positional disorder (Figure 3.21a). The atoms involved are Ni1, S1, S2, C1, C2, C3, C4 and N2 and they are disordered over two positions. The major component is present 93.876(3) % of the time as was refined anisotropically. The minor component was also successfully refined anisotropically. The above-mentioned atoms had thermal displacement parameter constraints applied to them. Within the NCS2 moiety, the characteristic delocalisation of *p*-electron of dithiocarbamate anion is observed in the bond lengths of the C—N

and C—S [C—S = 1.725(2)Å and C—N = 1.304(2) Å] which are very short compared to the single C—N bond length (1.47 Å) and C—S (1.81Å) [35]. The Ni1–S1 and Ni1–S2 bond lengths are very close at 2.1947(5) and 2.2167(5) Å. However, the Ni1–N1 bond length 1.850(4) is significantly shorter than the Ni1–P1 bond length 2.2298(4). The difference is ascribed to the good *p*-acceptor property of triphenylphosphine, and supports a good interaction between the nitrogen and the phosphorus in the complex [39]. There is evidence of intermolecular hydrogen bonding interactions and no intramolecular hydrogen bonding in the crystal structure, as shown in Figure 3.21 (a) The intermolecular N2—H2···S3 hydrogen bonds involved the hydrogen on the nitrogen atom and the S3 atom of the isocyanate group. A $\pi-\pi$ ring interactions was absent in the system. The molecular structure diagram showing the packing of the complex, viewed down the crystallographic *a*-axis and *b*-axis are presented in Figures 3.21 b and c respectively.

3.14.5.2 Description of crystal structures of [NiL^7(NC)(PPh$_3$)]

Crystallographic data for **[NiL^7(NC)(PPh$_3$)]** are given in Table 3.13 and selected bond lengths and angles are presented in Table 3.14. Figure 3.22 presents the molecular drawing of **[NiL^7(NC)(PPh$_3$)]**. The systematic absences in the diffraction data were uniquely consistent for the space group *C*2/*c* that yielded chemically reasonable and computationally stable results of refinement [1-6]. There are two symmetry-independent molecules in the asymmetric unit, one consisting of the entire Ni(II) complex and the second is a disordered triphenylphosphine moiety. The nickel is in the +2 oxidation state and charge balance comes from the one bound cyano ligand and one dithiocarbamate molecule where the negative charge is spread over both S atoms in the dithiocarbamate. The expected heteroleptic Ni(II) complex was obtained with a triphenylphosphine molecule also forming part of the crystal structure. Both symmetry independent molecules in the asymmetric unit exhibits extensive positional disorder. The triphenylphosphine molecule is disordered over two positions with the major component of the disorder being present 54.778(2)% of the time, and all atoms were refined anisotropically. The minor component was also successfully refined anisotropically. The Ni(II) complex exhibited positional disorder in the ethyl/hydroxyethyl groups. The major component of the disorder is present 74.728(6)% of the time and all atoms involved were successfully refined anisotropically.

The asymmetric unit of the complex contains one Ni(II) atom which is bound to one isocyanate and one dithiocarbamate molecule. The angles surrounding the nickel atom, are the *cis*: C1—Ni1—S2= 170.87 (11)°, C1—Ni1—P1=91.05 (11)°, C1—Ni1—S1=91.71 (11)°, S2—Ni1—S1 = 79.22 (3)°; while the *trans* angles: S1—Ni1—P1= 176.67 (4) °, and C2—S2—Ni1 = 85.75 (11)°, confers on the molecule a monoclinic structure. The Ni—S bond lengths are 2.2013(9) and 2.2079(9) Å and

the C2—N2 and C1—N1 bond lengths are 1.309(12) and 1.153(5) Å, respectively. The short C2—N2 distance, as compared to the normal bond distances for C—N and C=N (1.47 and 1.28 Å) indicates that the π electron density is delocalized over the S_2CN segment [42].

Table 3.13: Summary of crystal data and structure refinement for **[NiL²(NSC)(PPh₃)]** and **[NiL⁷(NC)(PPh₃)]**.

Complex	**[NiL²(NSC)(PPh₃)]**	**[NiL⁷(NC)(PPh₃)]**
Empirical formula	$C_{27}H_{23}N_2NiPS_3$	$C_{42}H_{40}N_2NiOP_2S_2$
Formula weight	561.33	773.53
Crystal size (mm)	0.13 x 0.13 x 0.44	0.38 × 0.25 × 0.22
Crystal system	Triclinic	Monoclinic, C2/c
Temperature (K)	100	100
Crystal habit	Plank, dark red	light orange blocks
Space group	*P*	C2/c (no. 15)
a (Å)	9.3486(6)	36.798(4)
b (Å)	9.8811(6)	10.3589(10)
c (Å)	13.7004(8)90	20.233(2)
α (°)	9.3486(6)	90
β (°)	84.5700(1)90	95.485(2)
γ (°)	85.0720(1)	90
V [Å**3]	1255.13(13)	7677.1(13)
Z	2	8
*D*calc (g cm^{-3})	1.485	1.339
F(000)	580	3232
Dataset	12:12; -13:13; -18:18	-49:49, -13:13, -27:27
μ(MoKa) (/mm)	1.11	0.733
Tot.,Uniq.Data,	36245, 6370, 0.031,	9598, 7189
R(int)	0.029	0.073
Observed reflections *I*> 2σ(*I*)	5808	7913
Nref, Npar	6370, 331	9598, 682
Final *R*, w*R2, S*	0.029, 0.072, 1.02	0.068,0.173, 1.14
Max.residual density [e/Å^3]	0.43	2.38
Min. residual density [e/Å^3]	-0.45	-0.41
θ range (°)	-0.21	2.0-28.4

Table 3.14: Selected bond distances and angles

$[NiL^2(NCS)(PPh_3)]$	
Bond	distances (Å)
Ni1—S1	2.1947 (5)
Ni1—S2	2.2167 (5)
Ni1—P1	166.80 (2)
Ni1—N1	2.2298 (5)
S1—C1	1.8501 (14)
S2—C1	1.725 (2)
S3—C2	1.7092 (19)
P1—C10	1.6292 (16)
P1—C16	1.8197 (15)
P1—C22	1.8252 (15)
P1—Ni1A	1.8238 (15)
N1—C2	2.074 (7)
N1—Ni1A	1.162 (2)
C1—N2	2.169 (6)
Bond	angles (°)
S1—Ni1—S2	78.68 (2)
S1—Ni1—P1	93.482 (17)
S2—Ni1—P1	167.88 (5)
N1—Ni1—S1	91.26 (4)
N1—Ni1—S2	97.62 (4)
N1—Ni1—P1	86.27 (6)
C1—S1—Ni1	85.96 (6)
C1—S2—Ni1	112.44 (5)
C10—P1—Ni1	106.61 (7)
C10—P1—C16	102.51 (7)
C10—P1—C22	104.40 (18)
C10—P1—Ni1	104.40 (18)
C16—P1—Ni1	106.07 (5)

$[NiL^7(NC)(PPh_3)]$.	
Bond	distances (Å)
Ni1—C1	1.860 (4)
Ni1—P1	2.1862 (9)
Ni1—S2	2.2079 (9)
Ni1—S1	2.2079 (9)
S1—C2	1.719 (3)
S2—C2	1.732 (3)
P1—C19	1.813 (3)
P1—C13	1.822 (3)
P1—C7	1.827 (3)
N1—C1	1.153 (5)
C2—N2A	1.309 (12)
Bond	Angle (°)
C1—Ni1—P1	91.05 (11)
C1—Ni1—S2	170.87 (11)
C1—Ni1—S1	91.71 (11
S2—Ni1—S1	79.22 (3)
P1—Ni1—S1	176.67 (4)
C2—S2—Ni1	85.75 (11)
S1—C2—S2	109.10 (18)
N2A—C2—S1	125.5 (5)
C19—P1—C13	106.71 (16)
C13—P1—Ni1	109.85 (11)
C7—P1—Ni1	117.26 (11)
N1—C1—Ni1	177.2 (3)

(a)

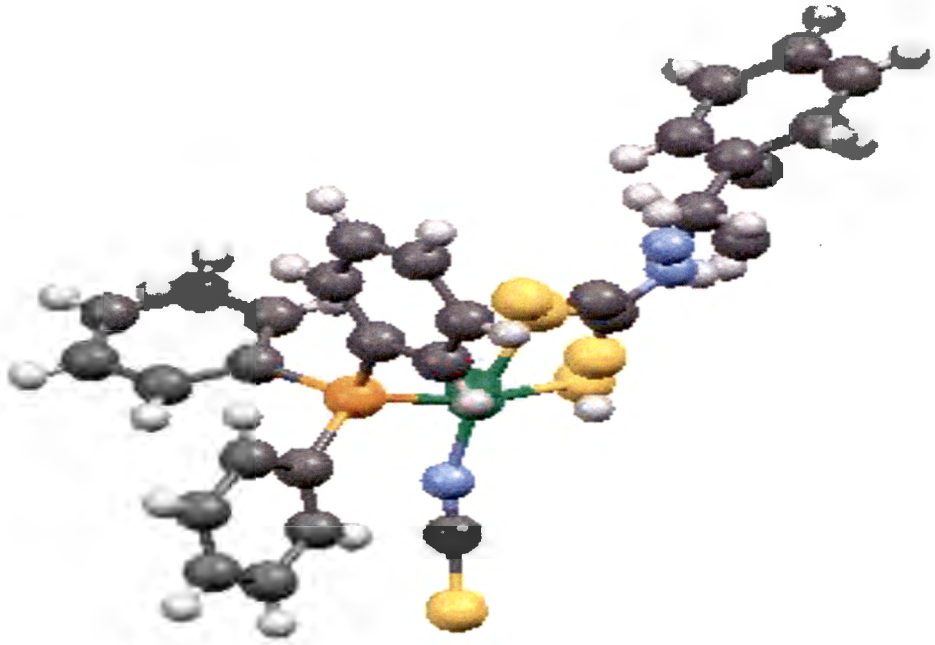

(b)

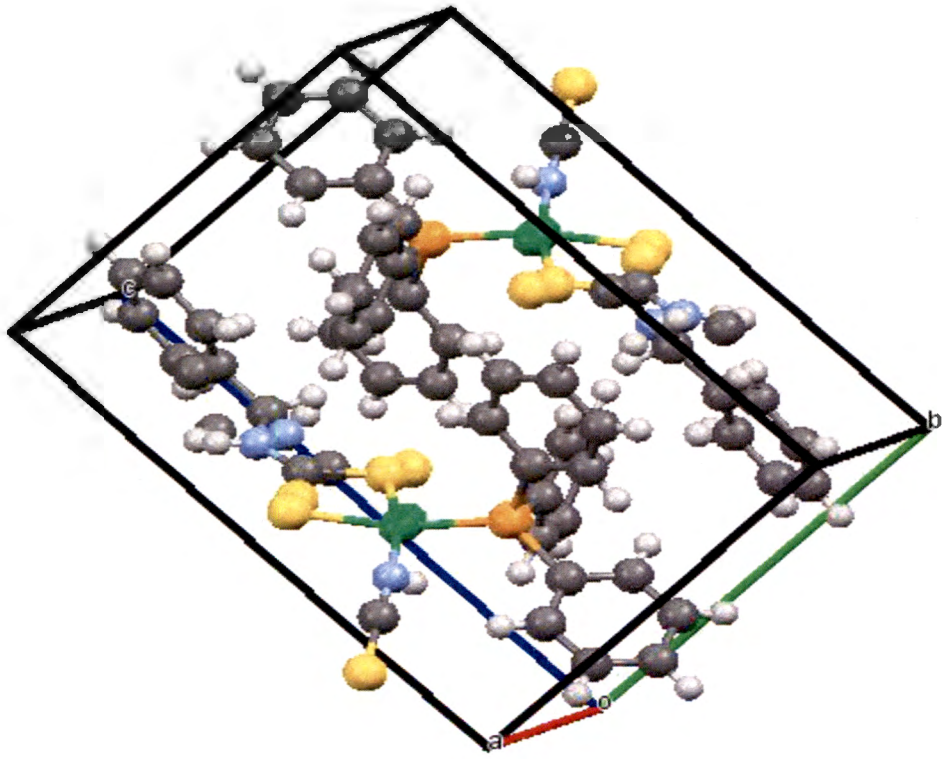

Figure 3.20: (a) Molecular structure and (b) packing diagram of **[NiL^2(NCS)(PPh$_3$)]**

(c)

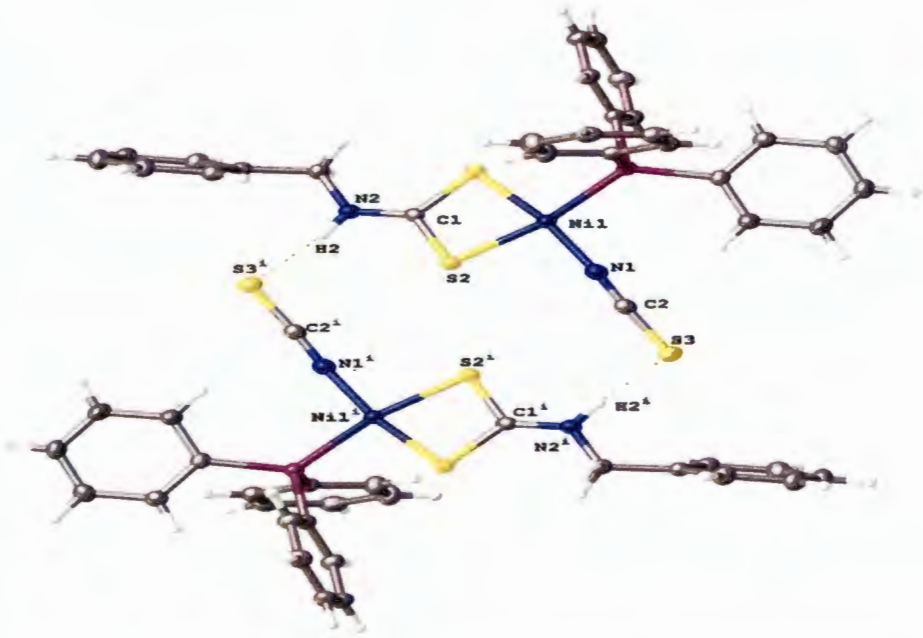

Figure 3.21(a): Molecular structure diagram showing the hydrogen bonding contacts (yellow dashed lines) for the complex 2. (Symmetry code: (i) -*x*+2, -*y*, -*z*+1)

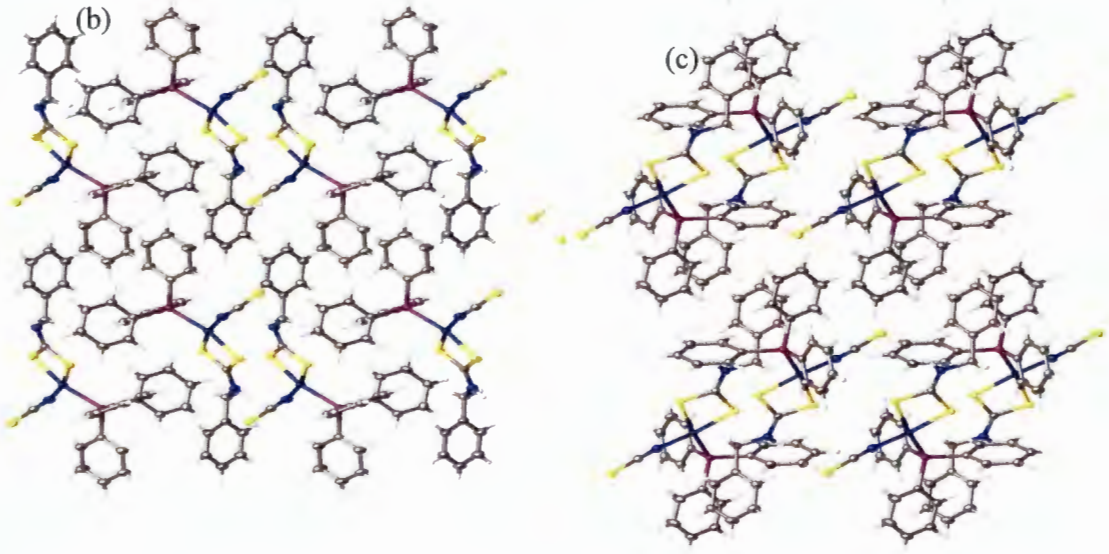

Figure 3.21: Molecular structure diagram showing the packing of complex 2 viewed down the crystallographic (b) a-axis and (c) b-axis. Yellow dashed lines show the H-bond contacts

(a)

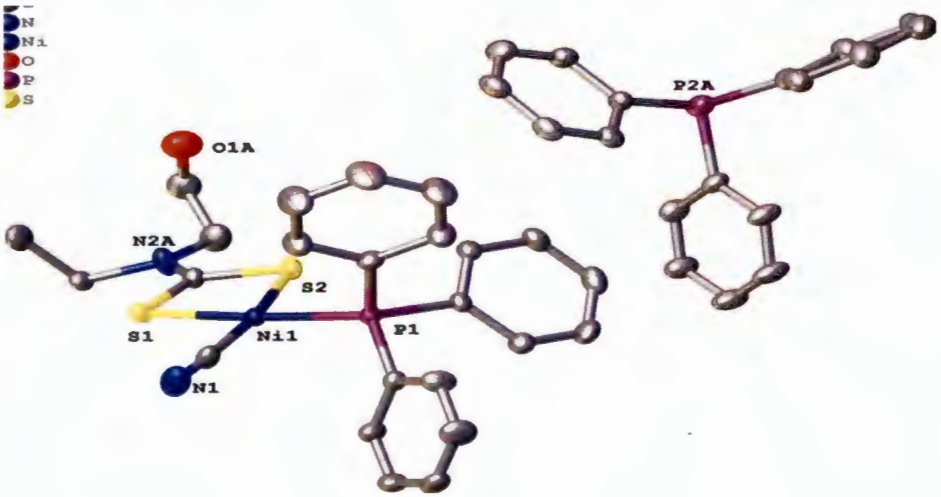

(b)

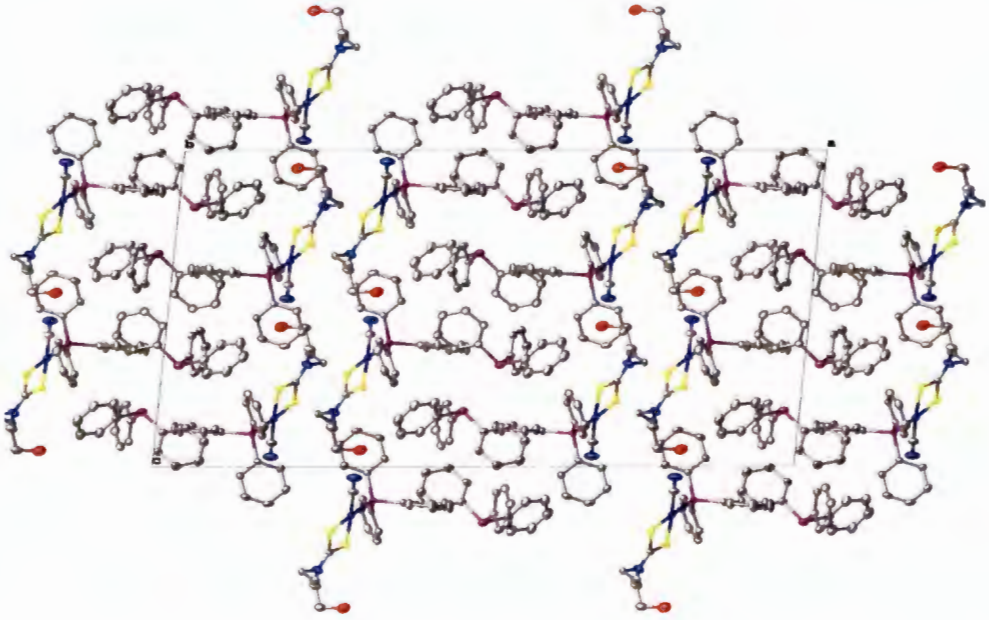

Figure 3.22: A molecular drawing shown with 50% probability ellipsoids, showing (a) only the major disorder component of the molecule of the asymmetric unit, and **(b)** packing diagram of **[NiL^7(NSC)(PPh$_3$)]**viewed down the b-axis

3.14.5. Thermal decomposition studies of the mixed ligand complexes of Ni(II) dithiocarbamate complexes

Figures 3.22 - 3.25 present the overlapped TGA/DTG graphs of the complexes. The relevant data from the thermal decomposition are presented in Table 3.15. The parent complex **[Ni(L^2)$_2$]** showed a well-defined two steps decomposition (Figures 3.22). The first step appeared between 169 – 194 °C, with a 35% mass loss which corresponded to the loss of the benzyl group, and the formation of thiocyanate intermediate. The second step started instantaneously after the first with a 73% loss in the range 194 – 255 °C to yield NiS2 as residue [43][44] (mass: found 3.03; calculated, 3.22 mg). The heteroleptic complex, **[NiL^2(NSC)(PPh$_3$)]** also gave a two-step decomposition. The first step occurred between 187 and 206 °C, and with a 70% loss due to the decomposition of the ligand molecules and the formation of thiocyanate (found, 4.50; calculated, 4.00). The second step decomposition in the range 207 – 300 °C with a 93% loss yielded the NiS residue (found, 1.920; calculated, 2.430) [45].

The decomposition profile of **[NiL^2(NC)(PPh$_3$)]** is presented in Figure 3.22. It showed that the complex decomposed in one step in the range 194-347 °C with 77% loss and yielded nickel sulphide (NiS_2) directly in the single step (mass: found, 4.01; calculated, 3.90). The overlapped graphs showed that the substitution of the sulphur atoms in the NiS4 chromophore of complex **[Ni(L^2)$_2$]** by the P and N atoms in complexes **[NiL^2(NSC)(PPh$_3$)]** and **[NiL^2(NC)(PPh$_3$)]** resulted in an increase in the decomposition temperature of the mixed ligand complexes. This indicates that the mixed ligand complexes have higher thermal stability than the parent complex. This is contrary to the earlier reported studies [46] where the replacement of the sulphur atoms in the NiS4 chromophore resulted in a reduction in the temperature of decomposition of the mixed ligand complexes. This difference in thermal behaviour could be due to the changes in substituents at the nitrogen of dithiocarbamate which could affect the properties of the complexes.

In the TGA of **[NiL^6(NCS)(PPh$_3$)]** and **[NiL^6(NC)(PPh$_3$)]** complexes, the first decomposition step occurred in the temperature range 189 – 239°C and 191 – 244°C with a 29 and 31% loss respectively. This corresponded to the decomposition of the organic molecules and the formation of thiocyanate. The second step decomposition in the range 250 – 310 and 254 -310 °C with a 76 and 75% loss yielded the NiS residue respectively. The final products of the thermolysis of the complexes were consistent with 1:1 nickel: sulphide phases. The replacement of the sulphur atoms in the NiS4 chromophore of the parent complexes with P and N atoms resulted in an increase in the decomposition temperatures, showing a higher thermal stability.

[NiL^7(NCS)(PPh$_3$)] complex presented a two-step decomposition profile. The first step of decomposition occurred in the range 204-274 °C with 32% loss of the organic molecule. After this

step, the residual mass obtained (found: 10.30, cald: 11.09) indicated isothiocyanate as intermediate product. The second step of decomposition occurred in the range 280-341 °C with 83% weight loss, and the weight of the residual product found/cald: 2.60/2.57 mg corresponded to NiS. Complex **[NiL^7(NC)(PPh$_3$)]** gave a single step decomposition in the range 266-351 °C with 82% loss, the mass of the residue (found/cald: 2.87/2.56 mg) corresponded to NiS_2. After this step, the decomposition profile maintained a plateau up to 700 °C indicating no further change. For the **[NiL^5(NCS)(PPh$_3$)]** and **[NiL^5(NC)(PPh$_3$)]** complexes, a single step decomposition pattern was followed, with the loss of all the methylene and the PPh_3/SCN/CN groups resulting in 84 and 91% loss, and yielding NiS residue with mass of 1.09 and 1.01 mg respectively.

From the results presented in Table 3.15, higher decomposition temperatures were observed in all the heteroleptic complexes. This showed that the heteroleptic complexes have higher thermal stability than the parent compounds, and could be due to the new addition of **PPh3, CN and NCS** to dithiocarbamates

All of the complexes showed almost the same pattern of TG profiles with similar weight loss and decomposition stages. The complexes decomposed to their corresponding nickel sulphide and, so are potential single source precursors for nickel sulphide nanoparticle

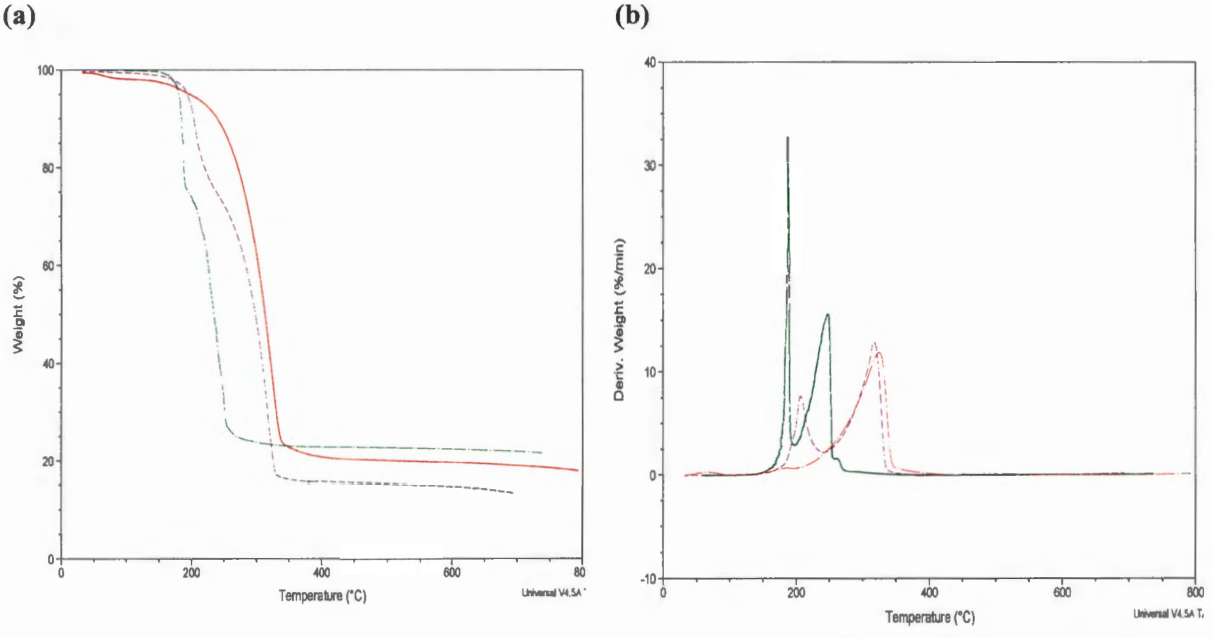

Figure 3.22: Overlapped TG/DTG curves of the compounds: **[Ni(L^2)$_2$]** (green), **[NiL^2 (NCS)(PPh$_3$)]** (Purple) and **[NiL^2 (CN)(PPh$_3$)]** (red).

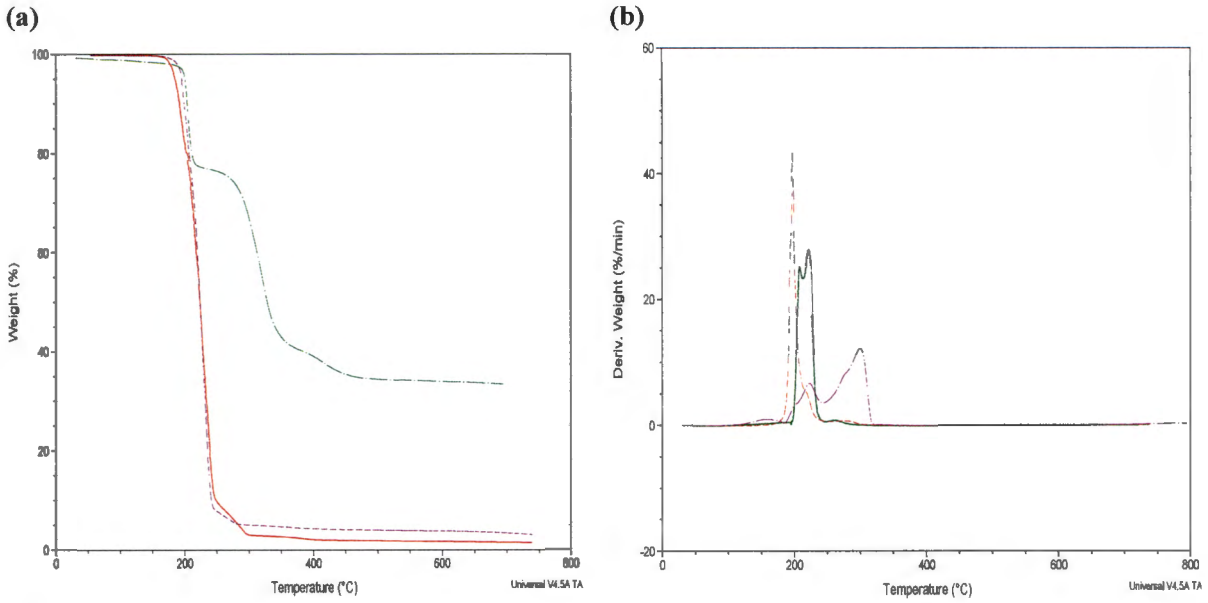

Figure 3.23: Overlapped (a) TG and (b) DTG curves of the compound: **[Ni(L^6)$_2$]** (green), **[NiL^6 (NSC)(PPh$_3$)]** (purple) and **[NiL^6 (CN)(PPh$_3$)]** (red).

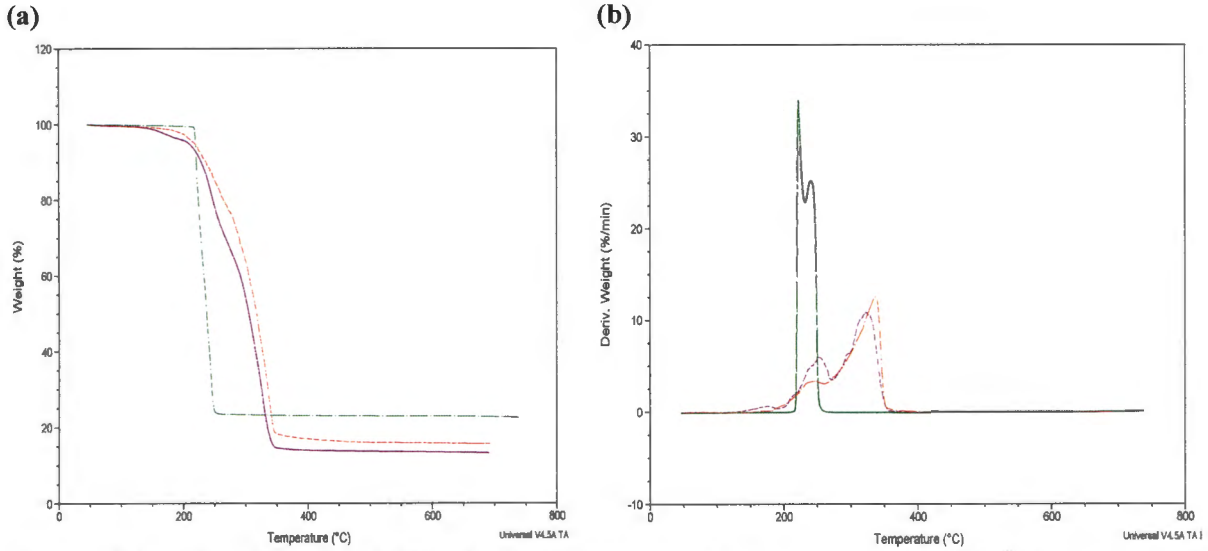

Figure 3.24: Overlapped (a) TG (b) DTG curves of the compound: **[Ni(L^7)$_2$]** (green), **[NiL^7 (NSC)(PPh$_3$)]** (Purple) and **[NiL^7(CN)(PPh$_3$)]** (red).

Table 3.15: Thermal stability data for the mixed ligand complexes of **$[Ni(L^2)_2]$, $[Ni(L^6)_2]$ and $[Ni(L^7)_2]$**

Compoud	Decomposition Range (◦c)	Peak temp (◦c)	Weight loss (%)	Product obtained	Residualmass: found/cald
$[Ni(L^2)_2]$	169 -194	187	73	NiS_2	3.027/3.221
	194-255				
$[NiL^2(NSC)(PPh_3)]$	187-206	285	93	NiS	1.920/2.430
	207-300				
$[NiL^2(CN)(PPh_3)]$	194-347	327	77	NiS_2	4.011/3.904
$[Ni(L^6)_2]$	195 -275	221	75	NiS	2.77/2.79
$[NiL^6(NSC)(PPh_3)]$	189 – 239	225	29	CS_2NiPPh_3	11.30/11.94
	250 - 310	302	76	NiS	2.75/2.70
$[NiL^6(CN)(PPh_3)]$	191 – 244		31	CS_2NiPPh_3	11.00/10.90
	254 -310	315	75	NiS	2.81/2.79
$[Ni(L^7)_2]$	212 – 258	222	76	NiS	3.10/2.97
$[NiL^7(NSC)(PPh_3)]$	204 - 274	247	32	$RNCS_2Ni$	10.30/11.09
	280 - 341	322	83	NiS	2.60/2.57
$[NiL^7(CN)(PPh_3)]$	266 - 351	337	82	NiS_2	2.87/2.56

3.15 Conclusion

Four different series of group 10 metal complexes have been synthesized using dithiocarabamate ligands prepared from primary and secondary amine, and represented as L^1 - L^5 ; and also dithiocarabamte ligands prepared from secondary amines derived from Schiff base compounds and represented as, L^6 - L^{10}. Further functionalization with P and N donor atoms afforded the formation of adducts and mixed ligand complexes comprising of 2, 2-bipyridine, 1, 10-phenanthroline, triphenylphosphine, isothiocyanate and thiocyanate. The complexes were characterized by elemental analysis, FTIR and NMR analysis. Some of the complexes were further characterized by single crystal X-ray analysis which confirmed that the geometry around the metal ions is distorted square planar geometry. The studies also revealed that M-S bond lengths increased down the group from Ni to Pt as confirmed from the crystal structure and also in the increase in FTIR vibration of the C=N and the ^{13}CNMR signal of NCS_2. Thermal decomposition studies revealed that all the complexes were thermally stable and the stability increased down the group. The introduction of the new groups increased the thermal stability of the parent complexes. All the

compounds decomposed into their respective metal sulphides making them suitable as single source precursors for metal sulphide nanoparticles.

REFERENCES

[1] APEX2, SADABS and SAINT, Bruker AXS Inc., Madison, Wisconsin, USA, (2010)

[2] G.M. Sheldrick, Acta Crystallogr. A71 (2015) 3.

[3] G.M. Sheldrick, Acta Crystallogr. C71 (2015) 3

[4] C.B. Hübschle, G.M. Sheldrick, B. Dittrich, J. Appl. Crystallogr. 44 (2011) 1281.

[5] E. Sathiyaraj, G. Gurumoorthy, S. Thirumaran, New J. Chem. 39 (2015) 5336.

[6] R.T. Li, P.Y. Ding, M. Han, M.S. Cai, Synth. Commun. 28 (1998) 295.

[7] A. Manohar, K. Karpagavel, A. Murugan, Int. J. ChemTech Res. 6 (2014) 474.

[8] I. Ali, W.A. Wani, K. Saleem, M. Hseih, Polyhedron 56 (2013) 134.

[9] R. Pelgrift, A. J. Friedman, Adv. Drug Delivery Rev. 65 (2013) 1803.

[10] E. Sathiyaraj, T. Srinivasan, S. Thirumaran, D. Velmurugan, J. Mol. Struct. 1102 (2015) 203.

[11] F. Bonati, S. Cenini, R. Ugo, J. Organomet. Chem. 9 (1967) 395.

[12] Y. Shi, W. Chu, Y. Wang, Inorg. Chem. Commun. 30 (2013) 178.

[13] D.C. Onwudiwe, P.A. Ajibade, B. Omondi, J. Mol. Struct. 987 (2011) 58.

[14] F. Chioma, A.C. Ekennia, C.U. Ibeji, S.N. Okafor, D.C. Onwudiwe, A.A. Osowole, O.T. Ujam, J. Mol. Struct. 1163 (2018) 455.

[15] T.L. Yang, W.W. Qin, Pol. J. Chem. 80 (2006) 1657.

[16] G.A. Kolawole, A.A. Osowole, J. Coord. Chem. 62 (2009) 1437.

[17] A.P. Balasubramaniam, A. Peuronen, M. Lahtinen, M. Manickavachagam, E. Kolehmainen, E. Haapaniemi, M. Sillanpï Polyhedron. 123 (2017) 453.

[18] A.N. Gupta, V. Kumar, V. Singh, K.K. Manar, M.G.B. Drew, N. Singh, CrystEngComm. 16 (2014) 9299.

[19] M. Delepine, Compt.Rend., 146 (1908) 981.

[20] M. A. Bernard and M.M Borel, Bull. Soc Chim. Fr. (1969) 423.

[21] S. Budagumpi, R.A. Haque, A.W. Salman, Coord. Chem. Rev. 256 (2012) 1787.

[22] S. Saeed, N. Rashid, M. Ali, R. Hussain, Eur. J. Chem. 13 (2010) 2000.

[23] G. Hogarth, Mini-Rev. Med. Chem. 12 (2012) 1202.

[24] G.M. De Lima, D.C. Menezes, C.A. Cavalcanti, J.A.F. Dos Santos, I.P. Ferreira, E.B. Paniago, J.L. Wardell, S.M.S.V. Wardell, K. Krambrock, I.C. Mendes, H. Beraldo, J. Mol.

Struct. 988 (2011) 1.

[25] I.A. Guzei, Programs Gn, University of Wisconsin-Madison, Madison Wisconsin, USA, 2007 - 2013.

[26] G. Hogarth, Transition Metal Dithiocarbamates: 1978-2003, Prog. Inorg. Chem. 53 (2005).

[27] P. Jamuna Rani, S. Thirumaran, S. Ciattini, Spectrochim. Acta - Part A Mol. Biomol. Spectrosc. 137 (2015) 1164.

[28] G.G. Mohamed, Z.H.A. El-Wahab, Spectrochim. Acta - Part A Mol. Biomol. Spectrosc. 61 (2005) 1059.

[29] S.A. Bhat, J.T. Mague, M.S. Balakrishna, J. Organomet. Chem. 809 (2016) 21.

[30] K.S. Siddiqi, S.A.A. Nami, Lutfullah, Y. Chebude, J. Braz. Chem. Soc. 17 (2006).

[31] Z. Travnicek, R. Pastorek, V. Slovak, Polyhedron 27 (2008) 411.

[32] S.S. Chavan, S.K. Sawant, V.A. Sawant, G.K. Lahiri, Inorg. Chem. Commun. 14 (2011) 1373.

[33] P.J. Rani, S. Thirumaran, S. Ciattini, Phosphorus, Sulfur Silicon Relat. Elem. 188 (2013) 778.

[34] R. Reyes-martínez, R. Mejia-huicochea, J.A. Guerrero-alvarez, H. Höpfl, H. Tlahuext, Arkivoc. 2008 (2008) 19.

[35] D.C .Onwudiwe, P.A. Ajibade, Int. J. Mol. Sci. 12 (2011) 5538.

[36] M. Garai, D. Dey, H. Ram, A. Roy, N. Kole, B. Biswas, , Polyhedron. 129 (2017) 114.

[37] A. Manohar, V. Venkatachalam, K. Ramalingam, U. Casellato, R. Graziani

Polyhedron, 16 (1997)1971.

[38] D.C. Onwudiwe, A.C. Ekennia, E. Hosten, J. Coord. Chem. 69 (2016) .

[39] M. Ahamad, R.M. Rao, G. Rafi, M. Jaffer, J. Sreeramulu, Arch. Appl. Sci. Res. 4 (2012) 858.

[40] D. C. Onwudiwe , C. A. Strydom, O.S. Oluwafemi , New J. Chem., 37 (2013) 834.

[41] E. Sathiyaraj, S. Thirumaran, S. Ciattini, Phosphorus, Sulfur Silicon Relat. Elem. 191. (2016) 1042.

[42] P.J. Heard, Prog. Inorg Chem. 53 (2005) 1

[43] E. Sathiyaraj, G. Gurumoorthy, S. Thirumaran. New J. Chem. 39 (2015) 5336.

[44] S. Saeed, N. Rashid, M. Ali, R. Hussain, Eur. J. Chem. 13 (2010) 2000.

[45] S. Thirumaran, K. Ramalingam, Transition Met. Chem. 25 (2000) 60.

[46] K. Lemma, S.K.C. Elmroth, L.I. Elding. Dalton Trans. (2002) 1281.

[47] F.W.B. Einstein, J.S. Field, Acta Crystallogr. 30 (1974) 2928.

[48] F. Dumestre, M. Chaudret, B. Amiens, C. Fromen, M.C. Casanove, M.J. Renaud, P. Zurcher, P. Angew, Chem. Int. Ed. (2002) 41 4286.

[49] M. Soenmez, A. Levent, and M. Sekerci, Russian J. Coord Chem.30 (2004) 655

[50] A. N. Vasiliev, A. D. Polackov, Molecules, 5 (2000) 1014

CHAPTER FOUR

4.0. Synthesis of group 10 metal sulphide nanoparticles

Chapter Summary

This chapter presents the synthesis and characterization of nanoparticles obtained using some of the Ni(II), Pd(II) and Pt(II) dithiocarbamate complexes synthesized in chapter 3 as single source precursor compounds. The chapter has been divided into three sections:

(i) The synthesis and characterization of nickel sulphide, palladium sulphide and platinum sulphide nanoparticles obtained using Ni(II), Pd(II), Pt(II) complexes of dithiocarbamate obtained from primary amines.

(ii) The synthesis and characterization of nickel sulphide, palladium sulphide and platinum sulphide nanoparticles obtained using Ni(II), Pd(II), Pt(II) complexes of dithiocarbamate obtained from secondary amines.

(iii) A study of the effect of different synthetic conditions such as temperatures, various growth time and different capping molecules on the optical and structural properties of nickel suphide nanoparticles.

- Representative Ni(II) complexes of dithiocarbamate obtained from a primary amine **$[Ni(L^2)_2]$,** and a secondary amine **$[Ni(L^6)_2]$,** were utilized as precursor compounds.
- Nickel dithiocarbamate was chosen for this study based on the following: (a) cost effectiveness, and (b) its ability to exhibit nanoparticles which has a wide array of phases.

4.1. Introduction

Metal sulphides are important class of compounds with a very rich properties and exhibit different crystalline phases. Many occur naturally in the earth crust; thus, they are abundant and cheap. They also have applications in different fields such as in medicine, environment, agriculture, and electronics [1]. However, these applications are limited when in the bulk stage and can be enhanced by their size dependant properties when in the nanometre dimension.

Different methods can be employed for the conversion of materials from their respective precursor complexes to the nanoscale dimension.

Solvothermal decompositions of precursors are generally preferred for nanoparticle synthesis. In this process, the solvents serve the duo purpose of acting as both the heat sink and capping agents. The solvothermal single source precursor approach involves the use of a single complex which bears both the metal and the anion of interest [2]. This method has many advantages over others: the presence of the bridging and chelating organic ligands can give rise to monodispersed nanoparticles which acquire some important structural properties from the precursor compounds. It allows intimate interactions between the molecules leading to homogenous distribution of the metal ion, thereby preventing molecular aggregation. The reaction occurs under relatively mild reaction conditions and the organic molecules are very volatile giving rise to pure and metastable phases [3].

Many metal dithiocarbamate compounds have been utilized as single source precursors for the preparation of metal sulphides due to their direct M-S bond. As a result of the special and unique physicochemical properties of transitional metal sulphides, they have found great and important applications in a variety of areas such as catalysis and in nanomaterial. Different phases of Ni_xS_y nanoparticles have been successfully prepared by solvothermal synthesis using the metal dithiocarbamates as the single source precursor. The plethora of binary nickel sulphide system comprises of the naturally occurring phases such as NiS_2 (vaesite), Ni_3S_2 (heazlewoodite), Ni_3S_4 (polydymite), Ni_9S_8(godlevskite), β-NiS (millerite) and α–NiS (hexagonal) [4] and the synthesized and sulfur-rich phase Ni_7S_6 [5]. Phase displayed by Ni_xS_y nanoparticles depends on the synthetic route adopted, capping agents employed and the temperature of preparation [6]. Revaprasadu *et al.*, have reported the synthesis of different mineral phases of nickel sulphide nanoparticles with various capping agents [5].

Noble metal nanoparticles, including those of palladium (Pd) and platinum (Pt), display strong catalytic activities and stability with unique properties for specific scientific and technological applications. They have found relevance in many fields including catalysis, fuel cells, in electronic industries as semiconductors due to their ease of formation of active sites. They have gained increasing attention as more promising catalysts for hydrogenation and aromatic amine reduction than the other transitional metals [7]. A lot of crystalline phases of palladium sulphide and platinum sulphides are also known such as PdS (vysotskite), PdS_2, Pd_3S, Pd_4S, $Pd_{16}S_7$ [8]; PtS (cooprite), PtS_2, Pt_2S_4 [9], and even mixture of phases; (Pt-Pd)S, and (Pt-Pd-Ni)S (Braggite) [10]. Phases displayed are also dependent on the conditions of reactions including, synthetic route, capping agents and the temperature of preparation. Musetha *et al.,* have deposited PdS_2 and Pt films using palladium and platinum dithiocarbamates as single source precursors [11].

Since the size and morphology of the prepared nanoparticles are determined by the temperature of synthesis, the type of precursor compounds, the capping agent and reaction time, these variables have been considered in these studies in order to have an insight into their effects on the nanoparticles obtained. Long chain amine coordinating solvents including hexadecylamine (HDA), oleylamine (OLA), and octadecylamine (ODA) have been explored as capping agents. The function of the capping agents is to separate the nucleation and growth process, in order to aid the formation of small sized monodispersed nanoparticles with desirable properties, which is governed by the structures and properties of the capping materials. Other properties such as morphology, photo-catalytic activities, mechanical stability and toxicity of the nanoparticles can also be varied by the choice of the capping agents. For example, HDA (with chemical formula $C_{16}H_{35}N$) and ODA (with formula $C_{18}H_{39}N$) behave similarly as both are long chain saturated primary aliphatic amines, while OLA ($C_{18}H_{37}$) with an unsaturation at 9-10 position in its chain often behave differently from the other two [12]. However, all can act as good crystallization control agents in the nanoparticle crystal growth stage, to inhibit nanocrystal overgrowth [13].

4.2. Chemicals

All chemicals; hexadecylamine (HDA), oleylamine (OLA), octadecylamine (ODA), trioctylphosphine(TOP), toluene, methanol, ethanol were purchased from Sigma Aldrich and used as obtained without further purification.

4.3. Instrumentation

Nanoparticles synthesized were characterized by X-ray diffraction (XRD) measurement recorded over a 2θ range of 20–90° using a Bruker D8 Advanced, equipped with a proportional counter with Cu Kα radiation ($k = 1.5405$ A, nickel filter). Transmittance electron microscopy (TEM) performed on a TECNAI G2 (ACI) instrument operated at an accelerating voltage of 200 kV. Fourier transform infrared (FTIR) were obtained using Bruker alpha-P FTIR spectrophotometer, measured in the range of 4000–400 cm^{-1}. UV/visible spectra were measured using a Perkin-Elmer λ20 UV-vis spectrophotometer, and photoluminescence studies (PL) were obtained using Perkin-Elmer LS 45 Fluorescence spectrophotometer.

4.4 Synthesis of nanoparticles

In a typical procedure, about 0.25 g of each complex was dispersed in trioctylphosphine (TOP) and injected into a nitrogen degassed 4 g of preheated hexadecylamine (HDA) at 120 °C in a 250 mL round bottom three neck flask. A sudden drop in temperature of about 15 °C was followed by a sharp change in colouration depending on the type of precursor compounds used. The reaction temperature was maintained for 1 h and subsequently terminated. Thereafter, the temperature of the mixture was reduced to about 70 °C and excess methanol was added to flocculate the HDA capped metal sulphide nanoparticles. The nanoparticles were isolated by centrifuging three times at 6000 rpm for 15 min each, rinsed 3 times with ethanol and allowed to dry.

4.5. Results and discussion on the nanoparticles prepared using Ni(II), Pd(II) and Pt(II) complexes of dithiocarbamate obtained from primary amine

The Ni(II), Pd(II) and Pt(II) complexes of dithiocarbamate synthesized using primary amine were employed for the synthesis of nanoparticle due to their good decomposition profile into their respective sulphides. The precursor complexes were thermolyzed in the temperature range 160 - 190 °C. Hexadecylamine was employed as the capping molecule because of its high electron-donating ability and capping density, which helps to control the structural characteristics of the resultant nanoparticles. In addition, it helps in particle stabilization as it binds well to the surfaces of the particles thereby causing repulsion between them [14]. It, thus, functions as a high boiling point solvent, as reducing and also as capping agents.

4.5.1.1 Characterization of nickel sulphide nanoparticles obtained using $[Ni(L^1)_2]$, $[Ni(L^3)_2]$, and $[Ni(L^4)_2]$, as single source precursors

For convenience and easy discussion, the nickel sulphide nanoparticles obtained by using **$[Ni(L^1)_2]$, $[Ni(L^3)_2]$, $[Ni(L^4)_2]$, and $[Ni(L^5)_2]$,** as single source precursors have been represented as NiS1, NiS2, NiS3 and NiS4 respectively.

4.5.1.1.2. X-ray diffraction studies of NiS1, NiS2, NiS3 and NiS4

The powder X-ray diffraction pattern of **NiS1, NiS2, NiS3 and NiS4** nanoparticles obtained in the temperature range 160-190 °C, gave different phases of nickel sulphide nanoparticles. Representative diffraction patterns are presented in Figure 4.1. The diffraction pattern of NiS1 is shown in Figure 4.1a. The peaks of NiS1 with miller indices of (100), (101), (102), (110), which could be indexed to the hexagonal α-NiS phase (JCPDS card no. 00-002-1277)[15]. NiS2 and NiS3 gave similar pattern which are shown in Figure 4.1b with the same phase of α-NiS (JCPDS card no. 00-002-1280)[16], with indices at (001), (110), (101), (300), (021), (211), (131), (410), (401), (321), (330) and (021). NiS4 yielded $NiSO_4 \cdot 6H_2O$, Nickelhexahydrite (JCPDS card no. 00-026-1288) with indices at (110), (112), (202), (114), (204), (311), (402), (136), (138), (131), (311) [17] as presented in Figure 4.1c. The observed phase in NiS4 might be as a result of the oxidation of the NiS to the sulphate, perhaps due to the presence of trapped air/oxygen during the synthesis process in the solvothermal reaction system.

The crystallite sizes have been calculated using Scherrer's equation: $D = K\lambda/b\cos\theta$. Where, b = FWHM (Full-width at half-maximum of diffraction peak), calculated from the diffraction angle broadening, λ is the wavelength of X-ray (1.5406 Å) Cu Ka radiation, k is the position of the maximum of the diffraction peak, usually takes a value of about 0.9 and is the so-called shape factor. The most intense peaks with miller indices of (1 0 2), (0 2 1), (2 0 2) for NiS1, NiS2, NiS3 and NiS4 respectively were used for the calculation. The estimated crystallite sizes from this relation were 10.4, 9.11, 9.11 and 7.36 nm respectively.

All the diffraction peaks were clearly sharp and intense which is an indication that the particles were crystalline. The diffraction patterns showed that little variation in the substituents on the precursor compounds could cause slight changes in the phases of the nanoparticles produced.

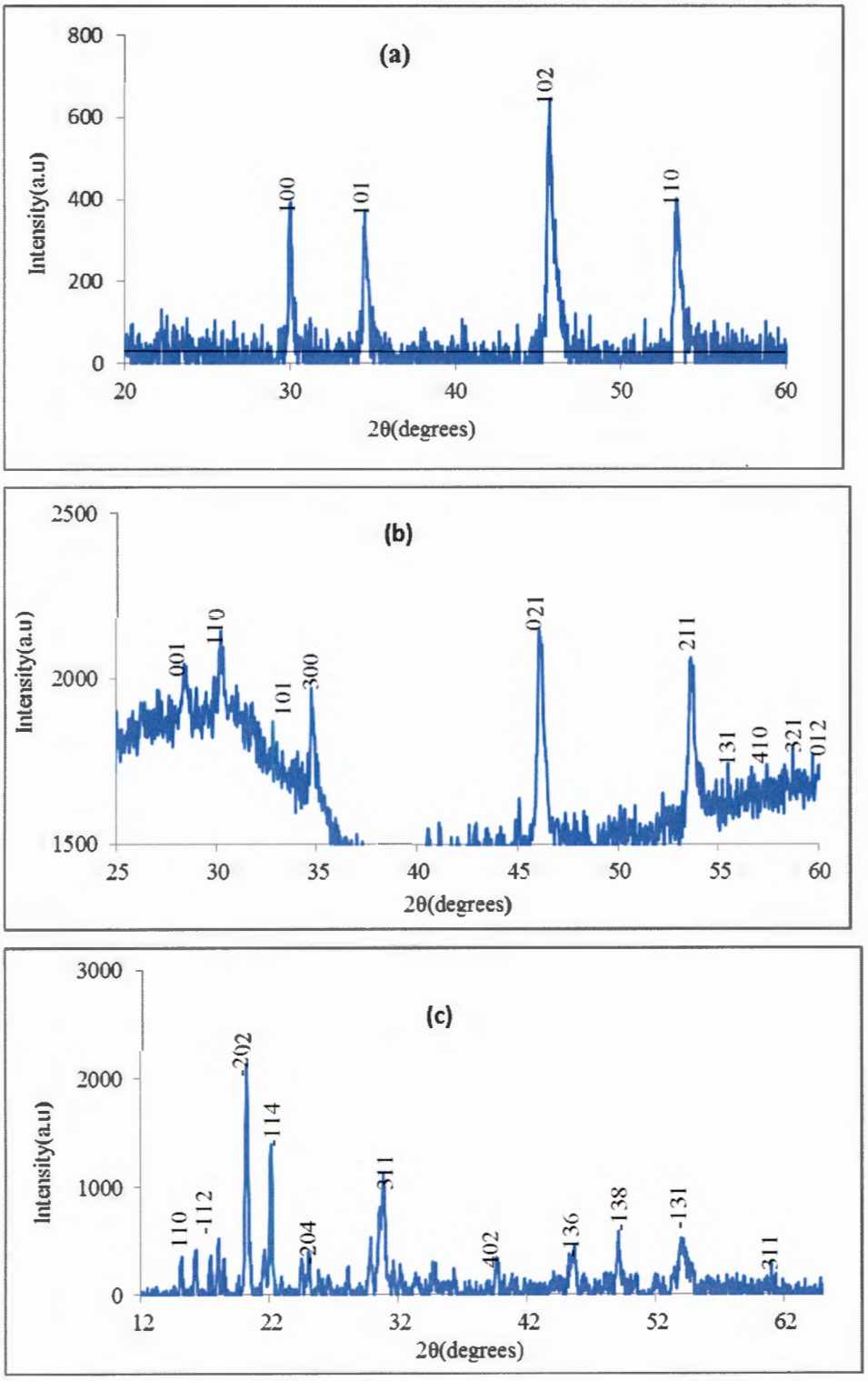

Figure 4.1: X-ray diffraction pattern of (a) NiS1, (b) NiS2 and NiS3, (c) NiS4

4.5.1.1.3. TEM studies of NiS1, NiS2, NiS3 and NiS4.

The TEM micrograph of the HDA capped **of NiS1, NiS2, NiS3 and NiS4 nanoparticles** are represented in Figure 4.2. The TEM images showed that all the nanoparticles have well-defined monodispersed dot-like/speherical shaped morphology. The monodispersity of the nanoparticles appeared to increase with increase in chain length. The nanoparticles have various sizes apart from differences in their shapes. The NiS1 (Fig. 4.2a) displayed a size range of 3.2 to 14.7 nm, with the average size of 8.3 nm; NiS2 (Fig. 4.2b) has average size of 6.1 nm, with minimum size of 2.8 and a maximum size of 10.1 nm, while NiS3 (Fig. 4.2c) has average size of 5.5 nm and the size variation in the range 2.7 to 8.7 nm. This showed that as the chain length of the alkyl substituents increased, the size of the nanoparticles produced decreased. Variations in size distribution of the nanoparticles are also a noticeable dissimilarity; NiS3 with the smallest size displayed the widest size distribution. All the particles are well dispersed, which implies the absence of agglomeration.

The particle size of NiS4 ranges between 2.70 -7.91 nm, and the TEM image showed that the smaller particles aggregated into secondary particles due to high surface energy as represented in Figure 2d. This perhaps is the effect of the aliphatic diamine which distinguished it from the other ligands; they appeared to be of spherical shape [18]. The energy dispersive X-ray (EDX) gives the elemental composition of the prepared nanoparticles. The result showed the peaks corresponding to the nickel and sulphur constituents as represented in Figure 4.3.

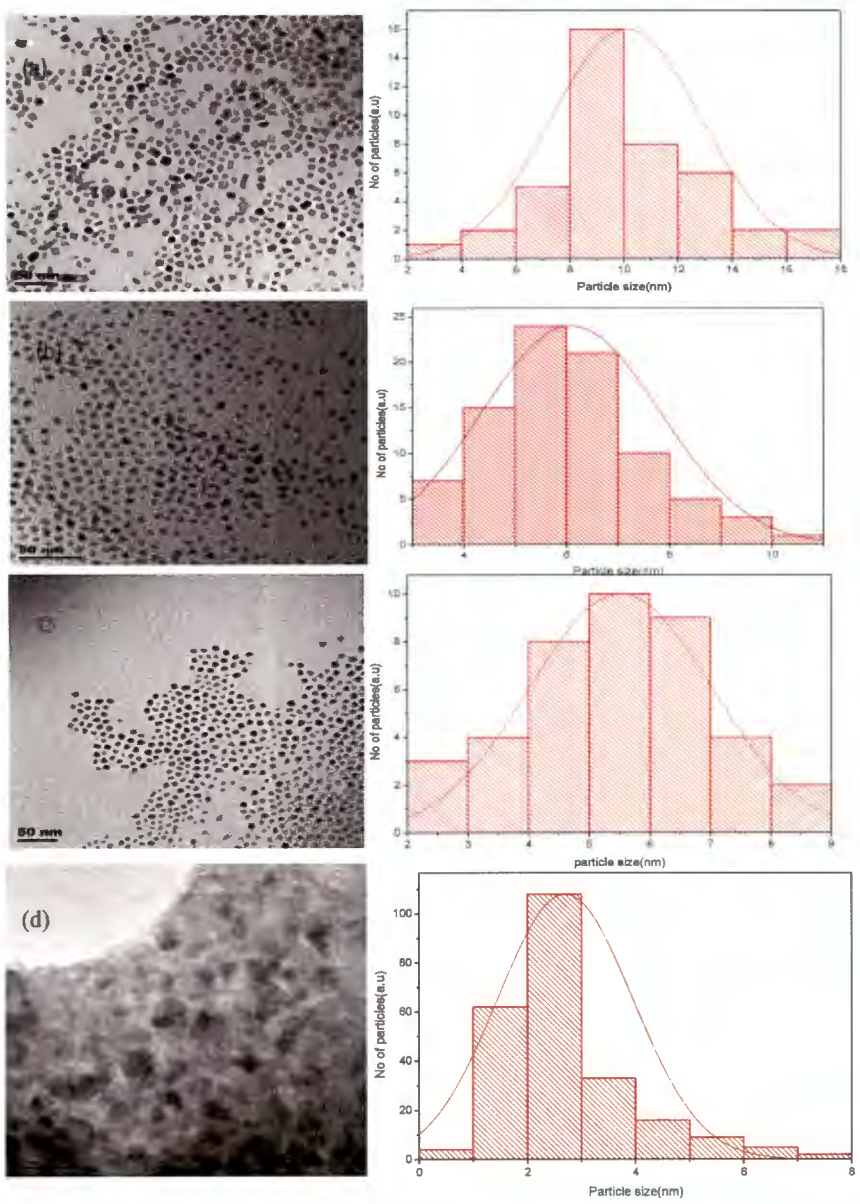

Figure 4.2: TEM micrographs of HDA-capped (a) NiS1 (b) NiS2 (c) NiS3 (d) NiS4, with their respective particle size distribution histogram.

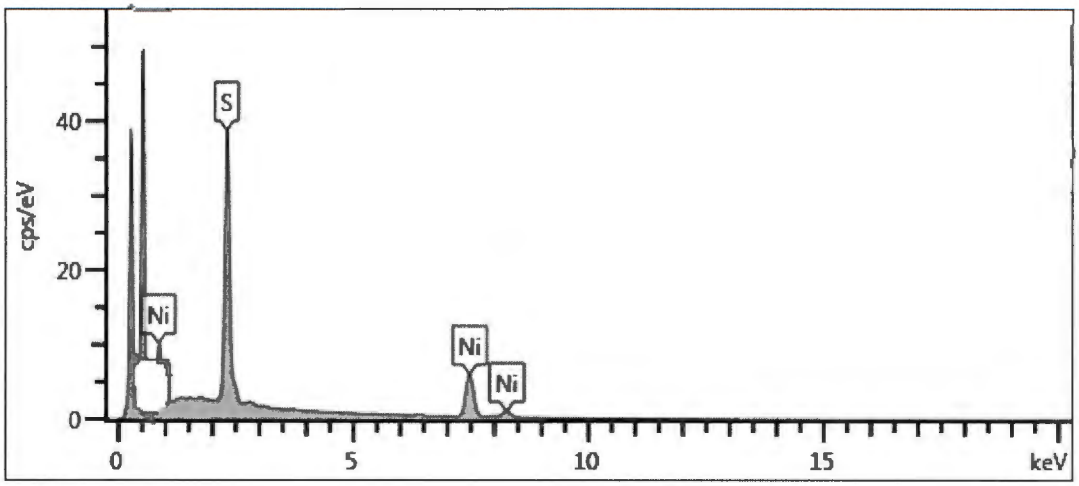

Figure 4.3: EDX of NiS nanoparticles

4.6.1.1.4. Optical studies of NiS1, NiS2, NiS3 and NiS4.

4.6.1.1.4.1 UV-vis spectroscopic studies of NiS1, NiS2, NiS3 and NiS4.

UV-vis absorption spectra were used to study the optical properties of the nickel sulphide nanoparticles. The band gap energy was determined using the Jan Tauc relation (Figure 4.4 inset). This function is based on the relationship between absorption coefficient (α) and photon energy (*hv*) [19]

$A h\nu = \alpha\,(h\nu - Eg)^{n}$

where *hv* represent the photon energy, E*g* is the optical band gap which corresponds to transitions indicated by the value of *n*, and *n* is ½ (0.5) or 2 for indirect allowed and forbidden transitions, and direct allowed and forbidden transitions respectively. In this study $n=1/2$. The α factor is a constant and it has separate values for different transitions.

By plotting $(\alpha h\nu)^{0.5}$ versus hv and extrapolating the linear portion of the graph to zero, the intercept of the *hv* axis gives the optical band gap (E_g) [20].

The UV-vis absorption spectra of the **NiS1, NiS2, NiS3 and NiS4** are shown in Figure 4.4. The respective band gap energies of the nanoparticles were calculated from the absorption spectra [21] and the obtained values were: 2.70 eV (459 nm), 2.80 eV (443 nm), 2.90 eV (427 nm) and 2.50 eV (496 nm), a blue shift of about 0.60, 0.70, 0.80 and 0.40 eV relative to the bulk value of 2.1 eV (590 nm) for NiS1, NiS2, NiS3 and NiS4 respectively. The trend of increase in band gap energy which implies decrease in particle size as the chain length of the substituents increases was also observed. This corroborates the observation made from the histogram of the TEM images discussed

in section 4.5.3. The NiS4, which consists of the aliphatic methylene chains, did not follow the same trend with the rest precursors which are aromatic phenyls with alkyl substituents. The diverse structural properties illustrate the different morphological behaviours observed, as optical properties and morphology of nanoparticles are dependent on the structure of precursor compounds.

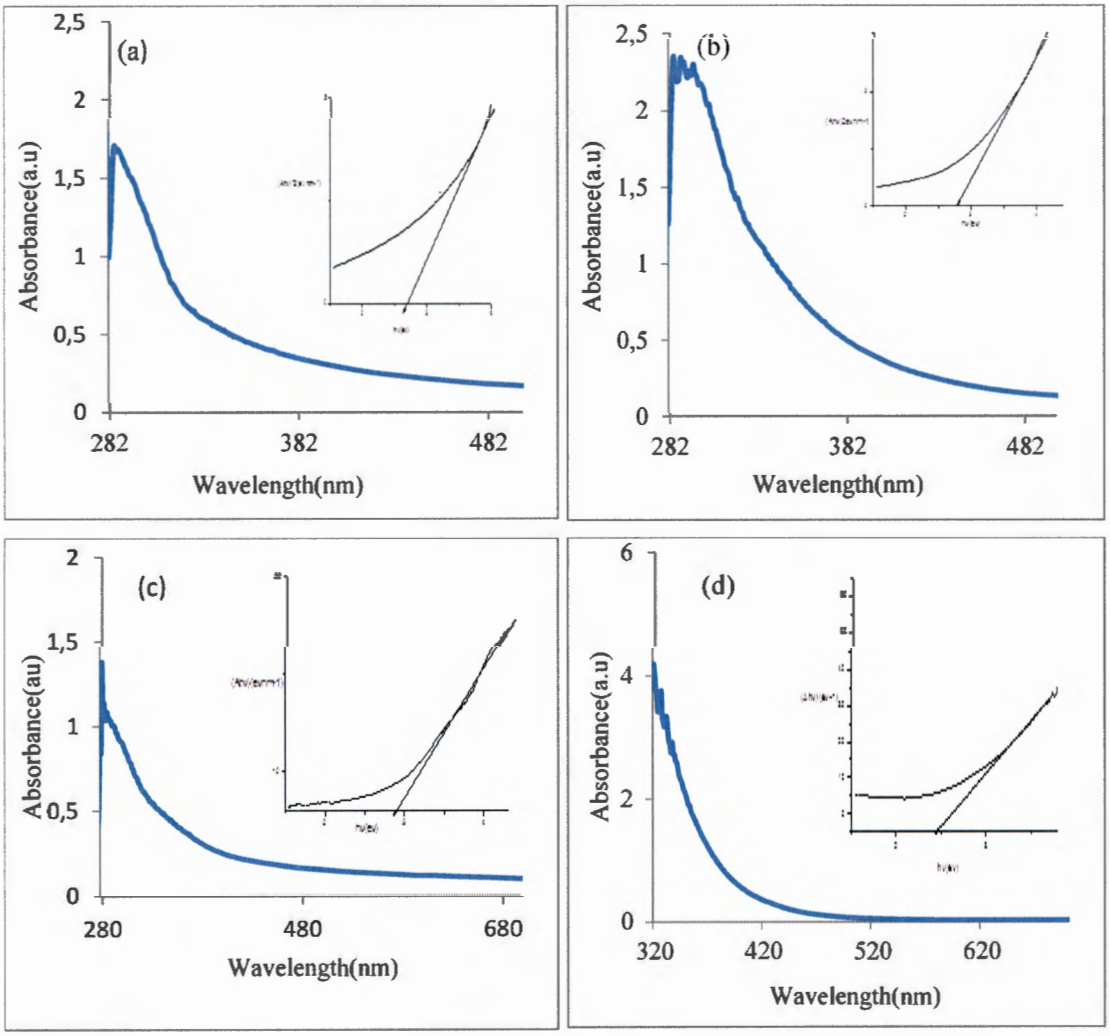

Figure 4.4: UV-vis of HDA capped (a) NiS1, (b) NiS2, (c) NiS3 and (d) NiS4 nanoparticles.

4.5.1.1.4.2. Photoluminescence studies of NiS1, NiS2, and NiS3

Photoluminescence spectroscopy is used to assess the charge migration, transfer and recombination processes in photo-excited nanoparticles [22]. The NiS1, NiS2, NiS3 nanoparticles showed similar photoluminescence spectra. Hence, representative PL spectrum for the four samples is shown in Figure 4.5. From the spectra, three emission peaks, recorded at the excitation wavelength of 260 nm were observed. The first one observed around 332 nm can be assigned to the electron hole

recombination of NiS nanoparticles, while the other peaks around 410 and 522 nm could be assigned to the intra-band transitions in the structure of the nanoparticles.

The high intensity of the peaks indicated the small size of the nanoparticles formed, the broadness indicate large size distribution and confirmed the effective surface passivation by the capping agent, which supports the size dependent quantum confinement effect of the nanoparticles.

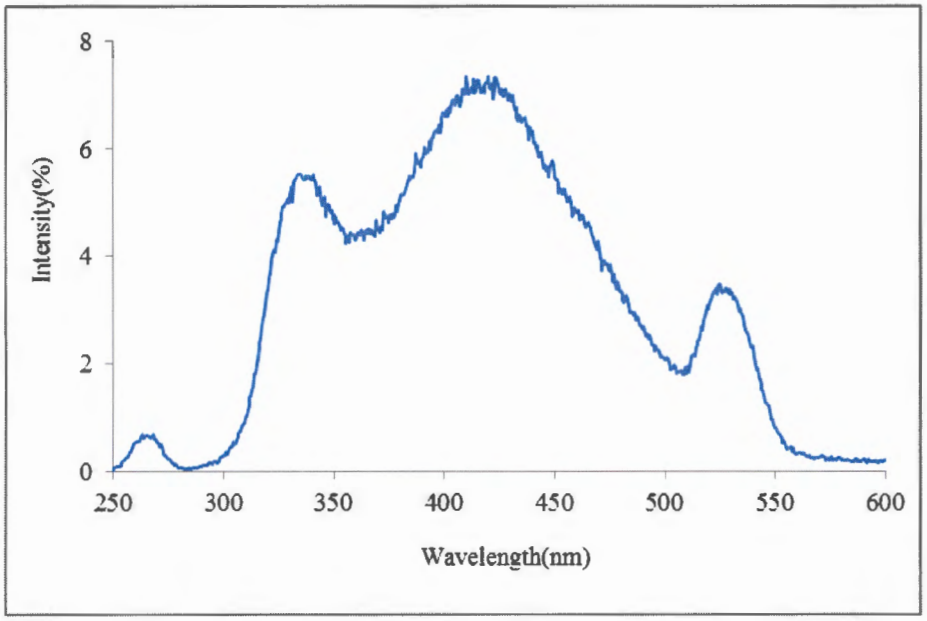

Figure 4.5: Representative PL spectra of the NiS1, NiS2, NiS3 nanoparticles

4.5.1.1.5. Infrared spectral studies of the NiS1, NiS2, NiS3 and NiS4 nanoparticles

The presence of HDA as the capping molecule on the surface of the NiS1, NiS2, NiS3 and NiS4 nanoparticles was confirmed using FTIR. The spectrum of the pure HDA was compared with that of the capped nanoparticles. Result of the analysis indicated that the most important peaks were observed at 3334 which could be ascribed to ν(N—H), and the band around, 2851 and, 2922 $cm^{-1}$are the asymmetrical and symmetrical ν(C—H) vibrations in the HDA respectively. Similar peaks were also found within the same environment in the spectra of the HDA capped NiS1, NiS2, NiS3 and NiS4 nanoparticles. The peak at 510 cm^{-1} is assigned to the stretching vibration due to Ni-S bond [23], which was not observed in the spectra of the pure HDA as shown in Figure 4.6. The similarities in the positions of appearance in the spectra of the pure HDA and their capped NiS nanoparticles revealed that the amine is involved as capping molecules for the nanoparticles. The results also confirmed the purity of the synthesized NPs because aside the vibrational modes of the

HDA ligands and the Ni-S, the absence of the aromatic C-H and N-CS2 stretching vibrations in the spectrum of nanoparticles confirmed the decomposition of dithiocarbamate molecule through the thermolysis process and subsequent formation of nickel sulphide nanoparticles. The EDX spectrum of NiS presented in Figure 4.6b showed the elemental composition to be Ni and S atoms

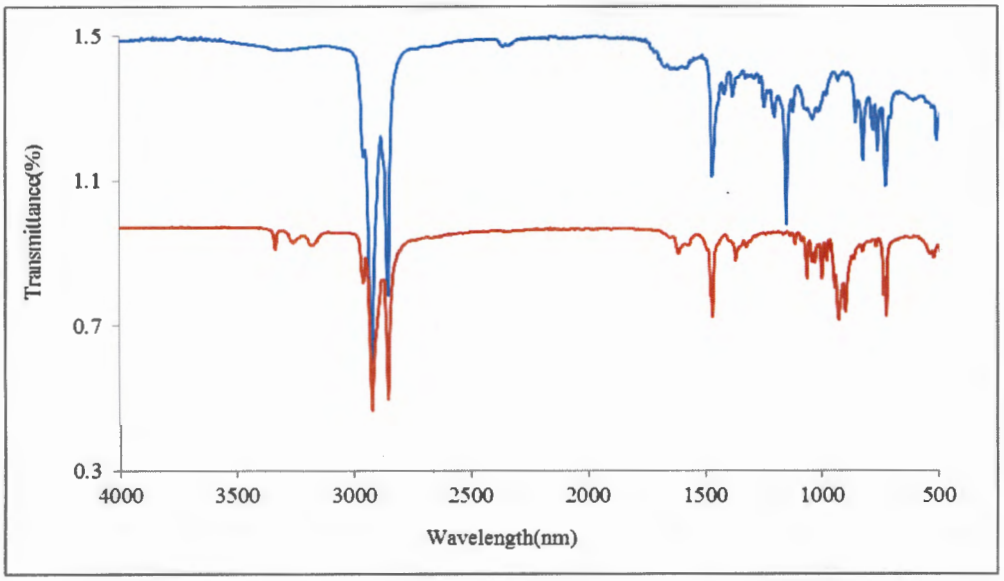

Figure 4.6a: A representative FTIR spectra for pure HDA (red) and HDA-capped nickel sulphide (blue) nanoparticles

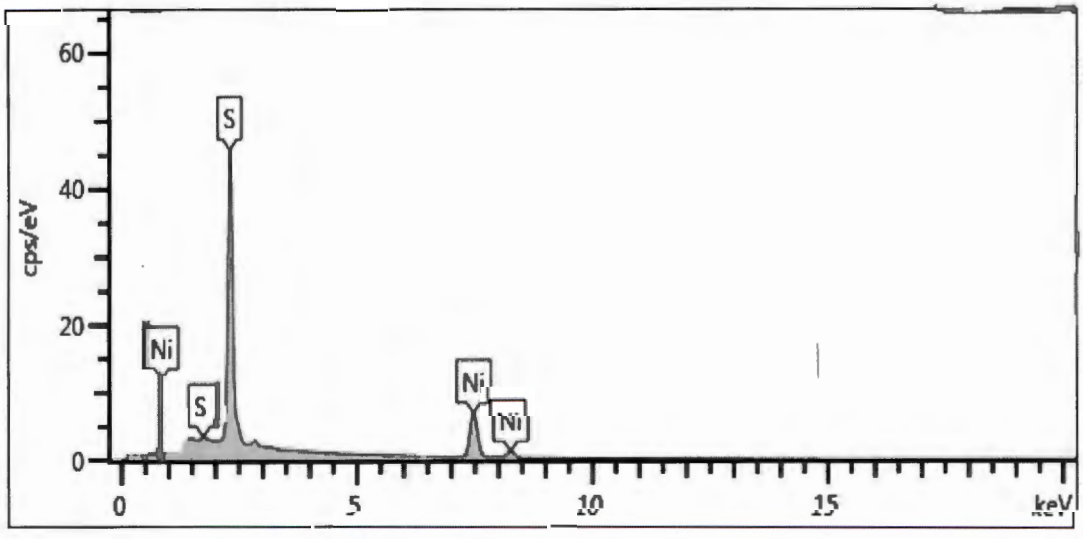

Figure 4.6b: A representative EDX spectra for HDA-capped nickel sulphide nanoparticles

Table 4.0: The band gap energies, particle phases and the estimated sizes of the NiS1, NiS2, NiS3 and NiS4 nanoparticles

Nanoparticle	Particle size from XRD (nm)	Particle size from TEM (nm)	Band gap energy (eV)	Particle Phase
NiS1	10.40	8.30	2.70	α-NiS (hexagonal)
NiS2	9.11	6.10	2.80	α-NiS
NiS3	9.11	5.50	2.90	α-NiS
NiS4	7.36	7.29	2.50	$NiSO_4$

4.5.1.2 Characterization of nanoparticles obtained using $[Pd(L^1)_2]$, $[Pd(L^2)_2]$, $[Pd(L^3)_2]$, and $[Pd(L^4)_2]$ and $[Pd(L^5)_2]$) as single source precursors

4.5.1.2.1 X-diffraction studies of nanoparticles obtained using $[Pd(L^1)_2]$, $[Pd(L^2)_2]$, $[Pd(L^3)_2]$, $[Pd(L^4)_2]$, and $[Pd(L^5)_2]$)

Two different X-ray diffraction patterns were observed for the nanoparticles obtained from this set of complexes. The nanoparticles obtained from **$[Pd(L^1)_2]$** and **$[Pd(L^2)_2]$,** have peaks corresponding to the (111), (200), (220), and (311) lattice planes of Pd crystals and are consistent with a face centered cubic (fcc) structure. Pd nanoparticles as a product of the thermolysis of Pd(II) dithiocarabamate has been reported in literature [24]. Lattice plane of (111) is a characteristic or diagnostic reflection peak for pure metallic Pd phase [25], which could be indexed to (card no. 00-046-1043). The diffraction patterns are presented in Figure 4.7a. The crystallite size has been calculated using the (1 1 1) diffraction peak at 38.8° using Scherrer's equation. The estimated crystallite size from this relation was 13.0 nm.

The nanoparticles obtained from **$[Pd(L^3)_2]$ and $[Pd(L^4)_2]$** gave vysotskite (PdS) phase [26] as shown in the diffractogram presented in Figure 4.7b. The patterns at 2θ values of 21.10°, 29.30°, 36.30°, 46.50°, 51.31°, 60.50°, 76.20° and 83.82° were indexed to (111), (00$\bar{2}$), (200), (1$\bar{0}$2), (201), (112), (121), (202) and with the crystallite size of 2.78 nm.

The narrowing of the peak widths in the patterns of (a) compared to (b) could be as a result of increase in crystallite size and phase uniformity of the particles [27].

[Pd(L^5)$_2$] also gave a different phase of PdS_2 cubic plane, represented by the diffractogram in Figure 4.6c. The diffraction peaks are indexed to miller indices (021), (210), (211), (113), and (023) with crystallite size obtained from the (021) diffraction peak to be 2.79 nm. The diffraction peaks were nearly sharp and intense which was an indication that the particles are crystalline and the narrowing of the peak widths could be as a result of increase in crystallite size and phase uniformity of the particles [11].

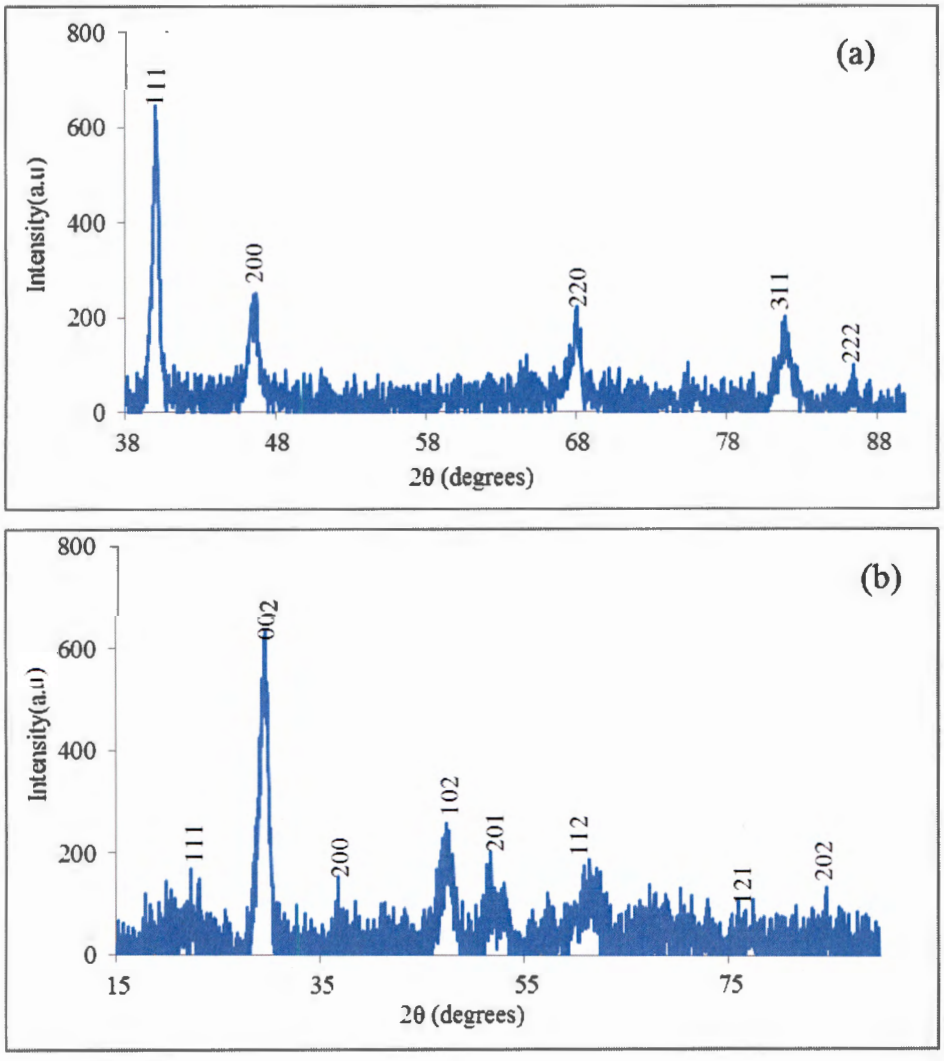

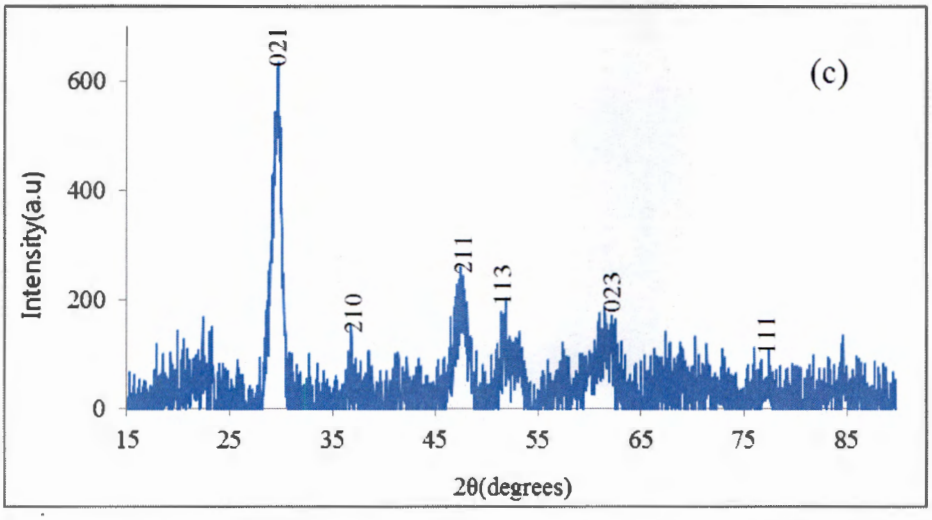

Figure 4.7: Representative X-ray diffractogram of nanoparticles obtained from (a) **[Pd(L^1)$_2$], and [Pd(L^2)$_2$],** (b) **[Pd(L^3)$_2$]** and **[Pd(L^4)$_2$],** and (c) and **[Pd(L^5)$_2$.**

4.5.1.2.2 TEM Studies of nanoparticles obtained using Pd(L^1)$_2$], [Pd(L^2)$_2$], [Pd(L^3)$_2$], [Pd(L^4)$_2$], and [Pd(L^5)$_2$]

The TEM images of the palladium nanoparticles obtained from [Pd(L^1)$_2$], and [Pd(L^2)$_2$], are presented in Figures 4.9 (a, and b) respectively. Figure 4.10 (a,b and c) is the TEM image of the palladium sulphide nanoparticles synthesized from [Pd(L^3)$_2$], [Pd(L^4)$_2$], and [Pd(L^5)$_2$] respectively. The nanoparticles are monodispersed, and of fairly spherical morphology with particle sizes in the range of 1.27 - 5.14 nm and the mean sizes range from 1.88-2.62 nm which is fairly a wide particle size distribution. The particles obtained from [Pd(L^2)$_2$] appeared to be a mixture of oval and spherical shapes with particle sizes in the range of 1.80 - 6.87 nm, as shown in Figure 4.9b. The nanoparticles are homogenously distributed and no large dense of flocs observed, which confirmed that the particles were well dispersed in solution. The selected area electron diffraction (SAED) of the particles obtained from [Pd(L^2)$_2$](Fig. 4.9b inset) showed clear diffraction rings which confirmed the crystallinity of the nanoparticles. The palladium sulphide nanoparticles are visibly smaller than the nickel sulphide nanoparticles, with well aligned and uniformly separated inter-particle distances. The EDX spectrum shown in Figure 4.8 confirmed the palladium and sulphur constituents of the nanoparticles. The presence of phosphorus might be from the TOPO in which the precursor complex was dispersed prior to injection into hot HDA, while the strong carbon peak is likely to have come from the carbon grid of the sample holder or from the HDA of the capping molecule.

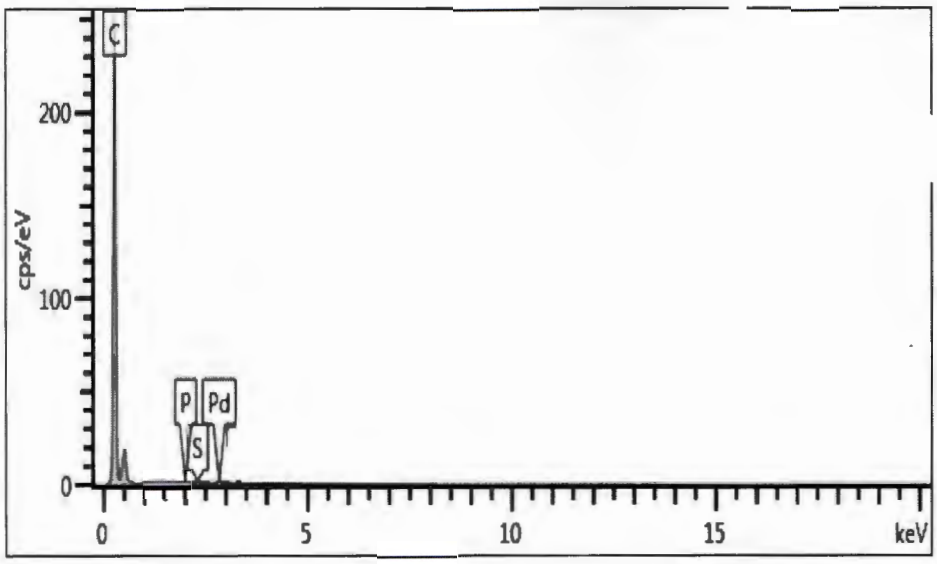

Figure 4.8 EDX of the PdS_x nanoparticles

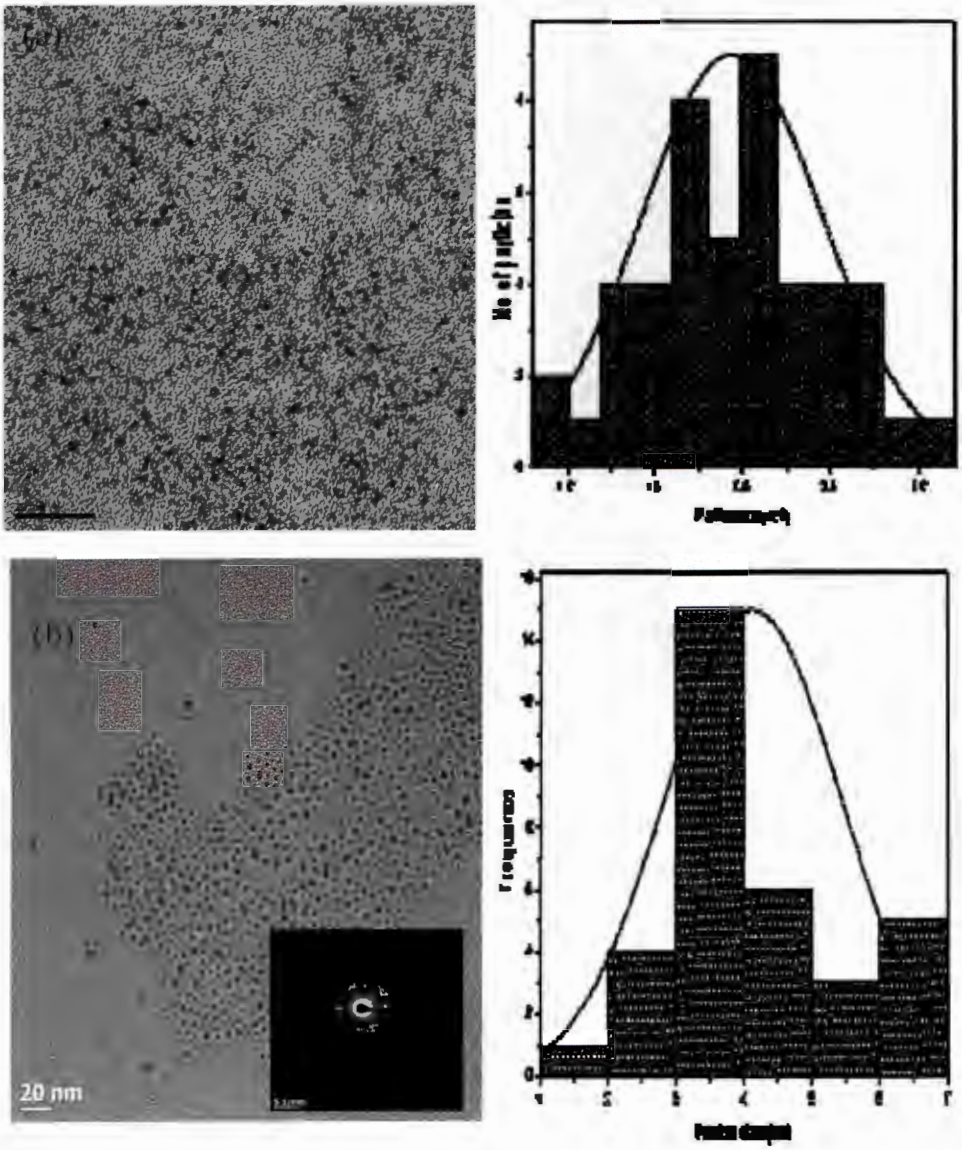

Figure 4.9: TEM micrographs of HDA-capped nanoparticles obtained from (a) $[Pd(L^1)_2]$ and (b) $[Pd(L^2)_2]$ (Pd crystal phase) The insert in (b) is the SAED for nanoparticles form $[Pd(L^2)$

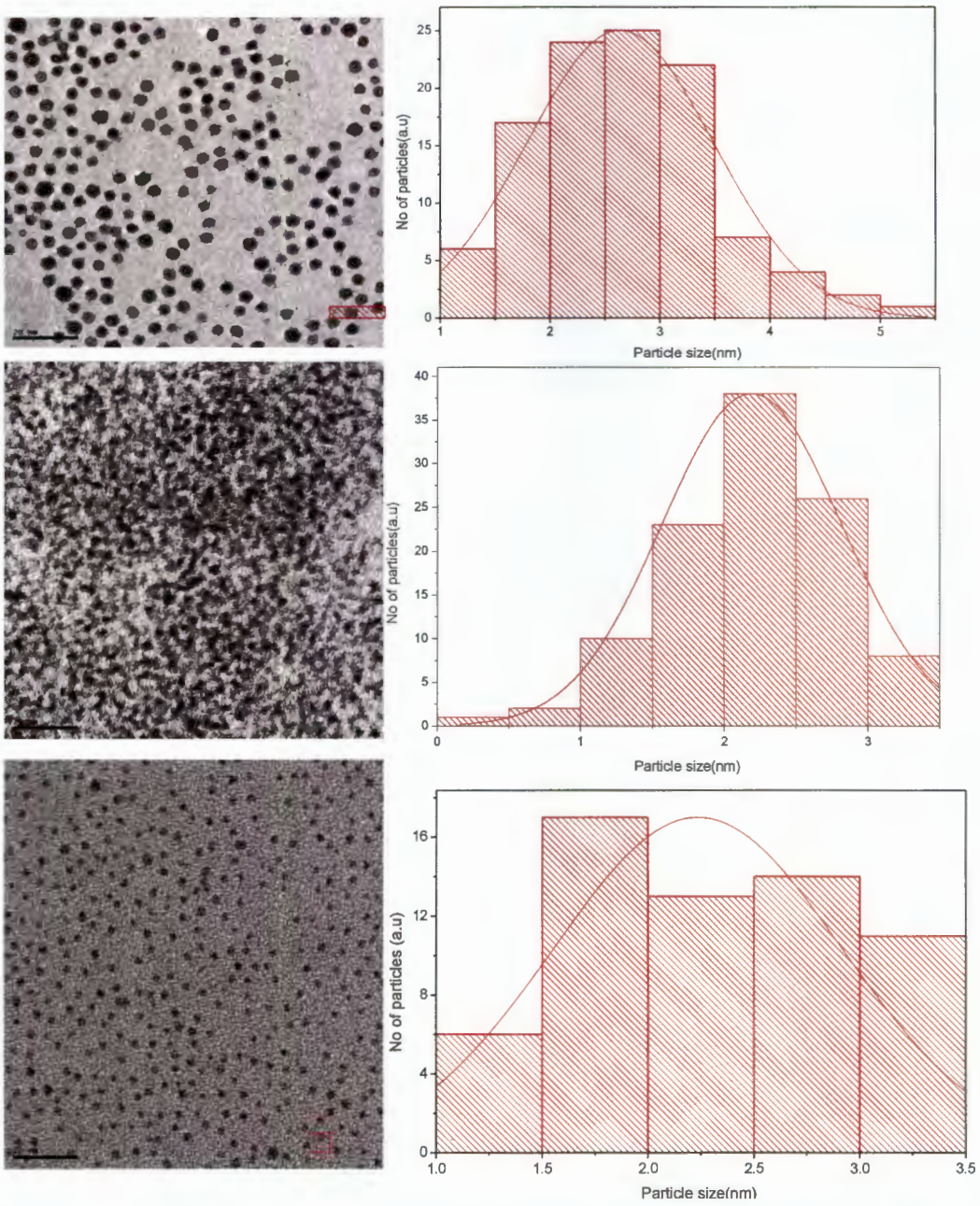

Figure 4.10: TEM micrographs of HDA-capped nanoparticles obtained from (a) $[Pd(L^3)_2]$, (b) $[Pd(L^4)_2]$, and (c) $[Pd(L^5)_2]$, (PdSx phases)with their respective particle size histogram.

4.5.1.2.3. Optical studies of the palladium sulphide nanoparticles obtained from $[Pd(L^1)_2]$, $[Pd(L^3)_2]$, and $[Pd(L^4)_2]$ as precursor complexes

4.5.1.2.3.1 UV-vis spectroscopic studies of the nanoparticles obtained from $[Pd(L^1)_2]$, $[Pd(L^3)_2]$, and $[Pd(L^4)_2]$

The UV-vis absorption spectra of the paladium sulphide prepared from **$[Pd(L^3)_2]$**, and **$[Pd(L^4)_2]$** are shown in Figure 4.11. The respective band gap energies of the nanoparticles were calculated using Tauc plots from the absorption spectra [29]. The calculated band gap energies were 3.40 eV (365), and 2.70 eV (459 nm) for the samples obtained from **$[Pd(L^3)_2]$**, and **$[Pd(L^4)_2]$** respectively. These were blue shift of about 1.40, and 0.70 eV relative to the bulk band gap value of 2.0 eV (620 nm) [28]. The trend of increase in band gap energy was observed for PdS3, and PdS4 which implies a decrease in particle size as the chain length of the substituents on the precursor increased. This was in line with the observation from the histogram of the TEM images discussed earlier.

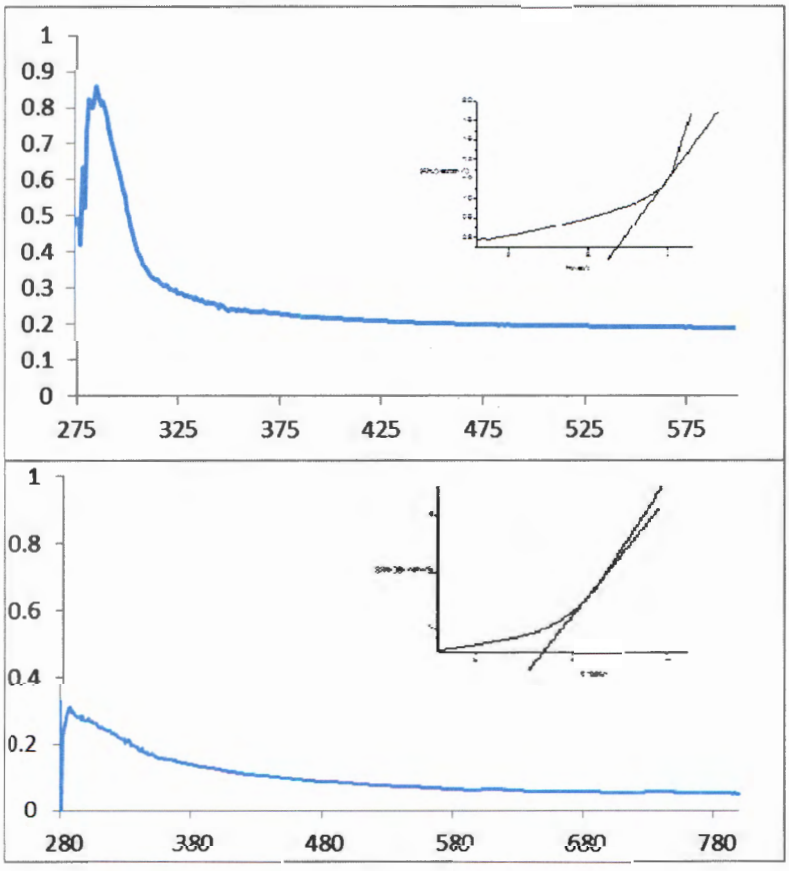

Figure 4.11: UV-vis of HDA-capped palladium sulphide nanoparticles prepared from $[Pd(L^3)_2]$ and $[Pd(L^4)_2]$

4.5.1.2.3.2 Photoluminescence studies of the palladium sulphide nanoparticles obtained from $[Pd(L^3)_2]$, and $[Pd(L^4)_2]$

The photoluminescence spectrum of representative PL spectra of palladium sulphide nanoparticles obtained from $[Pd(L^3)_2]$, and $[Pd(L^4)_2]$ are shown in Figure 4.12.

The emissions at 330 nm indicated that the PdS nanocrystals were in the quantum confinement regime. The multiple emissions at 430, 480 and 520 nm suggested intermolecular exciton interactions which are higher in palladium complexes due to larger 4d orbitals than 3d orbitals in nickel [29], and also due to band-edge emission as a result of quantum size effect. The emissions at the higher wavelength region at 595 and 645 nm could be due to the de-excitations from either 5S or Pd(4d) levels down to the Pd–S hybridization levels. The high intensity of the peaks showed the smaller size of the nanoparticles formed and the broad spectrum indicates large size distribution and confirms the effective surface passivation by the capping agent which supported the size dependent quantum confinement effect of the nanoparticles.

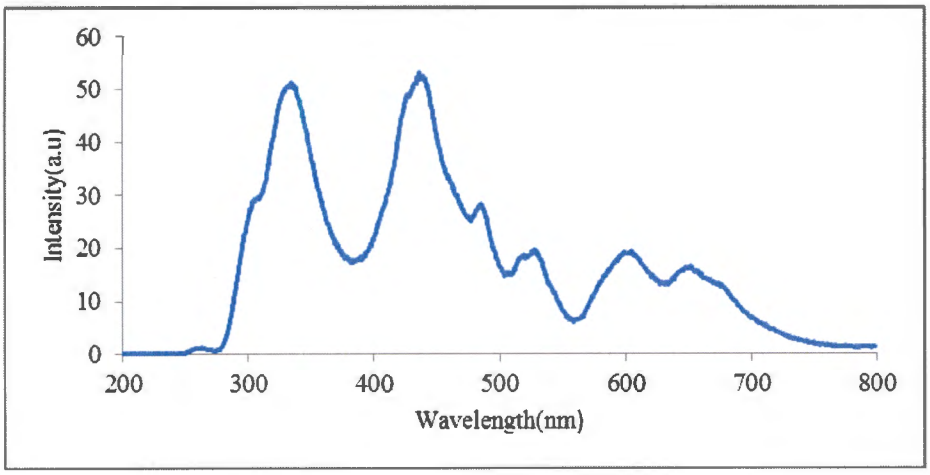

Figure 4.12: Representative PL spectra of PdS nanoparticle obtained from $[Pd(L^3)_2]$, and $[Pd(L^4)_2]$

4.5.1.3. Characterization of nanoparticles obtained from $[Pt(L^1)_2]$, $[Pt(L^2)_2]$, $[Pt(L^3)_2]$, $[Pt(L^4)_2]$, and $[Pt(L^5)_2]$

4.5.1.3.1 X-ray diffraction studies of the nanoparticles obtained from $[Pt(L^1)_2]$, $[Pt(L^2)_2]$, $[Pt(L^3)_2]$, $[Pt(L^4)_2]$, and $[Pt(L^5)_2]$

Two different X-ray diffraction patterns were observed for the samples obtained using the 5 complexes as single source precursors. The product of the thermolysis of **$[Pt(L^1)_2]$** yielded nanoparticles whose peaks at 2θ values of 28.27, 47.31 and 56.19◦ could be assigned to (100), (101) and (110) lattice planes of PtS nanoparticles, and matched with cooprite phase PtS as presented in Figure 4.13a [26]. The crystallite size has been calculated by applying Scherrer's equation as 3.10 nm using the 2θ value of the (1 0 0) diffraction peak. The samples prepared from the other four precursor compounds: **$[Pt(L^2)_2]$, $[Pt(L^3)_2]$, $[Pt(L^4)_2]$,** and **$[Pt(L^5)_2$** gave crystalline phase of the face-centered cubic platinum. This phase was consistent with the standard powder diffraction data for metallic polycrystalline Pt which could be indexed to JCPDS No 04-0802 diffraction patterns [11], as presented in Figure 4.13b. The solvothermal synthesis of nanoparticles involving Pt(II) dithiocarabamate complexes have been reported to usually result into metallic platinum or a mixture of PtS and Pt [11].

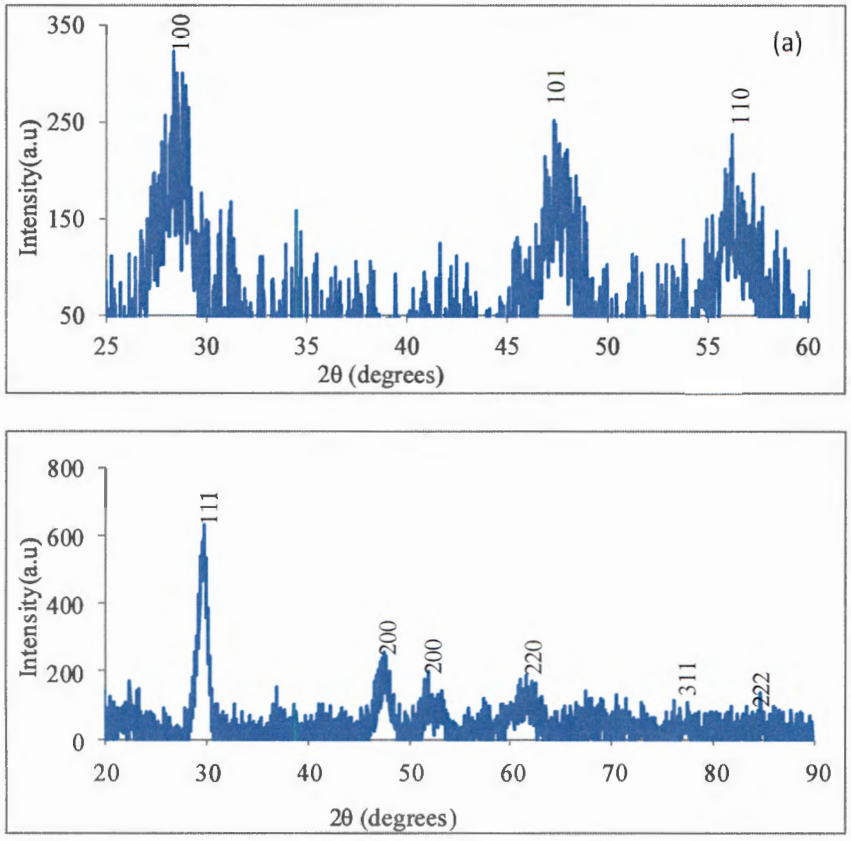

Figure 4.13: X-ray diffractogram of nanoparticles prepared from (a) **$[Pt(L^1)_2]$,** (b) **$[Pt(L^2)_2]$, $[Pt(L^3)_2]$, $[Pt(L^4)_2]$, and $[Pt(L^5)_2$** as precursor compounds.

4.5.1.3.2. TEM studies of the platinum sulphide nanoparticles obtained from $[Pt(L^1)_2]$

The TEM image in Fig.4.14 presents the platinum sulphide obtained from complex $[Pt(L^1)_2]$, while Fig.4.15 presents the TEM images for platinum nanoparticles obtained from $[Pt(L^2)_2]$, $[Pt(L^3)_2]$, $[Pt(L^4)_2]$, and $[Pt(L^5)_2]$. The nanoparticles were averagely spherical in shape, monodispersed with size ranges from 1.31-10.42, 1.58-6.62, 1.31-10.42, and 1.16-5.14 nm for $[Pt(L^1)_2]$, $[Pt(L^3)_2]$, $[Pt(L^4)_2]$, and $[Pt(L^5)_2]$ respectively, which suggests a wide particle size distribution. The average particle size ranges from 2.82-3.79 nm and with visible inter particle size separation which confirmed good passivation of the capping molecules on the nanoparticles' surfaces.

In the nanoparticles obtained from $[Pt(L^2)_2]$, ellipsoidal nanoparticles with size range of 6.15-15.94 nm were obtained. TEM micrograph revealed that approximately more than half of the particles were in form of a cluster, which suggests some degree of agglomeration. The selected area electron diffraction (SAED) pattern as inset showed that the nanoparticles obtained are crystalline as revealed by the rings. The EDX spectrum showed in Figure 4.16 represents the spectrum for the

platinum sulphide nanoparticles. The constituents are platinum and sulphur while the appearance of carbon atom could have been from the HDA capping agent.

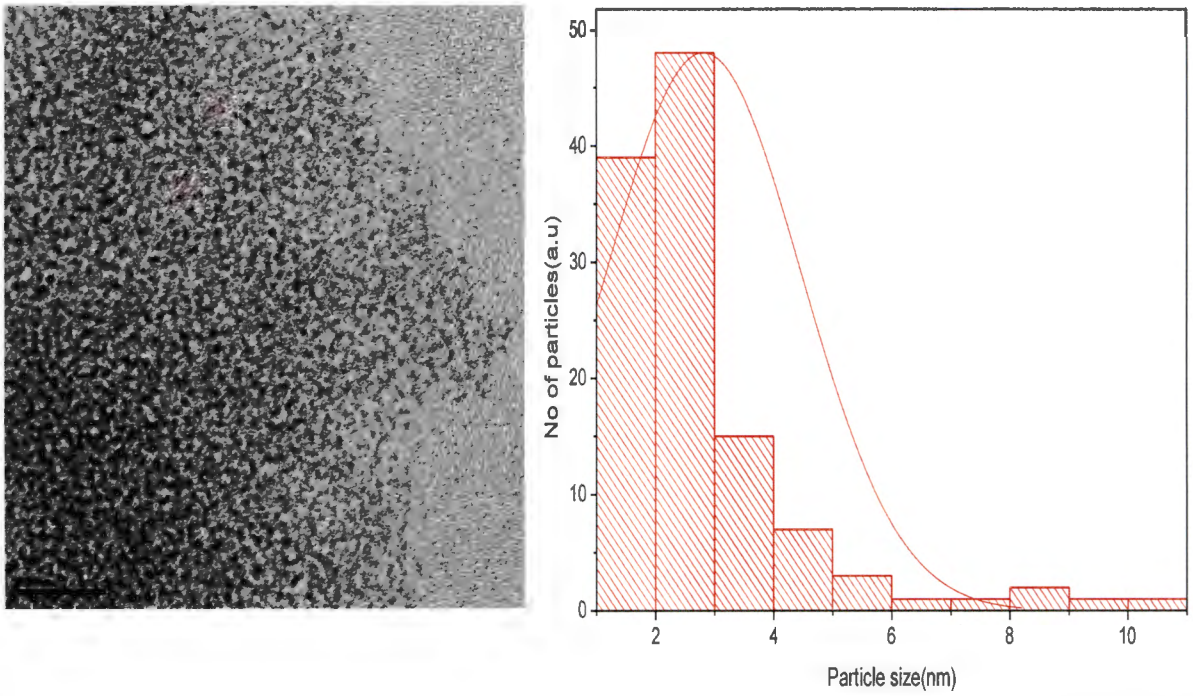

Figure 4.14: TEM micrographs of HDA-capped platinum sulphide nanoparticles obtained from **[Pt(L^1)$_2$],** with its particle size distribution histogram

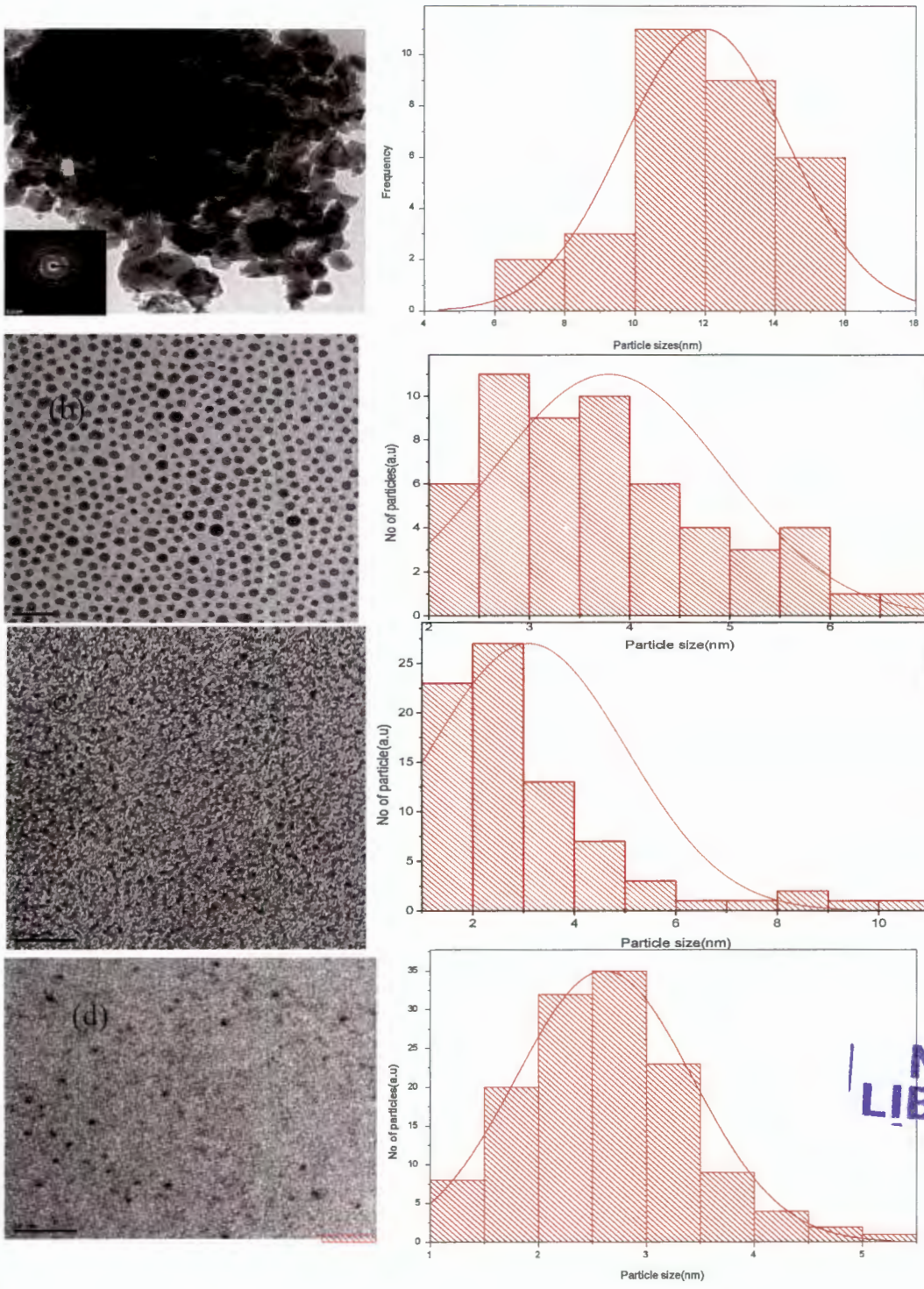

Figure 4.15: TEM micrographs of HDA-capped Pt nanoparticles obtained from **$[Pt(L^2)_2]$, $[Pt(L^3)_2]$, $[Pt(L^4)_2]$ and $[Pt(L^5)_2]$,** with their particle size distribution histogram.

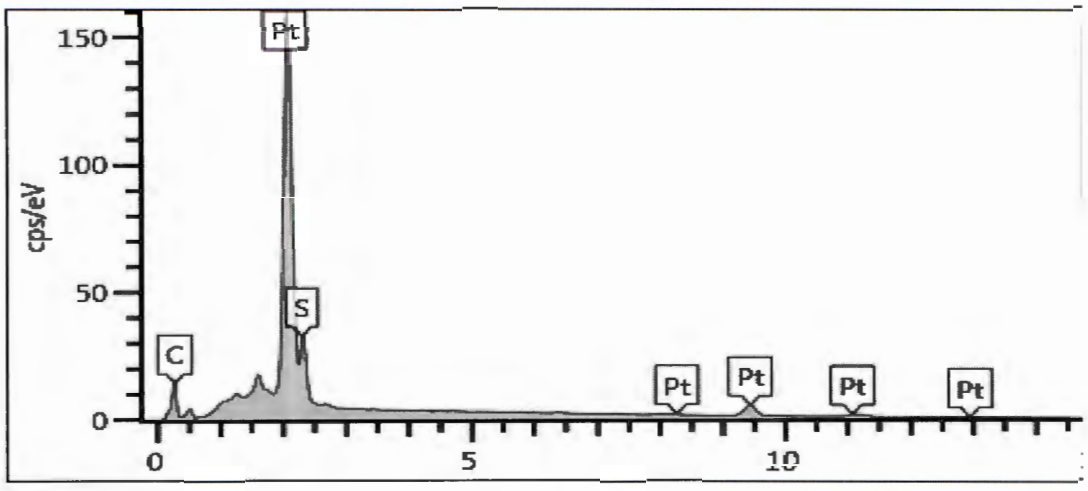

Figure 4.16: EDX of platinum sulphide nanoparticles

4.5.1.3.3. Optical studies of the platinum sulphide nanoparticles obtained from $[Pt(L^1)_2]$

4.5.1.3.3.1 UV-vis spectroscopic studies of PtS nanoparticles

The UV-vis absorption spectra of the PtS prepared from **$[Pt(L^1)_2]$** as precursor molecule is shown in Figure 4.17. The band gap energy of the nanoparticles was calculated on the basis of TAUC plots from the absorption spectra. The calculated band gap energies was 3.40 eV (365 nm), a blue shift of about 1.40eV (620 nm). The increase in the band gap energy with respect to the bulk is a consequence of quantum confinement.

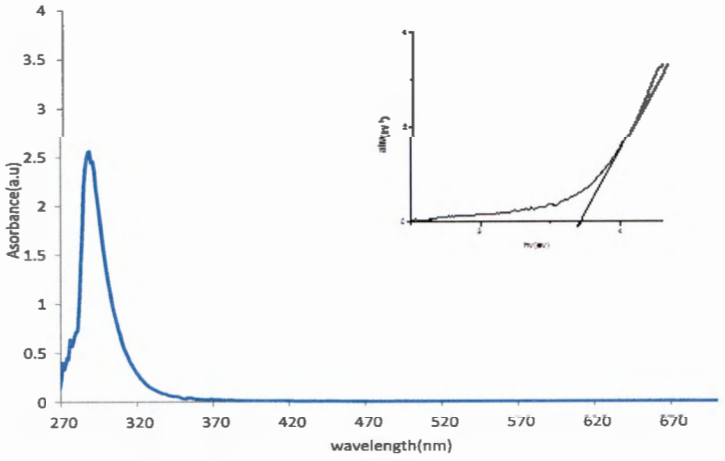

Figure 4.17: UV-vis of HDA capped PtS nanoparticles synthesized form from $[Pt(L^1)_2]$. Inset is the Tauc plot.

4.5.1.3.3.2 Photoluminescence studies of PtS nanoparticles

The photoluminescence spectrum of of platinum sulphide nanoparticles obtained from $[Pt(L^1)_2]$ is shown in Figure 4.18.

The emissions at 330 nm indicated that the PtS nanocrystals are in the quantum confinement regime. The larger 5d orbitals of the platinum transition metal gave rise to multiple emissions at slightly higher wavelengths than that of palladium at 434, 483 and 519 nm suggesting intermolecular exciton interactions due to larger 5d orbitals than both 4d and 3d orbitals in palladium and nickel, respectively [29], and also due to band-edge emission as a result of quantum size effect. The broad emission at the near IR region are separated into two peaks at 593 and 640 nm and is due to electronic transitions in the interfacial region respectively [30],[31], which could be ascribed to the de-excitations from either 6S or Pt(5d) levels down to the Pt–S hybridization levels. The high intensity of the peaks show the smaller size of the nanoparticles formed and the broad spectrum indicates large size distribution and confirms the effective surface passivation by the capping agent which supports the size dependent quantum confinement effect of the nanoparticles.

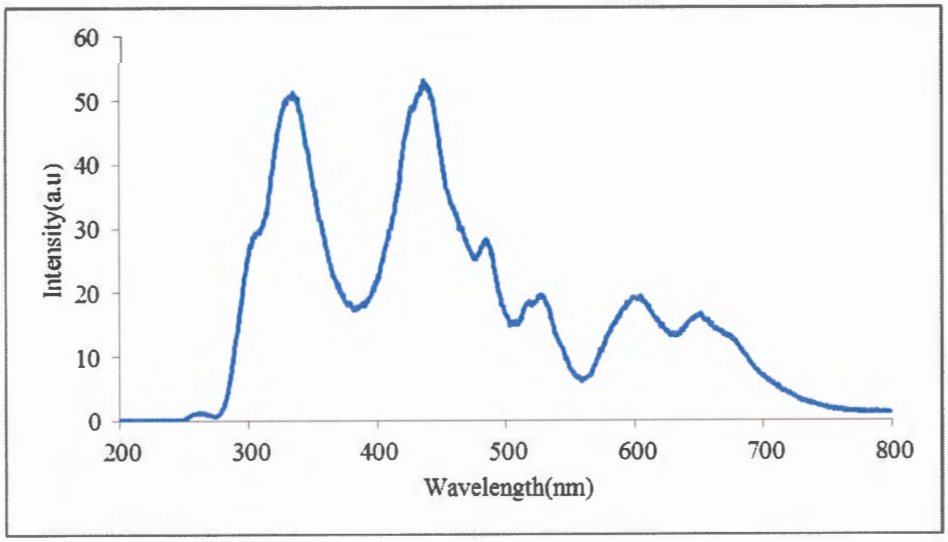

Figure 4.18: Representative PL spectra of PtS nanoparticle from primary amines

4.5.2. Results and discussion of the nanoparticles prepared using Ni(II), Pd(II) and Pt(II) complexes of dithiocarbamate obtained from secondary amine

The Ni(II), Pd(II) and Pt(II) complexes of dithiocarbamate derived from secondary amine were utilized for the synthesis of nanoparticles. TGA studies of these compounds revealed their good

thermal stability and the decomposition into their pure respective metal sulphides with little or no impurities. The precursor complexes were thermolyzed in the temperature range of 160-220 °C, based on their TGA decomposition profile. The products of thermolysis of these complexes gave an insight into various structural and morphological changes on the nanoparticles produced as a result of slight variation in the substituents on dithiocarbamate. It is noteworthy, that the structure of the precursor compounds influences the optical properties and morphologies of the synthesized nanoparticles [32]. HDA was employed as the capping molecule because of its high electron-donating ability and capping density, which aids the control of the structural characteristics of the resultant nanoparticles in a precise manner as it blocks the active site of the growing surfaces [33]. It, thus, plays the role of a high boiling point solvent as well as both reducing and capping agent.

4.5.2.1 Characterization of nickel sulphide nanoparticles obtained using $[Ni(L^7)_2]$ - $[Ni(L^{10})_2]$ as precursor compounds

The nickel sulphide nanoparticles obtained from $[Ni(L^7)_2]$ - $[Ni(L^{10})_2]$ were characterised to determine their optical and morphological properties.

4.5.2.1.2 X-ray diffraction studies of nickel sulphide nanoparticles obtained from $[Ni(L^7)_2]$ - $[Ni(L^{10})_2]$

The nanoparticles synthesized from these compounds gave the diffraction pattern which showed different phases of nickel sulphide nanoparticles. Representative diffraction patterns are presented in Figures 4.19a-c. The diffractogram in Figure 4.15a shows peaks that can be indexed to the hexagonal phase of NiS, and α-$NiS_{1.19}$. The reflection patterns identified as (100), (101), (102) and (110) correspond with the JCPDS card no. 00-002-1277. Similar phase has been reported with a peak that matches with (220) plane of $NiS_{1.97}$ [34]. The crystallite size has been calculated from 2θ of the (1 0 2) diffraction peak using Scherrer's equation and the estimated crystallite size of NiS from the equation is 10.4 nm.

Figure 4.19b is a representative of the diffractogram of nickel sulphide nanoparticles obtained from **$[Ni(L^8)_2]$** and **$[Ni(L^9)_2]$.** Both have patterns that are comparable to the planes of α- $NiS_{1.03}$ [35]. The reflection planes are in good agreement with JCPDS card no. 00-002-1273, with miller indices of (101), (110), (202) and (210). Nickel sulphide obtained using **$[Ni(L^{10})_2]$** as precursor complex has base-centered orthorhombic Godlevskite phase, Ni_9S_8, [36], which matches with JCPDS card no 00-022-1193 as presented in Figure 4.19c. The crystallite size has been calculated from 2θ of the (1 0 1) diffraction peak for α-NiS prepared from **$[Ni(L^8)_2]$** and **$[Ni(L^9)_2]$** and (2 0 2) diffraction peak

was used for Ni_9S_8, using Scherrer's equation. Estimated crystallite sizes from this relation were found to be 3.0 and 6.0 nm respectively. All the diffraction peaks were intense and clearly sharp, which is an indication that the particles were crystalline. Since no other peaks were observed in the diffraction patterns, it was a confirmation of the purity of the nanoparticles. The diffraction patterns showed that, variations on the phenyl substituents could have slight changes in the phases of the nanoparticles produced, as the different phases observed reflect the structure of the different ligands.

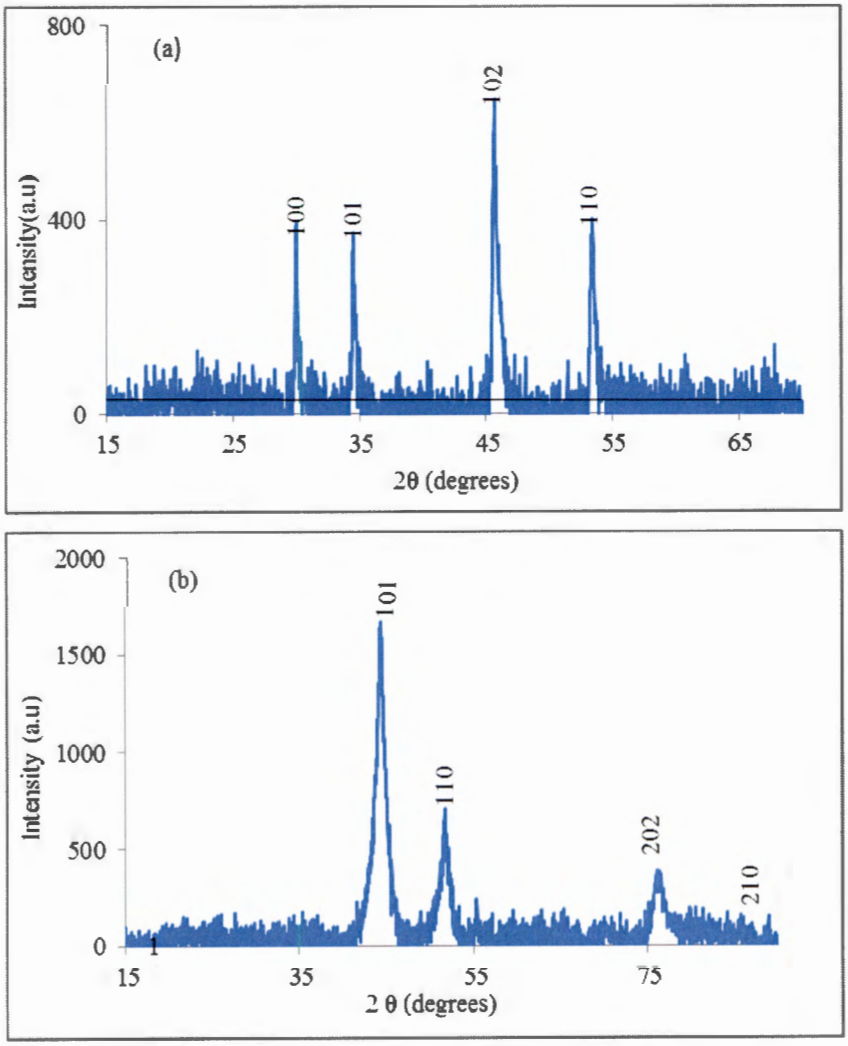

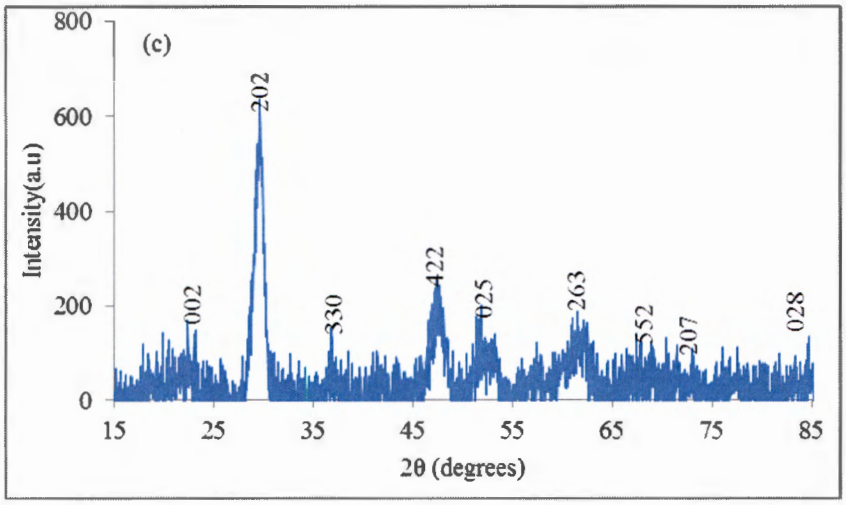

Figure 4.19: X-ray diffraction pattern of (a) α-$NiS_{1.19}$, (b) α- $NiS_{1.03}$ and (c) Ni_9S_8 **obtained from** $[Ni(L^7)_2]$ - $[Ni(L^{10})_2]$

4.5.2.1.3. TEM studies of nickel sulphide nanoparticles obtained from $Ni(L^7)_2]$ - $[Ni(L^{10})_2]$

Figures 4.20 a-d depict the TEM micrograph of nickel sulphide nanoparticles obtained from $[Ni(L^7)_2]$ - $[Ni(L^{10}{}_2]$. The nanoparticles synthesized from $[Ni(L^7)_2]$, α-$NiS_{1.19}$ showed triangular morphology, while α-$NiS_{1.03}$ (prepared from $[Ni(L^8)_2]$) showed well dispersed dot-like shape. On the other hand, the nanoparticles synthesized from $[Ni(L^9)_2]$ displayed oval shaped nanostructures and the Ni_9S_8, $[Ni(L^{10})_2]$ presented a mixture of spherical and triangular shape morphologies. All the samples were monodispersed. Average particle sizes were estimated to be 6.01, 7.53, 4.70 and 8.20 nm for the samples prepared using $[Ni(L^7)_2]$, $[Ni(L^8)_2]$, $[Ni(L^9)_2]$ **and** $[Ni(L^{10}{}_2]$ respectively. Particle size distribution of all the nickel sulphide nanoparticles are apparently narrow as revealed by the particle size histogram shown in Figure 4.16. The particles are almost uniformly distributed. These nanoparticles have identifiable boundaries which confirmed that the capping molecule is well absorbed on the surfaces of the particles to prevent aggregation.

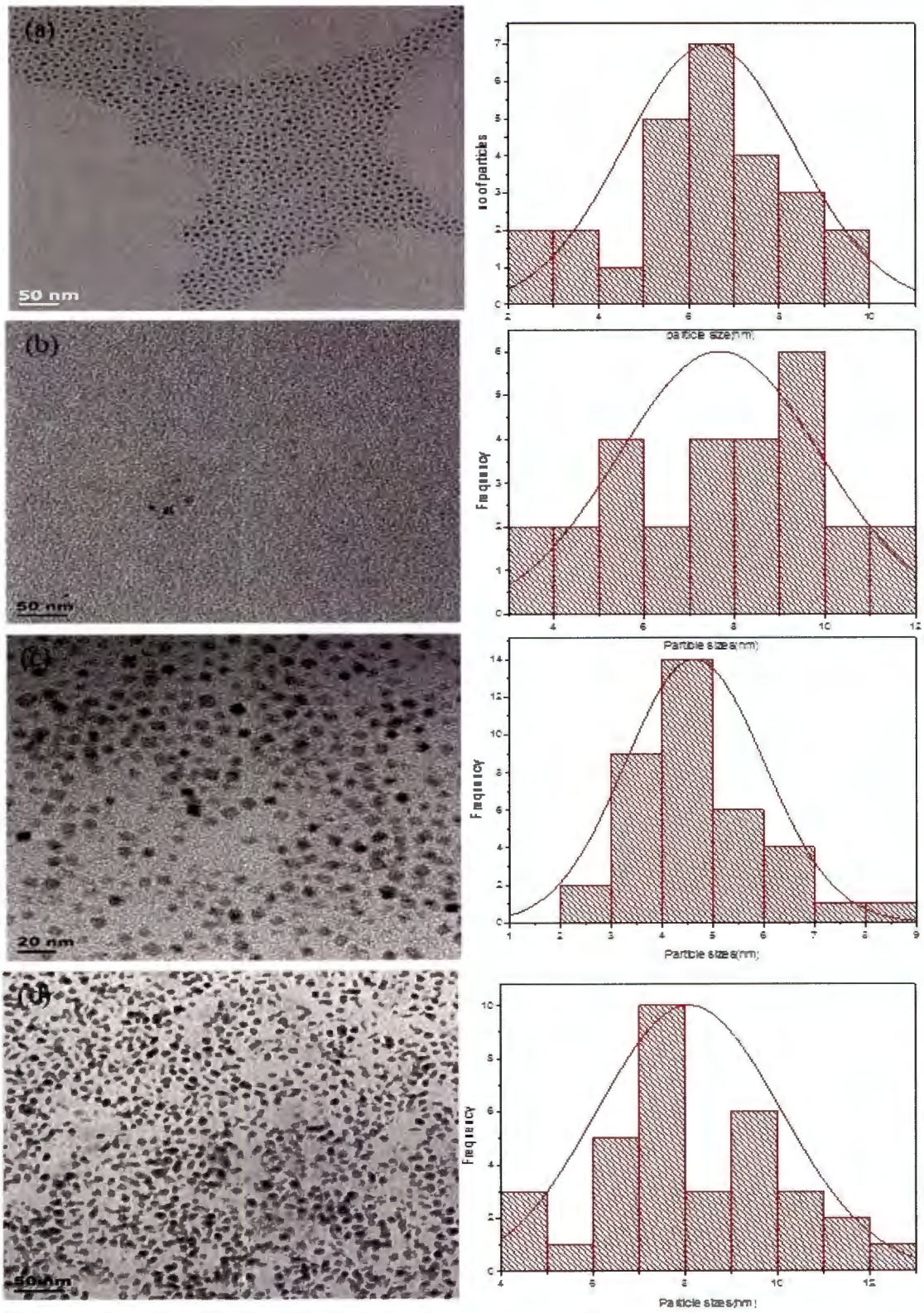

Figure 4.20: TEM micrographs of HDA-capped nickel sulphide nanoparticles synthesized using (a) **$Ni(L^7)_2$], (b) $Ni(L^8)_2$], (c) [$Ni(L^9)_2$] and (d) [$Ni(L^{10}{}_2$]** with their respective particle size distribution histogram.

4.5.2.1.4. Optical studies of nickel sulphide nanoparticles obtained from $Ni(L^7)_2$] - $[Ni(L^{10})_2]$

4.5.2.1.4.1 UV-vis spectroscopic studies of α-$NiS_{1.19}$, α-NiS and Ni_9S_8

The UV-vis absorption spectra of the nickel sulphide nanoparticles prepared from **$Ni(L^7)_2$]** - **$[Ni(L^{10})_2]$** complexes as precursor molecule are shown in Figures 4.21 (a-d). The respective band gap energies of the nanoparticles were calculated from the absorption spectra. The calculated band gap energies were: 3.36 eV (369 nm), 2.60 eV (477 nm), 2.50 eV (496 nm) and 2.30 eV (539 nm) for samples obtained from **$Ni(L^7)_2$], $Ni(L^8)_2$], $[Ni(L^9)_2]$** and **$[Ni(L^{10}{}_2]$** respectively. The values of the band gap energies indicated blue shift of about 1.26, 0.50, 0.40 and 0.20 eV respectively, relative to 2.1 eV (590 nm) of bulk nickel sulphide. The different structural properties reflect the change in morphologies observed, as optical properties and morphology of nanoparticles are dependent on the structure of precursor compounds. The complex, **$Ni(L^7)_2$]** contains the aliphatic methylethanol group. Complexes **$Ni(L^8)_2$], $[Ni(L^9)_2]$** and **$[Ni(L^{10}{}_2]$** contain both bridging and chelating ligands as a result of the combination of the carboxylformaldehyde, naphthalene and nitroaniline rings from the Schiff base compounds, which impart on the structural properties of the nanoparticles produced. The band gap energies were about 2.3-2.6 eV lower than the bulk.

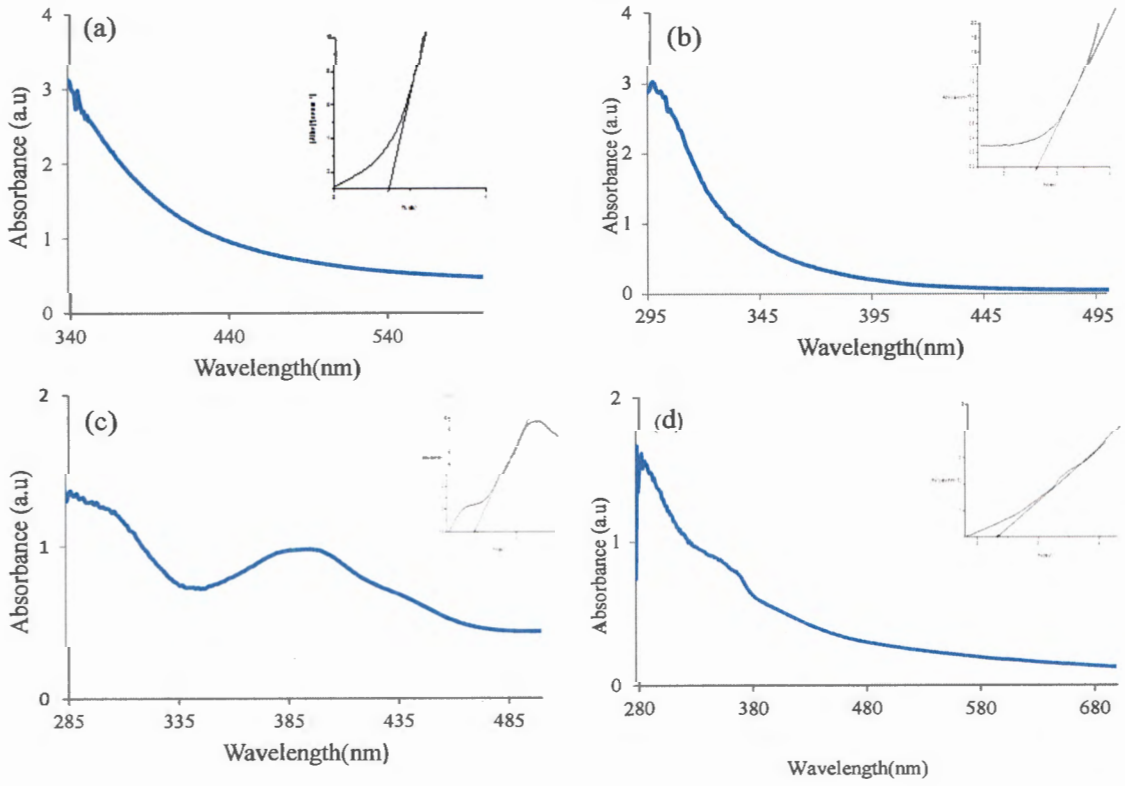

Figure 4.21: UV-vis of HDA capped nickel sulphide nanoparticles synthesized using (a) **$Ni(L^7)_2$],** **(b) $Ni(L^8)_2$], (c) $[Ni(L^9)_2]$ and (d) $[Ni(L^{10}{}_2]$**, with their respective Tauc plots.

4.5.2.1.4.2 Photoluminescence studies of nickel sulphide nanoparticles obtained from $Ni(L^7)_2$] - $[Ni(L^{10})_2]$

The photoluminescence spectrum shown in Figure 4.18 is the representative PL spectra of the nickel sulphide nanoparticle prepared using nickel complexes of dithiocarbamate obtained from the secondary amines. The photoluminescence study was conducted at room temperature and at an excitation wavelength of 260 nm. An emission peak centered on 330 nm, which is assigned to the electron hole recombination of nickel sulphide nanoparticles, was observed. The other peaks at higher wavelength around 408, 520 and 645 nm could be assigned to the intra-band transitions within the structure of the nickel sulphide nanoparticles during excitation.

The high intensity of the peaks is an indication of small size of the nanoparticles formed which could be the consequence of the effective surface passivation by the capping agent. Hence, this supports the size dependent quantum confinement effect of the nanoparticles.

4.5.2.1.5. Infrared spectral studies of nickel sulphide nanoparticles obtained from $Ni(L^7)_2$] - $[Ni(L^{10})_2]$

The capping function of the HDA molecules on the NiS nanoparticles was confirmed with FTIR. The spectrum of the pure amine was compared with that of the capped nanoparticles. Based on the analysis of the capping agents, the most important peaks were observed at 3334 cm^{-1} ascribed to ν(N—H); the peak around 2851 cm^{-1} was due to asymmetrical ν(C—H), and at 2922 cm^{-1} was ascribed to symmetrical ν(C—H) vibrations. Comparable peaks could be found around 3330, 2917, and 2849 cm^{-1} in the spectra of the HDA-capped nickel sulphide nanoparticles. The similarities in the positions of appearance of the peaks in the spectrum of the pure HDA capping molecules and the nanoparticles, with slight shift to higher frequencies revealed that the capping agents are integral parts of the capped nanoparticles. The bending vibration due to the Ni-S bond was found in the range 502-508 cm^{-1} and only on the spectra of the nanoparticles.

The summary of the characterization of nickel sulphide nanoparticles obtained from $[Ni(L^7)_2]$ - $[Ni(L^{10})_2]$ is presented in Table 4.3

Table 4.3: Summary of data of nickel sulphide nanoparticles obtained from $Ni(L^7)_2$] - $[Ni(L^{10})_2]$

Nanoparticle/precursor complex	Particle size From XRD (nm)	Particle size From TEM (nm)	Band gap energy(eV)	Particle Phase
α-$NiS_{1.19}$, $[Ni(L^7)_2]$	10.40	6.01	3.36	α-NiS(hexagonal
α-$NiS_{1.03}$, $[Ni(L^8)_2]$	3.00	7.53	2.60	$NiS_{1.03}$
α-$NiS_{1.03}$, $[Ni(L^9)_2]$	3.00	4.70	2.50	$NiS_{1.03}$
Ni_9S_8, $[Ni(L^{10})_2]$	6.00	8.20	2.30	Ni_9S_8

4.5.2.2. Characterization of palladium sulphide nanoparticles obtained from $[Pd(L^6)_2]$ and $[Pd(L^7)_2]$ as precursor compounds

Palladium sulphide nanoparticles, in the series of nanoparticles obtained from dithiocarbamate from secondary amine, were only prepared from complexes **$[Pd(L^6)_2]$** and **$[Pd(L^7)_2]$,** and used as representative samples for this series. This is because the yields obtained from other complexes (Schiff base) were not sufficient for thermolysis reaction that could yield reasonable products.

4.5.2.2.1 X-ray diffraction studies of palladium sulphide nanoparticles obtained from $Pd(L^6)_2$] and $[Pd(L^7)_2]$

The nanoparticles synthesized from **$Pd(L^6)_2$] and $[Pd(L^7)_2]$** gave diffraction patterns of the same phase of palladium sulphide. A representative diffraction pattern is presented in Figure 4.22. The pattern has peaks at 2θ values of 21.5, 29.6, 36.3, 46.3, 56.5, 61.4, 71.9 and 76.7 degrees, which could be associated with Pd_4S phase with miller indices of (002), (202), (212), (222) and (111) which matches with JCPDS card no 00-010-0335 [8]. The crystallite size has been calculated from the (0 0 2) diffraction peak using Scherrer's equation. Estimated crystallite size from this relation was 2.3 nm. The intense and sharp diffraction peaks are indication that the particles were crystalline and the broad peaks confirmed the small size of the nanoparticles.

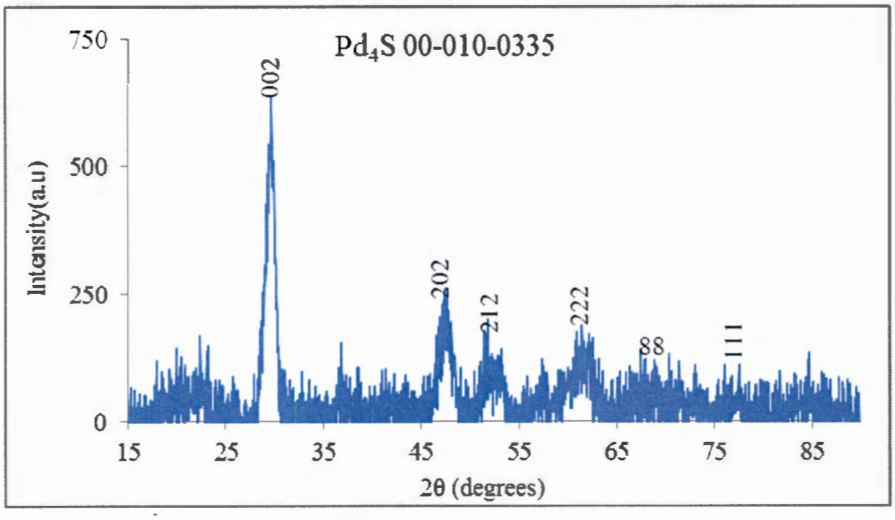

Figure 4.22: Representative X-ray diffraction pattern for PdS obtained from **Pd(L^6)$_2$] and [Pd(L^7)$_2$]** complexes.

4.6.2.2.2. TEM studies of palladium sulphide nanoparticles obtained from [Pd(L^6)$_2$] and [Pd(L^7)$_2$]

The TEM image for the palladium sulphide nanoparticles revealed dot shaped and spherical morphology with uniform inter-particle separation, as represented by Figure 4.23. The sizes are in the range 1.47 - 8.67 nm, and 1.44-3.91 nm, with average particle size of 3.45 and 2.40 nm. This showed a fairly wide particle size distribution with size decreasing with increase in chain length of substituents.

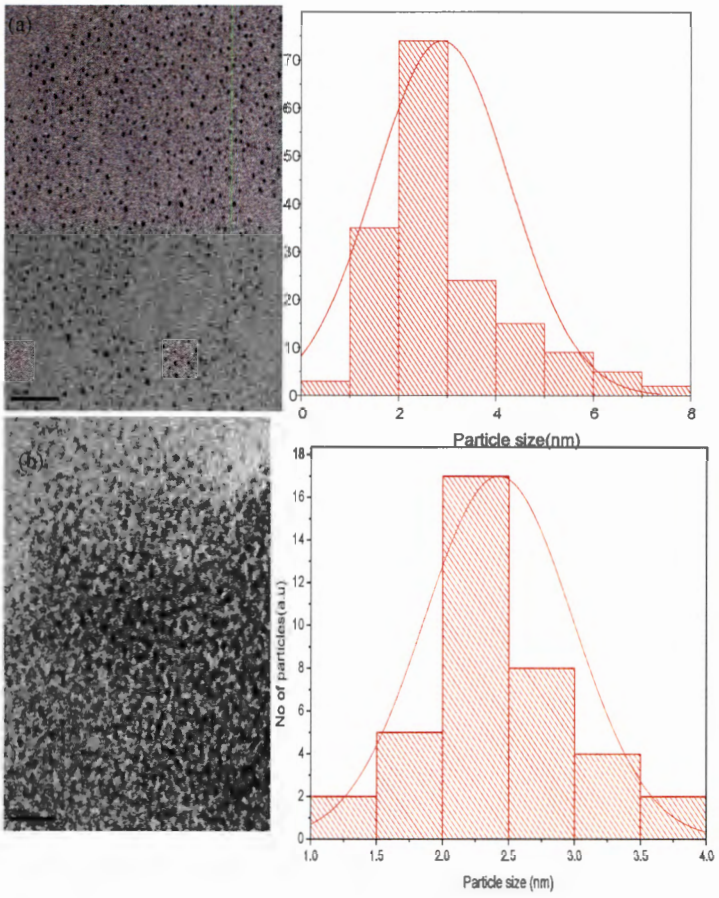

Figure 4.23: TEM image of PdS obtained from $Pd(L^6)_2]$ and $Pd(L^7)_2]$.

4.5.2.2.3. Optical properties of palladium sulphide nanoparticles obtained from $Pd(L^6)_2]$ and $Pd(L^7)_2]$ and $L^7)]$

4.5.2.2.3.1 UV-vis studies of PdS obtained from $Pd(L^6$ and $L^7)]$

The UV-vis absorption spectra of PdS nanoparticles prepared from **$Pd(L^6)_2]$** and **$Pd(L^7)_2]$** are shown in Figures 4.24. The respective band gap energies of the nanoparticles were calculated from the absorption spectra [29]. The band gap energies were 3.81 eV (326 nm) and 3.63 eV (350 nm), which implied a blue shift of about 1.81 and 1.63 eV relative to the bulk value of 2.0 eV (590 nm) for PdS obtained using **$Pd(L^6)_2]$** and **$Pd(L^7)_2]$** as precursor compounds respectively.

The observed trend was a decrease in band gap energy as the chain length of the nanoparticles increased, and since increase in band gap energies is synonymous with the reduction in particle size, this revealed that particle size increased with increase in chain length of precursor complexes.

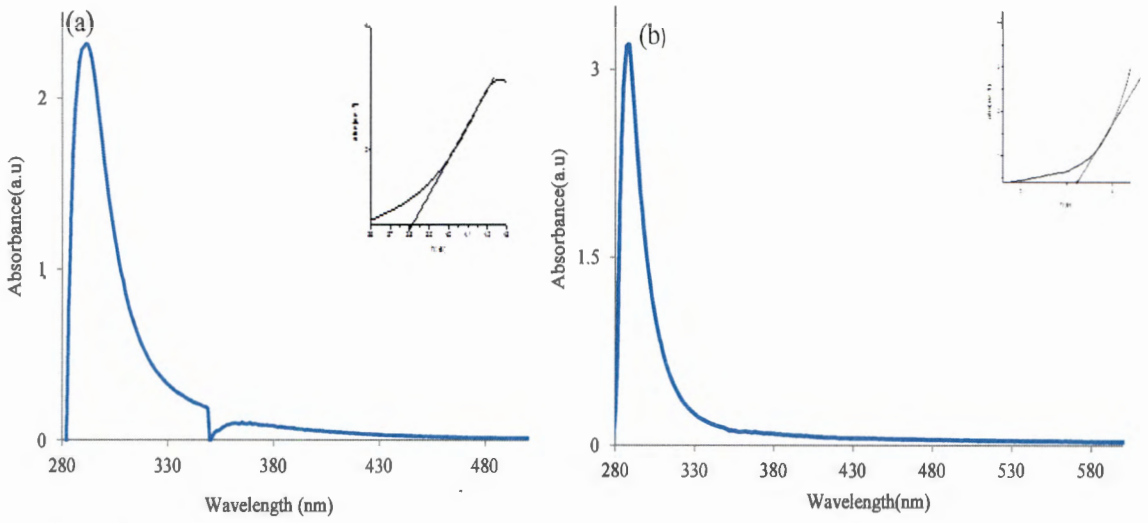

Figure 4.24: UV-vis of HDA-capped PdS nanoparticles synthesized using (a) **[Pd(L^6)$_2$]** and (b) **[Pd(L^7)$_2$],** with their respective Tauc plots.

4.5.2.2.4. Infrared spectral studies of palladium sulphide nanoparticles obtained from [Pd(L^6)$_2$] and [Pd(L^7)$_2$],

The FTIR spectra revealed the capping function of the HDA amine molecule on the PdS nanoparticles. The spectrum of the pure capping agent was compared with that of the capped nanoparticles. The most important peaks were observed at 3334 cm^{-1}, ascribed to ν(N—H), at 2851 and 2922 cm^{-1} cm^{-1} due to asymmetrical and symmetrical ν(C—H) vibrations repectively in the spectrum of the HDA. Comparable peaks could be found around 3048, 2925, and 2853 in the HDA-capped PdS nanoparticles. The similarity in the positions of appearance in both spectra confirmed the presence of the capping molecule on the surface of the nanoparticles. The slight shift of these peaks in the spectra of the nanoparticles indicated coordination, which was expected to result in weakening of the bonds around the coordination site. The peak at the far IR region of 533 cm^{-1} was assigned to the stretching vibration due to Pd-S bond [23], which was not observed in the spectra of the pure HDA. The results also confirmed the purity of the synthesized NPs because apart from the vibrational modes of the HDA ligands and the Pd-S, the absence of the thioureide C=N, C-S or N-CS_2 peaks from the functional groups present in the precursor dithiocarbamate complexes confirmed the decomposition of dithiocarbamate complexes through the thermolysis process and subsequent formation of palladium sulphide nanoparticles.

4.5.2.3. Characterization of nanoparticles obtained from $[Pt(L^6)_2]$ and $[Pt(L^7)_2]$ as precursor compounds

The PtS nanoparticles obtained from **$[Pt(L^6)_2]$ and $[Pt(L^7)_2]$** as single source precursor were also used as representative for the platinum sulphide synthesized from the series of platinum complexes used as precursor compounds.

4.5.2.3.1 X-ray diffraction studies of nanoparticles obtained from $[Pt(L^6)_2]$ and $[Pt(L^7)_2]$

The platinum sulphide nanoparticles obtained from both compounds gave similar diffraction patterns, with peaks associated to the face-centered cubic platinum which is consistent with the standard powder diffraction data for metallic crystalline Pt. This could be indexed to JCPDS 04-0802 diffraction patterns [11], as presented in Figure 4.25. The particle size has been calculated from 2θ of the (1 1 1) diffraction peak using Scherrer's equation and crystallite size from this relation is estimated to be approximately 3.2 nm. The diffraction peaks are also sharp and intense due to increase in crystallinity, phase uniformity and small size of the particles.

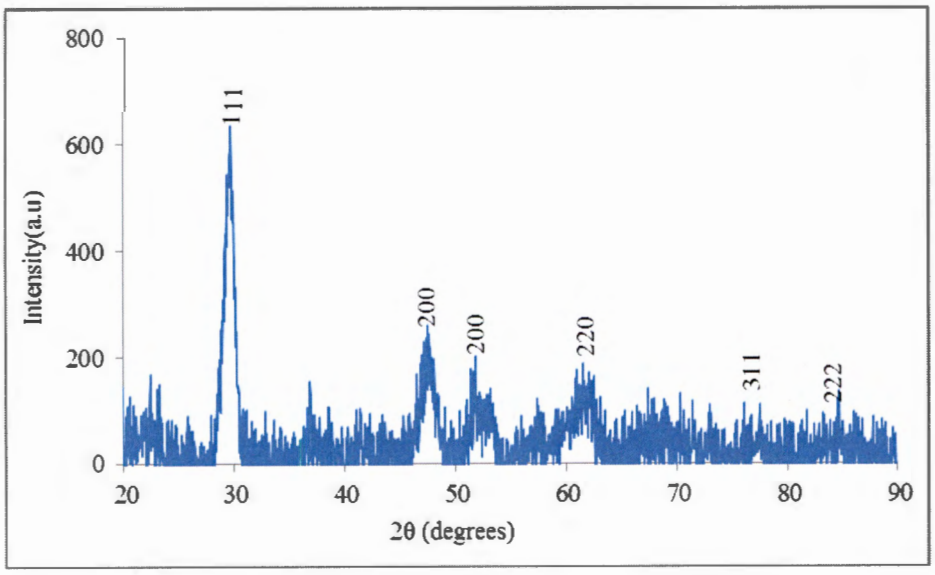

Figure 4.25: X-ray diffraction pattern for Pt nanoparticles obtained from **$[Pt(L^6)_2]$ and $[Pt(L^7)_2]$**

4.5.2.3.2. TEM studies of nanoparticles obtained from $[Pt(L^6)_2]$ and $[Pt(L^7)_2]$

Figure 4.26 shows the TEM images of nanoparticles obtained from $[Pt(L^6)_2]$ and $[Pt(L^7)_2]$. The particles appear spherical in shape with sizes in the range 2.51-10.42 nm and 1.47-4.15 nm and average particle size of 4.80 and 2.82 nm respectively. The particle size also decreases with increase

in chain length of substituent and nanoparticles obtained from $[Pt(L^6)_2]$ were distinctly monodispersed compared to the nanoparticles obtained from $[Pt(L^7)_2]$.

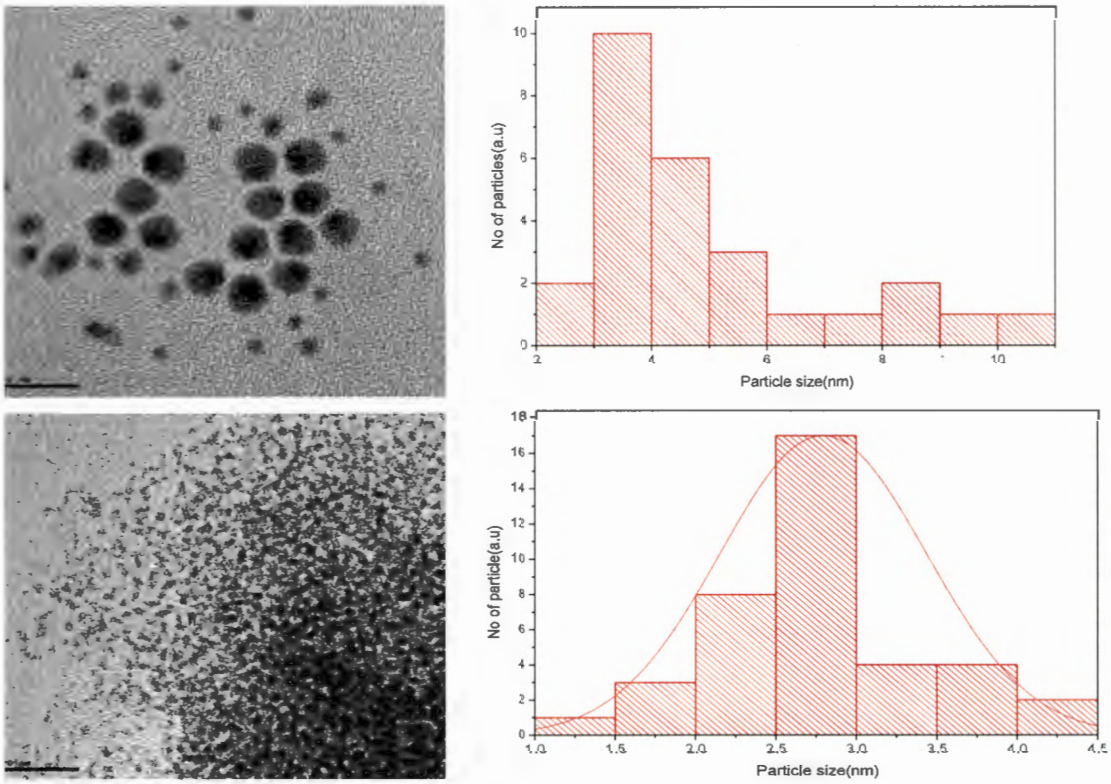

Figure 4.26: TEM images of Pt nanoparticles obtained from $Pt(L^6)_2]$ and $Pt(L^7)_2]$.

Table 4.4: Summary of characterization data of Palladium sulphide and platinium nanoparticles obtained from $[M(L^6)_2]$ and (b) $[M(L^7)_2]$, M = Pd and Pt

Nanoparticle/precursor compounds	Particle size from XRD (nm)	Particle size from TEM (nm)	Band gap energy (eV)	Particle Phase
Pd_4S /**$[Pt(L^6)_2]$**	2.30	3.45	3.81	Pd_4S
Pd_4S /**$[Pt(L^7)_2]$**	2.30	2.40	3.63	Pd_4S
$Pt/[Pt(L^6)_2]$	3.20	4.80	_	Pt metal
$Pt/[Pt(L^7)_2]$	3.20	2.82	_	Pt metal

4.6. A study of the effect of change in synthesis conditions: temperatures, growth time and capping molecules on the properties of nanoparticles using nickel suphide as representative.

To study the effects of the difference in temperature, capping agents and reaction time on the nanoparticles prepared, $[Ni(L^2)_2]$ and $[Ni(L^6)_2]$ obtained from dithiocarbamate derived from primary and secondary amines respectively were employed as precursor compounds. The same procedure described in section 4.4 was adopted for the two compounds. For the study of the effect of temperature variation, thermolysis was carried out at 150, 160, 190 and 220 °C using HDA as capping agent. For the study of the effect of different capping agents, hexadecylamine (HDA), oleylamine (OLA) and octadecylamine (ODA) were used and the reaction was conducted at 180 and 190 °C. For the study of the effect of change in growth time, aliqouts were taken after 15, 30, 45 and 60 min of reaction time.

4.6.1. X-ray diffraction studies of (NiL^2) and (NiL^6) nanoparticles

Nickel sulphide nanoparticles could appear in different phases. Hence, XRD analysis is an important technique used to ascertain the different possible crystalline phases of the synthesized nanoparticles. The powder X-ray diffraction patterns of the nanoparticles synthesized from $[Ni(L^2)_2]$ and $[Ni(L^6)_2]$ (as precursor compounds) thermolysed at 120, 150 and 180 °C yielded similar crystalline phase of nickel sulphide nanoparticles. Representative diffraction patterns are presented in Figure 4.27. The diffraction patterns in Figure 4.27a revealed pure phase of heazlewoodite Ni_3S_2 with 2θ values that could be assigned to (101), (110), (003), (202), (113), (122), (303), (014), (401), (105), and (134) which match with the JCPDS No: 00-044-1418 [37]. The crystallite size determined using the (110) diffraction peak and Debye Scherrer's equation estimated the diameters to be 4.58 nm for the samples prepared at 120, 150, and 180 °C respectively. The XRD pattern obtained using the same concentration of the samples and different capping agents including HDA, OLA and ODA, is presented in Figure 4.27b, and showed no phase variation. The diffraction pattern could be indexed to (202), (104),(401) of the pure phase of heazlewoodite Ni_3S_2. The sizes of the nanoparticles obtained from OLA and ODA capped Ni_3S_2 nanoparticles were also estimated using Scherrer's relation and were about 3.50 nm. The diffraction pattern showed that, by using the complex $[Ni(L^2)_2]$ as precursor molecule, the temperature of decomposition and capping molecules had no effect in altering the phases of the as-prepared nickel sulphide nanoparticles.

For $[Ni(L^6)_2]$, which was synthesized using dithiocarbamate obtained from secondary amine, the thermolysis of the compound at 160, 190 and 200 °C using HDA as capping agent also gave the same phase of nickel sulphide nanoparticles represented by the diffraction pattern in Figure 4.23a. The diffraction patterns obtained when OLA was used as capping agent and thermolysis at 190 °C are presented in Figure 4.27c. The sharp and intense peaks clearly indicate that the particles were crystalline; and the peaks could be indexed to pure alpha phase, $NiS_{1.03}$, which matches with JCPDS No: 00-002-1273 [32]. The absence of other observable peaks in the diffraction pattern is a confirmation of the purity of the nanoparticles. The diffraction pattern showed that, when complex $[Ni(L^6)_2]$ was utilized as precursor, the temperature of decomposition had no effect on the crystalline phases of the nickel sulphide nanoparticles prepared. However, the use of OLA as capping molecules gave nickel sulphides of different phases, probably due to the effect of the unsaturation in the ligand chain on the morphology of the nanoparticles.

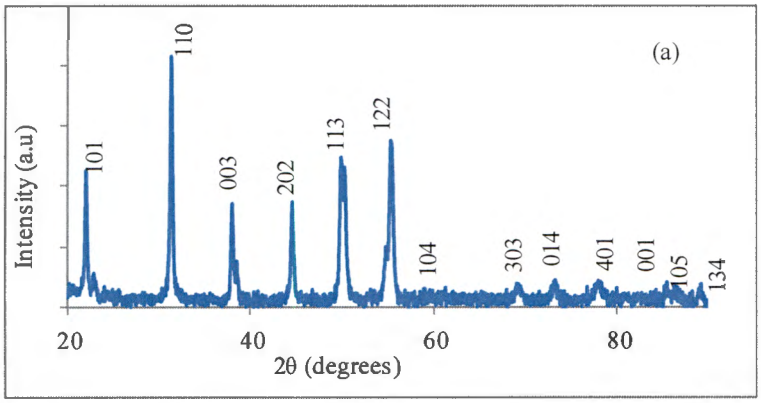

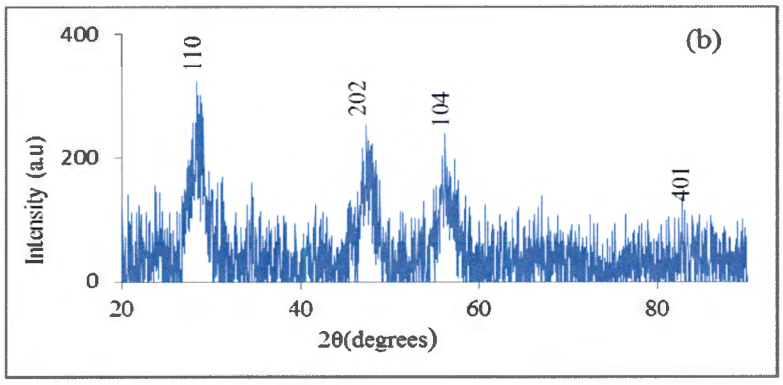

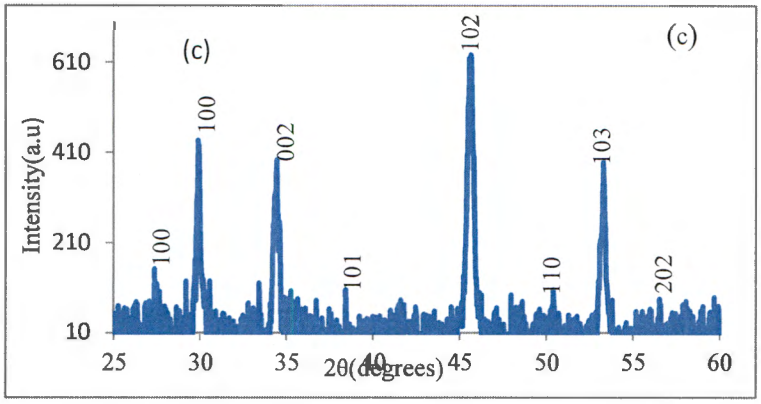

Figure 4.27: XRD of (a) Ni_3S_2 nanoparticles obtained at thermolysis temperature of 120, 150 and 180 °C, (b) OLA-capped Ni_3S_2 nanoparticles prepared at 150 °C using $[Ni(L^2)_2]$ complex, (c) OLA-capped $NiS_{1.03}$ nanoparticles obtained at 190 °C using $[Ni(L^6)_2]$.

4.6.2. TEM studies of the nanoparticles obtained from $[Ni(L^2)_2]$ and $[Ni(L^6)_2]$

The TEM micrograph of the HDA capped Ni_3S_2 nanoparticles obtained from $[Ni(L^2)_2]$ revealed a combination of dot-like and irregular shaped particles, while the ODA capped Ni_3S_2 nanoparticles gave a well-defined monodispersed dot-like morphology. Both the ODA and HDA-capped Ni_3S_2 displayed similar morphology as shown in Figures 4.28a and b. The OLA–capped Ni_3S_2 exhibited clearly irregular shapes which are distinctly different from the other samples obtained using ODA and HDA as capping molecules, as shown in Figure 4.28c. OLA has been reported to exhibit cis configuration, which promotes the formation of rods with low regularity and less opportunity for long range organization [39]. This might be responsible for the irregular morphology of the OLA-capped Ni_3S_2. Beside the differences in morphologies of the three different amine capped Ni_3S_2 nanoparticles, the size variation and size distribution of the nanoparticles are also noticeably dissimilar. The OLA-capped Ni_3S_2 has mean size of 7.51 nm, which is the largest, and are associated with the widest size distribution (3.20-13.90 nm) as revealed by the histogram obtained from the TEM micrograph.

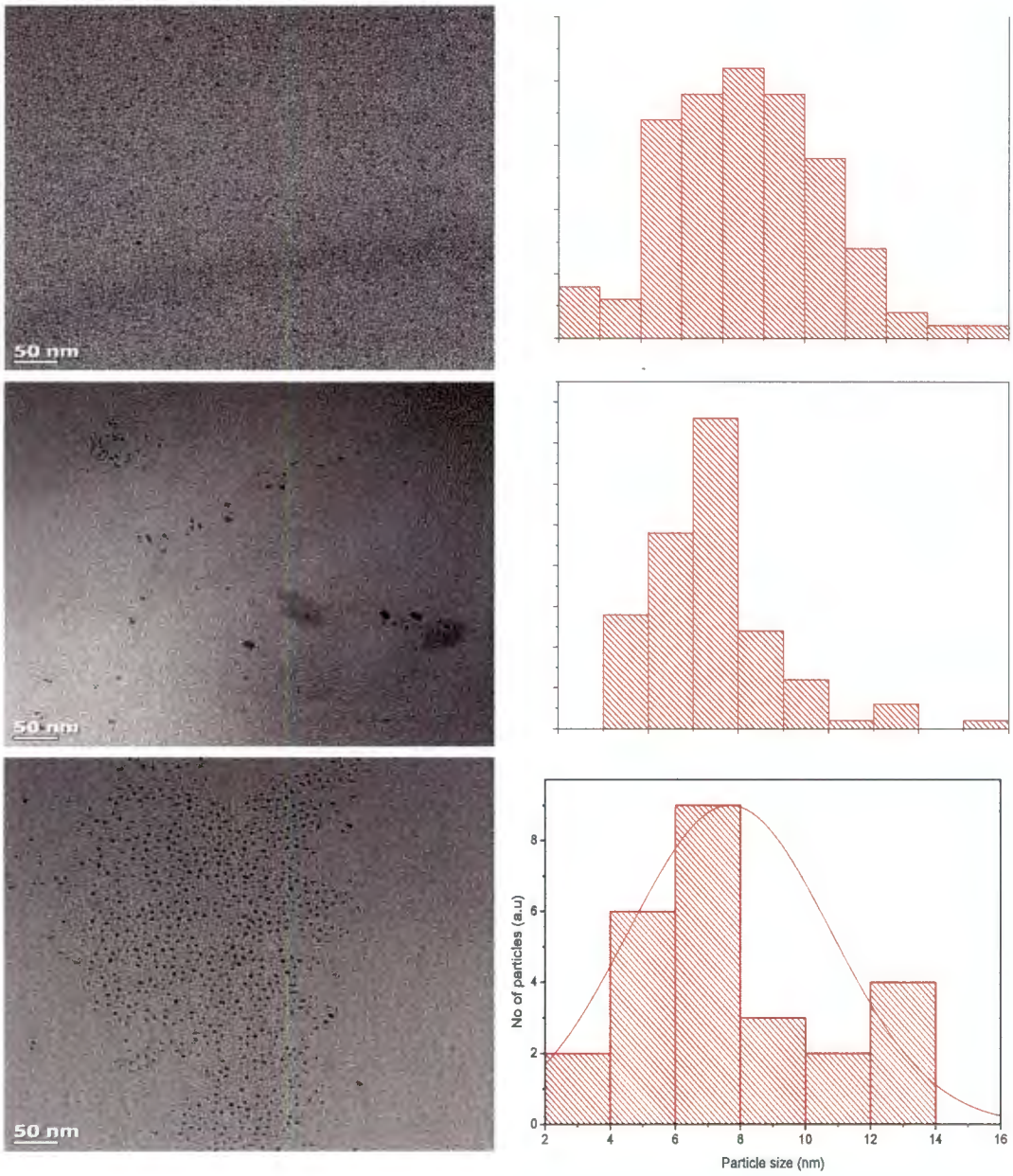

Figure 4.28: TEM micrographs of (a) HDA (b) ODA, and (c) OLA-capped Ni_3S_2 nanoparticles obtained using $[Ni(L^2)_2]$ as precursor complex at 180 °C, with their respective particle size histogram.

Figures 4.29 a and b present the TEM micrograph of the HDA capped Ni_3S_2 nanoparticles prepared from $[Ni(L^2)_2]$ complex at 120 and 150 °C respectively. The nanoparticles prepared at 120 °C, showed very small size and well defined dot shaped particles (Figure 4.29a).The corresponding particle size distribution histogram revealed an average particle size of 2.47 nm. The samples prepared at 150 °C and shown in Figure 4.29b presents uniformly distributed nanoparticles with average particle size of 3.01 nm. The TEM images showed that nanoparticles were effectively capped by the organic molecules as they have uniform inter-particle separation confirming that they are well separated from each other [40]. Figure 4.28a presents HDA-capped Ni_3S_2 nanoparticles obtained at 180 °C, and which has estimated average particle size of 3.32 nm. A slight widening of size distribution as the thermolysis temperature increased from 120 – 180 °C is noticeable, with significant difference in morphology occurring at 180 °C. The nanoparticles at this temperature appeared pseudo-spherical compared to the nanoparticles at lower temperature which are dot shaped. This observation confirmed that nanoparticles' size increases with increase in temperature of thermolysis [41].

The TEM micrograghs which showed the effect of different capping molecules on the morphology and size of the nanoparticles are presented in Figures 4.30(a-c). In contrast to the shape observation in the Ni_3S_2 nanoparticles obtained from $[Ni(L^2)_2]$, the Ni_3S_2 obtained using $[Ni(L^6)_2]$ complex as precursor revealed TEM micrograph that exhibited a combination of irregular shaped platelets of HDA capped Ni_3S_2 with mean size of 5.34 nm. The ODA capped Ni_3S_2 showed monodispersed dot-shaped morphology with mean size of 5.72 nm. The OLA capped NiS has a wider particle size distribution with monodispersed irregular rectangular shaped nanoparticles with mean size of 11.4 nm. It has the largest particle size compared to the nanoparticles obtained from the other two capping molecules [14].

The HDA-capped Ni_3S_2 nanoparticles prepared using $[Ni(L^6)_2]$ as precursor complex at 160, 190 and 220 °C growth temperatures is presented in Figures 4.31a, b and c respectively. Difference in particle morphology with variation in temperature is very conspicuous. A slight broadening of particle size distribution was also detected as the thermolysis temperature increased from 160 to 220 °C (3.55 – 13.90 nm). The mean particle sizes also increased from 3.55 to 5.34 nm, indicating the growth of nanoparticle as a direct function of temperature. All the nanoparticles are distinctly monodispersed with narrow size distributions.

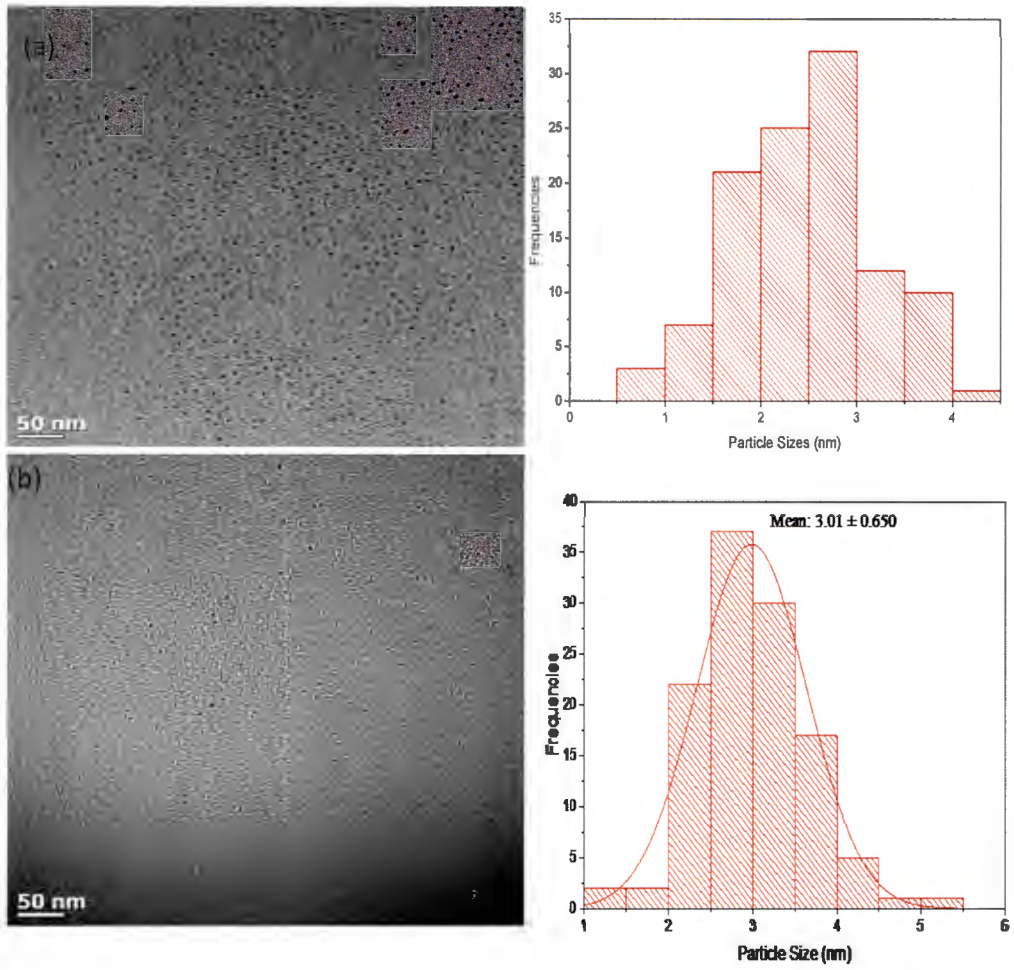

Figure 4.29: TEM micrographs of HDA-capped Ni_3S_2 obtained using $[Ni(L^2)_2]$ as precursor at (a) 120, (b) at 150 ° C, with their respective particle size distribution histogram

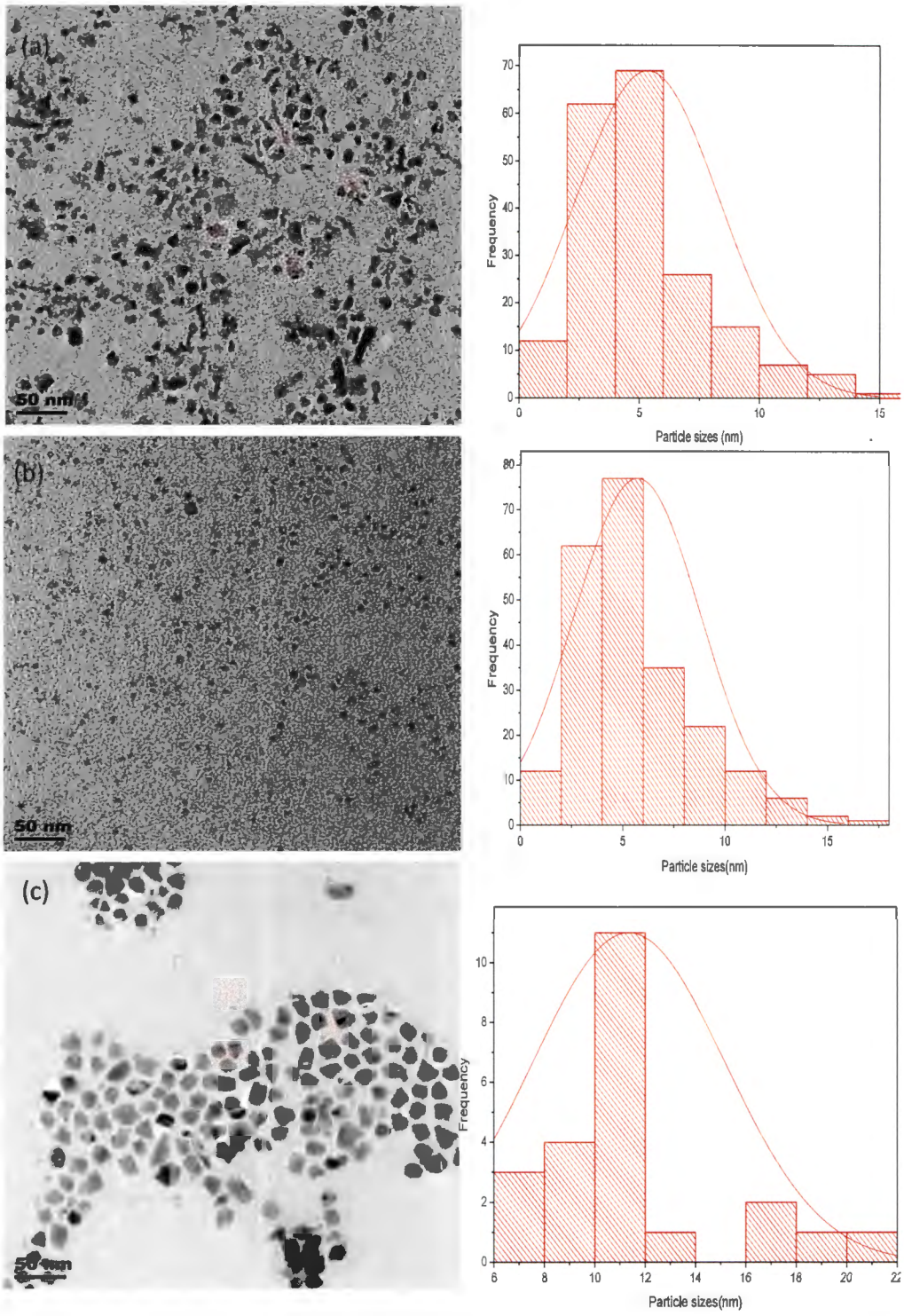

Figure 4.30: TEM micrographs of (a) HDA, (b) ODA, and (c) OLA - capped nickel sulphide nanoparticles obtained using $[Ni(L^6)_2]$ as precursor at 190 ° C, with their respective particle size distribution histogram.

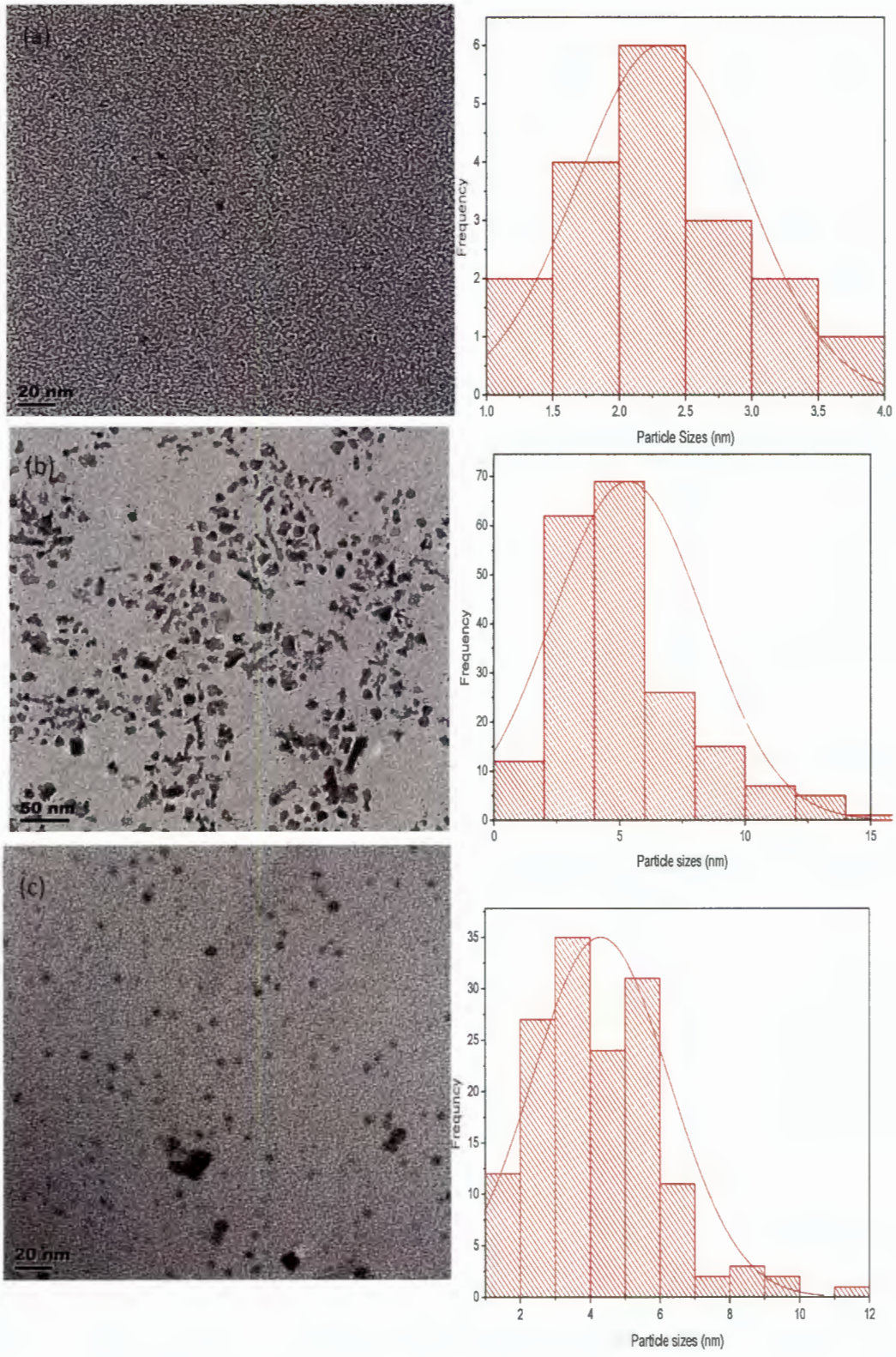

Figure 4.31: TEM micrographs of HDA-capped Ni_3S_2 obtained using $[Ni(L^6)_2]$ as precursor at (a) 160, (b) 190 °C , (c) 220 °C, with their respective particle size distribution histogram.

4.6.3. Optical properties of the nanoparticles obtained from $[Ni(L^2)_2]$ and $[Ni(L^6)_2]$

4.6.3.1 UV-vis spectroscopic studies of the nanoparticles obtained from $[Ni(L^2)_2]$ and $[Ni(L^6)_2]$

The optical excitation of electrons in materials whose sizes are in the nano dimension produces an abrupt increase in absorption at the wavelength which corresponds to its band gap energy. This process, which occurs across the band gap, is allowed and it is known as the optical absorption edge [42]. Both the position of the band edge and shape of the absorption shoulder depend on properties of the reaction system such as the type of surfactants used, temperature and time. It also depends on some properties of the nanoparticles such as size and size distribution [33].

The overlapped UV-vis absorption spectra of the Ni_3S_2 prepared using $[Ni(L^2)_2]$ and $[Ni(L^6)_2]$ as precursor compounds, and HDA as capping molecule at 160, 190, and 220 °C are shown in Figure 4.28. The obtained absorption spectra were employed to calculate the respective band gap energies from their absorption onset [43]. In the nanoparticles synthesized using $[Ni(L^2)_2]$ (Figure 4.32a), the calculated band gap energies were: 3.77, 3.51, and 3.08 eV which corresponded to 329, 353, and 402 nm for the samples obtained at 160, 190, and 220 °C respectively. In the spectra of the nanoparticles obtained using $[Ni(L^6)_2]$ (Figure 4.32b), following the same respective sequence, the band gap energies were estimated as 3.50, 3.55, and 3.77 eV, which corresponded to 354, 349 and 329 nm (354 nm), 3.55 (349 nm), 3.77 eV (329 nm). A blue shift relative to the bulk nickel sulphide (2.1 eV, 590 nm) [44] were observed for the samples obtained using both $[Ni(L^2)_2]$ and $[Ni(L^6)_2]$ at all studied temperature. The nanoparticles exhibited quantum confinement effect even with increase in temperature of thermolysis. It is noteworthy that the wavelength of the maximum excitonic absorption increased with temperature rise and this lead to increase in the size of the nanoparticles [45].

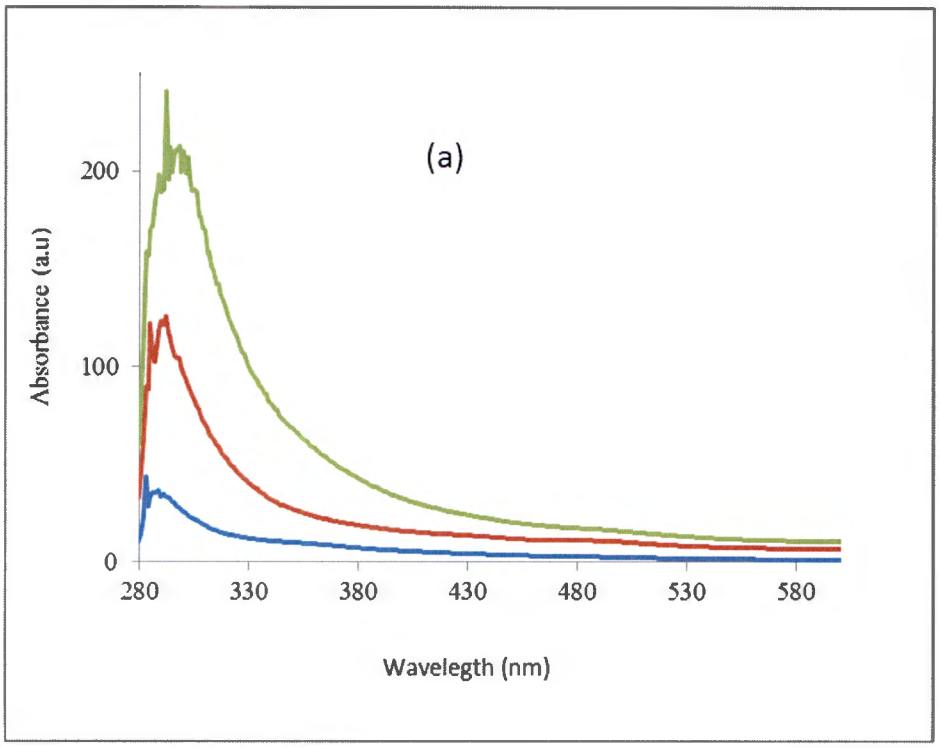

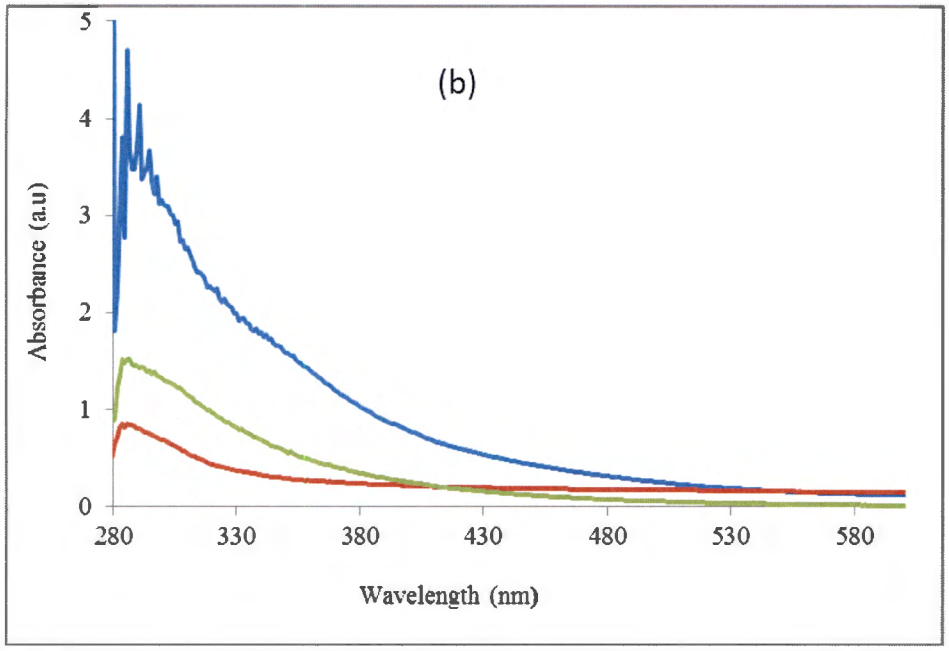

Figure 4.32: **UV-vis spectra of the nanoparticles obtained from $[Ni(L^2)_2]$ and $[Ni(L^6)_2]$**

4.6.3.2. Photoluminescence studies of the representative NiS nanoparticles.

Figure 4.33 presents the representative photoluminescence spectra of nickel sulphide nanoparticles obtained at an excitation wavelength of 260 nm (λ_{260}). The emission peak centred on 330 nm was observed in all reactions, which could be assigned to the electron hole recombination in nickel

sulphide nanoparticles [4]. Other peaks appear at higher wavelengths. These emissions could be assigned to the intra-band transitions within the structure of the nickel sulphide nanoparticles during excitation. Emissions around 400 and 420 nm could be as a result of the de-excitation between S (3p) levels and Ni (3d) levels, while emissions between 500 - 800 nm is attributable to the de-excitations from either S (3s, 3p) or Ni (3d) levels down to the Ni–S hybridization levels [48]. The high intensity of the peaks affirmed the small size of the nanoparticles formed with increase in reaction time.

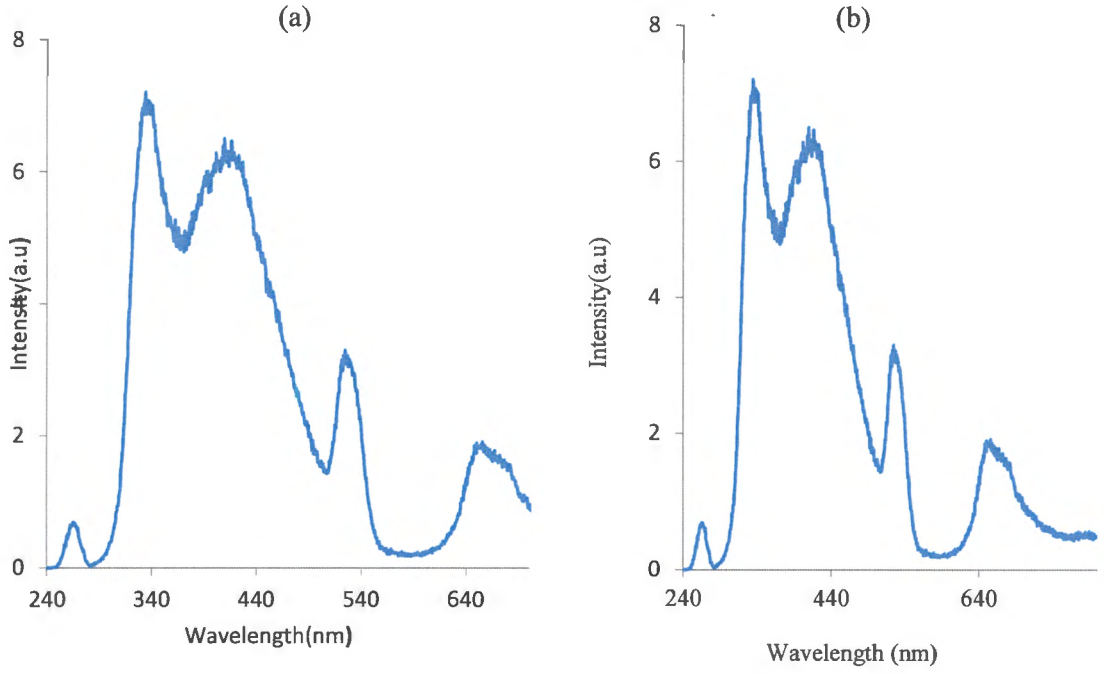

Figure 4.33: PL spectra of nickel sulphide nanoparticle obtained using (a) $[Ni(L^2)_2]$ and (b) $[Ni(L^6)_2]$ as precursor compound

4.6.5. Infrared spectral studies of representative nickel sulphide nanoparticles

Qualitative details of the interaction between the three capping molecules: HDA, OLA and ODA, and the nickel sulphide nanoparticles could be explored using FTIR. The infrared spectra of the pure capping agents were compared with that of the capped nanoparticles as represented in Figure 34. Based on the analysis of the capping agents, peaks were observed around 3334 cm^{-1} , which could be ascribed to ν(N—H) vibration, and the peaks due to asymmetrical and symmetrical ν(C—H) vibrations were identified around 2920 and 2850 cm^{-1}. Similar peaks were also identified in the same environment in the spectra of the nanoparticles. The similarities in the positions of

appearance in the spectrum of the pure capping molecules (HDA, ODA and OLA) and their respective capped Ni_3S_2 nanoparticles is an indication that all the capping agents are integral part of the capped nanoparticles. Similar results have been reported for the interactions of HDA [20], ODA [37] and OLA [49] with capped metal sulphide nanoparticles.

The strong peak around 510 cm^{-1} in the spectra nanoparticles, which was not observed in the spectra of the pure HDA/ODA/OLA, is assigned to the stretching vibration due to Ni-S bond. Apart from the vibrational modes of the capping molecules- HDA/ODA/OLA, and the Ni-S, the absence of the aromatic C-H and N-CS_2 stretching vibrations in the spectra of the nanoparticles confirmed the decomposition of dithiocarbamate compound; thus, the results also confirmed the purity of the synthesized NPs from the contamination by the incomplete decomposition of the starting precursor compounds.

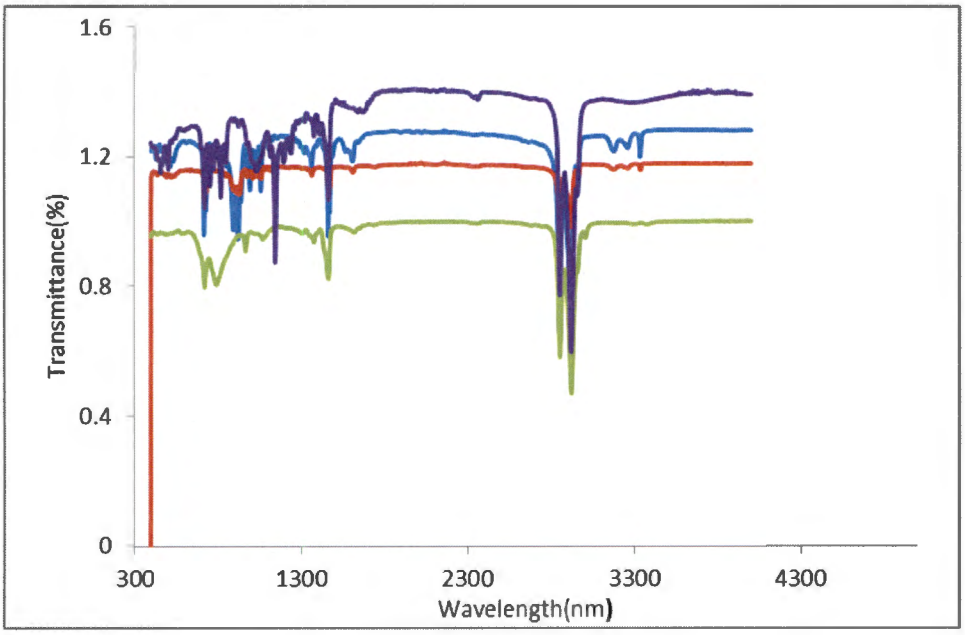

Figure 4.34: Overlapped FTIR spectra of pure HDA (blue), OLA (Green), ODA (red) and nickel sulphide (purple) nanoparticles.

4.7 Conclusion

Group 10 metal dithiocarbamate derivatives have been utilised as single source precursors to prepare metal sulphides nanoparticles with various optical and structural properties. The variations of the alkyl substituents on the nitrogen of the dithiocarbamate have pronounced effect on the structure of the complexes, which in turn influences the properties of the prepared nanoparticles. The good yield of the nickel dithiocarbamate was utilised in the study of the effect of the synthesis conditions such as temperature, variation of capping agents and growth time on the optical and morphology of the synthesized nanoparticles. The three capping agents chosen for the study were hexadecyl amine (HAD), octadecylamine (ODA) and oleylamine (OLA). The ligands were chosen based on their chain length, good thermal stability and reported stabilising properties associated with nanoparticles. The X-ray diffraction patterns revealed that the use of HDA and ODA as capping molecules gave the same phase while different phases were observed with OLA as capping agent. Six different phases were observed for the nickel sulphide nanoparticles viz: hexagonal α-NiS phase, α-NiS, $NiSO_4 \cdot 6H_2O$, Nickelhexahydrite, α-$NiS_{1.19}$, base-centered orthorhombic Godlevskite phase, Ni_9S_8 and (heazlewoodite), Ni_3S_2. There were four different phases obtained for the palladium nanoparticles; crystalline metallic Pd, vysotskite PdS, cubic plane PdS_2 and Pd_4S and two phases for the platinum nanoparticles; cooprite PtS and polycrystalline metallic Pt. The results of the TEM analysis showed that the ODA and HDA-capped nanoparticles were well-defined monodispersed dot-like and irregular shaped particles. The OLA–capped nanoparticles showed clearly irregular shapes distinct from the other two capping molecules. All the nanoparticles gave well-defined monodispersed nanostructures with the monodispersity increasing with increase in chain length of the substituents and with decrease in the size of the nanoparticles produced. All the nanoparticles exhibited quantum confinement even at higher temperature of thermolysis, with increase in band gap energy which implies decrease in particle size as the chain length of the substituents increases. The FTIR analysis, used to probe the functional groups on the surface of the nanoparticles, showed that the capping agents were integral part of the capped nanoparticles and the absence of the aromatic C-H and N-CS_2 stretching vibrations confirmed the purity of the nanoparticles formed.

The metal chalcogenide is practically a vast and an infinite area of research, because of the versatile technological applications, with structure and properties that could easily be manipulated to suit

several and different purposes [50]. Many derivatives have been synthesized from the numerous structural functionalization and modifications employed; morphological elucidation of the new forms has also become an easy task because of modern characterization tools that are available and easily accessible.

REFERENCES

[1] H. L. Beal, P. G. Etchegoin and R. D. Tilley, J. Phys. Chem. C 114, 3817 (2010).

[2] N. Hollingsworth, A. Roffey, H.U. Islam, M. Mercy, A. Roldan, W. Bras, M. Wolthers, C.R.A. Catlow, G. Sankar, G. Hogarth, N.H. De Leeuw, Chem. Mater. 26 (2014) 6281.

[3] S. N, Vercellotti, G. White J, A.Fegan, C.Wagner, Bischof, Mol.Pharm. 9 (2012) 2146.

[4] A.F. Hepp, M.J. Kulis, J.S. Mcnatt, N. V Duffy, M.D. Hoops, P.E. Fanwick, J. Masnovi, J.E. Cowen, R.N. Dominey, Decomposition of Nickel Dithiocarbamates : Effect of Precursor Structure and Processing Conditions on Solid-State Products, (2016).

[5] G. Kullerud R. A. Yund, Journal of Petrology 3 (1962) 126.

[6] C. Gervas, S. Mlowe, M.P. Akerman, I. Ezekiel, T. Moyo, N. Revaprasadu, Polyhedron. 122 (2017) 16.

[7] W. Xu, J. Ni, Q. Zhang, F. Feng, Y. Xiang, X. Li, J. Mater. Chem. A. 1 (2013) 12811.

[8] R. Bhatt, S. Bhattacharya, R. Basu, A. Singh, U. Deshpande, C. Surger, S. Basu, D.K. Aswal, S.K. Gupta, 539 (2013) 41.

[9] A. Zubkov, T. Fujino, N. Sato and K. Yamada, J. Chem.Thermodyn, 30 (1998) 571.

[10] M.C.Sabine, V. Roland, K.W. Merkle, The Canadian Mineralogist, 40 (2002) 571.

[11] P.L. Musetha, N. Revaprasadu, G.A. Kolawole, R.V.S.R. Pullabhotla, K. Ramasamy, P. O'Brien, Thin Solid Films. 519 (2010) 197.

[12] M. Masab, H. Muhammad, F. Shah, M. Yasir, M. Hanif, Mater. Sci. Semicond. Process. 81 (2018) 113.

[13] S. Mourdikoudis, L. M. Liz-Marzan, Chem. Mater. 25 (2013) 1465.

[14] J.B. Parise, Acta Crystallogr. Sect. B, 36 (1980) 1179.

[15] C. Sun, M. Ma, J. Yang, Y. Zhang, P. Chen, W. Huang, X. Dong, Sci. Rep. 4 (2014) 1.

[16] N. Nickel, S.L. Structures, Synthesis of Novel Nickel Sulfide Layer-Rolled Structures (2001) 1278.

[17] E.N. Volkova, I. Demidov, Russ. J. Appl. Chem. 83 (2010) 1874.

[18] J. Xu, D. Bhattacharyya, Environ. Prog. 24 (2005) 358.

[19] S.B Sibokoza, M.J. Moloto, N. Moloto, P.N. Sibiya, Chalcogenide Lett. 14 (2017) 69.

[20] S. N. Shukla, P. Gaur and N. Rai, Appl. Nanosci. 5 (2015). 583.

[21] M. Kristl, B. Dojer, S. Gyergyek, J. Kristl, Heliyon. 3 (2017) 1.

[22] Y. Chen, X. Gu, C.-G. Nie, Z.-Y. Jiang, Z.-X. Xie, C.-J. Lin, Chem. Commun. 1 (2005) 4181.

[23] N. Sonker, J. Bajpai, A.K. Bajpai, A. Mishra, Nano-Structures and Nano-Objects. 14 (2018) 1.

[24] P. Ajibade, N. Botha, Nanomaterials. 7 (2017) 32.

[25] Wei Xu, Jun Ni, Qunfeng Zhang, Feng Feng, Yizhi Xiang , Xiaonian Li. J. Mater. Chem. A, 1(2013) 12811.

[26] M.A. Malik, P. O'Brien, N. Revaprasadu, J. Mater. Chem. 12 (2002) 92.

[27] M A. Malik, P. O'Brien, N Revaprasadu, J .Mater Chem. 11 (2001) 2382.

[28] J.C.W. Folmer, J.A. Turner, B.A. Parkinson, J. Solid State Chem. 68 (1987) 28.

[29] Y. Hu, J.F. Chen, W.M. Chen, X.H. Lin, X.L. Li, Adv. Mater. 15 (2003) 726.

[30] Q. W.Chen, D. L Zhu, C. Zhu, J. Wang, Y. G. Zhang, Appl. Phys.Lett. 82 (2003) 1018.

[31] X.Li, Y.Xie, Y. Xu, C. Z.Wu, Z. Q.Li, J. Solid State Chem. 179 (2006) 56 .

[32] P.Mohanpuria, N.K.Rana, S.K.Yadav. J.Nanopart.Res. 10 (2008) 507.

[33] D.C. Onwudiwe, C. Strydom, O.S. Oluwafemi, S.P. Songca, Mater. Res. Bull. 47 (2012) 4445.

[34] C. Wei, Q. Ru, X. Kang, H. Hou, C. Cheng, D. Zhang, Appl. Surf. Sci. 435 (2018) 993.

[35] B.P.O'Brien, J. Waters, Deposition of Ni and Pd Sulfide Thin Films via Aerosol-Assisted

CVD (2006) 620.

[36] G. Barim, S.R. Smock, P.D. Antunez, D. Glaser, R.L. Brutchey, Nanoscale. 10 (2018).

[37] L. Polavarapu, N. Venkatram, W. Ji, Q-H. Xu, ACS Appl. Mater. Interfaces, 1 (2009) 2298.

[38] M.G. Neelgunda, B. Karthikeyanb, S. A. Shivashankar, A. Oki, Appl. Surf. Sci. 356 (2015) 726.

[39] J. Osuntokun, P.A Ajibade, Superlatt. Microstruct, 83 (2015) 89.

[40] F. Dumestre, M. Chaudret, B. Amiens, C. Fromen, M.C. Casanove, M.J. Renaud, P. Zurcher, P. Angew, Chem. Int. Ed. 41 (2002) 4286.

[41] W. Jiang, B. Kim, J. Rutka, W. Chan, Nat. Nanotechnol. 3 (2008) 145.

[42] V. Kumar, S. Kr, T.P. Sharma, V. Singh, 12 (1999) 115.

[43] L.E. Brus, J. Phys. Chem. 90 (1986) 2555.

[44] J.Tauc, Mater. Res. Bull., 3 (1968) 37.

[45] T. Vossmeyer, L. Katsikas, M. Giersig, I.G. Popovic, K. Diesner, A. Chemseddine, A. Eychmüller, H. Weller, J. Phys. Chem. 98 (1994) 7665.

[46] M. Salavati-Niasari, F. Davar, M. Mazaheri, Mater. Res. Bull. 44 (2009) 2246.

[47] A. Koji, J. Iqbal, R. Yu, Z-J Zhang, Front. Mater. Sci. 5 (2011) 311.

[48] E. C. Linganiso, S. D. Mhlanga, N. J. Coville and B. W. Mwakikunga, J. Alloys Compd., 552(2013) 345.

[49] J. Osuntokun, P.A. Ajibade, D.C. Onwudiwe, Superlattices Microstruct. 100 (2016) 605.

[50] F.A. Devillanova Handbook of Chalcogen Chemistry, University of Cagliari, Italy (2007).

[51] J. J. Vittal, M. Ng, T.Acc. Chem. Res. 39 (2006) 869.

[52] M. A.Malik, N. Revaprasadu, P. O'Brien, Chem. Mater. 13 (2001) 91.

[53] W. Han, M.Gao, Cryst. Growth Des. 8 (2008) 1023.

[54] B. Geng, X. Liu, J. Ma, Q. Du, Mater. Sci. Eng., B 145 (2007)17.

[55] B. Ludolph, M. A. Malik, P. O'Brien, N. Revaprasad, J. Chem. Commun.17 (1998) 1849.

[56] S. Nagaveena, S. N. Kumar, C. K. Mahadevan, Inter. J. Eng Res. 3 (2013)1214.

[57] H. Wang, J.R. Zhang, X.N. Zhao, S. Xu, J.-J. Zhu, Mater. Lett. 55 (2002) 253.

[58] B. Yuan and W. Luan, Funct Mater Lett. 7 (2014) 1.

[59] C. Buchmaier, M. Glanzer, A. Torvisco, P. Poelt, K. Wewerka, B. Kunert, K. Gatterer, G.Trimmel, T. Rath, J Mater Sci 52 (2017)10898.

[60] B.A Prakasam, M. Lahtinen, A.Peuronen, M.Muruganandham, E. Kolehmainen, E. Haapaniemi, M. Sillanpa, Inorg. Chim. Acta. 425 (2015) 239.

[61] I.J.Ferrer, P.Díaz-Chao, A.Pascual,C. Sánchez, Thin Solid Films, 515 (2007) 5783.

[62] R. Yamamoto, Japanese Patent S61-215661 (1986).

[63] S. Dey , V. K. Jain, Platinum Metals Rev. 48 (2004) 16.

[64] D. Nguyen-manh, P. S. Ntoahae, D. G. Pettifor, P. E. Ngoepe, Mol. Simul. 22(1999)23.

[65] P. Raybaud, J. Hafner, G. Kresse, H. Toulhoat, J. Phys. Condens. Matter.9 (1997) 11107.

[66] Q. Pan, K. Huang, S. Ni, F. Yang, D. He, Mater Res. Bull. 43(2008)1440.

[67] S. Boldish, W. White, Am. Mineral. 83 (1998) 865.

[68] L.C. Kanchana, R. Mucherla, Y. Aparna, M. Ramchander, D. Ravinder, K. Jaipal, P. Veerasomaiah, D. Shridhar, Mater. Res. 20 (2017) 256.

[69] M.G. Neelgunda, B. Karthikeyanb, S. A. Shivashankar, A. Oki, Appl. Surf. Sci. 356 (2015) 726.

CHAPTER FIVE

5.0 biological studies of the synthesized complexes

5.1. Introduction

Metal-based drugs have given remedies to many diseases since ancient times, for instance, the Greek physicians administer silver in the treatment of wounds and ulcers, while the Egyptians sterilized water with copper because of its antimicrobial properties [1].Transition metals have become very versatile in all spheres of life, but most importantly in medicine, after the coincidental discovery of cisplatin (diamminedichloroplatinum(II) as a very powerful chemotherapeutic agent for the treatment of various forms of cancer [2]. Cisplatin has been reported to exhibit cellular division, making it the most powerful drug, with very high antitumor activities. The potency has been attributed to the consequence of its interaction with DNA, which impedes their replication.

The major setback of this Pt based drug is bioavailability and selectivity between diseased and healthy cells. Therefore, derivatizations of the Pt-drug with appropriate substitution within a wide range of ligand or ligand combinations are continuously being investigated to improve the performance of cisplatin. Since the central metal ion of the complexes plays an important role in biological processes, the exploration of other transition metals in biological applications becomes imperative. The presence of metal ions in complexes facilitates the coordination to important residual structures at the active site of the substrate. They also help to catalyse the generation of reactive oxygen species (ROS) due to their high affinity for small molecules, which play an important role in modulating drug-induced cytotoxic responses and affect cell pathogenesis [3]. The nature of metal ions, as electron deficient, makes them bind and interact effectively with important biological molecules which are electron rich. Thus, provides the opportunity for biological modulation [4].

Organic ligands also play an important role in determining favourable interactions and activities between metal complexes and DNA. So, when dithiocarbamate ligands are utilized they can block metal interaction with sulphur-containing renal proteins, which can efficiently form transition metal dithiocarbamate complexes; with wide spectrum of biological activities and resistance. Furthermore, the enzyme mimics of organo-sulphur compounds have made them to be particularly useful in biological systems. Their high protolytic dissociation makes them more useful under physiological condition.Thus, heteroaromatic, nitrogen bases with M-N bonds form complexes with metal ions which may be considered as models for substrate–metal ion–enzyme interactions [5].

The increase in the outbreak of new infectious diseases coupled with the increase in drug resistance pathogens have also aroused the interest of chemists in the quest for new and effective compounds with improved pharmacological potentials. Interest in transition metal complexes has increased because of their biological properties as a result of their simple ligand exchange mechanism. The group 10 metal complexes have been explored in a number of biological areas due to their antimicrobial and anticancer properties. This has opened the way to new medical research involving heavy metals and group 10 metals in particular as excellent therapeutic agents against numerous diseases. Their actions have been suggested to be based mainly on the strong interactions between metals and DNA of certain target cells through both covalent and non-covalent interactions, such as electrostatic interactions, intercalation as well as direct coordination bond formation [6].

Since the coordination chemistry of Pd(II) and Pt(II) are similar, coupled with the higher solubility, greater cytotoxity of Pd over Pt based drugs, and with reduced cross resistance, Pd-based drugs have become an excellent choice for the search for a successor to cisplain [6]. Similarly, Ni interacts with iron found in the haemoglobin and is also involved in the transmission of genetic code (DNA, RNA). It is one of the elements containing bio-essential metal ions [7], and so, can add to the current generation of antibiotics as antibacterial and antifungi agents. The group 10 triad (Ni, Pd, Pt), with all the important therapeutic applications stated above, when combined with dithiocarbamate ligands to form group 10 dithiocarbamate complexes help in the recognition of target sites and are therefore explored for enhanced biological activities. They might hold the potential as good alternative to cisplatin, thus contribute to the generations of future drugs which could minimise or overcome some of the drawbacks that are associated with the use of cisplatin and other resistant and toxic antibiotics.

5.2 Experimental

5.2.1 Antimicrobial studies

Agar well diffusion method was used to determine the antibacterial activities of the complexes. The bacteria strains used were the Gram positive *S. aureus and B. cerues* and Gram negative *K. pneumonia*, *P. aeruginosa* and *E. coli,* while the fungi strains were *C. albican* and *A. flavus.*

The base plates were prepared using autoclaved Muller–Hinton agar (MHA), after drying for 24 h, 0.5 McFarland culture were carefully swabbed on the surface of the solidified media and allowed for about 15 min to dry. Then, the agar plate surface was inoculated with the microbial inoculum by using a sterilized cotton swab over the entire agar surface to make a layer of growth, and air dried

for about 10 min. A sterile cork borer was then used to bore a hole on the solidified agar surface and about 5 µL of 12.5, 25.0, and 50.0 µg/mL of each complex was introduced into the well. The agar plates were air dried for about 10 min and then incubated at 37 °C for 24 h. Zones of inhibition were recorded by measuring the diameter of inhibitory zones on the agar surface around the disks which relates directly to the sensitivities of the microorganism species to the samples tested.

The minimum inhibitory concentration (MIC) was determined by broth dilution method. Different concentrations of the compounds: 1, 2, 3, 4 and 5 mg/mL were prepared by dilution method from a stock solution. Each well of the microtiter plate (96 wells) was filled with 100 µL of nutrient broth, 20 µL of the test organism (10^6 CFU/mL) and 80 µL of different concentrations of the compounds. The control wells contained broth only or broth and test organisms. About 20 µL of 1.25 mg/mL of 3-(4,5-dimethylthiazol-2-yl)-2,5-diphenyltetrazolium bromide (Sigma-Aldrich) was introduced into each well and incubated for 30 min. The observation or non-observation of a purple coloration indicates microbial growth and MIC, respectively [8].

5.2.2 Anti- cancer studies

Human cervical carcinoma (HeLa) cells were obtained from the ATCC, Manasas, USA, and cultured in 25 cm^2 tissue culture flasks in EMEM (Lonza BioWhittaker, Verviers, Belgium) containing 10% fetal bovine serum, 100 U mL^{-1} penicillin, and 100 μgmL^{-1} streptomycin. Cell viability was investigated in the HeLa cell line using the MTT assay in a 96-well plate containing 2.5×10^2 cells/well in 100 µL EMEM. Cells were incubated overnight at 37 °C. The medium was, thereafter, replaced and the samples were added at various concentrations (25, 50, 100, and 1500 µg/mL). Cells were then incubated for 48 h at 37 °C, followed by the MTT assay. A positive control with untreated cells was included, together with 5-Fluorouracil as a standard. For the assay, the medium was replaced with fresh medium containing 10% MTT reagent (5 mg/mL in PBS), and incubated for 4 h at 37 °C. This was then removed, and the insoluble formazan crystals were dissolved in 100 µL of DMSO, followed by reading of the absorbance at 570 nm in a Mindray MR-96A microplate reader (Vacutec, Hamburg, Germany) using DMSO as the blank. Assays were done in triplicate [9].

5.3 Results and discussion

5.3.1 Antimicrobial studies

5.3.1.1 Antimicrobial studies of the Ni(II), Pd(II) and Pt(II) complexes of dithiocarbamate prepared from primary amines

All the compounds were screened at three different concentrations of 10, 25 and 50 µg/mL. However, significant zones of inhibition were obtained at 50 µg/mL and were taken as the minimum inhibitory concentration of the metal complexes against the microbes: Gram positive *S. aureus and B. cerues*), Gram negative (*K. pneumonia*, *P. aeruginosa* and *E. coli*) and two fungi organisms (*C. albican* and *A. flavus*).

The metal complexes gave varied antimicrobial activities ranging from moderate to very active. The presence of -NH, a hydrophilic group, on the complexes of dithiocarbamate prepared from primary amines promotes the lipophilicity of the compounds through the lipid cell membrane of the microorganisms. This facilitates the inhibition of the bacteria by the complexes. The obtained data are presented in Table 5.1 and summarized as histogram in Figures 5.1 – 5.3. Complexes $[Ni(L^1)_2]$, $[Pd(L^1)_2]$, $[Pt(L^1)_2]$, $[Ni(L^2)_2]$, $[Pd(L^2)_2]$, and $[Pt(L^2)_2]$ (1-6) consist of the unsusbtituted phenyldithiocarbamates. The moderate activities observed, as presented in Figure 5.1, indicated the sole contribution of the aromatic ring from the phenyl group. *E. coli* was susceptible to all the complexes, while *P. aeruginosa* and *K. pneumonia* were susceptible to all the complexes except for $[Pd(L^1)_2]$ and $[Ni(L^2)_2]$ complexes respectively.

Complexes $[Ni(L^3)_2]$, $[Pd(L^3)_2]$, $[Pt(L^3)_2]$, $[Ni(L^4)_2]$, $[Pd(L^4)_2]$ and $[Pt(L^4)_2]$ (7 – 12) comprised of the methyl and ethyl substituted phenyldithiocarbamates. The antimicrobial results of these compounds, presented as histogram in Figure 5.2, indicated that they exhibited better antimicrobial activities than were observed in the unsusbtituted compounds. The presence of the methyl and ethyl substituents imparted greater stabilization of an adjacent charge on the phenyl rings. This decreased the polarity of the central metal ions by directing the positive charge towards the donor groups into the chelate formed during the coordination. This further strengthens the metal ligand bond thereby increasing the lipophilic nature of the metal which favours their effective infusion over the cell membrane of the microorganism, for more violent inhibition [8].

Compounds $[Ni(L^5)_2]$, $[Pd(L^5)_2]$ and$[Pt(L^5)_2]$ (13-15), obtained from dithiocarbamate prepared from the aliphatic hexamethylenediamine, exhibited low activity. Perhaps, the absence of the aromatic ring denies the compounds the expected collaborative effect which existed in other compounds with

aromatic group. As reflected in Figure 5.3, the metal complexes of the dithiocarbamate obtained from Schiff bases, $[Ni(L^{10})_2]$, $[Pd(L^{10})_2]$ and $[Pt(L^{10})_2]$ (27-29), showed improved activities against both bacteria and fungi organisms. The presence of the aromatic hydroxyl benzaldehyde on the hexamethylenediamine dithiocarbamate complexes help to promote their activities. These results indicated that complexes with aromatic rings have better antimicrobial activities than those with aliphatic chains.

On a general note, the Gram negative bacteria organisms were more susceptible to the complexes compared to the Gram positive bacteria organisms. This was probably due to the presence of an outer protective lipopolysaccharide membrane in Gram positive bacteria strains, which does not permit lipophobic materials into the cell, making penetration of the complexes intricate [10]. However, complexes $[Ni(L^4)_2]$, $[Pd(L^4)_2]$ and $[Pt(L^4)_2]$, which contain ethyl substituted phenyl were very active against both Gram positive and Gram negative bacterial strains. They were the most active of the metal complexes screened against the microbes. The complexes exhibited better antibacterial activity compared to their antifungal activity. Of all the metal complexes, $[Pt(L^3)_2]$ which contains the phenyl group bearing ethyl substituent exhibited the best antifungal activity against *C. albican* and *A. flavus*. However, Ketoconazole had better antifungal activity compared to the metal complexes. Similarly, Sulfamethoxazole had the best antibacterial activity against all the bacteria strains compared to the metal complexes except for $[Pt(L^3)_2]$ against *S.aureus*. In addition, complex $[Pt(L^3)_2]$ exhibited 89, 82 and 77% of the antibacterial activity of Sulfamethoxazole against *B. cereus, P. aeruginosa* and *S. aureus* respectively. The antimicrobial results of the compound $[Pt(L^3)_2]$ were better than the results reported for similar platinum dithiocarbamate complexes [10, 11], making the complex a probable lead compound in antimicrobial research.

Table 5.1 Summary of the antimicrobial screening of complexes 1–15

Compounds	*S. aureus* (mm)	*K. pneumonia* (mm)	*B. cereus* (mm)	*E. coli* (mm)	*P. aeruginosa* (mm)	*C. albican* (mm)	*A. flavus* (mm)
$[Ni(L^1)_2]$ (1)	-	11 ±0.4	-	10 ±0.4	11 ±0.7	-	-
$[Pd(L^1)_2]$ (2)	10 ±0.0	-	08 ±1.4	17 ±0.0	11 ±0.0	13 ±0.0	-

$[Pt(L^1)_2]$ (3)	08 ± 1.4	16 ±1.4	-	11 ±0.7	14 ±0.0	07 ±1.4	-
$[Ni(L^2)_2]$ (4)	10 ±1.4	-	-	11 ±0.0	10 ±1.4	07 ±1.4	-
$[Pd(L^2)_2]$ (5)	-	14 ±0.7	-	17 ±0.0	11 ±0.7	-	-
$[Pt(L^2)_2]$ (6)	-	13 ±0.0	-	12 ±0.7	14 ±0.0	-	-
$[Ni(L^3)_2]$ (7)	14 ±0.7	11 ±0.7	-	12 ±0.7	-	-	-
$[Pd(L^3)_2]$ (8)	-	13 ±0.0	-	15 ±0.7	11 ±0.0	11 ±1.4	-
$[Pt(L^3)_2]$ (9)	-	11 ±1.4	09 ±1.4	10 ±1.4	11 ±0.7	07 ±1.4	14 ±0.7
$[Ni(L^4)_2]$ (10)	18 ±1.2	17 ±0.7	20 ±0.7	18 ±04	15 ±0.7	12 ±0.7	-
$[Pd(L^4)_2]$ (11)	19 ±0.7	19 ±0.7	21 ±0.7	16 ±0.7	14 ±0.0	08 ±1.4	10 ±0.7
$[Pt(L^4)_2]$ (12)	26 ±0.0	20 ±0.7	23 ±0.7	20 ±0.4	23 ±0.7	15 ±0.4	12 ±1.4
$[Ni(L^5)_2]$ (13)	12±0.7	14±0.6	-	10±0.4	12±0.0	-	-
$[Pd(L^5)_2]$ (14)	05±0.0	05±0.0	04±0.4	-	06±0.6	-	06±0.4
$[Pt(L^5)_2]$ (15)		06±0.7		07±0.4			08±0.2

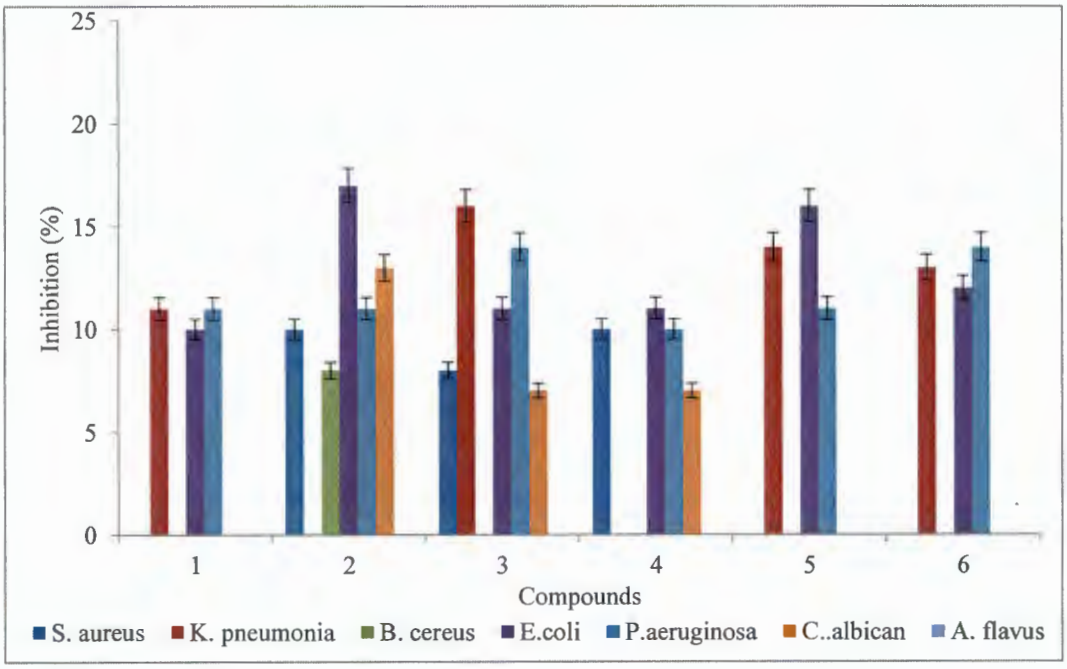

Figure 5.1: Histogram showing the antimicrobial activities of complexes 1 – 6

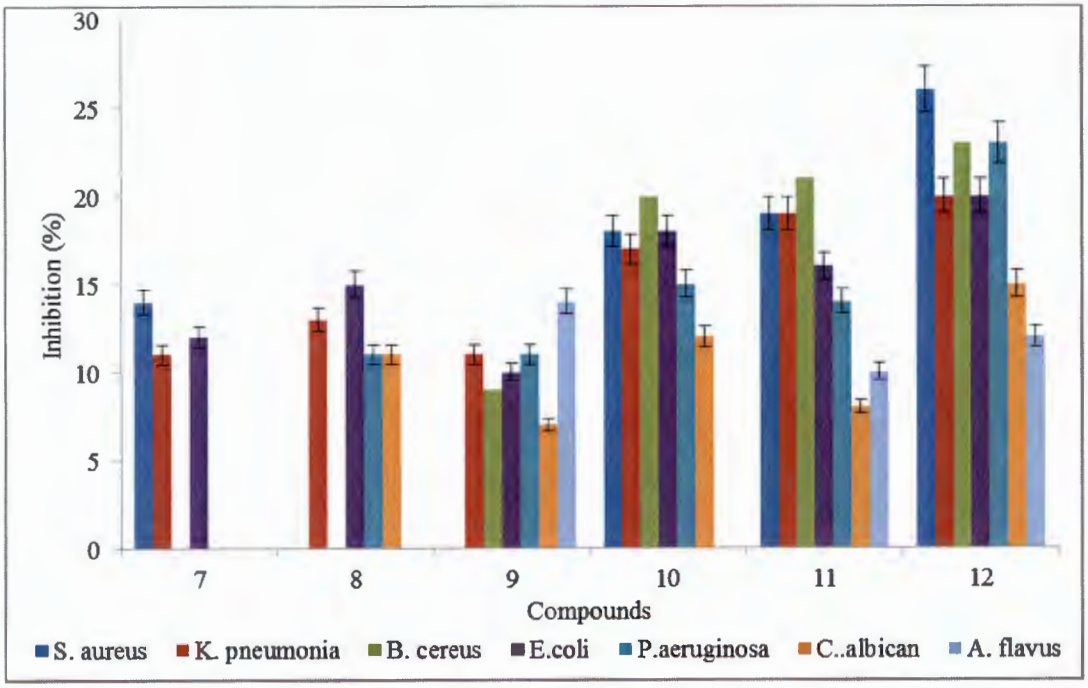

Figure 5.2: Histogram showing the antimicrobial activities of complexes 7 – 12

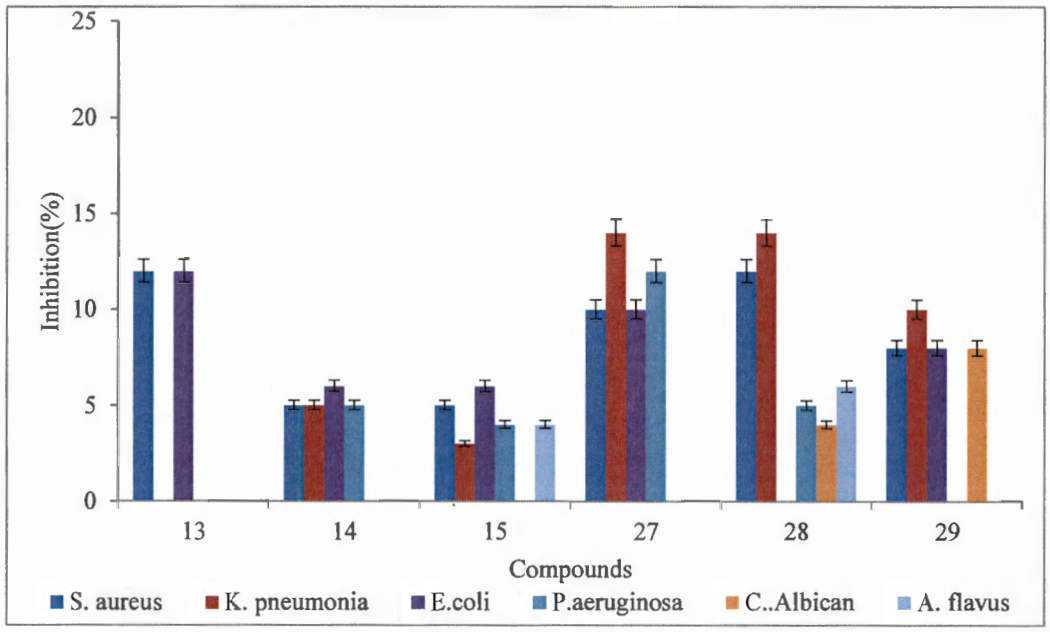

Figure 5.3: Histogram showing the antimicrobial activities of complexes 13 – 15, and 27-29

5.3.1.2 Antimicrobial studies of the Ni(II), Pd(II) and Pt(II) complexes of dithiocarbamate prepared from secondary amines

The first set of the metal complexes of dithiocarbamate prepared from secondary amines $[Ni(L^6)_2]$ - $[Pd(L^7)_2]$, (16-20) were the –OH containing substituents, summarised in Table 5.2 and presented in Figure 5.4. Their metal complexes showed better antimicrobial activities than the complexes of dithiocarbamate prepared from primary amines. This may be ascribed to the increased hydrophilicity of these compounds over compounds bearing no hydroxyl groups, which has imparted significant antimicrobial activities. The compounds were significantly active against both Gram negative and Gram positive bacteria organisms. They were also more active against *Candida albican* than the *Aspergillus flavus*. The presence of heteroatoms such as oxygen and nitrogen enhanced the activities of the compounds [9].

The second set of the compounds $[Ni(L^8)_2]$ – $[Pt(L^9)_2]$ (21-26), which were complexes of dithiocarbamate prepared from Schiff bases combined the hydrophilicity of the -OH group and the aromaticity of the extra ring on the compounds. The results are presented in Table 5.2 and Figure 5.5. They also gave significant antimicrobial activities against both Gram negative and Gram positive bacteria organisms. The presence of the heteroatoms (nitrogen) from the Schiff bases enhanced the activities and all the complexes showed high degree of antibacterial and antifungal activities.

Table 5.2: Summary of the antimicrobial screening of complexes 16-29

Compounds	*S. aureus*	*K. pneumonia*	*B. cereus*	*E. coli*	*P. aeruginosa*	*C. albican*	*A. flavus*
$[Ni(L^6)_2]$ (16)	17 ±1.4	15 ±0.0	19 ±0.7	12 ±1.4	16 ±0.7	11 ±0.7	-
$[Pd(L^6)_2]$ (17)	23 ±0.7	21 ±0.4	20 ±1.4	19 ±0.7	19 ±0.7	11 ±0.0	12 ±0.4
$[Pt(L^6)_2]$ (18)	28 ±0.4	20 ±0.0	26 ±0.7	16 ±0.7	22 ±1.4	12 ±0.7	11 ±0.7
$[Ni(L^7)_2]$ (19)	22 ±0.0	16 ±0.7	25 ±0.7	12 ±0.7	18 ±1.4	11 ±0.7	-
$[Pd(L^7)_2]$ (20)	20 ±0.7	23 ±0.0	23 ±0.7	19 ±0.0	20 ±0.7	17 ±0.4	-
$[Ni(L^8)_2]$ (21)	18 ±0.7	20 ±0.7	17 ±0.4	15 ±0.7	14 ±0.4	11 ±0.7	-
$[Pd(L^8)_2]$ (22)	21 ±1.4	19 ±0.0	24 ±0.4	13 ±1.4	17 ±0.7	12 ±0.0	07 ±0.7
$[Pt(L^8)_2]$ (23)	20 ±0.4	19 ±1.4	21 ±0.7	19 ±0.7	21 ±0.7	13 ±0.7	12 ±0.7
$[Ni(L^9)_2]$ (24)	19 ±0.7	17 ±0.7	20 ±0.0	21 ±0.7	17 ±0.7	13 ±1.4	10±±14
$[Pd(L^9)_2]$ (25)	23 ±0.0	21 ±0.0	24 ±0.7	21 ±0.4	23 ±0.7	13 ±1.4	14 ±0.7
$[Pt(L^9)_2]$ (26)	14±0.7	-	12±0.0	-	-	-	-
$[Ni(L^{10})_2]$ (27)	10±0.4	14±1.4	09 ±0.0	10±0.4	12±0.4	04±0.4	06±0.0
$[Pd(L^{10})_2]$ (28)	12±1.4	14±0.0	10 ±0.0	-	5±0.5	-	-
$[Pt(L^{10})_2]$ (29)	08±0.7	10 ±0.7	8±0.6	8±0.7	-	8±0.0	-

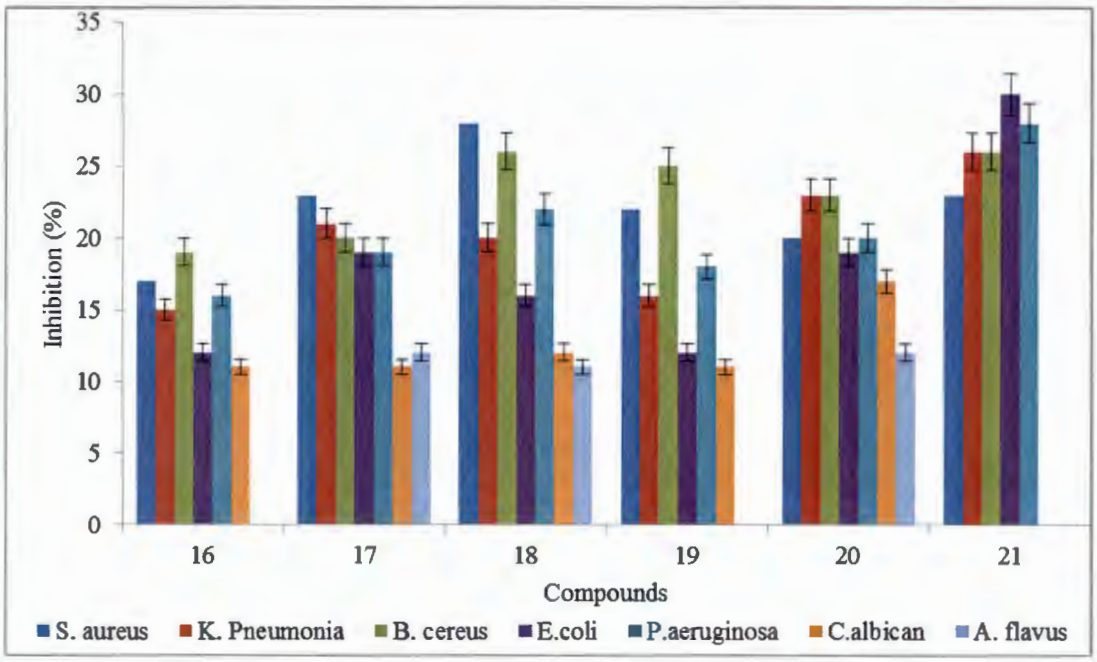

Figure 5.4: Histogram showing the antimicrobial activities of complexes 16 – 20

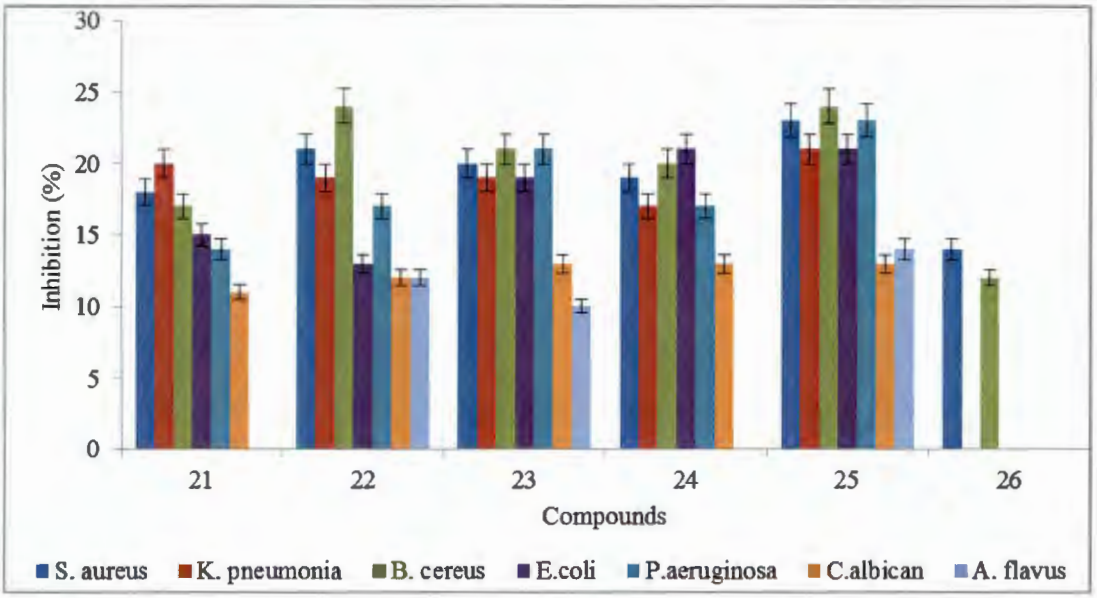

Figure 5.5: Histogram showing the antimicrobial activities of complexes 21 – 26

5.3.1.3 Antimicrobial studies of the adducts and mixed ligand complexes

The presence of aromatic and hetero-aromatic nucleus in compounds enhances their biological activities. In addition, when an active nucleus is linked to another nucleus, the resulting molecule

might possess greater potential for biological activities [10]. Nitrogen and sulphur containing heterocyclic compounds are known to show marked microbial activities [11]. All these properties have been confirmed by the observed activities recorded by the adducts and mixed ligands of the prepared complexes. The combined effects of the aromatic rings from the bipyridine, phenanthroline, triphenylphosphine and the nitrogen carrying isothiocyanate groups has yielded good antimicrobial activities. The results, as presented in Table 5.3, show that the adduct and mixed ligand compounds have more significant activities against the Gram negative *B. cereus and S. aureus* microorganisms than the Gram positive microorganisms. The adducts exhibited better antibacterial properties except for *P. aeruginosa* where very insignificant activity was recorded for some of the complexes. In general, the adducts have better activities than the mixed ligands complexes of triphenylphosphine and isothiocyanates.

Table5.3. Summary of the antimicrobial screening of complexes 30–35

COMPD	***S. aureus***	***K. pneumonia***	***B. cereus***	***E. coli***	***P. aeruginosa***	***C. albican***	***A. flavus***
$[Ni(L^1)_2bpy]$ (30)	15±0.7	-	12±0.7	10±0.0	-	09 ±0.7	10±0.4
$[Ni(L^1)_2ph]$ (31)	11±0.0	04±0.4	10±0.4	08±0.4	04±0.6	14 ±0.0	16 ±0.4
$[Ni(L^3)_2ph]$ (32)	-	22±0.7	18±1.4	10±0.6	-	16 ±0.7	19 ±0.7
$[Ni(L^3)_2bpy]$ (33)	26±1.4	28±0.6	28±0.6	30±0.7	04±0.0	18 ±0.7	05±0.0
$[Ni(L^4)_2bpy]$ (34)	-	-	12±0.4	12±0.6	05±0.4	15 ±0.4	06±0.7
$[Ni(L^4)_2ph]$ (35)	14±0.6	-	18±0.7	12±0.4	-	14 ±0.7	04±0.0

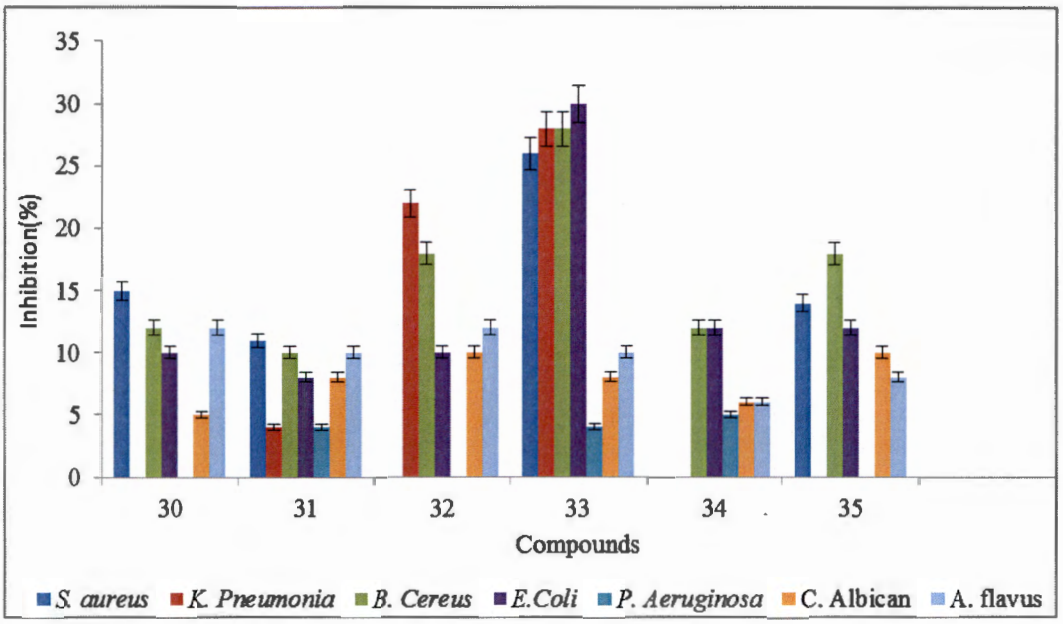

Figure 5.6: Histogram showing the antimicrobial activities of complexes 30- 35

Table 5.4 Summary of the antimicrobial screening of complexes 36–41

COMPOUND	*S. aureus*	*K. pneumonia*	*B. cereus*	*E.coli*	*P. aeruginosa*	*C. albican*	*A. flavus*
$[NiL^2(NCS)PPh_3]$ (36)	-	04±0.7	10±0.4	12±0.6	-	05 ±0.7	12±0.4
$[NiL^2(NC)(PPh_3)]$ (37)	07±0.6	10±0.4	10±0.6	08±0.6	-	08 ±0.0	10 ±0.4
$[NiL^6(NCS)(PPh_3)$(38)	05±0.6	15±1.4	21±0.6	26±0.6	06±0.6	10 ±0.7	12 ±0.7
$[NiL^6(NC)(PPh_3)]$ (39)	08±0.4	10±0.6	19±0.6	26±0.6	10±0.6	08 ±0.7	10±0.0
$[NiL^7(NCS)(PPh_3)$(40)	06±0.4	08±0.6	12±0.6	18±0.6	-	06 ±0.4	06±0.7
$[NiL^7(NC)(PPh_3)]$ (41)	08±0.6	10±0.6	14±0.6	23±0.6	08±0.6	10 ±0.7	08±0.0

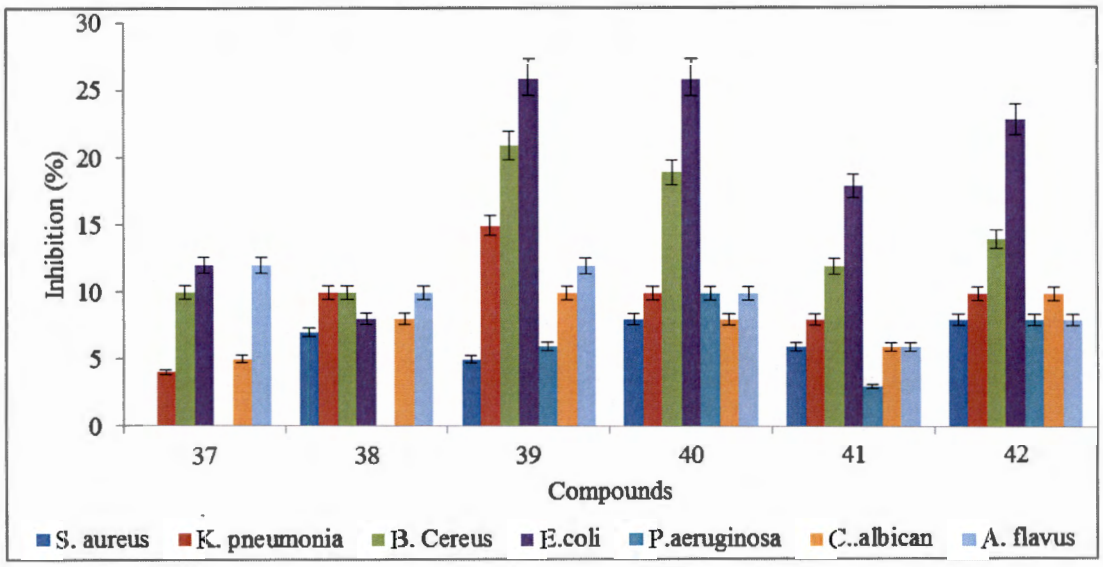

Figure 5.7: Histogram showing the antimicrobial screening of complexes 37–42

5.3.2 Anti-cancer studies of the complexes

The progress of new metal-based anticancer agents with alternative mechanisms of action from that of established compounds has been the centre of new drug development recently. This encompasses the development of organometallic complexes, as 'metals in medicine' where the metal can act as scaffold for functionalization and for more targeted, cancer cell-specific approach [15]. This trend involved the use of different metals for different targets, and also the inclusion of different bioactive ligands with varied substituents to help control the kinetic reactivity of the metal ions to target specific types of cancer cells [16]. To explore the development of new inorganic anti-cancer agents, which utilize the metal ion-base interaction, group 10 metal dithiocarbamate complexes were considered.

Several mechanisms have been proposed on the action of anticancer drugs [13], since it is possible to vary or modify the ligands around the metal centre, thereby changing the solubility, reactivity, electronic and steric properties. However, the lipophilicity of this drug plays a crucial role in the drug interaction with the cells. Thus, the presence of the phenyl group and the –NH groups of the primary amine can influence lipophilicity of the compounds and induce a π-π interaction with biomolecular cells. Interaction of dithiocarbamate nitrogenous bases with cancerous cell can inhibit cell proliferation thereby interfering with the DNA replication and transcription [17]. HeLa cell is an immortal cell line often used for research, and it is obtained from a common human cervical cancer [16].

5.3.2.1 Anti-cancer studies of the Ni(II), Pd(II) and Pt(II) complexes of dithiocarbamate prepared from primary amines

The IC_{50} levels of the complexes in the HeLa cell line obtained have been summarized in Tables 5.5-5.8. Most of the complexes synthesized from dithiocarbamate derived from primary amines have IC_{50} values in a range which showed better properties than the control, 5-Fluorouracil (5FU). Only $[Pt(L^1)_2]$ and Pd $[Pd(L^4)_2]$ complexes showed IC_{50} values greater than the standard. The dinuclear complexes, $[Ni(L^5)_2]$ $[Pd(L^5)_2]$, $[Pt(L^5)_2]$, showed IC_{50} values below the standard with the platinum complex exhibiting the best cytotoxic activity with IC_{50} value of 0.013. The enhanced higher cytotoxic activities could be ascribed to the coordinated and cooperative reactiveness of the two metal centres to give a significant drug-induced cytotoxic responses more than the mononuclear complexes. This is in agreement with the reports of Zhao *et al.*, [17] who reported the activities of dinuclear palladium complexes with IC_{50} values slightly lower than those recorded for cisplatin. The results are summarised in Table 5.5 and Figure 5.5.

Table 5.5: Viabilities (%) of the HeLa cell lines at different concentration for complexes 1 – 13

	Complex	25 μg mL^{-1}	50 μg mL^{-1}	100 μg mL^{-1}	150 μg mL^{-1}	IC_{50} μM
		100.00±0.79	100.00±0.79	100.00±0.79	100.00±0.79	-
Control 1	Cell only					
		104.09±2.43	104.09±2.43	104.09±2.43	104.09±2.43	
Control 2	Cell + 10 μl DMSO					-
5FU	5-Fluorouracil	36.57±4.15	27.47±6.14	23.54±2.90	17.72±4.34	40
		9.62±6.10	14.39±10.33	51.99±4.88		1.41
1	$[Ni(L^1)_2]$				45.76±5.93	
		58.084±6.218	51.044±3.820	31.230±14.510	15.112±16.924	41
2	$[Pd(L^1)_2]$					
3		85.215±15.814	87.830±11.811	85.441±11.014	13.704±10.103	112

	$[Pt(L^1)_2]$					
		60.09±8.59	53.77±7.75	55.33±10.54	66.13±11.93	74
4	$[Ni(L^2)_2]$					
	$[Ni(L^3)_2]$	9.34±7.67	11.86±4.44	8.44±10.39	19.07±11.70	0.013
5						
		4.92±16.69	3.76±16.81	12.64±1.35	0.59±11.69	14.12
6	$[Pd(L^3)_2]$					
		37.365±15.647	82.726±8.289	81.921±7.506	76.088±11.620	25
7	$[Pt(L^3)_2]$					
		50.817±7.472	34.121±7.680	33.719 ±6.494	27.030±14.347	20
8	$[Ni(L^4)_2]$					
		30.10±11.497	90.18±4.278	89.50±2.558	80.38±8.588	288
9	$[Pd(L^4)_2]$					
		175.08±0.31	216.06±7.65	216.31±7.29	210.33±5.31	$1.25X10^{10}$
10	$[Pt(L^4)_2]$					
		35.88±7.62	35.18±7.30	31.33±2.12	25.20±6.17	28.84
11	$[Ni(L^5)_2]$					
		51.38±14.28	46.56±12.62	43.98±10.77	12.74±11.13	35.48
12	$[Pd(L^5)_2]$					
		27.94±10.80	26.80±18.48	23.96±23.00	24.93±10.53	0.013
13	$[Pt(L^5)_2]$					

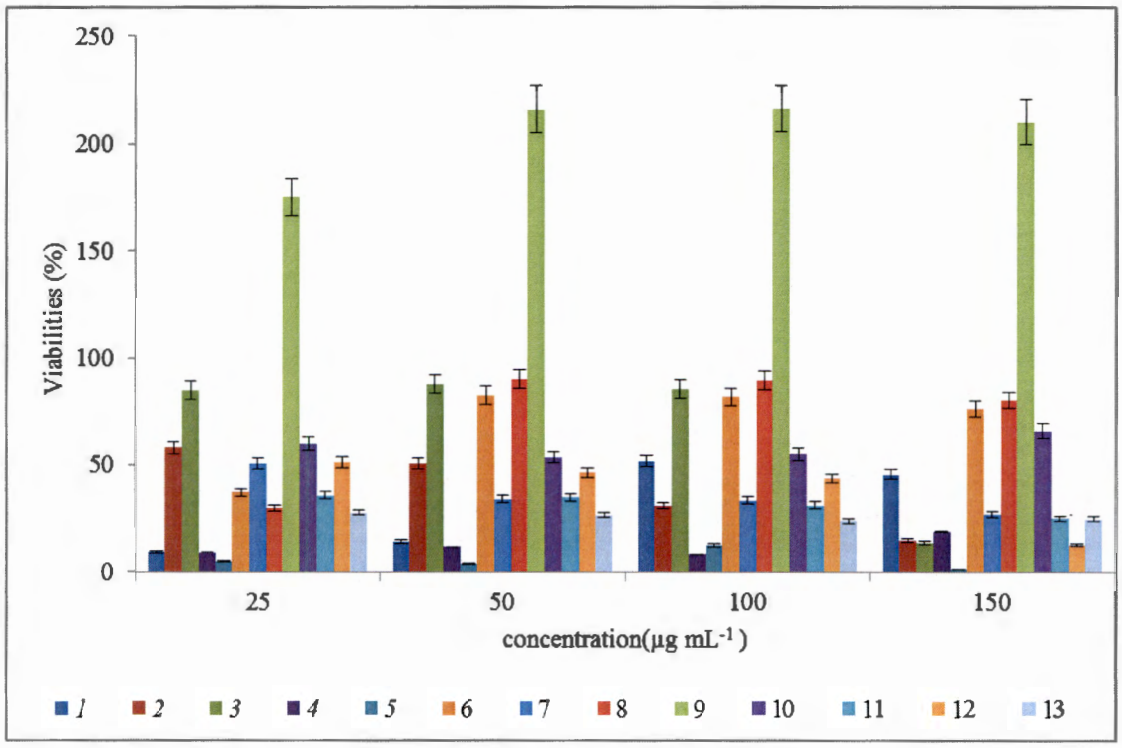

Figure 5.5: Histogram showing the MTT Assay of complexes 1 – 13.

5.3.2.2 Anti-cancer studies of the Ni(II), Pd(II) and Pt(II) complexes of dithiocarbamate prepared from secondary amines

The results of the cytotoxic studies of the Ni(II), Pd(II) and Pt(II) complexes of dithiocarbamate prepared from secondary amines (14- 20) are summarised in Table 5.6 and presented in Figure 5.6. Complexes $[Ni(L^8)_2]$, $[Ni(L^9)_2]$, $[Ni(L^7)_2]$ and $[Ni(L^6)_2]$ showed the highest anti-cancer activities with IC_{50} values of 6 $x10^{-13}$, 0.0056, 9.55 and 39.8 µM respectively, and below that of the standard. While the other complexes have IC_{50} values higher than those recorded for the standard.

Table 5.6: Viabilities (%) of the HeLa cell lines at different concentration for complexes 14 -20

	Complexes	25 μg mL^{-1}	50 μg mL^{-1}	100 μg mL^{-1}	150 μg mL^{-1}	IC_{50} μM
			100.00±0.79	100.00±0.79	100.00±0.79	-
Control	Cell only	100.00±0.79				
	$[Ni(L^6)_2]$	30.0±17.02	45.8±10.54	33.0±5.31	62.0±2.84	
14						39.81
	$[Pd(L^6)_2]$	20.4±7.84	23.2±7.25	28.5±10.52	10.3±14.73	
15						61.7
	$[Pt(L^6)_2]$	55.91±1.77	71.68±4.66	64.03±10.94	41.91±20.48	
16						131.8
	$[Ni(L^7)_2]$	39.15±15.70	31.32±8.02	38.33±2.60	37.44±7.76	
17						9.55
	$[Pd(L^7)_2]$	91.57±8.34	78.51±3.91	78.48±2.30	79.53±1.59	
18						1584
	$[Ni(L^8)_2]$	5.67±6.27	5.32±21.08	5.40±4.52	4.85±28.22	
19						6x10-13
	$[Ni(L^9)_2]$	12.10±17.15	7.14±8.87	5.75±14.96	6.96±5.17	
20						0.0056

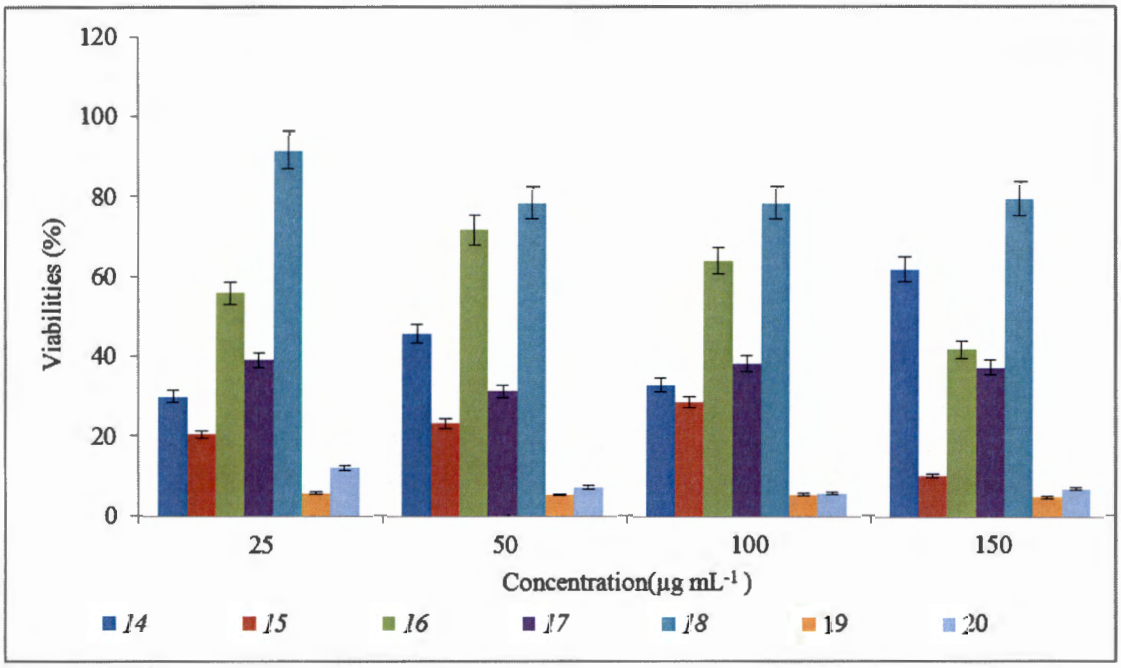

Figure 5.6: Histogram showing the MTT Assay for complexes 14 -20

5.3.2.3 Anti-cancer studies of the adducts and mixed ligand complexes

The adducts, $[Ni(L^4)_2bpy]$, $[Ni(L^4)_2ph]$ and $[Ni(L^3)_2bpy]$, which contain dithiocarbamate with ethyl substituents on the phenyl ring exhibited the highest anti-cancer activities in both series of the bipyridine and the phenanthroline adducts. They showed anti-cancer activities higher than the standard, while the remaining compounds have IC_{50} slightly higher than the standard. Complexes $[NiL^6(NC)(PPh_3)]$ and $[NiL^7(NC)(PPh_3)]$, of the series containing triphenylphosphine and cyanide, have lower IC_{50} values than the standard, and the values were also lower than that of the adducts of bipyridine and phenathroline. Thus, giving them higher anti-cancer activities. The presence of the -OH group, an active hydrophilic nucleus on complexes $[NiL^6(NC)(PPh_3)]$ and $[NiL^7(NC)(PPh_3)]$ linked with the chelating and bridging effect of the triphenylphosphine nucleus may have imparted higher anti-cancer activities. It is known that a chelate ring system reduces the polarity of the central metal atom as a result of the sharing of its positive charge with the ligand. This facilitates the infusion of the compounds efficiently over the lipid layer of the cell membrane leading to cell inhibition and termination [20-23]. The other complexes of the series have anti-cancer activities lower than that of the standard. The results are summarised in Tables 5.7 and Figures 5.8.

Table 5.7: Viabilities (%) of the HeLa cell lines at different concentration for complexes 21 – 26

	Complexes	25 μg mL^{-1}	50 μg mL^{-1}	100 μg mL^{-1}	150 μg mL^{-1}	IC_{50} μM
21	$[Ni(L^1)_2bpy]$	43.110±9.18	52.685±4.10	51.469±20.70	22.442±4.19	51.3
22	$[Ni(L^1)_2ph]$	157.497±3.80	136.424±3.73	64.590±5.28	16.059±12.32	64.6
23	$[Ni(L^3)_2ph]$	13.427±7.579	43.374±16.368	48.906±11.908	21.323±10.008	100
24	$[Ni(L^3)_2bpy]$	132.47±5.35	87.34±3.06	35.31±3.89	4.81±14.66	44.67
25	$[Ni(L^4)_2bpy]$	38.82±1.75	31.21±14.99	100.47±5.97	109.40±4.65	9.12

Table 5.8: Viabilities (%) of the HeLa cell lines at different concentration for complexes 27 – 31.

	Complex	25 μg mL^{-1}	50 μg mL^{-1}	100 μg mL^{-1}	150 μg mL^{-1}	IC_{50} μM
27	$[NiL^2(NCS)PPh_3]$	19.00±7.33	53.69±4.27	85.84±2.62	73.74±1.40	166
28	$[NiL^2(NC)(PPh_3)]$	79.20±8.47	78.50±2.50	96.41±7.50	93.68±11.02	97723
29	$[NiL^6(NCS)(PPh_3)]$	10.85±11.32	37.13±4.42	50.53±4.20	48.82±16.38	56.23
30	$[NiL^6(NC)(PPh_3)]$	7.59±5.45	11.01±9.50	9.85±14.84	14.92±15.88	2X10-9
31	$[NiL^7(NC)(PPh_3)]$	35.00±7.22	22.99±2.75	22.70±4.97	22.57±3.48	1.57

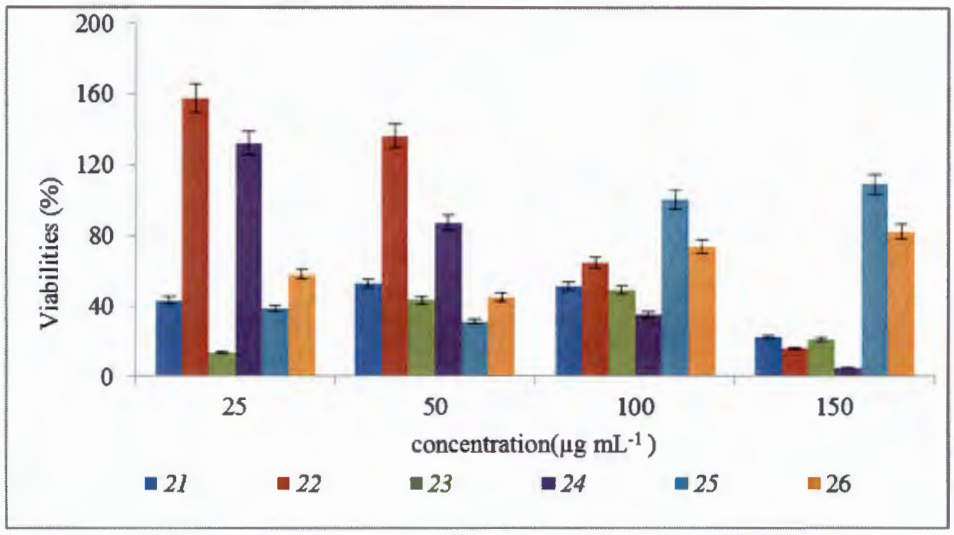

Figure 5.7: Histogram showing the MTT Assay of complexes 21 – 2

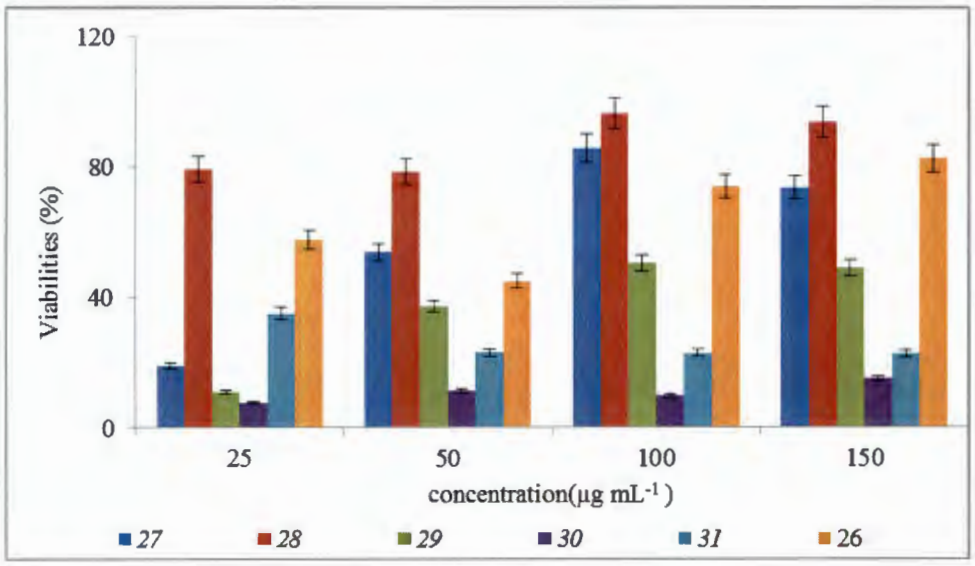

Figure 5.8: Histogram showing the MTT Assay of complexes 27 – 31.

5.4 Conclusion

Metal complexes which contain S chelating ligands such as dithiocarbamate are known to display pronounced biological activities. The results in this chapter of the thesis revealed that most of the complexes have moderate to good antibacterial, and antifungi properties. The *N*-ethylphenyldithiocarbamate complexes, $[Ni(L^4)_2]$, $[Pd(L^4)_2]$ and $[Pt(L^4)_2]$, exhibited the best activity than the other complexes in the same series. The presence of the -OH group on the *N*-alkyl-*N*-ethanol dithiocarbamate complexes, $[Ni(L^6)_2]$ – $[Pd(L^7)_2]$, increased the hydrophilicity of the

compounds. Hence, significant antimicrobial activities were observed over the other compounds not bearing hydroxyl group. An improved antimicrobial activity was observed for the adducts and mixed ligands complexes due to the contribution of N and S atoms on the activities of the complexes. In general, the adducts showed better activities than the mixed ligands with higher activities on the Gram negative *B. cereus and S. aureus* organisms than the Gram positive organisms.

The dinuclear complexes, $[Ni(L^5)_2]$ $[Pd(L^5)_2]$ and $[Pt(L^5)_2]$, derived from dithiocarbamate ligands prepared from primary amine gave the best anti-cancer activities than the other complexes of the dithiocarbamate ligands prepared from primary amine. Complexes $[Ni(L^8)_2]$, $[Ni(L^9)_2]$ which are the *N*-alkyl-*N*-phenyl dithiocarbamate compounds showed the highest anti-cancer activity towards HeLa cell with IC_{50} values of 6×10^{-13} and 0.0056 μM compared to 40 μM of the standard. The presence of the -OH group, an active hydrophilic group and the chelating effect of the triphenylphosphine on complexes $[NiL^6(NC)(PPh_3)]$ and $[NiL^7(NC)(PPh_3)]$ imparted higher anti-cancer activities with IC_{50} values of 2×10^{-9} and 1.57 μM, which implies better antitumour activities than the standard.

In general, the results obtained showed that most of the complexes displayed a concentration dependent profile with some good activities toward the HeLa cell line; with some of the complexes showing cyto-selectivity against this cell line. Some of the IC_{50} values obtained were much better than the standard drug, 5-Fluorouracil (5FU), with an IC_{50} value of 40 μM, while some of the complexes displayed high IC_{50} values which are comparable to the used standard drug due to selectivity or low cytotoxic activity as the case may be. This study and the results obtained have confirmed that little variations in molecular structure could enhance the biological activities of compounds and make them more effective as antimicrobial and anti cancer agents.

REFERENCES

[1] B. Rosenberg, L.Vancamp, T. Krigas, Nature 205 (1965) 698.

[2] B. Rosenberg, L.VanCamp, J.E Trosko, V.H. Mansour, Nature 222 (1969) 385.

[1] M.N. Patel, D.S. Gandhi, P.A. Parmar, Inorg. Chem. Commun. 15 (2012) 248.

[2] S. Medici, M. Peana, V.M. Nurchi, J.I. Lachowicz, G. Crisponi, M.A. Zoroddu, Coord. Chem. Rev. 284 (2015) 329.

[3] B. Desoize, C. Madoulet, Crit. Rev. Oncol. Hematol. 42 (2002) 317.

[4] R. Huang, A. Wallqvist, D.G. Covell, Biochem. Pharmacol. 69 (2005) 1009.

[5] S.B. Hong, F.M. Raushel, Biochemistry. 35 (1996) 10904.

[6] G. Hogarth, Mini Rev. Med. Chem. 12 (2012) 1202.

[7] E.C. Long, Acc. Chem. Res. 32 (1999) 827.

[8] M. Rowinska-Zyrek, M. Salerno, H. Kozlowski, Coord. Chem. Rev. 284 (2015) 298.

[9] Y. Ding, W.H. Zhu, Y. Xie, Chem. Rev. 117 (2017) 2203..

[10] M.K. Amir, Zia-Ur-Rehman, F. Hayat, S.Z. Khan, G. Hogarth, T. Kondratyuk, J.M. Pezzuto, M.N. Tahir, RSC Adv. 6 (2016) 110517.

[11] M.K. Amir, S.Z. Khan, F. Hayat, A. Hassan, I.S. Butler, Zia-ur-Rehman, Inorganica Chim. Acta. 451 (2016) 31.

[12] A.K. Mishra, S.B. Mishra, N. Manav, D. Saluja, R. Chandra, N.K. Kaushik, Bioorganic Med. Chem. 14 (2006) 6333.

[13] P. Zhang, P.J. Sadler, J. Organomet. Chem. 839 (2017) 5.

[14] M.K. Amir, S.Z. Khan, F. Hayat, A. Hassan, I.S. Butler, Zia-ur-Rehman, Inorganica Chim. Acta. 451 (2016) 31.

[15] M. Rizzotto, Metal Complexes as Antimicrobial Agents, A Search Antibact. Agents. (2012).

[16] John R. Masters, *Nature Reviews Cancer,* 2 (2002) 315–319.

[17] G. Zhao, H. Lin, S. Zhu, H. Sun, Y. Chen, J. Inorg. Biochem. 70 (1998) 219

[20] J. Borrás, G. Alzuet, S. Ferrer, C.T. Supuran,C.T. Supuran, A. Scozzafava, J. Conway (Eds.) CSC Press, Boca Raton (2004).

[21] A.S. Chaudhary, R. Singh, Bol. Soc. Quim, 47 (2002) 203.

[22] M. Carmen Sharaby, Spectrochim. Acta A, 62 (2005) 326.

[23] V.T. Kasmov, I. Karatal, F. Koksal, Spectrochim. Acta A. 56 (2000) 841.

[24] P. Zhang, P.J. Sadler, J.Organomet. Chem. 839 (2017) 5.

[25] V. Karunakaran, V.Balachandran, Spectrochim. Acta A 98 (2012) 229.

[26] A. Salim Abu-Surrah, H. Haitham, Y. Al-Sa'doni Maher Abdalla, Cancer Therapy 6 (2008) 1.

[27] M. C. Aragoni, M. Arca, A. F. Devillanova, F. Isaia,V. Lippolis, Cryst. Growth Des. 12 (2012) 2769.

[28] A.Y.Louie, T.J. Meade, Chem. Rev 99 (1999) 2711.

[29] A.Albert, S.D Rubbo, R.J. Goldacre, B.G .Balfour. Br J Exp Pathol, 28 (1947) 69.

[30] L. Marcheselli, C. Preti, M. Tagliazucchi, V. Cherchi, L. Sindellari, A. Furlani, A. Papaioann, V.Scarcia, Eur. J. Med. Chem.28 (1993) 347.

[31] R. Johari, G. Kumar, S. Singh, J. Indian Chem Council, 26(2009) 23.

[32] P. Mittal, V. Uma, Der Chemica Sinica 1(2010) 124.

CHAPTER SIX

6.0 Summary, conclusion and future studies

6. 1 Summary

The results obtained have shown the importance of group 10 metals in therapeutic applications. As transition metals, they possess many properties that give them advantages over the more common organic-based drugs. Since the reactivity of transition metal complexes are controlled by both the metal and the ligands, combining dithiocarbamate; a bulky chelating ligand with the metal ions provides an added advantage of higher stabilization with improved biological activities for the complexes. The use of single source precursor for the synthesis of metal sulphide nanoparticles can give rise to high quality, crystalline and monodispersed nanoparticles. This study therefore, reports the synthesis and characterization of group 10 metal dithiocarbamate complexes, their biological activities and their use as single source precursor for metal sulphide nanoparticles.

The work comprised of six chapters. Chapter one contained the introduction to group 10 metals, dithiocarbamate ligand and their properties, and nanoparticles overview. It ended with the aim, objectives and significance of the study.

Chapter two dealt with the detailed literature review of previous works on the synthesis of dithiocarbamate metal complexes and their biological relevance. It also presented the different synthetic routes to metal sulphide nanoparticles using different capping molecules.

In chapter three, the detailed synthesis and characterization of the dithiocarbamate ligands from primary, secondary and Schiff bases were reported. The use of these ligands in the synthesis of group 10 metal dithiocarbamate complexes and their characterization using various techniques such as elemental analysis, FTIR, UV-vis spectroscopic, ^{1}H NMR, ^{13}C NMR and some of the complexes by single crystal X-ray analysis were also highlighted. TGA analyses confirmed the thermal stability of the synthesized compounds. Some of the complexes were further functionalised into adducts and mixed ligand complexes by the introduction of P and N containing Lewis bases unto the parent complexes to improve the properties of the complexes for various applications.

The single source precursor synthetic routes to the formation of the metal sulphide nanoparticles from the metal complexes were described in chapter four Different long chain amine molecules (HDA, ODA and OLA) were utilized as capping agents at different reaction times and thermolysed at varied temperatures as dictated by the results from the TGA analyses. The optical properties of

the as-prepared nanoparticles were studied using UV-vis and PL spectroscopies, while the structural morphology and phases were determined with TEM, EDX and X-ray diffraction analyses.

The biological activities of the synthesized complexes were reported in chapter five. This involved the use of Gram positive and Gram negative bacteria and fungi organisms in the antmicrobial studies and the use of human cervical HELA cells in the anti-cancer studies. The antimicrobial activities were recorded as % inhibition at minimum concentration termed as minimum inhibition concentration (**MIC**) while the anti-cancer studies were recorded as inhibitor concentration, where the response is reduced by half, that is, concentration at half inhibition (IC50).

6.2 Conclusion

Forty two complexes of group 10 dithiocarbamate have been prepared in all; fifteen complexes were synthesized utilizing the dithiocarbamate obtained primary amine ligands, six complexes were prepared from dithiocarbamate obtained using the secondary amine and nine complexes were prepared from the dithiocarbamate obtained from Schiff base condensation reactions. Functionalization of the parent complexes further yielded six adducts and six mixed ligand complexes. All the complexes were characterized by different techniques. Elemental analysis confirmed the degree of purity of the complexes as the experimental results were comparable to the calculated values. The results from FTIR revealed the bidentate mode of bonding within the complexes and the presence of the thiouriede bands (C=N), ν(C-S) and M-S vibrations confirmed the complexation reaction between the dithiocarbamate ligands and the metal ions, with ν(C=N) vibrations increasing down the triad from Ni to Pt. The ν(C-S) vibrations indicated a symmetrically bidentate coordination of the $-CS_2$ group to the metal centre and the vibrations increased as the chain length of the substituents on the phenyl group increased. The UV-vis spectroscopic results gave the d-d transitions at the near IR region, while the ligand-metal- ligand transitions were observed at the far IR absorption peaks to confirm d^8 configuration and square planar geometry. ^1H and ^{13}C NMR signals support the formation of complexes as many signals in the spectra of the complexes were observed to be shifted compared to those in the uncoordinated ligands with the -NCS_2 signals increasing down the heavier atom complexes of each series. X-ray crystal structures of some of the complexes confirmed the distorted square planar geometry and bidentate bonding fashion of the dithiocarbamate ligands to the central metal. It was also observed that bond length increases down the group from Ni-S to Pt-S, which implies higher bond strength in Ni-S than Pt-S, while the bond length for both Pd-S and Pt-S are relatively close supporting their similar coordination modes and chemical properties. The decomposition patterns from the TGA occurred

via single step for some complexes or two step patterns for other complexes. The volatility decreased while the thermal stability increased down the group and also with the presence of the methyl and ethyl substituents on the phenyl ring. All the complexes decomposed into their respective metal sulphides, hence, were utilized as single source precursors (SSP) for the preparation of their respective metal sulphide nanoparticles. The precursor complexes were thermolyzed in the temperature range 160 - 220 °C. hexadecyl amine (HDA) was employed as the capping molecule for all the Ni(II) complexes obtained from dithiocarbamate prepared using the primary and secondary amines. To study the effect of different temperatures, growth time and capping molecules on the optical and structural properties of nickel suphide nanoparticles, **$[Ni(L^2)_2]$ and $[Ni(L^6)_2]$** which are representative of complexes prepared using dithiocarbamate obtained from primary and secondary amines respectively were utilised. Different capping agents ODA and OLA were used, and thermolysis was carried out at different temperatures and time. The Pd(II) and Pt(II) complexes synthesized using dithiocarbamate obtained from the secondary amines were represented as $[Pd(L^6)_2]$ and $[Pd(L^7)_2]$ for the nanoparticle synthesis. X-ray diffraction (XRD) analysis gave six different phases for the nickel sulphide nanoparticles: hexagonal α-NiS phase, α-$NiS_{1.03}$, $NiSO_4 \cdot 6H_2O$, nickelhexahydrate, α-$NiS_{1.19}$, base-centered orthorhombic Godlevskite phase, Ni_9S_8 and (heazlewoodite), Ni_3S_2. Four different phases for the palladium sulphide nanoparticles were observed; crystalline metallic Pd, vysotskite PdS, cubic plane PdS_2 and Pd_4S and two phases for the platinum nanoparticles; cooprite PtS and polycrystalline metallic Pt. The diffraction patterns also revealed that the use of HDA and ODA capping molecules gave the same phase while different phases were observed with OLA capping agent and the use of varied precursor complexes. The ODA and HDA-capped nanoparticles gave similar morphology from the TEM images, formation of well-defined monodispersed dot-like and triangular shaped particles were observed. In contrast, the OLA–capped nanoparticles showed clearly irregular shapes distinct from the other two capping molecules. However, all the nanoparticles gave well-defined monodispersed nanostructures with the monodispersity increasing with increase in chain length of the substituents and with decrease in the size of the nanoparticles produced. The capped nanoparticles were adequately passivated by the capping agents as FTIR spectra confirmed the purity of the nanoparticles formed. The band gap energies increased with decrease in particle size as the chain length of the substituents increased, and all the nanoparticles displayed quantum confinement effect.

The biological studies revealed that most of the complexes have moderate to good antibacterial and antifungi properties with the *N*-ethylphenyldithiocarbamate complexes, **$[Ni(L^4)_2]$, $[Pd(L^4)_2]$** and **$[Pt(L^4)_2]$,** exhibiting the best activity. The presence of the –OH group on the *N*-alkyl-*N*-ehtylethanol dithiocarbamate complexes, **$[Ni(L^6)_2]$ - $[Pd(L^7)_2]$** also enhanced their antimicrobial

activities. Most of the complexes showed a concentration dependent profile with cyto-selectivity and some good activities toward the HeLa cell line. The dinuclear dithiocarbamate complexes, **[Ni(L^5)$_2$] [Pd(L^5)$_2$]** and **[Pt(L^5)$_2$]** exhibited the best anti-cancer activities and the presence of the –OH group, and the chelating effect of the triphenylphosphine on complexes **[NiL^6(NC)(PPh$_3$)]** and **[NiL^7(NC)(PPh$_3$)]** also imparted higher anti-cancer activities.

Finally, the results from the studies have proven that novel group 10 metal dithiocarbamate complexes have been synthesized with quality properties, because according to George S. Hammond, 'the most fundamental and lasting objective of synthesis is not just the production of new compounds, but production of properties' [1] . The biological properties of these compounds have shown they can be incorporated into new classes of platinum group metals (PGM) for the development of new antibiotics and anti-cancer agents. Their metal sulphide nanoparticles could also improve the biological activities based on the nanoparticle drug delivery system to reduce toxicity and curb drug resistance. The small size and quantum confinement of the nanoparticles prepared can also afford their usefulness in catalysis, electronics and environmental contaminants degradation.

6.3 Recommendation for future studies

The following suggestions can be made for future works

(i) The catalytic properties of the synthesized complexes could be determined since nickel or supported nickel catalysts play an important role in chemical industry

(ii) The biological activities of the prepared nanoparticles can be studied to determine the improved activities over the bulk complexes based on the small size dimensions and nanoparticle drug delivery system.

(iii) Application of the nanoparticles in photocatalytic degradation of dyes can be determined for effective use in water and environmental remediation.

(iv) The formation of ternary and quartenary nanoparticles is an emerging field of research in nanoparticles synthesis, the prepared group 10 metals could be integrated together to form (Ni-Pd)S, (Ni-Pt)S,(Pd-Pt)S and (Ni-Pd-Pt)S nanoparticles for improved activities.

(v) The prepared nanoparticles can be incorporated as nanosize particles in the matrices of some polymer materials as nanocomposites to improve their strength for electronic properties.

(vi) Adducts of Pd(II) and Pt(II) dithiocarbamate could also be synthesised, using some N and P donor Lewis bases, in order to study the effects of the mixed ligands on their biological and nanoparticle properties.

REFERENCES

[1] George S. Hammond, Norris Award Lecture, 1968

APPENDICES

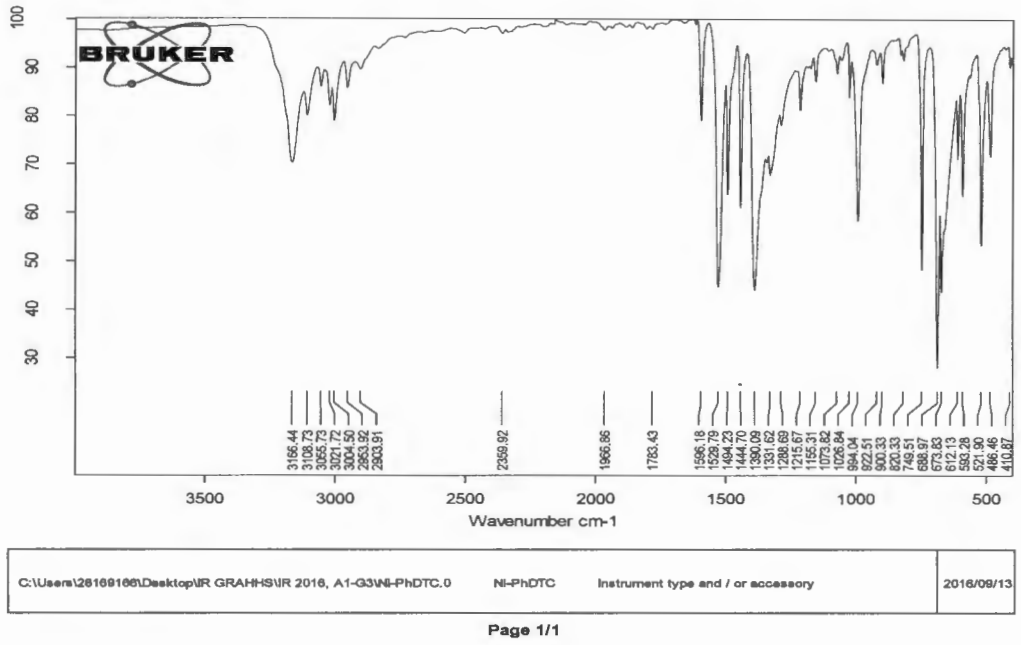

Figure S1:FTIR of $[Ni(L^1)_2]$

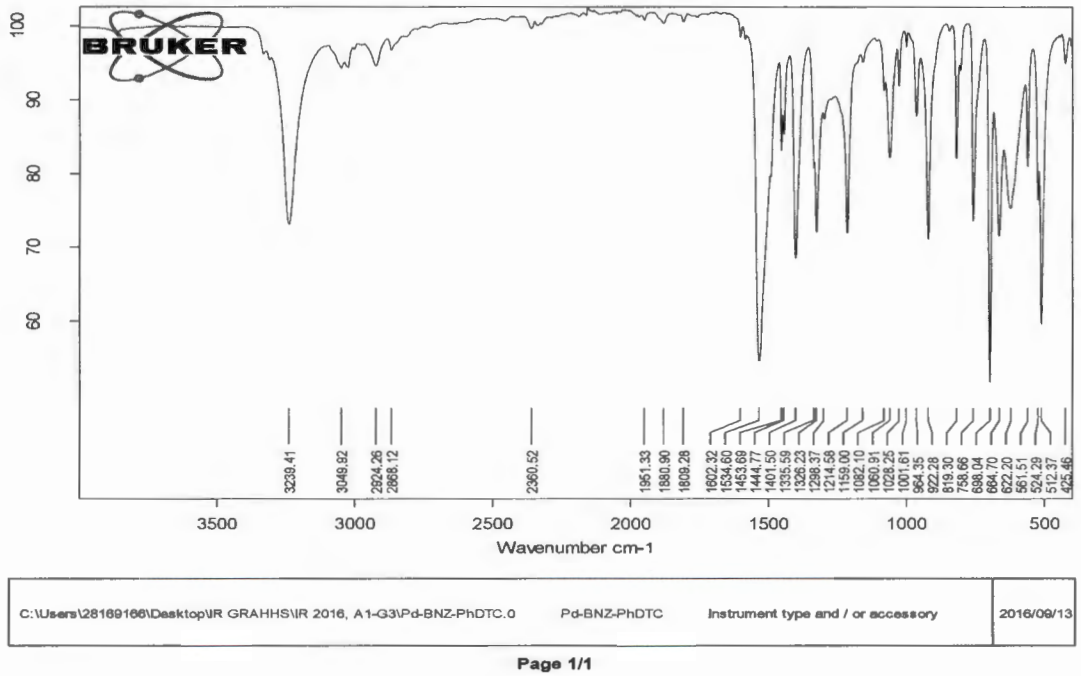

Figure S2: FTIR of $[Pd(L^2)_2]$

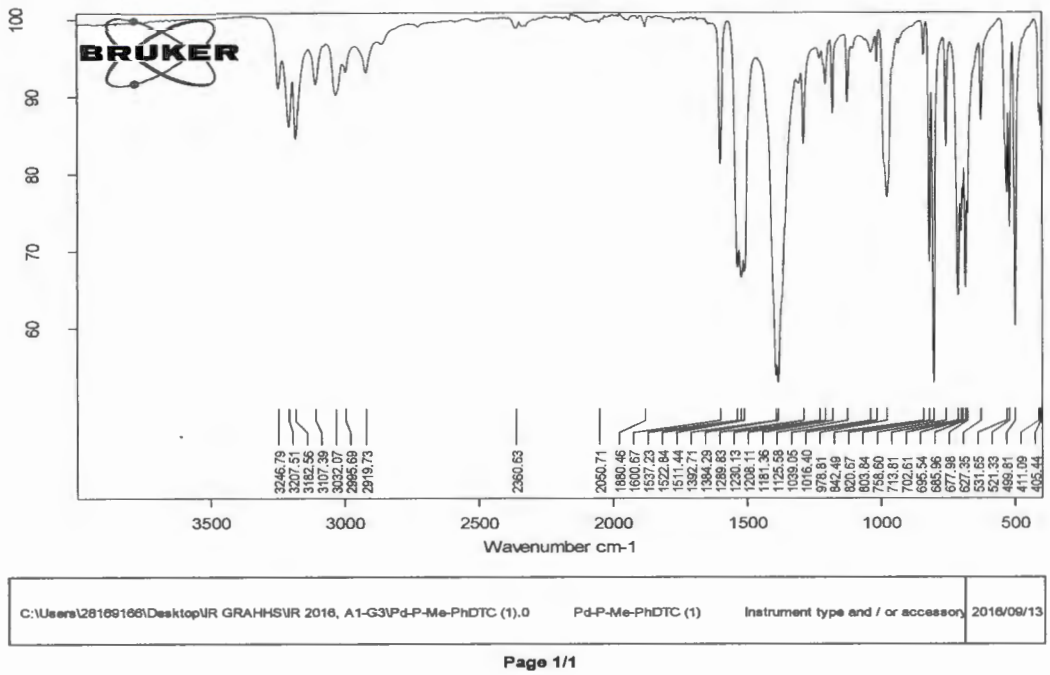

Figure S3: FTIR of $[Pd(L^3)_2]$

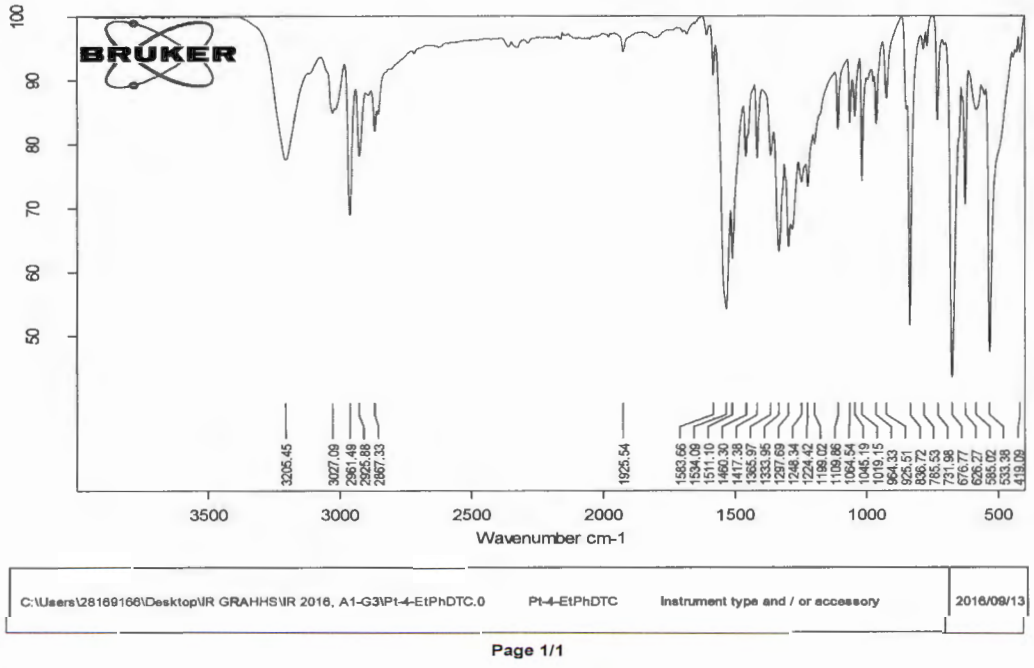

Figure S4: FTIR of $[Pt(L^4)_2]$

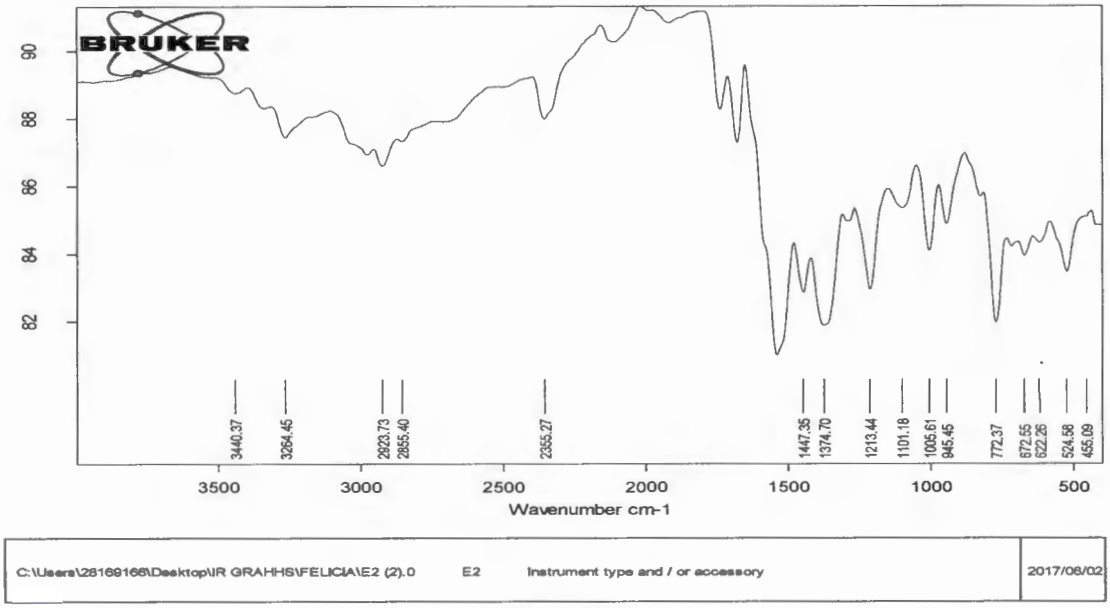

Figure S5: FTIR of $[Pd(L^5)_2]$

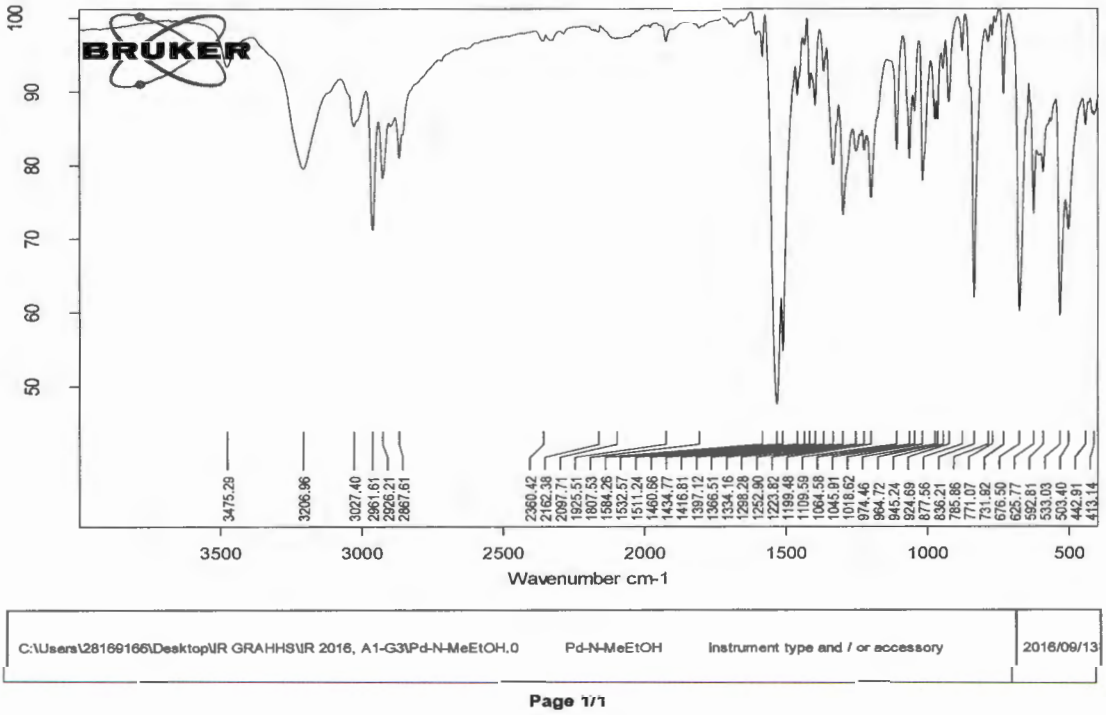

Figure S6: FTIR of $[Pd(L^6)_2]$

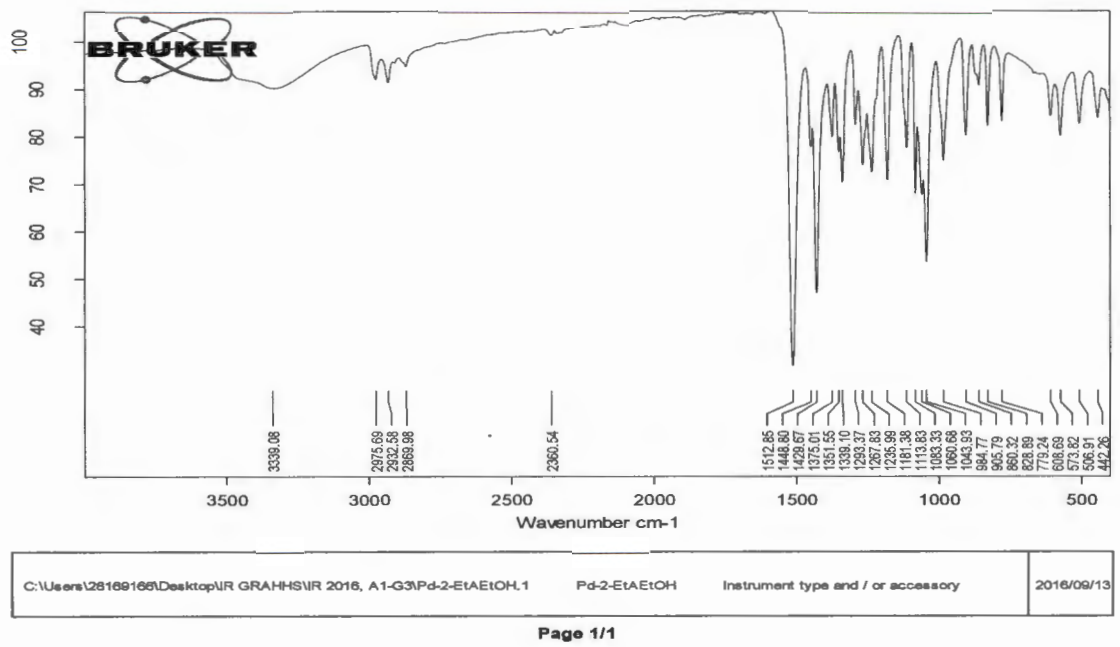

Figure S7: FTIR of $[Pd(L^7)_2]$

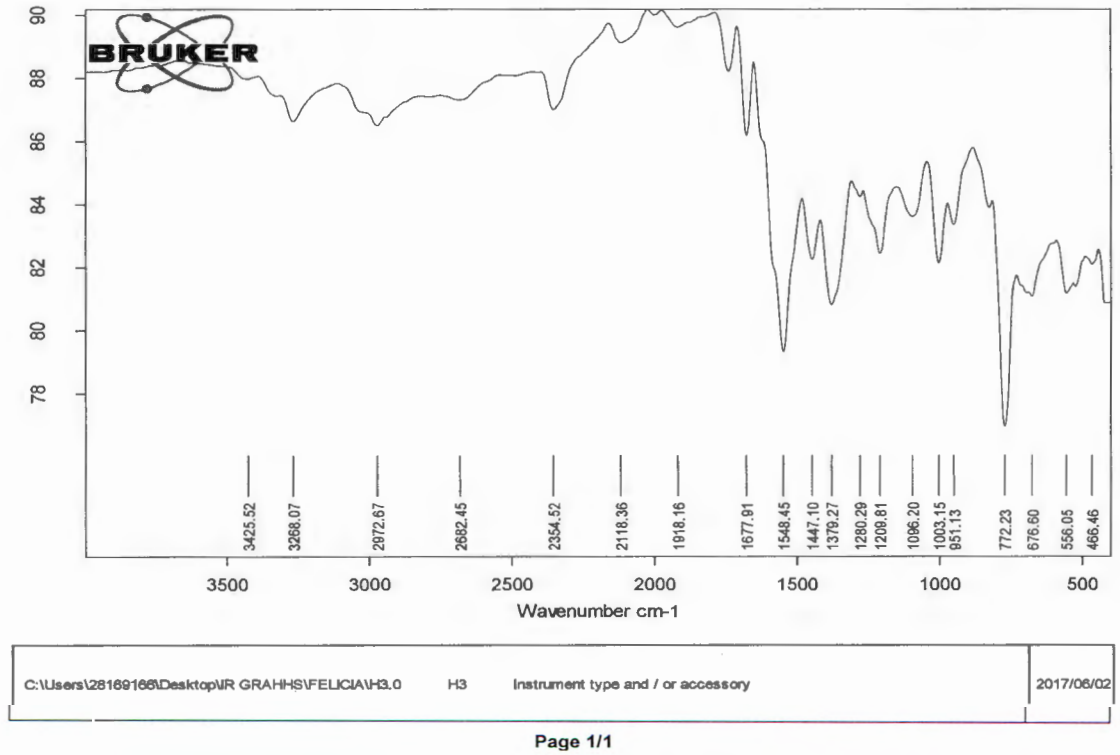

Figure S8: FTIR of $[Pd(L^8)_2]$

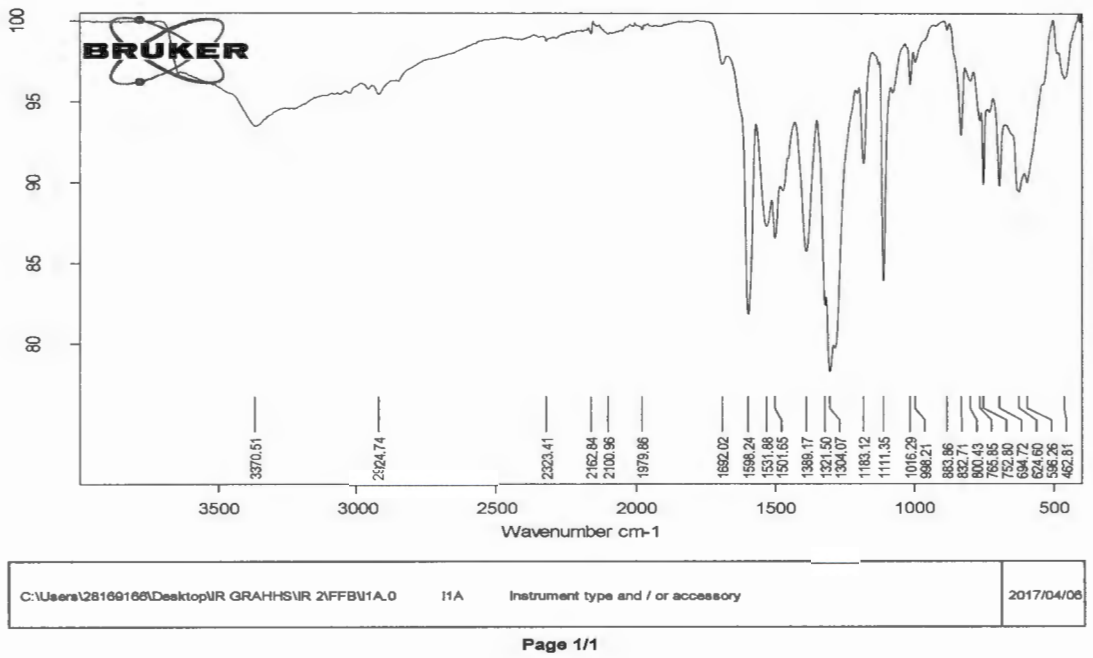

Figure S9: FTIR of $[Ni(L^9)_2]$

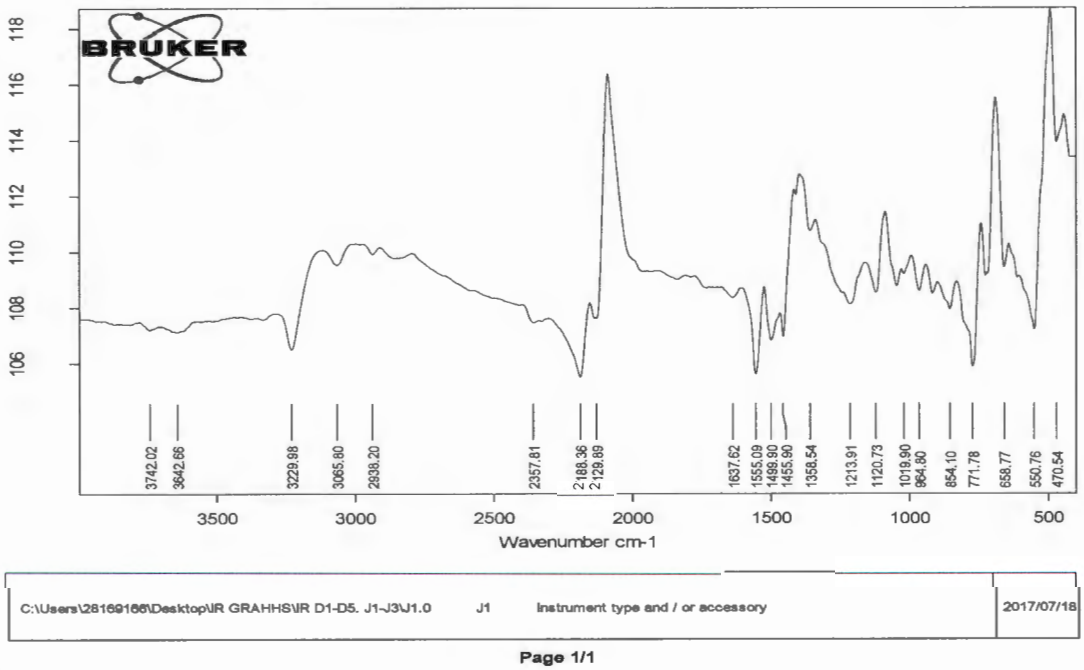

Figure S10: FTIR of $[Ni(L^{10})_2]$

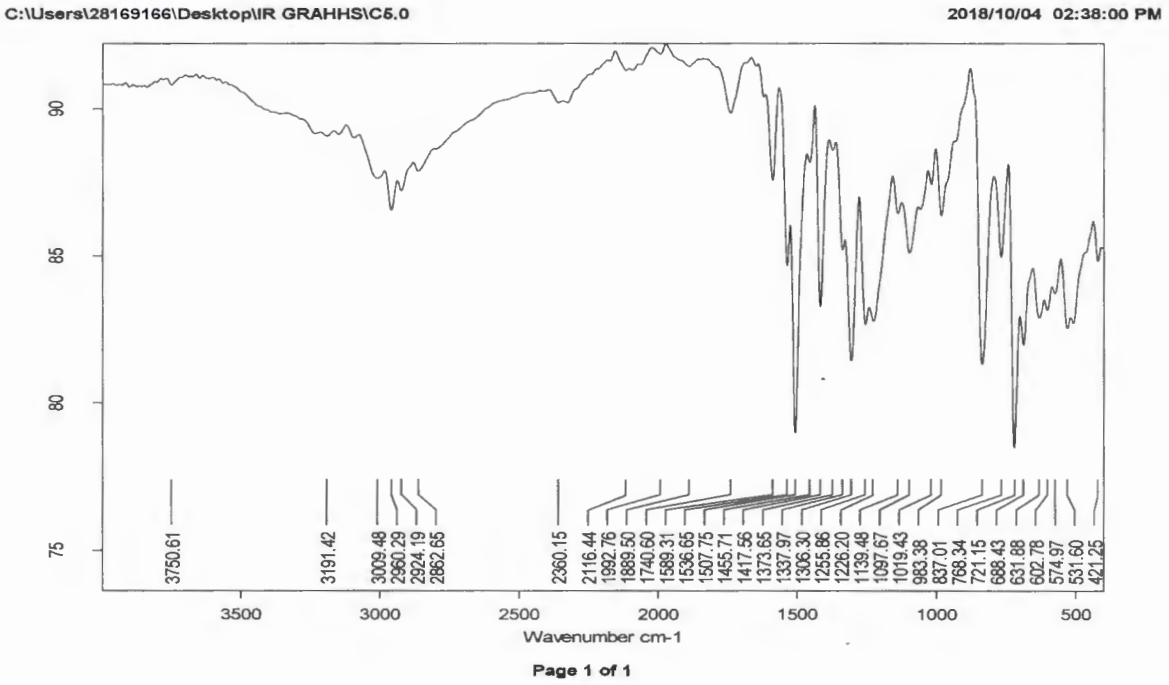

Figure S11: FTIR of $[Ni(L^4)_2phen]$

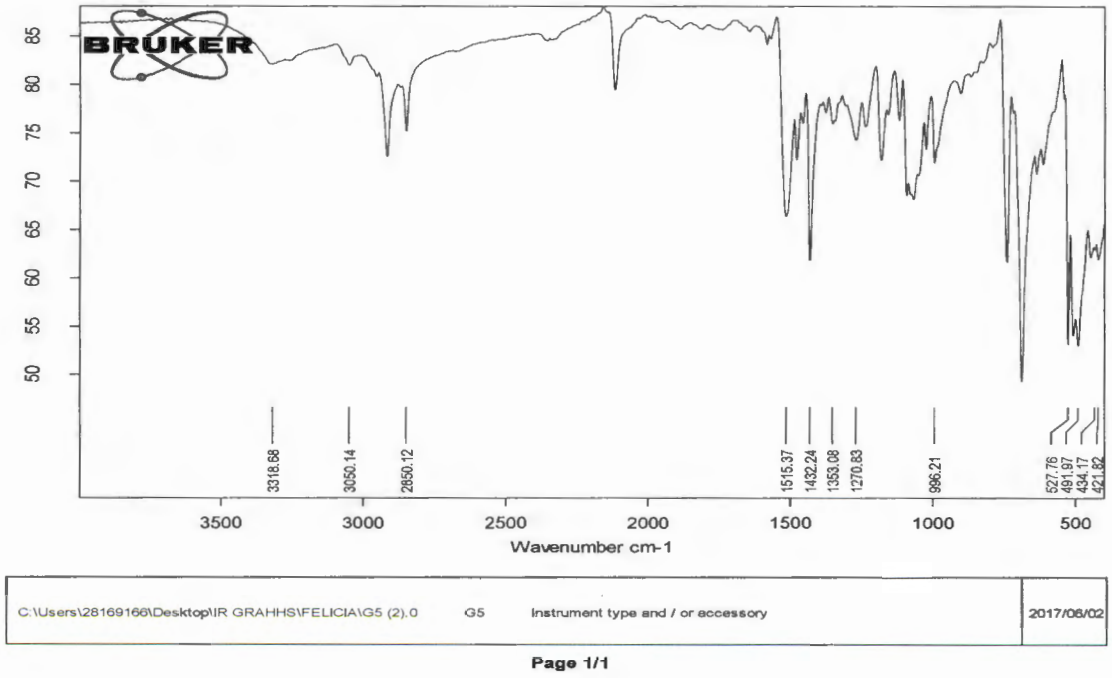

Figure S12: FTIR of $[NiL^7(NC)(PPh_3)]$

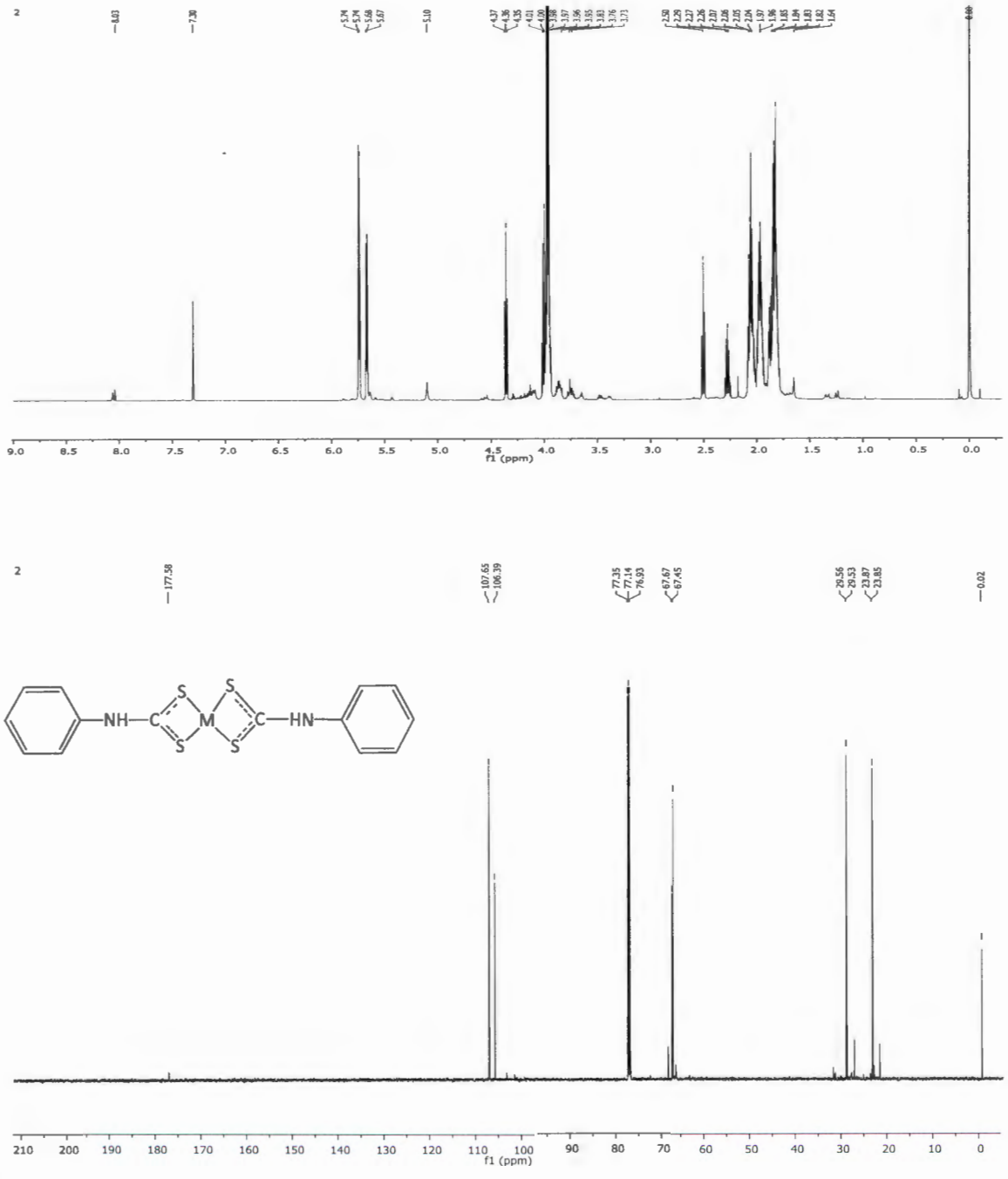

Figure S13: ^{1}H, ^{13}C NMR $[Pd(L^{1})_2]$

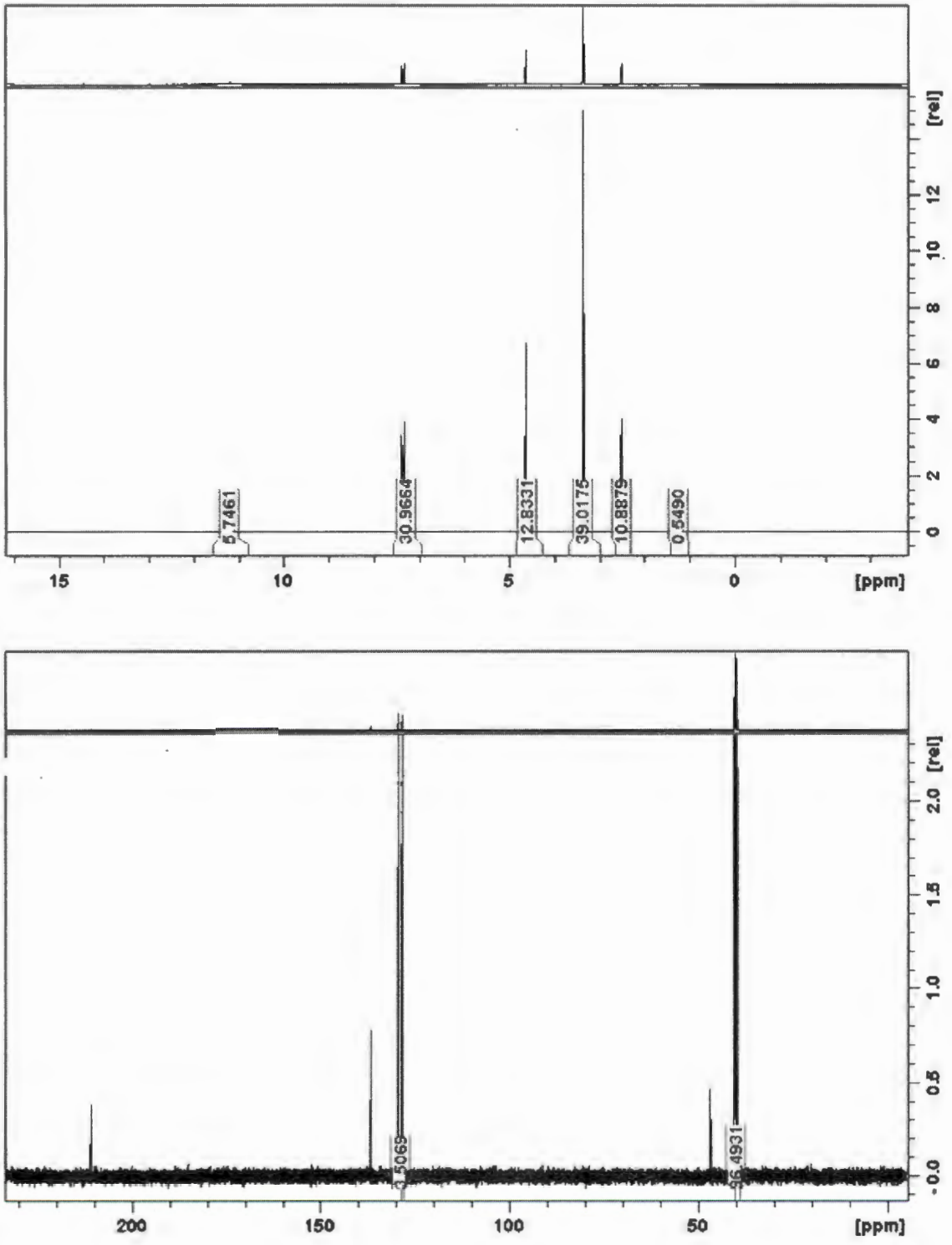

Figure S14: 1H, 13C NMR [Pd(L^2)2]

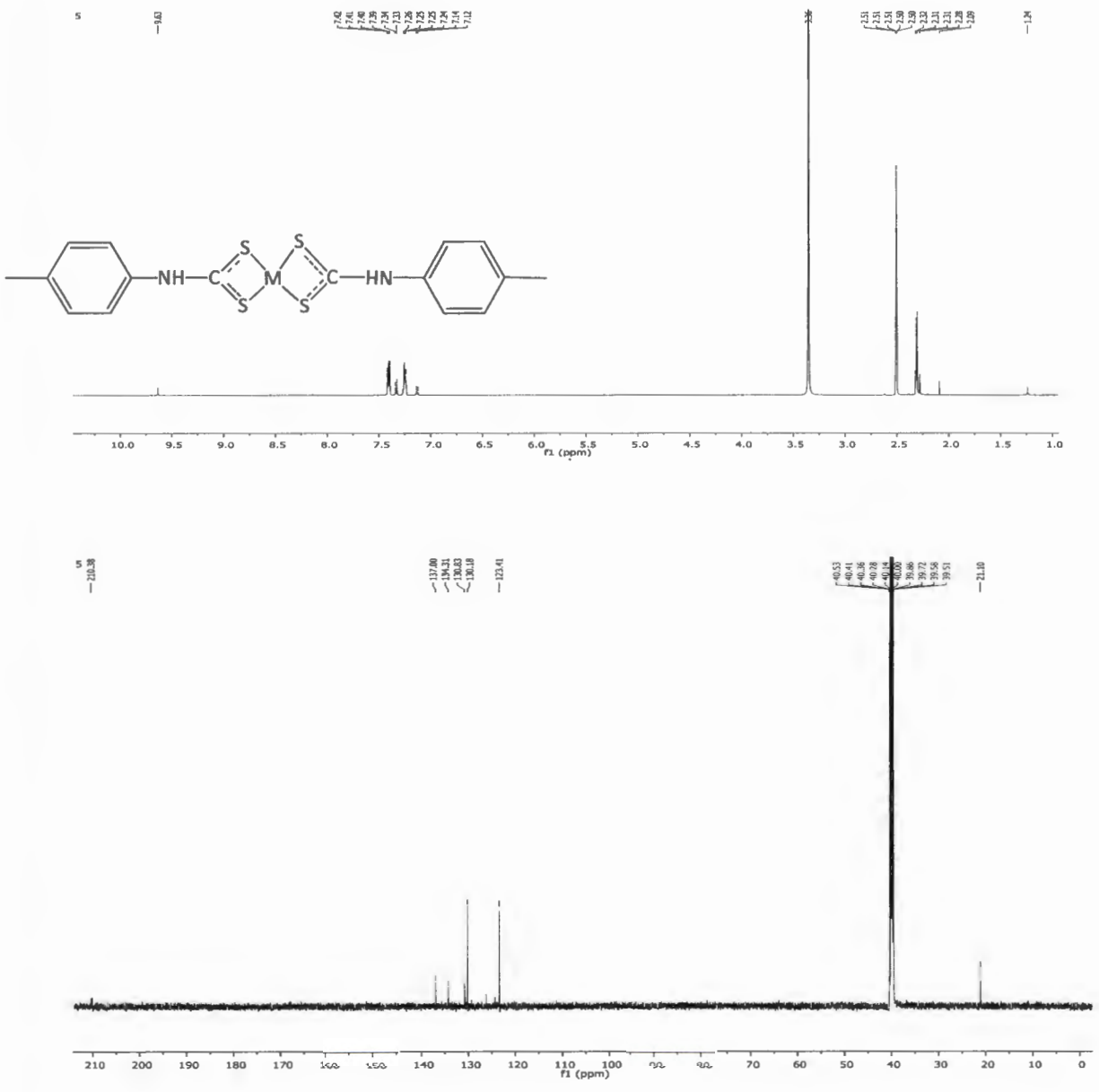

Figure S15: ^{1}H, ^{13}C NMR [Pd(L^{3})2]

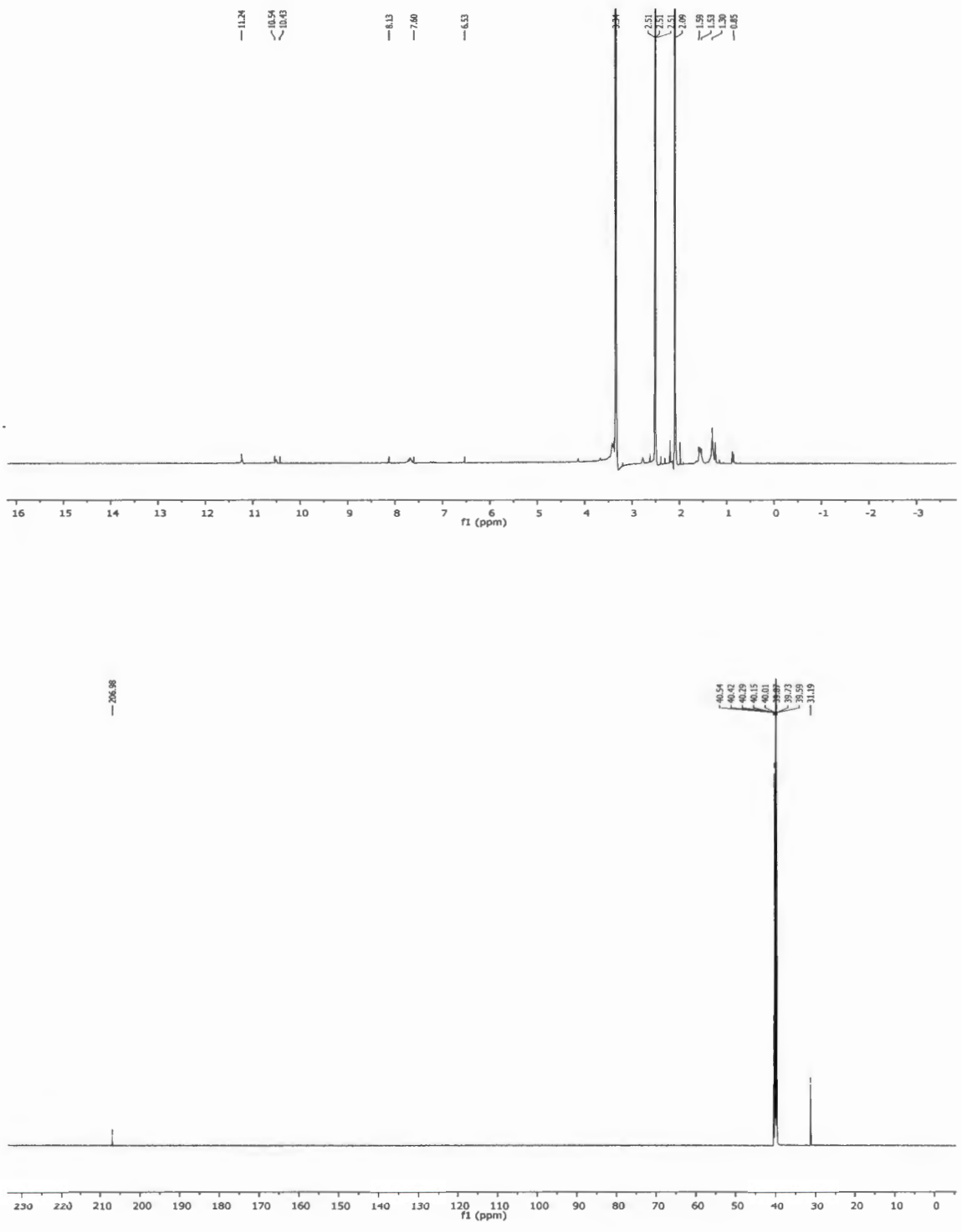

Figure S16: ^{1}H, ^{13}C NMR $[Pt(L^{5})_{2}]$

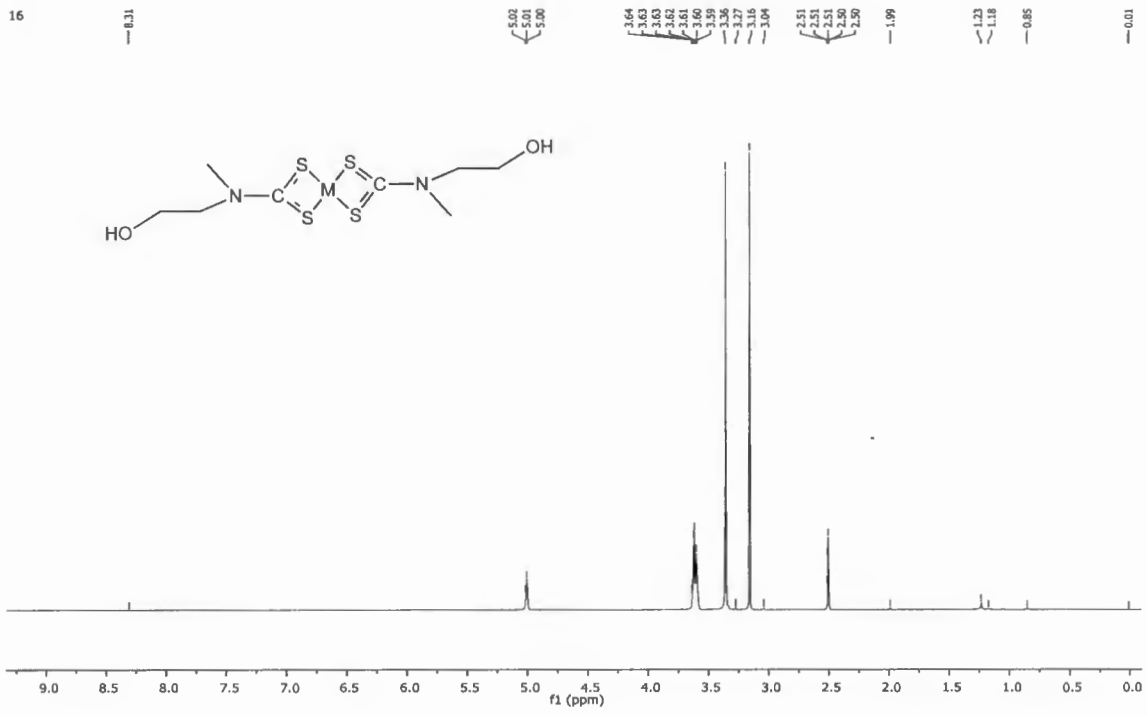

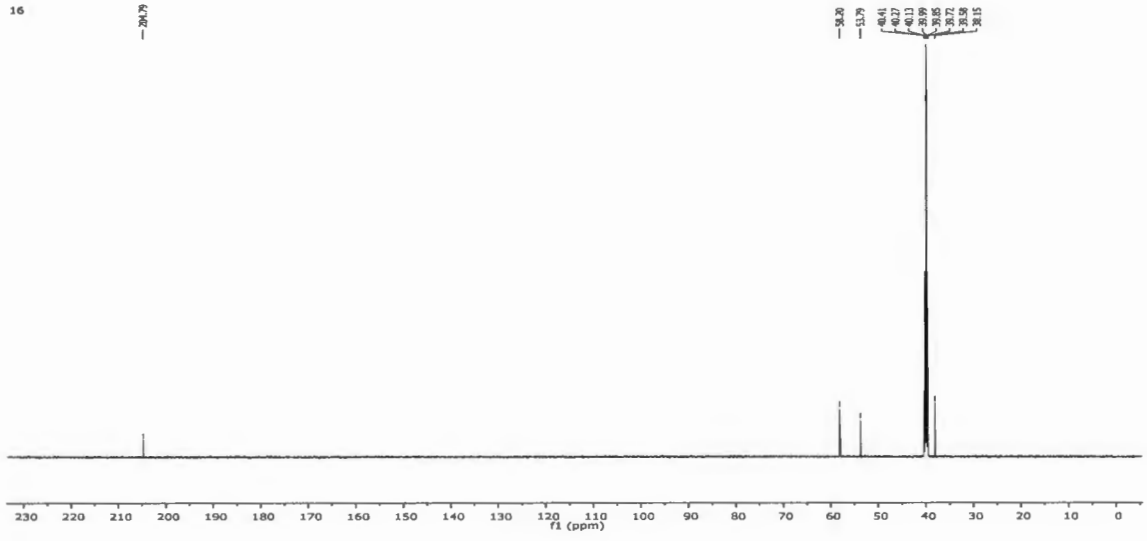

Figure S17: ^{1}H, ^{13}C NMR $[Ni(L^{6})_2]$

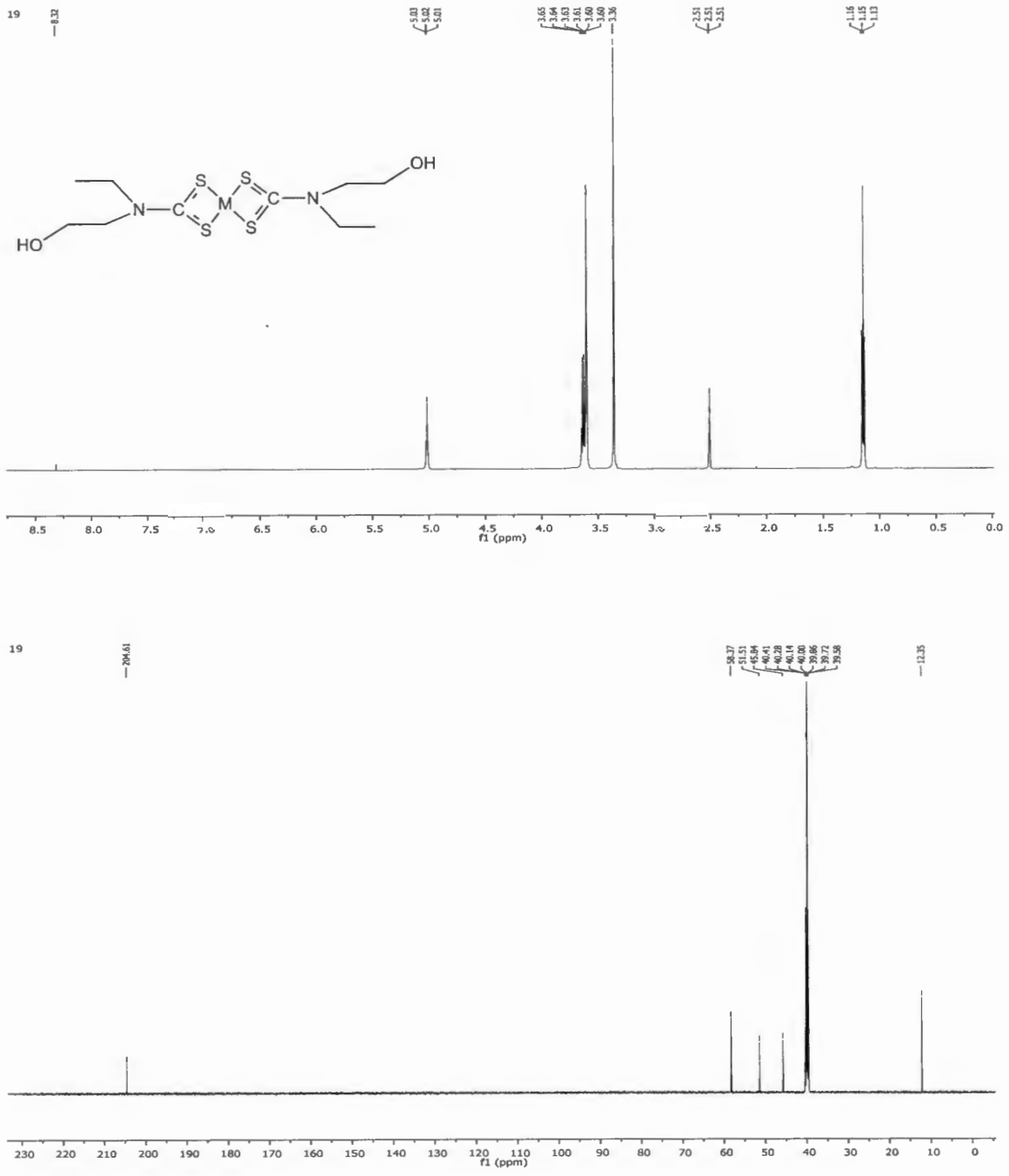

Figure S18: ^{1}H, ^{13}C NMR $[Ni(L^{7})_2]$

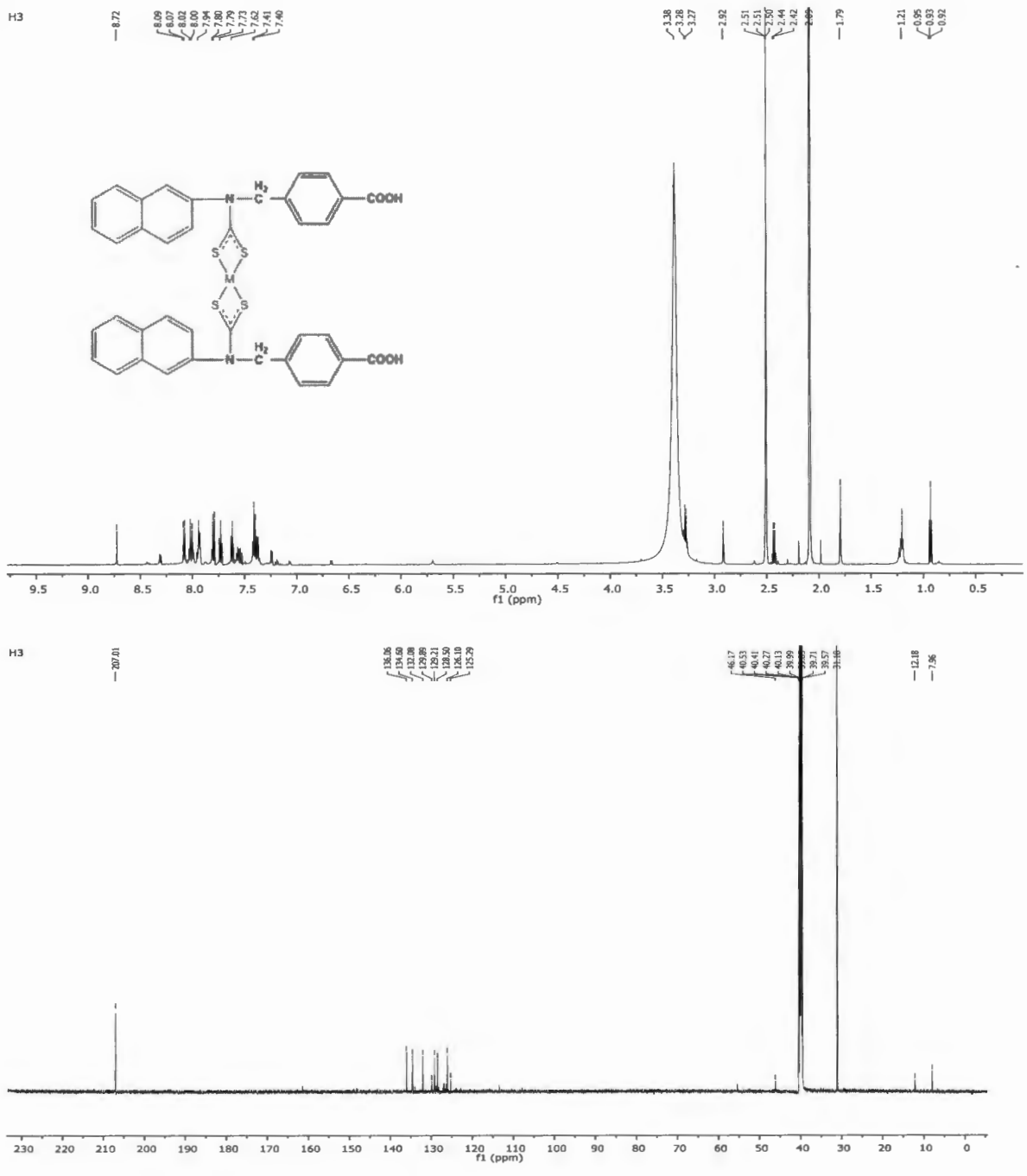

Figure S19: ^{1}H, ^{13}C NMR $[Pt(L^{8})_2]$

CCDC NUMBER

CRYSTAL	CCDC
$[Pd(L)_2]$	1849649
$[Pt(L)_2]$	1848912.
$[Pt(L^3)_2]$	1875081
$[Ni(L^2)_2]$	
$[Pt(L^2)_2]$	
$Pd(L^7)_2]$	1551524
$[NiL^2(NCS)PPh_3]$	1566642.
$NiL^7(NC)(PPh_3)]$	1573114